



NCS Technical Information Bulletin 88-1

Radiation Response Prediction of Single Mode Fibers

E.J. Friebele



Optical Sciences Division
Naval Research Laboratory
Washington, DC 20375

Final Report
March, 1988

This document has been approved
for public release and sale in
distribution is unlimited.

DTIC
ELECTE
31 MAR 1989
ca
E

89 3 30 00

AD-A206 211

Unclassified

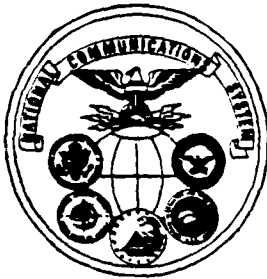
SECURITY CLASSIFICATION OF THIS PAGE

ADA206211

REPORT DOCUMENTATION PAGE

Form Approved
OMB No. 0704-0188

1a REPORT SECURITY CLASSIFICATION Unclassified		1b RESTRICTIVE MARKINGS	
2a SECURITY CLASSIFICATION AUTHORITY		3 DISTRIBUTION/AVAILABILITY OF REPORT Approved for public release; distribution unlimited. /A	
2b DECLASSIFICATION/DOWNGRADING SCHEDULE		5 MONITORING ORGANIZATION REPORT NUMBER(S)	
4 PERFORMING ORGANIZATION REPORT NUMBER(S) NCS TIB 88-1		7a NAME OF MONITORING ORGANIZATION	
6a NAME OF PERFORMING ORGANIZATION Naval Research Laboratory	6b OFFICE SYMBOL (If applicable)	7b ADDRESS (City, State, and ZIP Code)	
8a ADDRESS (City, State, and ZIP Code) Optical Sciences Division Washington, D.C. 20375		9 PROCUREMENT INSTRUMENT IDENTIFICATION NUMBER MIPR HC1001-6-40048	
3a NAME OF FUNDING SPONSORING ORGANIZATION National Communications System	3b OFFICE SYMBOL (If applicable) NCS-TS	10 SOURCE OF FUNDING NUMBERS PROGRAM ELEMENT NO 33127K PROJECT NO Q019 TASK NO WORK UNIT ACCESSION NO	
11 TITLE (Include Security Classification) Radiation Response Prediction of Single Mode Fibers			
12 PERSONAL AUTHOR(S) E. J. Friebele			
13a TYPE OF REPORT Final	13b TIME COVERED FROM TO	14 DATE OF REPORT (Year, Month, Day) March 1988	15 PAGE COUNT 250
16 SUPPLEMENTARY NOTATION			
COSATI CODES FIELD GROUP SUBGROUP		18 SUBJECT TERMS (Continue on reverse if necessary and identify by block number) Fiber Optic National Security Emergency Preparedness (NSEP)	
19 ABSTRACT (Continue on reverse if necessary and identify by block number) The primary result of this study is the demonstration of the feasibility of a predictive capability whereby the optical attenuation induced by nuclear fallout in a matched clad single mode fiber can be determined via a linear regression model whose inputs are core and clad dopant concentrations and fabrication parameters such as draw speed and tension and oxygen-to-reagent ratio. This study has shown the capability of developing a predictive model via multiple regression and has opened the possibility of further refinement to improve statistical confidence.			
20 DISTRIBUTION AVAILABILITY OF ABSTRACT <input checked="" type="checkbox"/> UNCLASSIFIED/UNLIMITED <input type="checkbox"/> SAME AS RPT <input type="checkbox"/> DTIC USERS		21 ABSTRACT SECURITY CLASSIFICATION Unclassified	
22a NAME OF RESPONSIBLE INDIVIDUAL A. H. Rausch		22b TELEPHONE (Include Area Code) 202-692-2124	22c OFFICE SYMBOL NCS-TS



NCS Technical Information Bulletin 88-1

Radiation Response Prediction of Single Mode Fibers

E.J. Friebele



Accession For	
NTIS GRA&I	<input checked="checked" type="checkbox"/>
DTIC TAB	<input type="checkbox"/>
Unannounced	<input type="checkbox"/>
Justification	
Title	
Distribution/	
Availability Codes	
Avail and/or	
Dist	Special
A-1	

Optical Sciences Division
Naval Research Laboratory
Washington, DC 20375

Final Report
March, 1988

NCS TECHNICAL INFORMATION BULLETIN 88-1

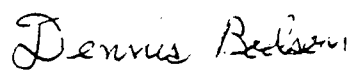
RADIATION RESPONSE PREDICTION OF SINGLE MODE FIBERS

JANUARY 1988

PROJECT OFFICER


A. H. RAUSCH
Electronics Engineer

APPROVED FOR PUBLICATION:


DENNIS BODSON
Assistant Manager
Office of Technology
and Standards

FOREWORD

The National Communications System (NCS) is an organization of the Federal government whose membership is comprised of 23 Government entities. Its mission is to assist the President, National Security Council, Office of Science and Technology Policy, and Office of Management and Budget in:

- o The exercise of their wartime and non-wartime emergency functions, and their planning and oversight responsibilities.
- o The coordination of the planning for and provision of National Security/Emergency Preparedness communications for the Federal government under all circumstances including crisis or emergency.

In support of this mission the NCS has initiated and manages the Electromagnetic Pulse (EMP) program. The major objective of this program is to significantly reduce the vulnerability of the U.S. telecommunication infrastructure to disabling damage due to nuclear weapon effects in direct support of the survivability and endurability objectives addressed by Executive Order 12472 and National Security Decision Directive 97. Nuclear weapon effects include EMP, Magnetohydrodynamic EMP (MHD-EMP), and fallout radiation from atmospheric detonations. The purpose of this Technical Information Bulletin is to provide the reader with information relating to the effects of fallout radiation on fiber optic cables which will become the predominant transmission media in the 1990's.

Comments, on this TIB are welcome, and should be addressed to:

Office of the Manager
National Communications System
ATTN: NCS-TS
Washington, DC 20305-2010
(202) 692-2124

RADIATION RESPONSE PREDICTION OF SINGLE MODE FIBERS

FINAL REPORT

March 23, 1988

E. Joseph Friebele, Principal Investigator
Optical Sciences Division
Naval Research Laboratory
Washington, DC 20375
(202) 767-2270

Andre H. Rausch, Program Manager
Technology and Standards
National Communications System
Arlington, VA 22204
(202) 692-5872

Funded by the National Communications System under MIPR HC1001-6-40048

CONTRIBUTING SCIENTISTS

Charles G. Askins

Louise A. Brambani⁺

Kenneth L. Dorsey⁺

David L. Griscom

Michael E. Gingerich

Calvin C. Harrington⁺

Cathy M. Shaw⁺

Tsung-Ein Tsai⁺⁺

Un-Chul Paek⁺⁺⁺

⁺ Sachs Freeman Associates, Inc., Landover, MD 20785

⁺⁺ GeoCenters, Inc., Suitland, MD 20746

⁺⁺⁺ AT&T Engineering Research Center, Hopewell Junction, NJ 08540

EXECUTIVE SUMMARY

BACKGROUND

Fiber optic transmission systems, because of their extraordinary channel capacity and decreasing cost, are rapidly becoming the preferred terrestrial transmission media of the nation's long distance, inter-city telecommunications infrastructure. Since the commercial telephone network forms the foundation for emergency communication in the event of a national crisis or emergency, additional requirements are placed on the fibers and components being installed. One of the most stressing environments for the fiber consists of fallout subsequent to a nuclear attack. The susceptibility of some types of commercially available fiber optic cable to optical darkening (and hence increased signal loss) from exposure to ionizing radiation raises serious questions about the survivability of such systems in the reconstitution phase of a nuclear conflict. There is a large body of knowledge available on the effects of gamma radiation on the older multimode fiber cables. However, there are critically important knowledge gaps with respect to the newer single mode cables which are employed in the inter-city fiber transmission links being installed today.

There is an urgent need to establish a data base of single mode fiber radiation responses in order to have the tools necessary to assess the National Security Emergency Preparedness (NSEP) utility of present and future fiber optic systems and to provide guidance on how to decrease their radiation susceptibility. These data will be used in the preparation of a multi-tier specification by the National Telecommunications and Information Administration Institute for Telecommunication Sciences (NTIA/ITS) for the National Communications System (NCS) to identify the measures to be incorporated into the design of commercial fiber optic networks to meet NSEP

survivability needs. The spectrum of threats with which the fiber optic systems must cope are: power loss, disruption by natural causes, physical security, EMP, and gamma radiation from nuclear fallout. The design parameters to be addressed by this specification will be those which tend to minimize disruption of service in the face of the above-mentioned threats and to greatly increase the probability of survival of optical fiber networks.

Unfortunately, fiber optic response data to gamma radiation do not exist over a sufficiently wide range of physical conditions necessary to satisfy the requirements of a hardness design specification. This is especially true in the case of single mode fibers and cables. Furthermore, there have been only limited efforts to develop a sufficient understanding of the relationship between fabrication parameters and radiation response so that the behavior of fiber optic waveguides in fallout radiation environments could be quantitatively predicted based on knowledge of fabrication parameters and fiber compositions.

PRESENT PROGRAM

This document is a final report of a two year program funded by NCS at NRL, which was the first systematic study of the interrelationship of fiber fabrication parameters and radiation-induced loss. A rudimentary regression model was developed for predicting the loss induced by a fallout exposure at -35 C.

The experimental and analytical studies carried out in this program addressed the problem of predicting the increase in optical loss in single mode fiber optic waveguides that occurs as a result of exposure to fallout from nuclear weapons. Those parameters of fiber design and manufacture that are critical to radiation hardness were identified and provided as input to the specification of fibers for lightwave communications systems capable of

satisfying National Security/Emergency Preparedness requirements.

This represents the first systematic study of the interrelationship of fiber parameters and radiation-induced loss. Because of the large parameter space, including core and clad dopants, and deposition and draw conditions, specific orthogonal matrix models were applied to the experimental design, resulting in a reduction from 248 to 24 fibers required for the study. A generic radiation environment for the fiber was derived from literature values and calculations. Fabrication parameters having a significant effect on radiation sensitivity and subsequent recovery have been identified, and the behavior of the fibers has been well-characterized after a 2000 rad exposure at -35 C. A kinetic model describing the recovery in quantitative terms has been applied to the data, and the kinetic parameters have been correlated with fabrication parameters.

RESULTS AND CONCLUSION

The primary result of present study is the demonstration of the feasibility of a predictive capability whereby the optical attenuation induced by nuclear fallout in a matched clad single mode fiber can be determined via a linear regression model whose inputs are core and clad dopant concentrations and fabrication parameters such as draw speed and tension and oxygen-to-reagent ratio. The radiation response and recovery has been quantified by fitting the data to an n-th order kinetic equation. The "initial" loss A_0 is a measure of the response of the fiber to the delayed gamma component, while the "permanent" incremental A_f loss is a measure of the fallout response.

The stepwise multiple regression procedure used here has shown that prediction of A_0 and A_f can be made with a fair degree of confidence in a few cases with one or two input variables:

1. For the Ge-F-doped silica clad fibers, A_0 is predicted from the effective

core [Ge] and the oxygen flow used during clad deposition. A_f is predicted from the effective core [Ge] and the oxygen flow used during core deposition.

2. For the P-F-doped silica clad fibers, A_0 is predicted from the draw tension and the oxygen flow used during clad deposition.

The regression results are more tenuous in other cases, likely due to the small sample size.

It was found in this study that no consistent, meaningful predictive capability could be derived for either the order of the kinetics n or the half-life of the radiation-induced loss τ . Once again, this result may be attributed to the small sample size, but additionally to the fact that there were significant outlying points in both populations. The value of kinetic order does not have a strong influence on either the delayed gamma or fallout radiation response, at least within the range of $2 \leq n \leq 4$. However, variations in the half-life τ do have a dramatic effect, and it is hoped that further studies will result in a predictive capability for this parameter.

The preliminary regression model developed for predicting radiation response requires as input not only the analyzed core and clad compositions, but their effective value determined by normalizing by the relative optical power transmitted in the core and clad at the operating wavelength. The core and clad compositions are determined by electron microprobe analysis, while the core diameter (measured by scanning electron microscopy) and the near field radiation pattern are required for normalization. In addition, parameters such as oxygen flow during core and clad deposition, draw speed and draw tension are also required as input in some cases. The former parameters can be measured from the fiber, albeit tediously, while the latter must be provided by the manufacturer before the regression equation can be used. Alternatively, fibers to be installed can be specified to have optimum

parameters for radiation hardness. In any event, the present study has shown the capability of developing a predictive model via multiple regression and has opened the possibility of further refinement to improve statistical confidence.

TABLE OF CONTENTS

EXECUTIVE SUMMARY	ii
BACKGROUND	ii
PRESENT PROGRAM	iii
RESULTS AND CONCLUSION	iv
LIST OF FIGURES	x
LIST OF TABLES	xviii
INTRODUCTION	1
BACKGROUND	1
PROGRAM	2
RADIATION ENVIRONMENT	3
REFERENCES	7
ORTHOGONAL MATRIX DESIGN AND ANALYSIS	11
INTRODUCTION	11
FACTORIAL DESIGN OF ORTHOGONAL MATRIX	12
Factors and Minimum Number of Experiments	12
Factorial Design of 2^4 Orthogonal Array.	13
ANALYSIS	14
Effects of Two-Level Factors	14
Effects of Three-Level Factors	14
Effects of Interactions between Two Factors	16
Statistical Analysis.	16
IMPLEMENTATION TO MODELLING RADIATION RESPONSE OF OPTICAL FIBERS . .	18

Assessment of the Method	18
Simulation	18
Simulation Results	21
Conclusions	24
MULTIPLE REGRESSION	24
REFERENCES	27
 PREFORM DESIGN	 51
PREFORM FABRICATION	53
ELECTRON PROBE MICROANALYSIS	56
REFERENCES	57
 OPTICAL CHARACTERIZATION	 71
REFERENCES	75
 RADIATION DAMAGE MEASUREMENTS	 85
TEST PROCEDURE	85
COMMERCIAL FIBERS	88
NRL PROTOTYPE FIBERS	92
REFERENCES	93
 KINETIC ANALYSIS	 118
REFERENCES	123
 EXPERIMENTAL RESULTS AND MODEL DEVELOPMENT	 135
RECOVERY DATA	135
ORTHOGONAL MATRIX ANALYSIS	137
Initial Attenuation	137

Final Attenuation	139
Order of the Kinetics	139
Half-Life of the Induced Attenuation	141
MULTIPLE REGRESSION ANALYSIS	143
Initial Attenuation	144
Final Attenuation	148
Order of Kinetics	151
Half-Life of Recovery	151
CONCLUSIONS AND FUTURE DIRECTIONS	220
CONCLUSIONS	220
FUTURE DIRECTIONS	222
REFERENCES	223

LIST OF FIGURES

2.1	Derivation of a function $f(N)$ by a graphic fit to 5 extracted point solutions for parameter N.	32
2.2	Extracted point solutions for a function of parameter E, plotted with the pseudo-function of E.	33
2.3	Extracted solutions for parameter E offset to align first point with pseudo-function.	34
2.4	Extracted solutions and function for parameter B.	35
2.5	Extracted solutions and function for parameter F.	36
2.6	Extracted solutions and function for parameter C.	37
2.7	Range of solutions for parameter C with level errors considered. . .	38
2.8	Range of solutions for parameter C with measurement errors considered.	39
2.9	Range of solutions for parameter C determined by both levels and measurement errors.	40
2.10	Cross term $A \times C$ plotted against range of A for six discrete levels of C.	41
2.11	Effect of cross terms on solutions for parameter C.	42
2.12	All modifiers affecting solutions for parameter C: levels and measurement error and cross terms.	43
2.13	Solutions for parameter E as affected by cross terms.	44
2.14	Solutions for parameter F with or without cross terms.	45
2.15	Range of solutions for parameter A due to all modifiers; weak function of A.	46
2.16	Range of solutions for parameter A due to all modifiers; strong function of A.	47
2.17	Range of solutions for parameter F with all modifiers; weak function	

of A.	48
2.18 Range of solutions for parameter F with all modifiers; strong function of A.	49
2.19 Range of solutions for B due to all modifiers.	50
3.1 Schematic of a typical MCVD apparatus. Not shown are the controls for maintaining accurate temperature of the reaction zone and tube dimension by providing back pressure.	69
3.2 Typical results of electron microprobe analysis showing weight percents of GeO ₂ , SiO ₂ , P ₂ O ₅ and F across the fiber core (centered 7.5 microns) and cladding.	70
4.1 Dynamic spatial filtering technique for determining refractive index profile of fiber preforms.	78
4.2 Apparatus for measuring single mode cutoff wavelength and spectral transmission of single mode fibers.	79
4.3 Apparatus for near-field measurement of the mode field diameter in the single mode fiber.	80
4.4 Refracted near field technique for measuring the fiber index profile.	81
4.5 Refractive index profile of a typical matched clad single mode fiber preform made in this study.	82
4.6 Spectral transmission ratio of bent and straight single mode fiber showing the large second mode cutoff and the location of the cutoff wavelength at 1.23 μ m	83
4.7 Typical spectral attenuation data for single mode fibers fabricated in this study.	84
5.1 Recovery of the attenuation induced in a Sumitomo single mode fiber by doses of 2000 and 400 rads.	99
5.2 Apparatus used for measuring the growth and recovery of the	

radiation-induced attenuation of the single mode fibers.	100
5.3 Raw recovery data of N=16 obtained without use of the reference fiber and detector.	101
5.4 Recovery data of N=16 obtained using the reference fiber and detector to reduce long term drifts in the laser diode output. . . .	102
5.5 Data set of N=16 obtained by selection of 30 data points from the set at logarithmic intervals.	103
5.6 Recovery data of Northern Telecom, NRL, Spectran, and Sumitomo single mode fibers and two NRL prototype fibers.	104
5.7 Recovery data of Corning commercial single mode fibers.	105
5.8 Recovery data of AT&T standard and rad-hard single mode fibers. . . .	106
5.9 Recovery data of a Lightwave Technologies, Inc. commercial single mode fiber.	107
5.10 Recovery data of a Schott commercial single mode fiber made by the plasma impulse chemical vapor deposition (PICVD) process.	108
5.11 Recovery data of a Philips single mode fiber made by the plasma chemical vapor deposition (PCVD) process.	109
5.12 Raw recovery data for N = 3.	110
5.13 Reduced and selected recovery data for N = 3.	111
5.14 Raw recovery data for N = 7.	112
5.15 Reduced and selected recovery data for N = 7.	113
5.16 Raw recovery data for N = 8.	114
5.17 Reduced and selected recovery data for N = 8.	115
5.18 Raw recovery data for N = 9.	116
5.19 Reduced and selected recovery data for N = 9.	117
6.1 Plots of kinetic equation (6.5) used to fit the recovery data of the radiation-induced attenuation measured in fibers of this study, showing the effect of variations in n.	126

6.2	Recovery of radiation-induced attenuation (points) in AT&T radiation-hardened and commercial single mode fiber and fits to kinetic model (lines).	127
6.3	Recovery of radiation-induced attenuation (points) in commercially-available Corning 1521 and 1524 single mode fibers and fits to kinetic model (lines).	128
6.4	Recovery of radiation-induced attenuation (points) in commercially-available and prototype Lightwave Technologies, Inc. single mode fibers and fits to kinetic model (lines).	129
6.5	Recovery of radiation-induced attenuation (points) in a commercial Northern Telecom single mode fiber and fit to kinetic model (line). .	130
6.6	Recovery of radiation-induced attenuation (points) in a Philips single mode fiber made by the plasma CVD process and fit to kinetic model (line).	131
6.7	Recovery of radiation-induced attenuation (points) in a Schott single mode fiber made by the plasma-enhanced CVD process and fit to kinetic model (line).	132
6.8	Recovery of radiation-induced attenuation (points) in commercial and rad-hard Spectran single mode fibers and fits to kinetic model (lines).	133
6.9	Recovery of radiation-induced attenuation (points) in Sumitomo standard Ge-doped silica and pure silica core (Z) single mode fibers and fits to kinetic model (lines).	134
7.1	Recovery of radiation-induced attenuation in pure silica clad single mode fibers (points) and fits to the generalized kinetic recovery equation (lines).	175
7.2	Recovery of radiation-induced attenuation in matched clad single mode fibers with level 3 Ge in the core (points) and fits to the	

generalized kinetic recovery equation (lines).	176
7.3 Recovery of radiation-induced attenuation in matched clad single mode fibers with level 2 Ge in the core (points) and fits to the generalized kinetic recovery equation (lines).	177
7.4 Recovery of radiation-induced attenuation in matched clad single mode fibers with levels 1 or 2 Ge in the core and level 2 Ge in the clad down doped with F to maintain the proper index (points) and fits to the generalized kinetic recovery equation (lines).	178
7.5 Recovery of radiation-induced attenuation in matched clad single mode fibers with level 1 P in the clad down doped with F to maintain the proper index (points) and fits to the generalized kinetic recovery equation (lines).	179
7.6 Recovery of radiation-induced attenuation in matched clad single mode fibers with level 2 P in the clad down doped with F to maintain the proper index (points) and fits to the generalized kinetic recovery equation (lines).	180
7.7 Recovery of radiation-induced attenuation in matched clad single mode fibers with level 3 P in the clad down doped with F to maintain the proper index (points) and fits to the generalized kinetic recovery equation (lines).	181
7.8 Effect of Ge concentration in the core and clad (down-doped with F) on the initial damage level A_0 of fibers of the first group.	182
7.9 Effect of P concentration in the clad (down-doped with F) on initial damage level A_0 of fibers of the second group.	183
7.10 Effect of the ratio of oxygen carrier gas to reagent concentration during core and clad deposition on the initial damage level A_0 of fibers of the first group.	184
7.11 Effect of the ratio of oxygen carrier gas to reagent concentration	

during clad deposition on the initial damage level A_0 of fibers of the second group.	185
7.12 Effect of draw tension on initial damage level A_0 and permanent incremental loss A_f of fibers of the first group.	186
7.13 Effect of draw tension on initial damage level A_0 and permanent incremental loss A_f of fibers of the second group.	187
7.14 Effect of draw speed on initial damage level A_0 and permanent incremental loss A_f of fibers of the first group.	188
7.15 Effect of draw speed on initial damage level A_0 and permanent incremental loss A_f of fibers of the second group.	189
7.16 Effect of Ge concentration in the core and clad (down-doped with F) on the permanent induced attenuation A_f of fibers of the first group.	190
7.17 Effect of P concentration in the clad (down-doped with F) on the permanent induced attenuation A_f of fibers of the second group. . . .	191
7.18 Effect of ratio of oxygen carrier to reagent concentration during core and clad deposition on permanent damage level A_f of fibers of the first group.	192
7.19 Effect of Ge concentration in the core and clad (down-doped with F) on the order of the kinetics n of fibers of the first group.	193
7.20 Effect of P concentration in the clad (down-doped with F) on the order of the kinetics n of fibers of the second group.	194
7.21 Effect of ratio of oxygen carrier to reagent concentration during core and clad deposition on the order of the kinetics n of Phase 1 fibers.	195
7.22 Effect of ratio of oxygen carrier to reagent concentration during cladding deposition on the order of the kinetics n of fibers of the second group.	196

7.23 Effect of draw tension on the order of the kinetics n of Phase 1 fibers.	197
7.24 Effect of draw tension on the order of the kinetics n of fibers of the second group.	198
7.25 Effect of draw speed on the order of the kinetics n of fibers of the first group.	199
7.26 Effect of draw speed on the order of the kinetics n of fibers of the second group.	200
7.27 Effect of Ge concentration in the core and clad (down-doped with F) on the "half-life" τ of fibers of the first group.	201
7.28 Effect of P concentration in the clad (down-doped with F) on the "half-life" τ of fibers of the second group.	202
7.29 Effect of ratio of oxygen carrier to reagent concentration during core and clad deposition on the "half-life" τ of Phase 1 fibers.	203
7.30 Effect of ratio of oxygen carrier to reagent concentration during cladding deposition on the "half-life" τ of fibers of the second group.	204
7.31 Effect of draw tension on the "half-life" τ of Phase 1 fibers.	205
7.32 Effect of draw tension on the "half-life" τ of fibers of the second group.	206
7.33 Effect of draw speed on the "half-life" τ of fibers of the first group.	207
7.34 Effect of draw speed on the "half-life" τ of fibers of the second group.	208
7.35 Stepwise multiple regression results of A_0 over all fibers using as the independent variables the clad [Ge] and clad [P], both normalized by the fractional optical power.	209
7.36 Stepwise multiple regression results of A_0 using a population of	

Ge-F-doped and P-F-doped silica clad fibers.	210
7.37 Stepwise multiple regression results of A_0 using a population of Ge-F-doped silica clad fibers.	211
7.38 Stepwise multiple regression results of A_0 using a population of P- F-doped clad fibers.	212
7.39 Stepwise multiple regression results of A_f using a population of all fibers.	213
7.40 Stepwise multiple regression results of A_f using a population of Ge-F-doped and P-F-doped silica clad fibers.	214
7.41 Stepwise multiple regression results of A_f using a population of Ge-F-doped silica clad fibers.	215
7.42 Stepwise multiple regression results of A_f using a population of Ge-F-doped and pure silica clad fibers.	216
7.43 Stepwise multiple regression results of n using a population of all Ge-F-doped, P-F-doped, and pure silica clad fibers.	217
7.44 Stepwise multiple regression results of n using a population of all Ge-F-doped silica clad fibers.	218
7.45 Stepwise multiple regression results of τ using a population of all Ge-F-doped, P-F-doped, and pure silica clad fibers.	219

LIST OF TABLES

1.1	Prompt Gamma Dose and Corresponding Thermal Radiation at Various Distances From The Edge of Plastic Region (R_p)	8
1.2	Prompt Gamma Dose and Distance from Ground Zero Corresponding to Various Thermal Radiations	8
1.3	Distance from Ground Zero and Prompt Gamma Dose for Various Overpressures Calculated for Optimum Burst Height.	9
1.4	Total Prompt Gamma Dose Received by an Unburied Optical Fiber Cable 1.15 mi from a Surface Burst of a 300 kT Weapon	10
2.1.	2^4 Orthogonal Array	28
2.2.	Factorial Design for $3^3 \times 2^3$ Using Table 2.1	29
2.3	Experimental Factors for Phase 1 of the Matched Clad Design	30
2.4	Determination of the Significance of Each Control Parameter	31
3.1	Parameters for Phase 1 of the Matched Clad Design	58
3.2	Parameters for Phase 2 of the Matched Clad Design	59
3.3	Experimental Factors for Phase 1 of the Matched Clad Design	60
3.4	Experimental Factors for Phase 2 of the Matched Clad Design	62
3.5	Matched Clad Single Mode Fiber Parameters	63
4.1	Mass Spectrographic Analysis (ppmw) of Synthetic Silica Samples	77
5.1	Fiber core and cladding dopants and recovery parameters.	94
5.2	Fiber core and cladding dopants and recovery parameters sorted by order of recovery kinetics n.	95
5.3	Fiber core and cladding dopants and recovery parameters sorted by half-life of recovery s.	96
5.4	Fiber core and cladding dopants and recovery parameters sorted by initial induced attenuation A_0	97
5.5	Fiber core and cladding dopants and recovery parameters sorted by	

final or permanent induced attenuation A_f	98
6.1 Fiber core and cladding dopants and recovery parameters.	125
7.1 Analyzed and Power Weighted Core and Clad Dopant Concentrations, Draw Conditions, and Radiation Recovery Parameters	154
7.2 Stepwise Multiple Regression of A_0 , All Fibers	155
7.3 Stepwise Multiple Regression of A_0 , Excluding Silica Clad Fibers . .	157
7.4 Stepwise Multiple Regression of A_0 , Ge-F-Doped Silica Clad Fibers . .	160
7.5 Stepwise Multiple Regression of A_0 , P-F-Doped Silica Clad Fibers Only	162
7.6 Stepwise Multiple Regression of A_f , All Fibers	164
7.7 Stepwise Multiple Regression of A_f , Excluding Only Pure Silica Clad Fibers	165
7.8 Stepwise Multiple Regression of A_f , Ge-F-Doped Silica Clad Fibers Only	166
7.9 Stepwise Multiple Regression of A_f , Ge-F-Doped Silica Clad Fibers .	168
7.10 Stepwise Multiple Regression of n , All Fibers	170
7.11 Stepwise Multiple Regression of n , Ge-F-Doped Silica Clad Fibers . .	171
7.12 Stepwise Multiple Regression of τ , All Fibers	172
7.13 Summary of Regression Coefficients for Matched Clad Fibers	173

This page intentionally blank

CHAPTER 1

INTRODUCTION

BACKGROUND

Currently, telephone companies are installing extensive long line lightwave communication systems using single mode fibers as the data and voice transmission medium. Since the commercial telephone network forms the foundation for communication in the event of a national crisis or emergency, additional requirements are placed on the fibers and components being installed, such as unimpaired operation in the event of power loss, sabotage, disruption by natural causes, EMP, or nuclear fallout. One of the most stressing environments that the fiber might experience consists of the initial prompt gamma rays following a nuclear weapons detonation and the fallout subsequent to a nuclear attack. Indeed, it has been well-established that steady state radiation exposures can result in an incremental loss in single mode fibers of at least 0.001 dB/km-rad at 1.3 μm . [1] Since most of the commercially-available single mode fibers have intrinsic losses of 0.5 dB/km at 1.3 μm , a fallout exposure of 10^4 rads will result in at least a 3-fold increase in the optical attenuation of the most radiation-resistant fiber!

There have been extensive previous studies characterizing the behavior of optical fiber waveguides during and subsequent to various radiation exposures, including steady state ^{60}Co , proton and neutron irradiations, pulsed electron, and flash X-rays. [2-4] In general, the radiation response of fiber waveguides has been found to be a complex function of fiber parameters such as core/cladding dopants and profile, system parameters such as operational wavelength and temperature, and radiation parameters such as dose rate and total dose. [3]

Although numerous characterizations of the radiation sensitivity of both single mode and multimode fiber waveguides have been completed,[2-4] these have been carried out primarily on commercial or prototype fibers provided by fiber manufacturers with little or no documentation concerning the fabrication techniques and parameters. Nevertheless, the results have been encouraging. Various dopants such as phosphorus, which was shown to increase the permanent radiation damage in the fibers,[5] have been minimized or eliminated. The radiation hardness of fibers has increased as programs such as the US Army Fiber Optic Transmission System (Long Haul) have driven the vendors to improve their product.

Considering the large amount of fiber to be deployed in commercial telecommunications networks, it becomes an impossible task to individually test and qualify each waveguide. Since there have been virtually no systematic studies quantitatively relating fabrication parameters to radiation-induced loss, it is impossible at this time to correlate the large variation in radiation responses measured for single mode fibers to fabrication parameters, except on a very qualitative basis. Likewise, it is impossible to predict the behavior of an optical fiber in a radiation field or to identify on more than the most rudimentary basis the principal determinants of fiber radiation sensitivity.

PROGRAM

The experimental and analytical studies carried out in this program address the problem of predicting the increase in optical loss in single mode fiber optic waveguides that occurs as a result of exposure to prompt gamma or fallout from nuclear weapons. In principal, the approach is quite straightforward: A number of fiber optic preforms and fibers was fabricated with varying parameters such as core/cladding dopant and profile, deposition

conditions, and draw conditions, and these were tested under identical irradiation conditions. As a result, it has been possible to identify those parameters of fiber design and manufacture that are critical to radiation hardness and to provide them as input to the specification of fibers for lightwave communications systems capable of satisfying the National Security/Emergency Preparedness (NSEP) requirements. The program has also developed a regression algorithm permitting the systems designer to quantitatively predict the incremental loss in a fiber due to radiation exposure using as input a post-manufacturing microprobe analysis of the core/cladding composition and data of the fabrication parameters provided by the manufacturer. A spinoff of the regression analysis is the identification of means for reducing the fiber radiation sensitivity.

RADIATION ENVIRONMENT

In preparation for measuring the radiation response of the single mode fibers fabricated under the program, it was necessary to define a realistic set of test parameters for the NSEP environment. Because of the unavailability of data from sources such as the Defense Nuclear Agency, and because such data was likely to be quite scenario-specific, Reference 6 was used to define a more general set of test parameters. Basically two scenarios have been considered:

- a. Buried cable--the reduction in dose for 3 feet of earth is approximately 0.002-0.004 for initial gamma rays, 0.002-0.010 for initial neutrons, and 0.0002 for fallout (due to the lower energies of the latter). It was assumed that if the cable is outside the plastic zone (R_p in Table 1.1) surrounding the crater, there will be no physical damage due to stress on the cable. A possible source of damage is the thermal energy transmitted from the earth surface to the buried cable

which could ignite and char the polymer jacket and buffer. A calculation of the temperature rise due to the thermal loading has been performed and indicates that the increase in temperature is minimal in spite of the fact that for large-yield weapons, the thermal energy is extremely large, as shown in Table 1.1. Correspondingly, the prompt gamma dose is very high. Nevertheless, the radiation shielding of the earth reduces even the highest dose of 10 Mrads to 40 krad. It may not be realistic to expect the fiber to survive at the edge of the plastic zone; at twice this distance the thermal load is reduced to 1-9 kcal/cm² at the earth surface, and the prompt gamma dose at depth is on the order of 4000 rads.

b. Bridge crossings and surface cable--The major threats here are thermal radiation, which will ignite the cable or its support, and overpressure, which will destroy the supporting structure. Under the assumption of strategic weapons of ≥ 300 kT yield, the prompt gamma doses are ≤ 1800 rads for 20 psi overpressure and ≤ 2000 rads for a thermal load of 200 cal/cm². See Tables 1.2 and 1.3 for a complete compilation. It seems reasonable to assume that higher overpressures or greater thermal radiations would destroy the cable and/or support structure.

It is significant to note that for a given thermal load or overpressure, the prompt gamma dose increases drastically with decreasing weapon yield due to the fact that the distance from ground zero decreases. Although such weapons may be used to sabotage a telecommunications system, a large scale attack of low yield weapons on the continental US seems unlikely. Thus, the prompt threat may be simulated by an exposure in the krad range over a period of 30-60 sec.

Also in this vein, it is important to note that the primary threat to the system may not be the prompt radiation exposure since this is largely a point phenomenon. Connectivity of a system with properly-designed topology would be preserved in spite of the failure of one or more fiber optic links. Rather, the more serious threat appears to be fallout since it would expose a wide area to a high dose. The actual dose that a fiber cable would receive from fallout is difficult to predict due to the likelihood of large numbers of weapons being detonated and the dependence of fallout intensity on weather conditions such as wind and precipitation. However, it should be noted that the largest accumulated fallout dose 96 h following the 15 MT BRAVO test explosion was 7500 rads at a site was near ground zero. On the Rongelap Atoll approximately 100 miles downwind, the total accumulated fallout dose was 6000 rads.

If a fiber cable is strung between poles, it might be thought that the fact that it is raised a certain height above the ground where the fallout particles were accumulating might reduce the dose. However, calculations have been performed that show that this is not the case, and in fact no significant reduction is evident for reasonable fallout contour widths and pole heights. This is a result of the fact that a $1/r^2$ intensity dependence is only valid for point sources.

In the case of both prompt gamma and fallout, the whole fiber length will not be exposed to the maximum doses shown in the Tables, although the dose will be much more uniform in the fallout case. The prompt gamma dose will follow $1/r^2 = 1/(a^2 + b^2)$, where r is the straight-line distance between a point on the fiber and ground zero, a is the perpendicular distance between the fiber and ground zero, and b is the distance from the point to the perpendicular. Thus, the "effective" dose received by a fiber will be less than the peak dose at $b = 0$. An example is shown in Table 1.4 for a 300 kT

weapon detonated 1.15 mi from an unburied fiber; the corresponding peak thermal radiation at the earth's surface is 200 cal/cm^2 , and the maximum overpressure is 11.6 psi for surface burst. Similarly, the fiber transversing a fallout region will be more uniformly irradiated, but the dose will still be nonuniform. For example, in the BRAVO test, the 100 rad dose contour was approximately 65 miles in width, but the dose at the center of this contour increased to >3500 rads.

On the basis of the above analysis, it seemed reasonable to expose the fibers of the present study to a total dose of 2000 rads over a period of approximately 20 sec to simulate the prompt gamma dose, monitoring the growth of the radiation-induced loss during exposure and the recovery following the irradiation. Extrapolations to lower doses would be possible since it is our experience that the growth behavior is nominally linear in the 0-4000 rad range, and most nonlinear behavior occurs at higher doses.[2-4] If saturation occurred at higher doses, the 2000 rad exposure would permit extrapolation of the results, but it would overestimate the induced loss. This laboratory scenario would not mimic the behavior of the cable under fallout since the dose rate would be much less, and substantial recovery would be occurring simultaneously with the darkening. However, the "permanent" induced loss measured 24 h after the laboratory exposure of 2000 rads gives an indication of the response to a fallout exposure of the same dose.[7] Similar to the prompt gamma case, the growth and recovery data of the fiber exposed under these conditions could be used to extrapolate to the fallout case with some fair degree of confidence.

REFERENCES

1. E.J. Friebele, K.J. Long and M.E. Gingerich, Appl. Opt. 22 1754-1757 (1983).
2. E.J. Friebele, Opt. Eng. 18 552-561 (1979).
3. E.J. Friebele, C.G. Askins, M.E. Gingerich, and K.J. Long, Nucl. Inst. Meth. in Phys. Res. B1 355-369 (1984).
4. E.J. Friebele, K.J. Long, C.G. Askins, M.E. Gingerich, M.J. Marrone, and D.L. Griscom, Crit. Rev. Tech.: Opt. Materials in Radiation Environments (SPIE Vol. 541), P. Levy and E.J. Friebele, Ed. (SPIE, Bellingham, WA, 1985), pp. 70-88.
5. E.J. Friebele, P.C. Schultz and M.E. Gingerich, Appl. Opt. 19 2910-2916 (1980).
6. S. Glasstone and P.J. Dolan, The Effects of Nuclear Weapons (US Gov't Printing Office, Washington, DC, 1977).
7. E.J. Friebele, C.G. Askins and M.E. Gingerich, Appl. Opt. 23 4202-4208 (1984).

Table 1.1

Prompt Gamma Dose and Corresponding Thermal Radiation at Various Distances
From The Edge of Plastic Region (R_p)

Yield (kT)	Plastic Region (mi)	Prompt Gamma Dose (rems)			Thermal Radiation (cal/cm ²)		
		@ R_p	@ $2 \cdot R_p$	@ $10 \cdot R_p$	@ R_p	@ $2 \cdot R_p$	@ $10 \cdot R_p$
1	0.035	9.0E+05	2.0E+05	3,000.0	500	100	5
3	0.048	1.5E+06	6.0E+05	2,000.0	1,500	400	8
10	0.068	3.0E+06	1.0E+06	1,000.0	3,000	700	15
30	0.093	6.0E+06	1.0E+06	500.0	4,000	800	30
100	0.140	8.0E+06	1.0E+06	40.0	6,000	1,050	40
300	0.190	1.0E+07	9.0E+05	10.0	10,000	1,900	60
1000	0.275	1.0E+07	8.0E+05	0.2	14,000	3,000	100
3000	0.390	9.0E+06	4.0E+05	0.0	19,000	4,000	170
10000	0.560	5.0E+06	4.0E+05	0.0	30,000	7,000	280
20000	0.690	5.0E+06	4.0E+05	0.0	40,000	9,000	400

Table 1.2

Prompt Gamma Dose and Distance from Ground Zero
Corresponding to Various Thermal Radiations

Yield (kT)	20 cal/cm ²		50 cal/cm ²		100 cal/cm ²		200 cal/cm ²	
	r (mi)	d (rems)	r (mi)	d (rems)	r (mi)	d (rems)	r (mi)	d (rems)
1	0.19	30,000	0.13	100,000	0.10	150,000	0.07	400,000
3	0.32	15,000	0.21	90,000	0.16	150,000	0.12	300,000
10	0.59	2,500	0.39	28,000	0.29	90,000	0.21	250,000
30	1.02	200	0.66	4,000	0.50	30,000	0.32	100,000
100	1.88	2	1.29	300	0.86	3,000	0.63	30,000
300	3.60	0	2.20	3	1.53	100	1.09	10,000
1000	5.90	0	3.90	0	2.75	1	2.00	30
3000	9.80	0	6.60	0	4.80	0	3.40	1
10000	16.50	0	11.90	0	9.10	0	6.70	0
20000	22.50	0	17.00	0	12.70	0	9.40	0

Table 1.3

Distance from Ground Zero and Prompt Gamma Dose for Various Overpressures
Calculated for Optimum Burst Height. For Surface Burst, Overpressure is
Approximately 0.5 Times as Great.

Yield (kT)	2 psi		5 psi		10 psi		20 psi	
	r (mi)	d (rems)	r (mi)	d (rems)	r (mi)	d (rems)	r (mi)	d (rems)
1	0.78	30	0.42	1,000	0.27	10,000	0.17	40,000
3	1.12	5	0.62	500	0.39	5,000	0.25	40,000
10	1.68	0	0.92	120	0.59	2,500	0.37	30,000
30	2.42	0	1.31	25	0.85	1,000	0.54	15,000
100	3.60	0	1.97	2	1.26	150	0.80	7,000
300	5.20	0	2.85	0	1.81	11	1.15	1,800
1000	7.90	0	4.10	0	2.70	0	1.71	200
3000	11.30	0	6.20	0	3.90	0	2.50	25
10000	17.00	0	9.20	0	5.90	0	3.75	
20000	21.50	0	11.70	0	7.50	0	4.70	

Table 1.4

Total Prompt Gamma Dose Received by an Unburied Optical Fiber Cable 1.15 mi
from a Surface Burst of a 300 kT Weapon

Distance from Normal Point (mi)	Dose (Rems)
0.0	1,800
0.1	1,200
0.2	1,000
0.3	800
0.4	500
0.5	400
0.6	300
0.7	250
0.8	200
0.9	150
1.0	100
1.2	90
1.4	40
1.6	30
1.8	20
2.0	15
2.5	7
3.0	3

CHAPTER 2

ORTHOGONAL MATRIX DESIGN AND ANALYSIS

INTRODUCTION

Fabrication of matched clad single mode fibers by the MCVD method involves experimental factors such as core and cladding dopants, oxygen flows during deposition, draw tension, and draw speed. To develop a relationship between these experimental parameters and the resultant radiation response would involve varying each factor among two or more levels. In principle, one could attempt to vary one factor at a time, but this procedure is not always desirable or practical. In the present study, we have chosen 6 factors in which three have three levels and the other three have two levels. The total number of experiments required to establish a relationship between the fabrication parameters involved and radiation response when only one factor is varied at a time is $3^3 \times 2^3 = 216$, which is an intractable problem. If we want to improve experimental error by taking two observations for each combination of fabrication parameters and estimate the effect of the factors using average response, 532 preforms and fibers must be prepared and irradiated! In addition, if interactions between factors are present, the one-factor-at-a-time design often results in misleading conclusions [1].

In this chapter, the procedure of using factorial design of an orthogonal array to reduce the required number of experiments is presented [1-3]. In factorial design experiments, all possible combinations of the levels of each factor are investigated for each complete trial or replication of an experiment. Thus, the method is more efficient than one-factor-at-a-time experiments and obviously less time-consuming. Furthermore, a factorial design is necessary to avoid misleading conclusions when interactions between factors may be present. Finally, factorial designs allow the effects of one factor to be estimated at several levels of other factors, yielding

conclusions that are valid over a wider range of experimental conditions.

FACTORIAL DESIGN OF ORTHOGONAL MATRIX

Factors and Minimum Number of Experiments. To optimize the experimental conditions for determining the relationship between the fiber fabrication parameters and their radiation response, we consider the following factors with their levels in order to select :

A_i = [Ge] in core (no F) $i = 1, 2, 3$

B_i = [Ge] in clad, F to match clad index $i = 1, 2, 3$

C_i = [O₂]/Reagents in core $i = 1, 2$

D_i = [O₂]/Reagents in clad $i = 1, 2$

E_i = Draw tension $i = 1, 2, 3$

F_i = Draw speed $i = 1, 2$

If we were to use a one-factor-at-a-time experiment, $3^3 \times 2^3 = 216$ experiments would be needed to determine the effect of each factor. In the orthogonal array design to be presented in section B, the number of experiments needed to estimate the effect of each factor, including some interactions between two factors, is only 16.

In order to decide the type of orthogonal array to be used among 2^k and 3^k ($k = 2, 3, 4, \dots$) orthogonal arrays, we should estimate the minimum number of experiments required to derive the parameters from our experimental results. Obviously, the absolute minimum number of experiments needed is equal to the number of parameters to be determined.

For an arbitrary factor P with n levels, the degrees of freedom is n-1. The degrees of freedom for the interaction between two factors with levels m and n is (m-1) x (n-1). Since the number of parameters to be determined is the sum of the degrees of freedom of each factor plus 1, the minimum number of experiments required can then be estimated.

In our case, we have three factors at three levels and three factors at two levels. Therefore, if interactions between factors are not present (or are arbitrary suppressed), the minimum number of experiments required is $(2 \times 3) + (1 \times 3) + 1 = 10$. However, if we consider all interactions between two factors and suppress all interactions between three or more factors, the minimum number of experiments needed becomes

$$(2 \times 3) + (1 \times 3) + (4 \times 3) + (2 \times 9) + (1 \times 3) + 1 = 43.$$

Since it takes a considerable amount of time to carry out one experiment (involving the fabrication of an MCVD preform with the proper core and clad dopant levels, drawing an optical fiber, and performing the radiation test), a more reasonable number of experiments is in the range of 10 to 20. Thus the array to be used is a 2^4 orthogonal array which involves 16 experiments (2^3 and 3^2 orthogonal arrays do not have a large enough number of experiments, while the 3^3 array has too many to be practical in this study). Some interactions between two factors can also be studied in this factorial design using an orthogonal array.

Factorial Design of 2^4 Orthogonal Array. A 2^4 orthogonal array [1] is shown in Table 2.1. This array has the property that when the results of the experiments are summed for a given level in any column, all the levels of the other columns are summed with equal frequency, and presumably cancel out (this is a property of orthogonal arrays and hence the name). This orthogonal array can be used for designing experiments to study phenomena involving four two-level factors, including all possible interactions between two, three and four factors. It can also be modified to study phenomena involving factors with three levels. One of these modified designs is shown in Table 2.1, which is obtained from the orthogonal array of Table 2.1 by combining columns 1 and 2 for factor A, columns 3 and 4 for factor B, and columns 7 and 8 for factor E

using the following correspondences for these three-level factors:

(1, 1) --- 1, (2, 1) --- 2, (2, 2) --- 2, (1, 2) --- 3.

This is the factorial design used in our experiments. In addition, some of the interactions between two factors (factors DF, CF, and BC) can also be studied (see section III).

ANALYSIS

Effects of Two-Level Factors. The two-level factors (such as factors C, D, and F which correspond to the columns 5, 6, and 9 of Table 2.1, respectively), can be analyzed for each level by dividing I_i and J_i of Table 2.1 by 8 ($i = 5, 6, \text{ and } 9$). This is possible because the factorial design of Table 2.2 is orthogonal with respect to these two-level factors. That is,

$$C_1 = I_5/8, \quad C_2 = J_5/8$$

$$D_1 = I_6/8, \quad D_2 = J_6/8$$

and

$$F_1 = I_9/8, \quad F_2 = J_9/8.$$

Effects of Three-Level Factors. Since the factorial design of Table 2.2 is not orthogonal with respect to three-level factors (level 2 appears twice as often as levels 1 and 3), simple averaging will not work. However, notice that the sub-arrays of Table 2.2 (which are divided by the dashed line) are orthogonal arrays with respect to the levels of each of the factors in that sub-array. Therefore, the level of each factor can be estimated and compared within each sub-array. For factor A, the values of levels 1 and 2 can be estimated in the upper orthogonal array (corresponding to experiments #1 to #8),

$$A_1 = (R_1 + R_3 + R_6 + R_8)/4, \quad A_2^u = (R_2 + R_4 + R_5 + R_7)/4$$

The values of the levels 2 and 3 of the factor A can also be calculated in this way using the lower array (corresponding to experiments #9 to #16) since

it is likewise orthogonal:

$$A_3 = (R_{10} + R_{12} + R_{13} + R_{15})/4, \quad A_2^d = (R_9 + R_{11} + R_{14} + R_{16})/4.$$

Notice that

$$A_2 = J_A/8 = (A_2^u + A_2^d)/2 = A_2^u + (A_2^d - A_2^u)/2 = A_2^d - (A_2^d - A_2^u)/2.$$

The effect of the levels 1 and 2 can also be estimated by comparing

$$A_1 + (A_2^d - A_2^u)/2$$

and

$$A_2^u + (A_2^d - A_2^u)/2 = A_2.$$

Similarly, for levels 2 and 3, we can compare

$$A_2^d - (A_2^d - A_2^u)/2 = A_2$$

and

$$A_3 - (A_2^d - A_2^u)/2.$$

Thus, the values of the three levels of factor A can be estimated by comparing

$$A_1 + W_A, \quad A_2 = J_A/8, \quad \text{and} \quad A_3 - W_A$$

where

$$W_A = (A_2^d - A_2^u)/2.$$

In the same way, the values of the three levels of factors B and E can be estimated by comparing

$$B_1 + W_B, \quad B_2 = J_B/8, \quad B_3 - W_B$$

for factor B, and

$$E_1 + W_E, \quad E_2 = J_E/8, \quad E_3 - W_E$$

for factor E,

where

$$B_1 = (R_1 + R_2 + R_5 + R_6)/4,$$

$$B_3 = (R_{11} + R_{12} + R_{15} + R_{16})/4,$$

$$W_B = (R_9 + R_{10} + R_{13} + R_{14} - R_3 - R_4 - R_7 - R_8)/8$$

$$E_1 = (R_1 + R_2 + R_7 + R_8)/4$$

$$E_3 = (R_{11} + R_{12} + R_{13} + R_{14})/4$$

and

$$W_E = (R_9 + R_{10} + R_{15} + R_{16} - R_3 - R_4 - R_5 - R_6)/8.$$

Effects of Interactions between Two Factors. The value of the levels of column DF in Table 2.2 (corresponding to column 10 in Table 2.1) is

$$\begin{aligned} DF_1 - DF_2 &= I_{10} - J_{10} \\ &= (R_1 + R_2 + R_3 + R_4 + R_9 + R_{10} + R_{11} + R_{12})/8 - \\ &\quad (R_5 + R_6 + R_7 + R_8 + R_{13} + R_{14} + R_{15} + R_{16})/8 \\ &= \{(R_2 + R_3 + R_{10} + R_{11})/4 - (R_1 + R_4 + R_9 + R_{12}) \\ &\quad - [(R_6 + R_7 + R_{14} + R_{15})/4 - (R_1 + R_4 + R_9 + R_{12})/4] \\ &\quad - [(R_5 + R_8 + R_{13} + R_{16})/4 - (R_1 + R_4 + R_9 + R_{12})/4]\}/2 \\ &= \{DF_{22} - DF_{11} - [DF_{21} - DF_{11}] - [DF_{12} - DF_{11}]\}/2 \end{aligned}$$

where DF_{ij} is the average of results when factor D is at level i and factor F at level j. This last expression states that the difference between levels 1 and 2 of the column DF is the difference when both factors are varied minus those when one factor is varied at a time. That is, the value of the levels of the column DF is the interaction between factors D and F. Similar conclusions can be obtained for columns CF and BC.

Statistical Analysis. We have so far obtained the value of each factor and some interactions between two factors. How much confidence do we have on these values? To answer this kind of question, statistical analysis should be carried out.

The variance of column i, V_i , in Table 2.1 is

$$V_i = 8 \times (I_i/8 - R)^2 + 8 \times (J_i/8 - R)^2 = (I_i - J_i)^2/16$$

where R is the mean value of the results of all the 16 experiments with $f_i = 15$ degrees of freedom. We have for the two-level factors,

$$V_C = (I_5 - J_5)^2/16, \quad V_D = (I_6 - J_6)^2/16, \quad V_F = (I_9 - J_9)^2/16$$

$$V_{DF} = (I_{10} - J_{10})^2/16, \quad \text{and} \quad V_{CF} = (I_{11} - J_{11})^2/16,$$

with degrees of freedom = 1. Since the three-level factors are the combinations of two-level columns, their variances are the sums of the corresponding columns [1]. That is,

$$V_A = V_1 + V_2, \quad V_B = V_3 + V_4, \quad V_E = V_7 + V_8, \quad \text{and} \quad V_{BC} = V_{12} + V_{13},$$

with degrees of freedom = 2.

The total variance of these 16 experiments with 15 degrees of freedom is the sum of the variances of each specified factor plus the random error. Among these, we have assigned two degrees of freedom for factors A, B, E and BC, and one degree of freedom for factors C, D, F, DF and CF. Two degrees of freedom are left, which must be associated with the two unspecified columns 15 and 16. Therefore, the variance of the random error, V_e , must be the sum of the variances of columns 15 and 16 with $f_e = 2$ degrees of freedom. That is,

$$V_e = V_{15} + V_{16}.$$

The significance of each factor can then be estimated using an F distribution [1]. The standard variation S_i of factor i with variance V_i and degrees of freedom f_i is

$$S_i = V_i/f_i.$$

The standard variation of the random error S_e is

$$S_e = V_e/f_e.$$

Let the ratio of the standard variation of factor i to that of random error be F_0 . If $F_0 > F_a(f_i, f_e)$ (F-distribution with numerator f_i degrees of freedom, denominator f_e degrees of freedom and percentage point a [1]), then the percentage confidence for concluding factor i has significant effect is $100\% - a$.

IMPLEMENTATION TO MODELLING RADIATION RESPONSE OF OPTICAL FIBERS

As described in the preceeding sections, the orthogonal matrix analysis (OMA) permits an experimental design where several of the considered manufacturing set points change with each experiment in a carefully chosen manner, thereby minimizing the total number of required experiments. A few correctly formulated samples are capable of registering the effects of discrete changes in all the variables. The output of the matrix is a set of instantaneous (or point) solutions of each parameter's function. However, these solutions are offset by the constant average of the contributions of all the other parameters. There are only as many point solutions of a variable as there are discrete levels entered in the matrix. If the number of point solutions is small, only the low order components of the function can be extracted with certainty over the experimental range of the variable.

Assessment of the Method. The intrinsic characteristics of the matrix method combine with details of the data being processed to determine the significance of the results. A complete expression of the model would include both independent (single-variable) terms and interdependent (multi-variable, interactive) terms, each with components ranging from linear to higher orders. While a matrix with low sampling density is best-suited to detect linear or low-order dependencies, the presence of other dependencies can influence the indicated forms of the variables. If the matrix is not designed to address interactions between specific variables, an assessment of sensitivity to such cross terms should be considered. Finally, imprecision in the experimental method and finite signal-to-noise in measurements alter the assumptions of the orthogonal matrix analysis method.

Simulation. To investigate the impact of the preceeding observations on the

validity of the analysis method, a simulation of the matrix employed in this project was carried out through a computer spread-sheet program. The dimensions and internal structure of the experimental matrix were replicated, and a set of generic functions was substituted for the unknown forms of the six variables of the first matrix (Table 2.3). The postulated functions, which have no relevance outside the context of this simulation, were:

$$f(A) = x \exp[(A - 3)/y] - z \quad (2.1)$$

$$f(B) = 2 \exp[(B - 3)/20] - 0.3 \exp[-(0.2B)/2] + 1 \quad (2.2)$$

$$f(C) = 2 |C - 2| \quad (2.3)$$

$$f(D) = 2 |D - 1.5| \quad (2.4)$$

$$f(E) = 6 \{1 - \exp[-(E - 20)/30]\} \quad (2.5)$$

$$f(F) = \exp[-F + 0.5]. \quad (2.6)$$

The selected functions serve merely to test the ability of the matrix analysis method to successfully extract several classes of functions. Included are functions with minima appearing within the range of the variable (functions C and D), a nearly linear curve with slight positive curvature (functions A and B), a rapidly decaying exponential (F), and a slowly decreasing function of positive curvature (E). In addition, cross terms of $A \times C$ and $B \times D$ represent interactions not specifically considered by the matrix.

Experimental imprecision is included by randomly offsetting the input levels of each parameter over a range. This would correspond to variations of a parameter from its design setpoint; in the simulation some attempt has been made to reflect the actual range encountered during the production of the fiber samples in this study. Inclusion of this modification in the simulation results is referred to as "levels error".

The third modifier to the matrix is an error range in the results column. This would correspond to signal-to-noise limitations in the measured radiation response of each of the samples and is referred to as "instrument error."

Again, this modifier is introduced as a random offset from the values of the results. The amplitude of this "error" was set at 1 dB/km, a figure well above the actual accuracy of a typical measurement of <0.2 dB/km.

This simulation was conducted simultaneously with many of the actual irradiation measurements. Before the final version of the simulation was implemented, an attempt was made to scale the pseudo-functions of the model to approximate the observed radiation responses. While this adjustment was largely subjective, it is felt that an improvement in the fidelity of the simulation was effected.

With the simulator it was possible to isolate origins of discrepancies between the hypothetical functions of the parameters (equations 2.1-2.6) and the extracted forms. A fully successful "analysis" simulation would be one in which the extracted point solutions exactly overlay the known function for that variable. Figure 2.1 illustrates the method of graphically fitting a set of point solutions derived from a matrix analysis with a "best fit" curve. The horizontal coordinate is the range of the parameter, and the vertical axis is the response of the experiment to the range of the variable. In this example, the setting for parameter N would have ranged over five discrete levels through the course of the experiment. The matrix would yield five point solutions which are then plotted in the figure at their respective range settings. If the plotted curve were the true function of the parameter (i.e., the radiation response of the fiber as a function of N), then a perfect analysis would place all the pairs on the curve.

An important feature of orthogonal matrix analysis is depicted in the first simulation results shown in Figs. 2.2 and 2.3: the point solutions for a parameter have a valid vertical displacement ("calculated effect" in the figures), only in relation to each other. The difference between Figs. 2.2 and 2.3 is that the extracted point solutions in Fig. 2.3 are offset such that

the left-most data point is made to align with the hypothesized curve. As suggested above, the relative offset is equal to the average contribution of the remainder of the parameters. A fundamental assumption of OMA is that each level of the considered parameter in the matrix appear against every level of each of the others. In this manner, the average contribution of the other parameters is the same for all levels of the considered parameter. This average will then appear as a constant offset with each point solution of the considered parameter. The vertical position of the set of point solutions is, then, arbitrary. Formulations of how each of the point solutions are derived from the result column of the matrix are listed in Table 2.4

Simulation Results. The initial demonstration of the matrix was to perform an extraction of the various functions in the absence of any of the modifying conditions such as noise on the levels or responses. The levels errors, measurement errors and cross terms were all set to zero, and the fits of the point solutions vs. the corresponding functions were plotted in Figs. 2.3-2.6. In all cases, the fits were numerically exact.

The method for indicating the responses to both levels and measurement errors is to repeat the analysis 30 times as the error inputs are allowed to vary randomly. The nature of the actual experiment precludes multiple repetitions for the purpose of minimizing the adverse effects of levels error. Because of this, a simulation at any of the random levels of error gives a result which is as valid as that for any other level. The plotted simulation results show the maximum (diamonds), minimum (pluses), and mean (triangles) values of all simulated analyses for each point solution. The separation of the maxima and minima defines the resolution of the matrix point solutions. A somewhat different situation exists for the role of measurement errors-- while it is impractical to fabricate numerous preforms and fibers, it is at least

marginally practical to repeat the irradiation measurements to improve precision. For this simulation, a worst case situation of only one measurement will be assumed, however.

Fig. 2.7 indicates the reduced certainty of fitting two points on the curve of hypothetical function C in the presence of levels error. The vertical axis corresponds to the additional dB/km induced by radiation due to the various levels of C. Note how poorly two-point solutions define the shape of function C. Figure 2.8 is the corresponding plot addressing measurement errors, and Figure 2.9 is the cumulative effect of the two. A visual comparison of the two separate effects with their composite indicates that the two are not additive, but that one can dominate the other, rendering the smaller effect insignificant.

Cross-term interactions were included in the simulation for parameters $A \times C$ and $B \times D$. The response of parameters to the inclusion of such interactions may be expected to reflect whether the considered parameter is one with cross relations. The cross function of $A \times C$ vs. A is plotted in Figure 2.10 for six discrete levels of C. Figure 2.11 demonstrates the potentially dramatic influence of interactions when extracting the independent form of the variable. Finally the total effect of measurement noise, levels error and cross term influence on the point solutions is compared to the independent function of C (Fig. 2.12). Note that the range of the extracted values no longer includes the parent function. This is primarily the result of strong cross interactions not considered in the design of the matrix.

In light of the strong effect of cross terms on the extraction of parameter C, Figure 2.13 emphasizes the relative immunity of parameter E to the presence of $A \times C$ and $B \times D$. In Figure 2.14, there is no visible distortion of the solutions for F from the cross terms. Thus, the extraction of a parameter which does not appear in cross terms may be relatively unaffected by

cross terms in other parameters.

The amplitude of a given parameter relative to its noise modifiers will determine the signal-to-noise of the extracted solutions. Figures 2.15 and 2.16 are representations of the precision of the point solutions for A at two different amplitudes of the function of A. In both figures, levels and measurement noise and cross-term contributions are held constant. In agreement with intuition, a strong function of a parameter is more easily and more accurately detected than a weak function.

Level and/or measurement errors in one parameter will influence the successful extraction of another, particularly if the "noisy" parameter has a large magnitude relative to the second parameter. Function F and its point solutions are plotted in Figs. 2.17 and 2.18 for the amplitudes of A shown in Figs. 2.15 and 2.16 respectively. When the vertical range of A is 1.8 (Fig. 2.15) a dependency on F is apparent even in the worst case (Fig. 2.17). For a response to A ranging over 30 units, F cannot be detected for almost half of the tested cases. This type of interference can be exacerbated for parameter solutions strongly influenced by a cross term with A (i.e., C due to $A \times C$).

There may be cases where the function of a parameter is so small as to be undetectable as a result of even small amplitudes of any of the modifying effects. Parameter B is plotted in Figure 2.19 with the range of the solutions broadened by all of the effects. The postulated function of B gives a theoretical deflection of only approximately 0.4 units, a level overcome by any one of the effects individually. Such a parameter would be insignificant relative to the other parameters addressed, and serves to recognize that there is a finite limit to the sensitivity of the OMA technique. It is unlikely, however, that such a parameter would be reliably detected by any method not intended to specifically address its presence. Such a parameter would not be a significant determinant of radiation response.

Conclusions. The simulation of our experimental design has served to prove the fundamental ability of the OMA technique to fit functions of the several input parameters. The inclusion of modifiers to the input data reflecting experimental uncertainty indicates a reduction in the resolution of the extracted functions. Limited density in the number of input levels constrains the description of the functional forms to their low order components. Interactions between parameters are resolvable only if the matrix design includes such cases.

Judging by the apparent range of responses of the actual experimental fiber samples to irradiation, a number of functions will be detectable. Strong functions will be resolvable with only a minor degradation of the fit due to error contributions. Smaller terms may be detected, but with reduced certainty of their form.

Additional applications of OMA may better resolve specific terms through more specific matrices. A similar approach should permit elucidation of cross terms and higher order components missed by the experimental survey.

MULTIPLE REGRESSION

The advantages and characterization of the orthogonal matrix analysis technique have been described in the preceding sections. However, there are several drawbacks which impact the current study. Perhaps the most severe is that it is virtually impossible to fabricate a series of preforms where the core and/or clad dopant concentrations are held to precise levels. Although the MCVD process is capable of fabricating preforms in production where the dopant concentrations are maintained at constant, optimized levels, the nature of this study requires wide variations in process parameters. These in turn affect deposition conditions, and as a result, considerable variations in

dopant concentrations within a given level are found. If the concentration of a certain dopant is a major determinant of radiation response, it is improper to ignore these within-level variations in the analysis.

The very nature of the OMA method results in another drawback--derivation of the values of a factor at a given level depends on the cancellation of contributions from other factors. Thus, a large number of different cases, each weighted approximately equally, is required. If there are anomalous cases where either the fabrication parameters or radiation response results are deviant, the whole matrix analysis can be skewed.

Finally, it is difficult to derive a predictive equation from OMA because of the background offset in the results of a factor due to the averaged contributions of all the other factors. It would be necessary to fabricate a fiber with parameters chosen from the minima of all factors and then to use its response as an anchor by which to scale the data. If there were an error in the fabrication or measurement of this "anchor" fiber, all the subsequent predicted results would be erroneous.

To circumvent these problems, we have performed multiple regression analyses on the data, using the fabrication parameters such as core [Ge], clad [Ge], core oxygen-to-reagent ratio, clad oxygen-to-reagent ratio, draw tension and draw speed as predictors and the resultant radiation response as the dependent variable. The analyses were performed on an IBM-compatible AST Premium 286 desktop computer using the SPSS-PC+ code.

The results of the orthogonal matrix analyses of the data were used to test the validity of the assumption of multiple regression that the radiation response depended linearly on each factor. If this was not the case, the data were transformed to quasi-linear behavior using procedures such as exponentiation. Both the OMA and multiple regression analysis determined that certain factors were more influential in determining radiation response than

others. The correspondence of the results of the two techniques was used as a test to further strengthen the confidence in the predictive capability of the regression.

Of course, it was recognized that the statistical significance of the regression might not be great due to the very limited sample sizes of 16 and 8 for the P-free and P-doped fibers. Although it was tempting from a physical standpoint to include all factors in the regression analysis in order to determine the dependence of the radiation response on each one, the predictive capability of this procedure is severely degraded. Inclusion of a large number of factors improved the quality of the fit to the data since the number of factors (6) was close to the number of data points (16 or 8).

Indeed, if the number of factors and data points are equal, a perfect fit to the set of experimental data can be obtained. However, the confidence in the predictive capability is minimal in this case, so stepwise regression was used. Here, the factors are included in the regression equation one at a time. The first variable selected is the one with the largest correlation with the dependent variable, and it is included if the probability of an F-test of its regression coefficient is less than a certain value. The second variable is added based on the highest partial correlation. After each step the variables in the equation are examined to determine if the probability of an F-test of their regression coefficient is greater than a certain criterion, and if so, they are removed from the equation. This procedure continues until no more variables meet the entry and removal criteria. The quality of the resultant regression equation depends on the quality of the data, of course, but the significance of its predictive capability will be greater than in the case where all factors were included.

REFERENCES

1. D.C. Montgomery, "Design and Analysis of Experiments," 2nd Ed., John Wiley & Sons, New York (1984).
2. B.L. Raktoe, A. Hedayat and W. T. Federer, "Factorial Designs," John Wiley & Sons, New York (1981).
3. P.W.M. John, "Statistical Design and Analysis of Experiments," T h e Macmillan Company, New York (1971).
4. M.J. Norusis, "Introductory Statistics Guide," SPSS, Inc., Chicago (1983).

Table 2.1. 2^4 Orthogonal Array

	A		B		C	D	E		F	DF	CF	BC				
n	1	2	3	4	5	6	7	8	9	10	11	12	13	14	15	R
1	1	1	1	1	1	1	1	1	1	1	1	1	1	1	1	R ₁
2	2	1	1	1	2	2	1	1	2	1	1	2	2	2	2	R ₂
3	1	1	2	2	2	2	2	2	2	1	1	1	1	2	1	R ₃
4	2	1	2	2	1	1	2	2	1	1	1	2	2	1	2	R ₄
5	2	1	1	1	1	1	2	2	2	2	2	1	1	2	2	R ₅
6	1	1	1	1	2	2	2	2	1	2	2	2	2	2	1	R ₆
7	2	1	2	2	2	2	1	1	1	2	2	1	1	1	2	R ₇
8	1	1	2	2	1	1	1	1	2	2	2	2	2	2	1	R ₈
9	2	2	2	1	2	1	2	1	1	1	2	2	1	2	1	R ₉
10	1	2	2	1	1	2	1	2	1	1	2	1	2	1	2	R ₁₀
11	2	2	1	2	1	2	1	2	2	1	2	2	2	2	2	R ₁₁
12	1	2	1	2	2	1	1	2	1	1	2	1	2	2	2	R ₁₂
13	1	2	2	1	2	1	1	2	2	2	1	2	1	1	2	R ₁₃
14	2	2	2	1	1	2	1	2	1	2	1	1	2	2	1	R ₁₄
15	1	2	1	2	1	2	2	1	1	2	1	2	1	2	2	R ₁₅
16	2	2	1	2	2	1	2	1	2	2	1	1	2	1	1	R ₁₆

I_i I_1 I_2 I_3 I_4 I_5 I_6 I_7 I_8 I_9 I_{10} I_{11} I_{12} I_{13} I_{14} I_{15}

J_i J_1 J_2 J_3 J_4 J_5 J_6 J_7 J_8 J_9 J_{10} J_{11} J_{12} J_{13} J_{14} J_{15}

* I_i and J_i are the sum of the result R_j of experiments #j corresponding to level 1 and level 2, respectively, of factor i.

Table 2.2. Factorial Design for $3^3 \times 2^3$ Using Table 2.1

n	A	B	C	D	E	F	DF	CF	BC	14	15	Result
1	1	1	1	1	1	1	1	1	1	1	1	R ₁
2	2	1	2	2	1	2	1	1	2	2	2	R ₂
3	1	2	2	2	2	2	1	1	1	2	1	R ₃
4	2	2	1	1	2	1	1	1	2	1	2	R ₄
5	2	1	1	1	2	2	2	2	1	2	2	R ₅
6	1	1	2	2	2	1	2	2	2	1	1	R ₆
7	2	2	2	2	1	1	2	2	1	1	2	R ₇
8	1	2	1	1	1	2	2	2	2	2	1	R ₈

9	2	2	2	1	2	1	1	2	2	2	1	R ₉
10	3	2	1	2	2	2	1	2	3	1	2	R ₁₀
11	2	3	1	2	3	2	1	2	2	1	1	R ₁₁
12	3	3	2	1	3	1	1	2	3	2	2	R ₁₂
13	3	2	2	1	3	2	2	1	2	1	2	R ₁₃
14	2	2	1	2	3	1	2	1	3	2	1	R ₁₄
15	3	3	1	2	2	1	2	1	2	2	2	R ₁₅
16	2	3	2	1	2	2	2	1	3	1	1	R ₁₆

Table 2.3

Experimental Factors for Phase 1 of the Matched Clad Design

A_i = [Ge] in Core (no F)	$i = 1, 2, 3$
B_i = [Ge] in Clad, F to Match Clad	$i = 1, 2, 3$
C_i = Stoichiometry in Core	$i = 1, 2$
D_i = Stoichiometry in Clad	$i = 1, 2$
E_i = Draw Tension	$i = 1, 2, 3$
F_i = Draw Speed	$i = 1, 2$

Experimental Design Table for 6 Factors

n	A	B	C	D	E	F	R _i
1	1	1	1	1	1	1	R1
2	2	1	2	2	1	2	R2
3	1	2	2	2	2	2	R3
4	2	2	1	1	2	1	R4
5	2	1	1	1	2	2	R5
6	1	1	2	2	2	1	R6
7	2	2	2	2	1	1	R7
8	1	2	1	1	1	2	R8
9	2	2	2	1	2	1	R9
10	3	2	1	2	2	2	R10
11	2	3	1	2	3	2	R11
12	3	3	2	1	3	1	R12
13	3	2	2	1	3	2	R13
14	2	2	1	2	3	1	R14
15	3	3	1	2	2	1	R15
16	2	3	2	1	2	2	R16

Table 2.4

Determination of the Significance of Each Control Parameter

$$\bar{A}_1 = 1/4 (R_1 + R_3 + R_6 + R_8) + W_A$$

$$\bar{A}_2 = 1/8 (R_2 + R_4 + R_5 + R_7 + R_9 + R_{11} + R_{14} + R_{16})$$

$$\bar{A}_3 = 1/4 (R_{10} + R_{12} + R_{13} + R_{15}) - W_A$$

$$W_A = 1/8 (R_9 + R_{11} + R_{14} + R_{16} - R_2 - R_4 - R_5 - R_7)$$

$$B_1 = 1/4 (R_1 + R_2 + R_5 + R_6) + W_B$$

$$B_2 = 1/8 (R_3 + R_4 + R_7 + R_8 + R_9 + R_{10} + R_{13} + R_{14})$$

$$B_3 = 1/4 (R_{11} + R_{12} + R_{15} + R_{16}) - W_B$$

$$W_B = 1/8 (R_9 + R_{10} + R_{13} + R_{14} - R_3 - R_4 - R_7 - R_8)$$

$$C_1 = 1/8 (R_1 + R_4 + R_5 + R_8 + R_{10} + R_{11} + R_{14} + R_{15})$$

$$C_2 = 1/8 (R_2 + R_3 + R_6 + R_7 + R_9 + R_{12} + R_{13} + R_{16})$$

$$D_1 = 1/8 (R_1 + R_4 + R_5 + R_8 + R_9 + R_{12} + R_{13} + R_{16})$$

$$D_2 = 1/8 (R_2 + R_3 + R_6 + R_7 + R_{10} + R_{11} + R_{14} + R_{15})$$

$$E_1 = 1/4 (R_1 + R_2 + R_7 + R_8) + W_E$$

$$E_2 = 1/8 (R_3 + R_4 + R_5 + R_6 + R_9 + R_{10} + R_{15} + R_{16})$$

$$E_3 = 1/4 (R_{11} + R_{12} + R_{13} + R_{14}) - W_E$$

$$W_E = 1/8 (R_9 + R_{10} + R_{15} + R_{16} - R_3 - R_4 - R_5 - R_6)$$

$$F_1 = 1/8 (R_1 + R_4 + R_6 + R_7 + R_9 + R_{12} + R_{14} + R_{15})$$

$$F_2 = 1/8 (R_2 + R_3 + R_5 + R_8 + R_{10} + R_{11} + R_{13} + R_{16})$$

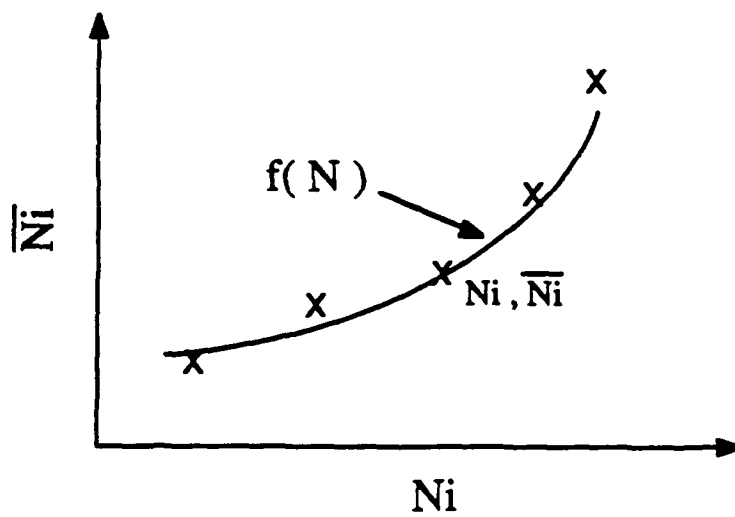


Figure 2.1 Derivation of a function $f(N)$ by a graphic fit to 5 extracted point solutions for parameter N .

E, No Offset

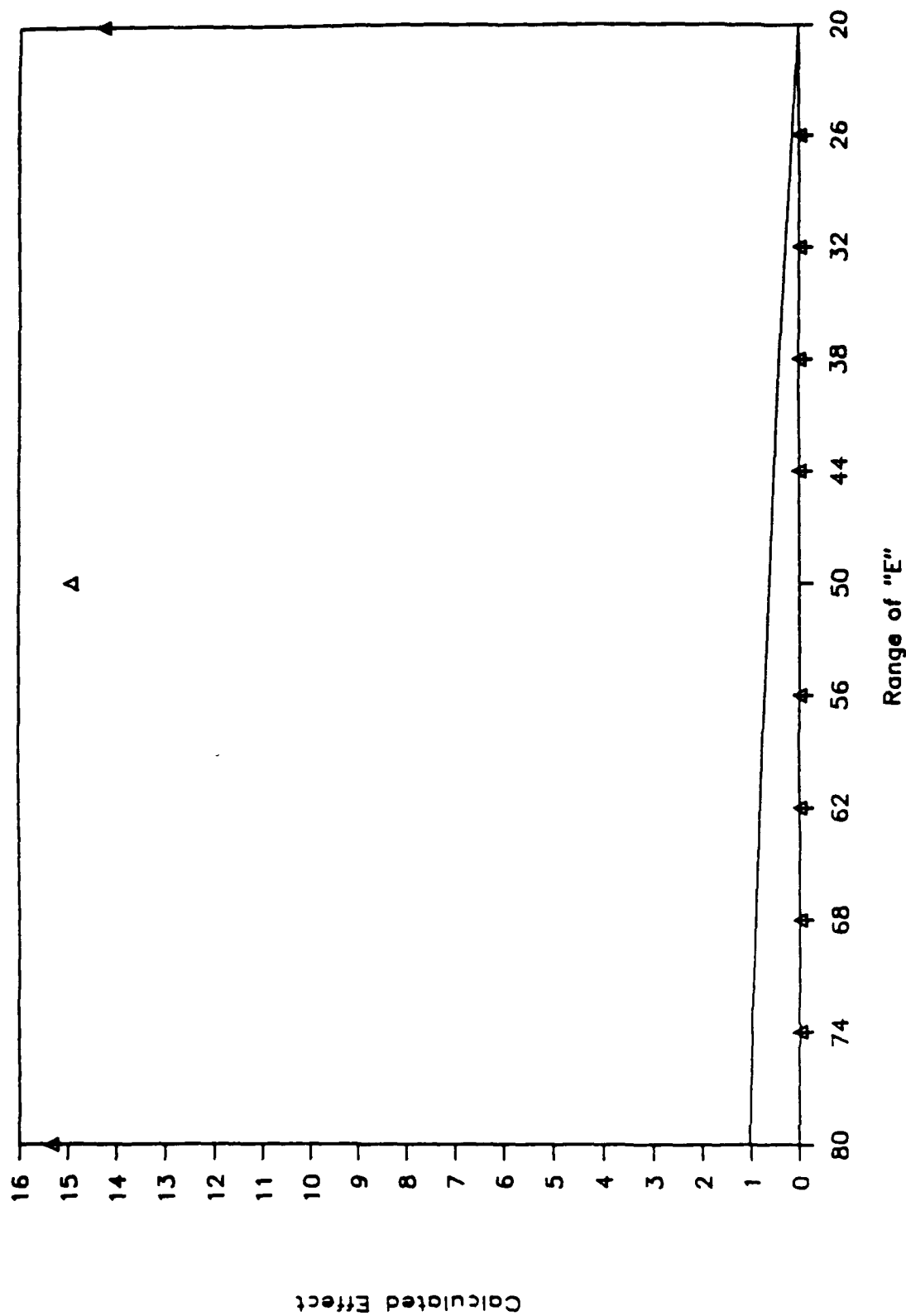


Figure 2.2 Extracted point solutions for a function of parameter E, plotted with the pseudo-function of E.

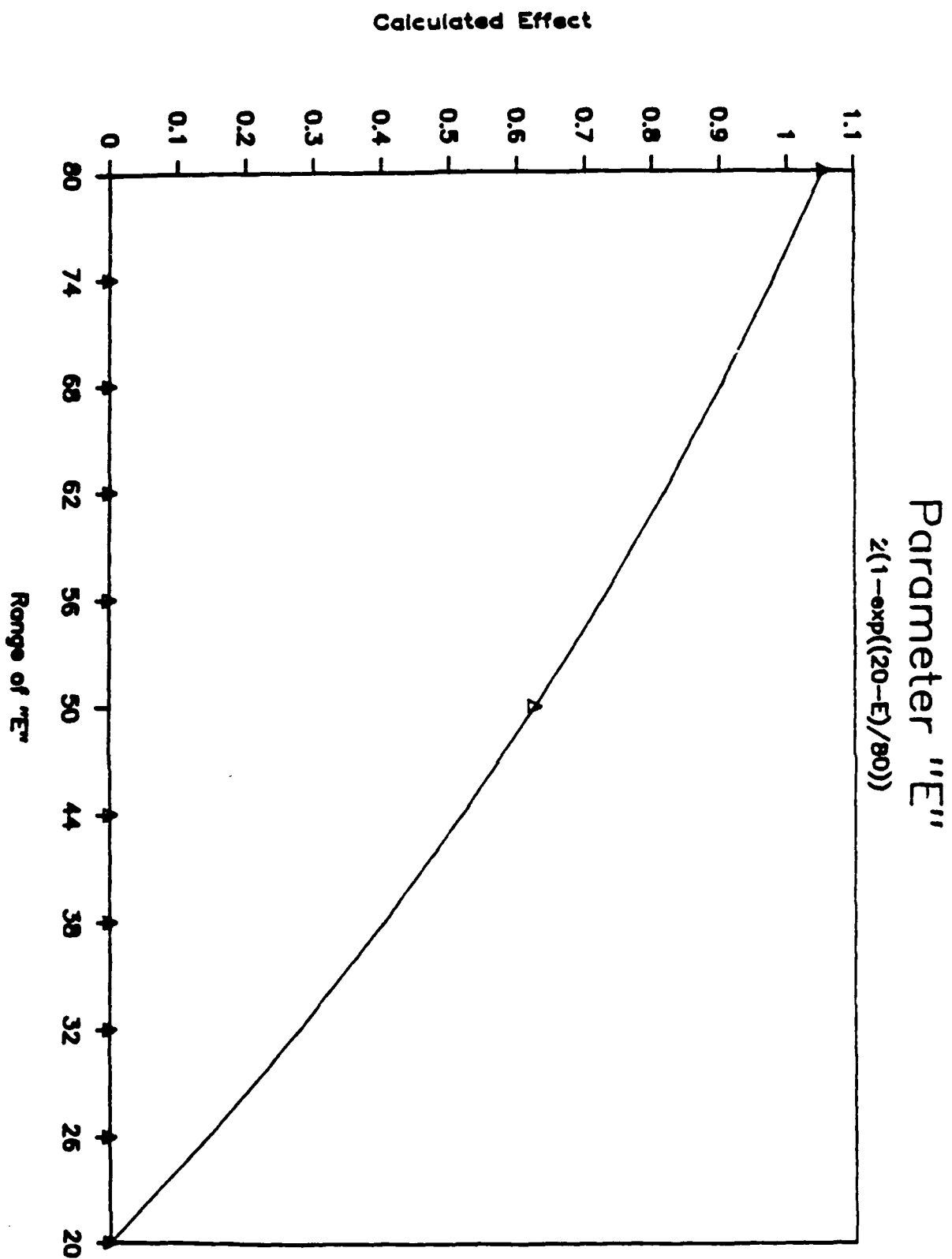
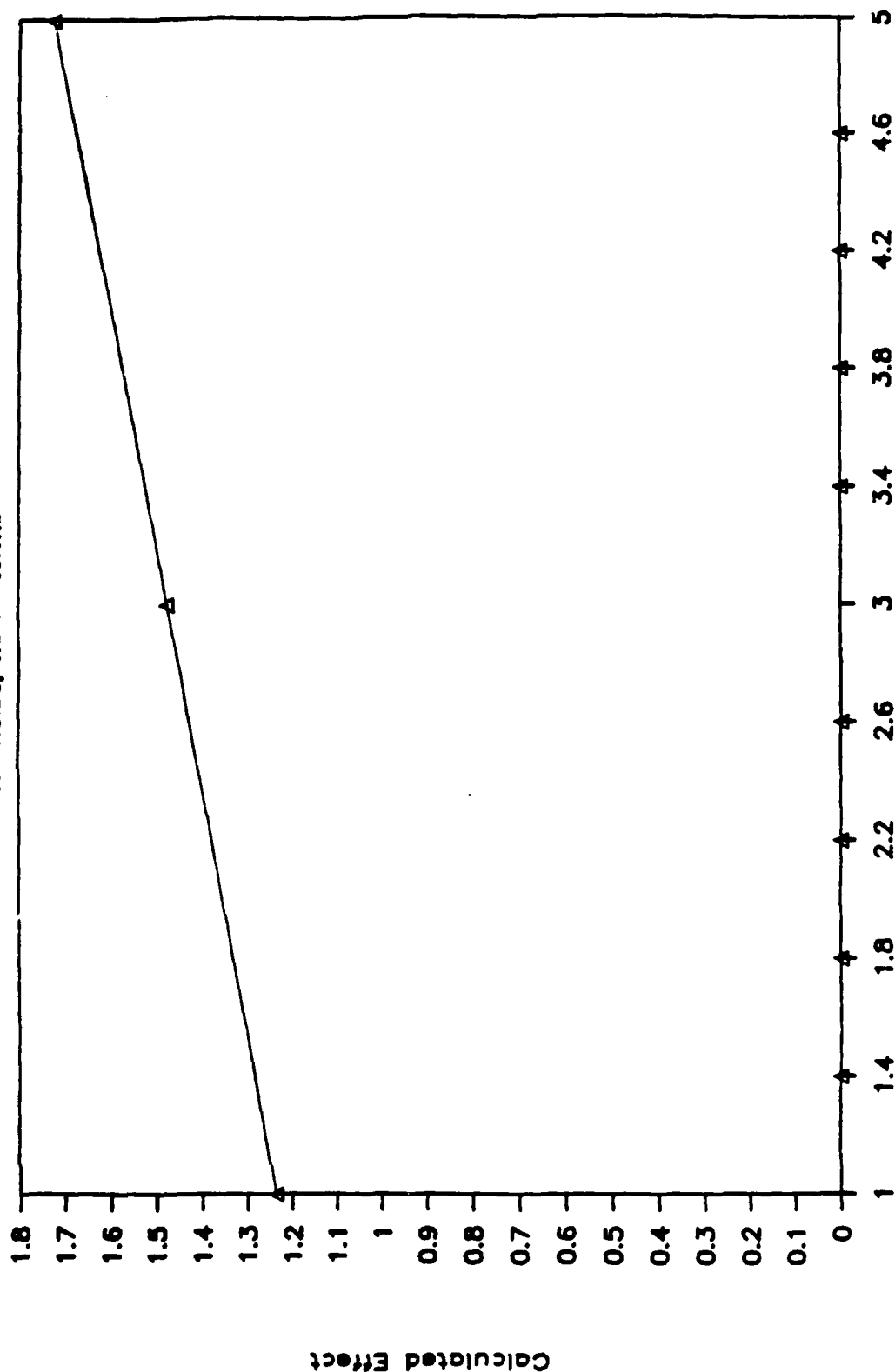


Figure 2.3 Extracted solutions for parameter E offset to align first point with pseudo-function.

Parameter "B"

No noise, no X-terms



Range of "B"

Figure 2.4 Extracted solutions and function for parameter B.

F

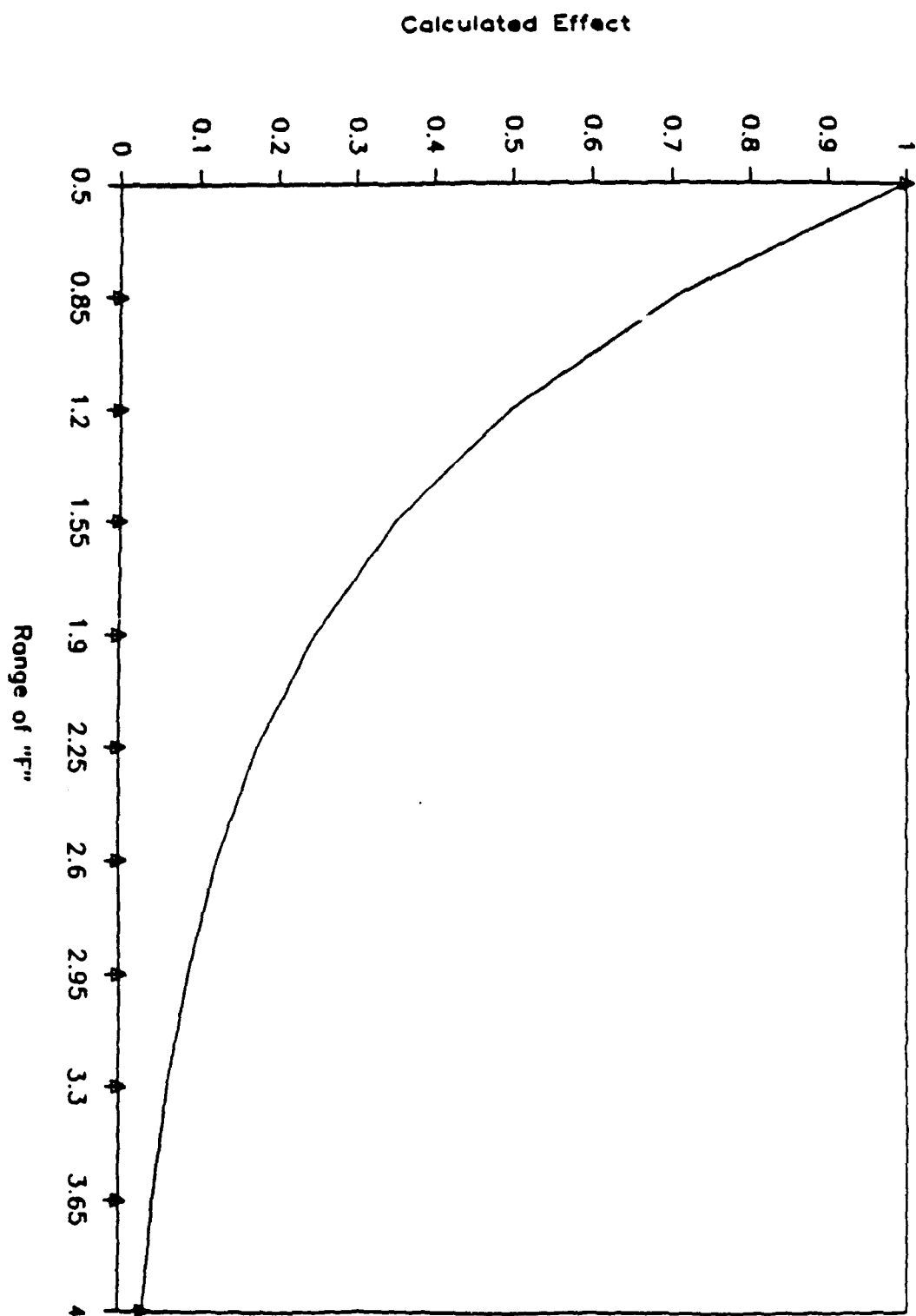


figure 2.5 Extracted solutions and function for parameter F.

Parameter "C" Noise OFF, X-Terms OFF

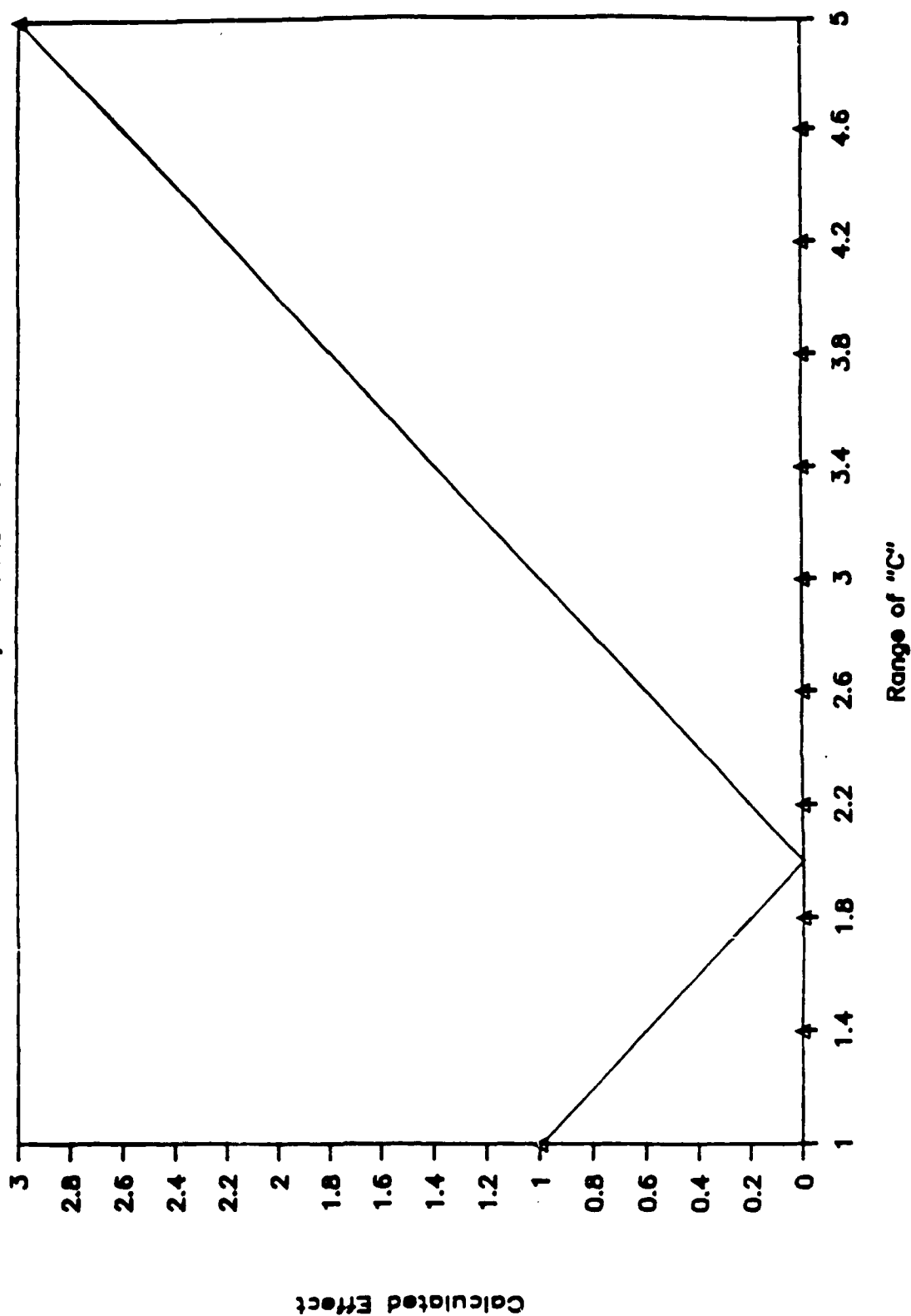


Figure 2.6 Extracted solutions and function for parameter C.

C, Level Error

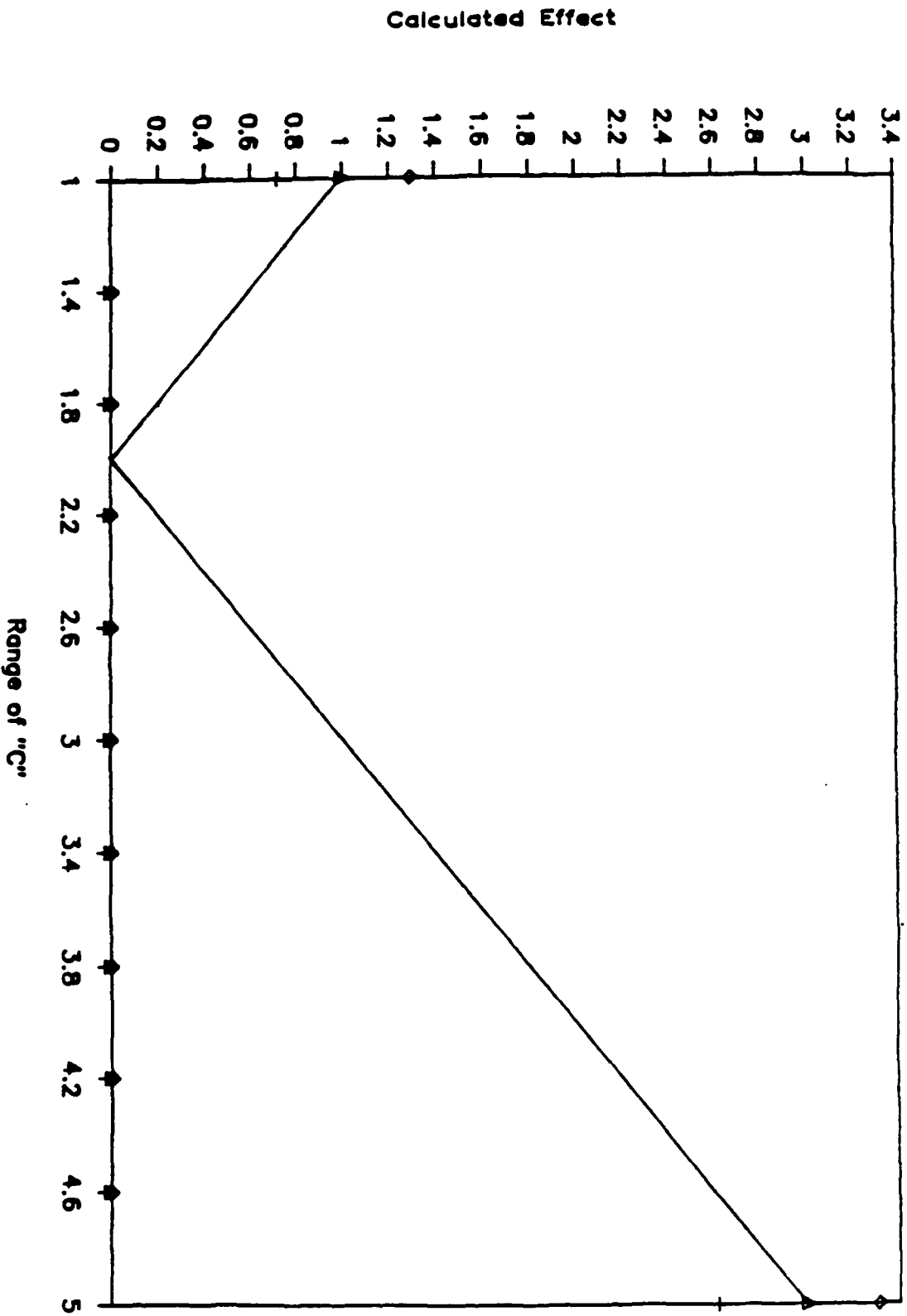
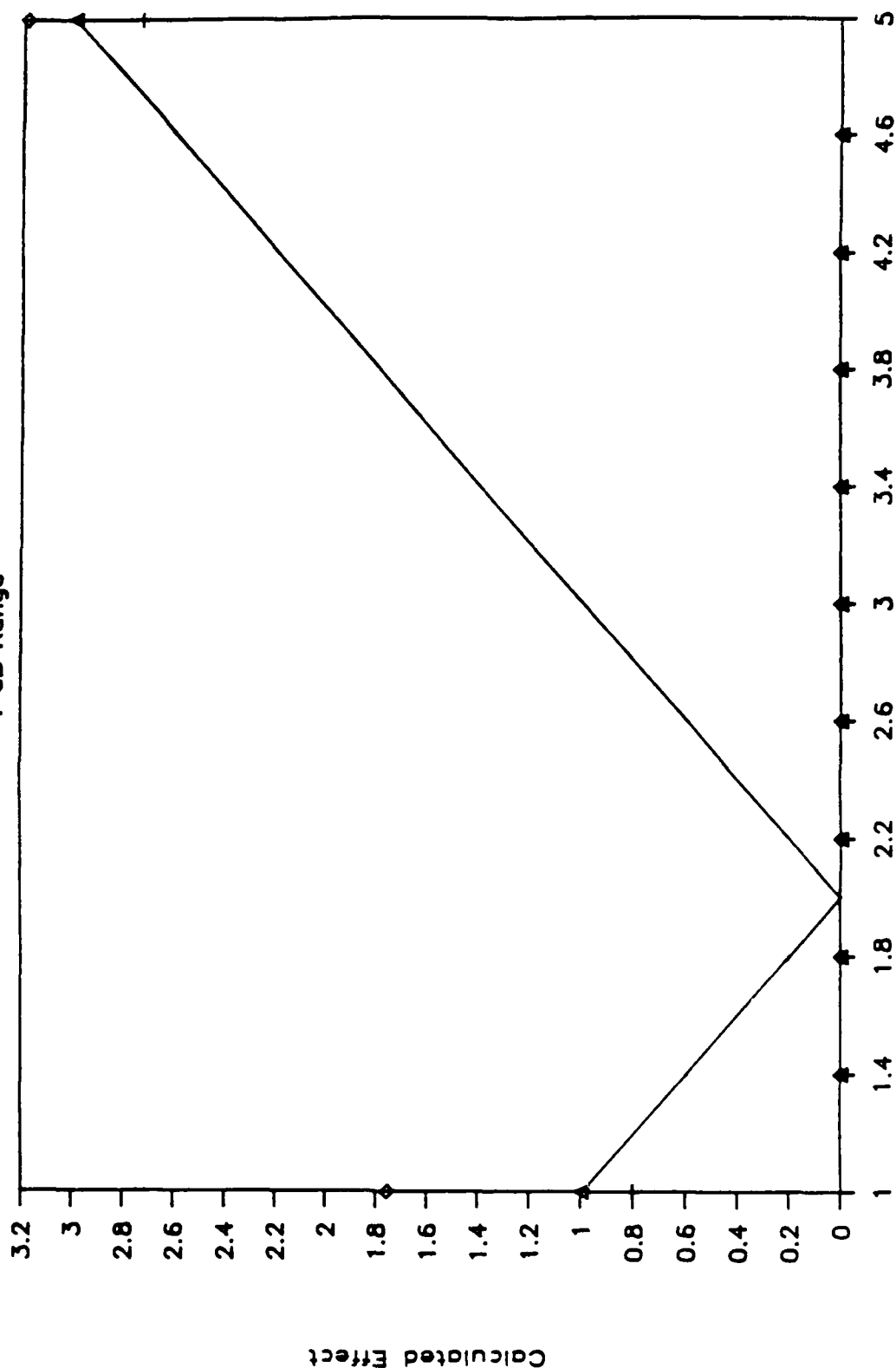


Figure 2.7 Range of solutions for parameter C with level errors considered.

C, Measurement Noise Only

1 dB Range



Range of "C"

Figure 2.8 Range of solutions for parameter C with measurement errors considered.

C, Levels and Measurement Error

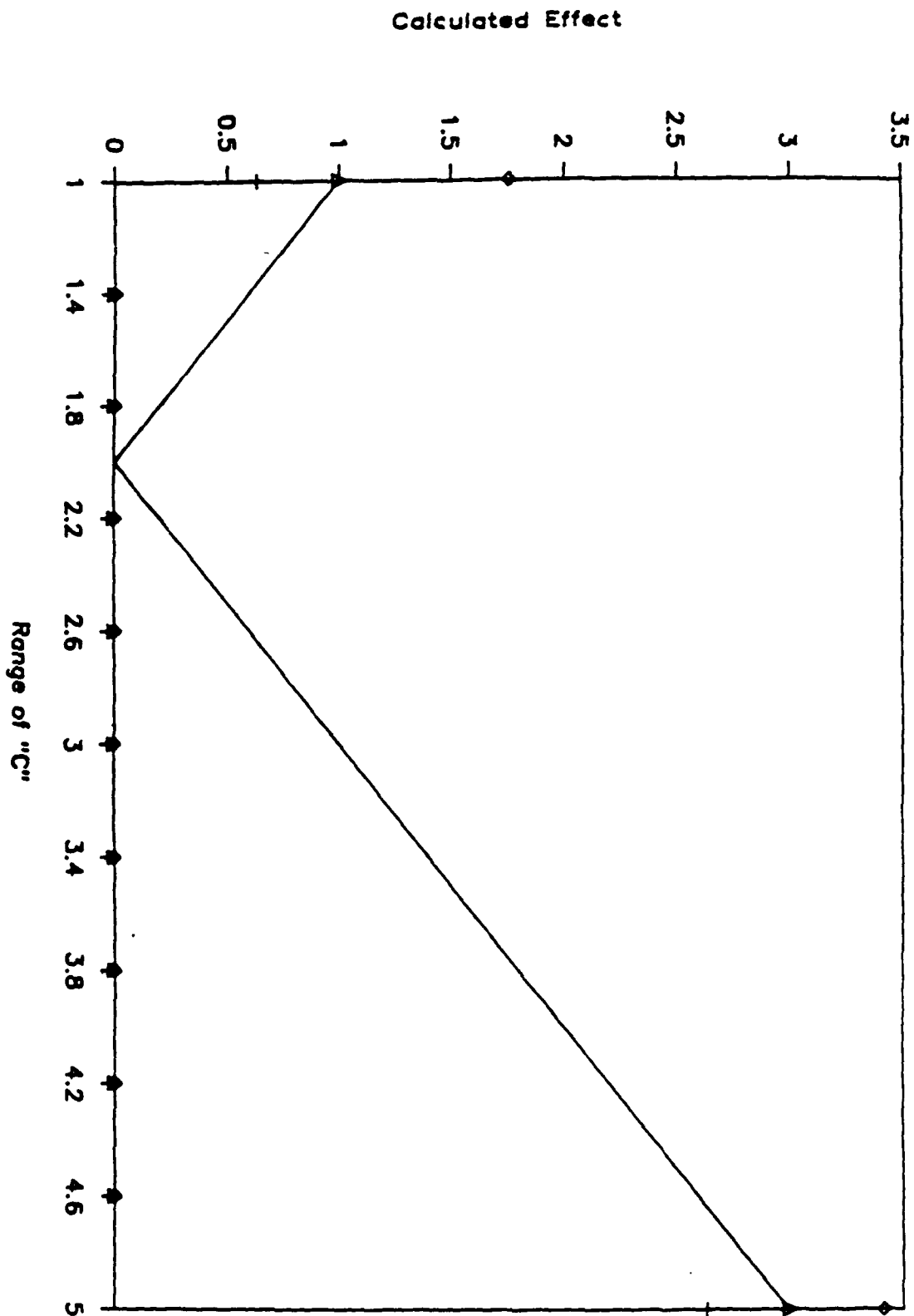


Figure 2.9 Range of solutions for parameter C determined by both levels and measurement errors.

A cross C

Six levels of C

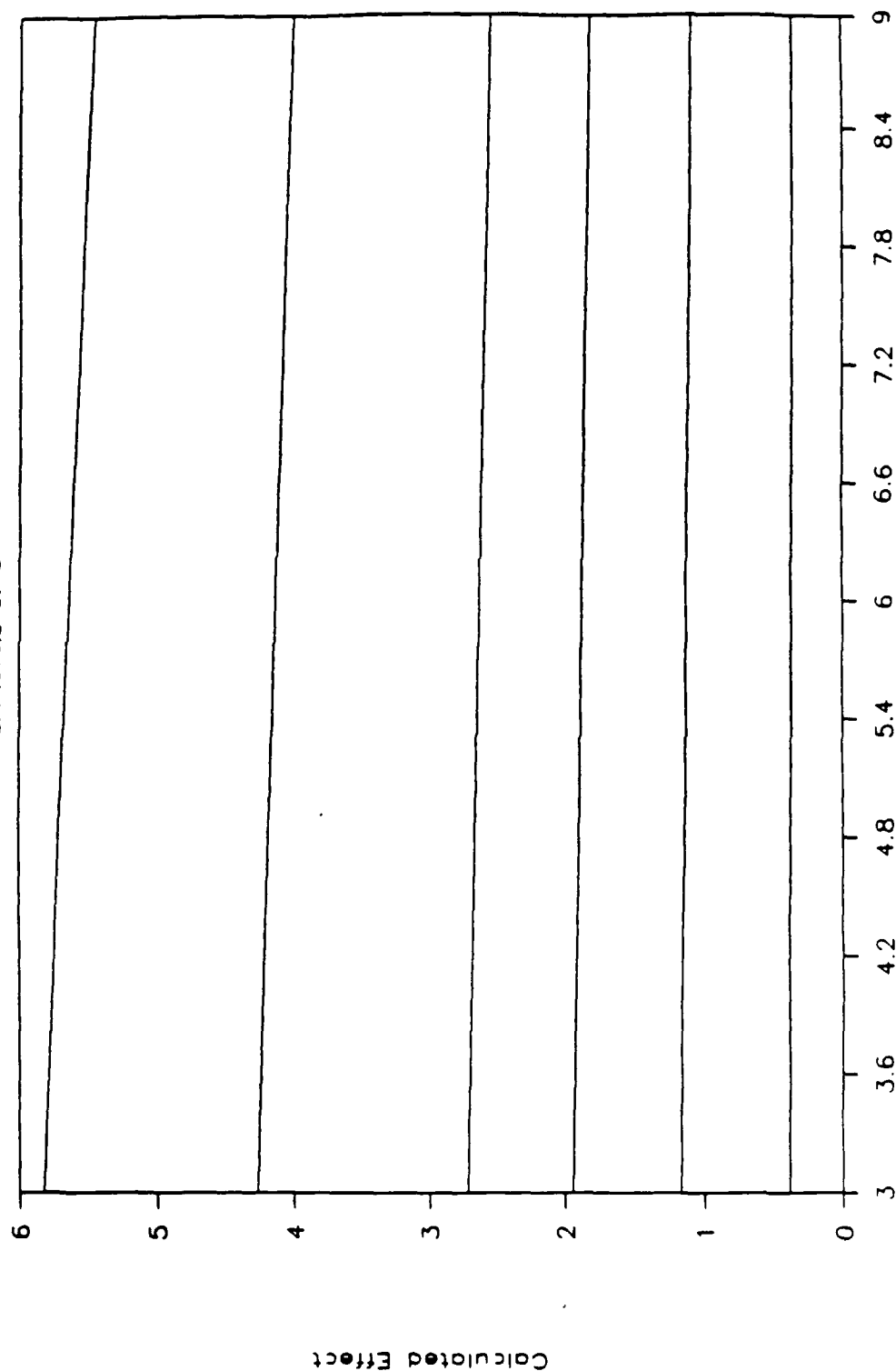


Figure 2.10 Cross term AxC plotted against range of A for six discrete levels of C.

C, Cross Term Effect

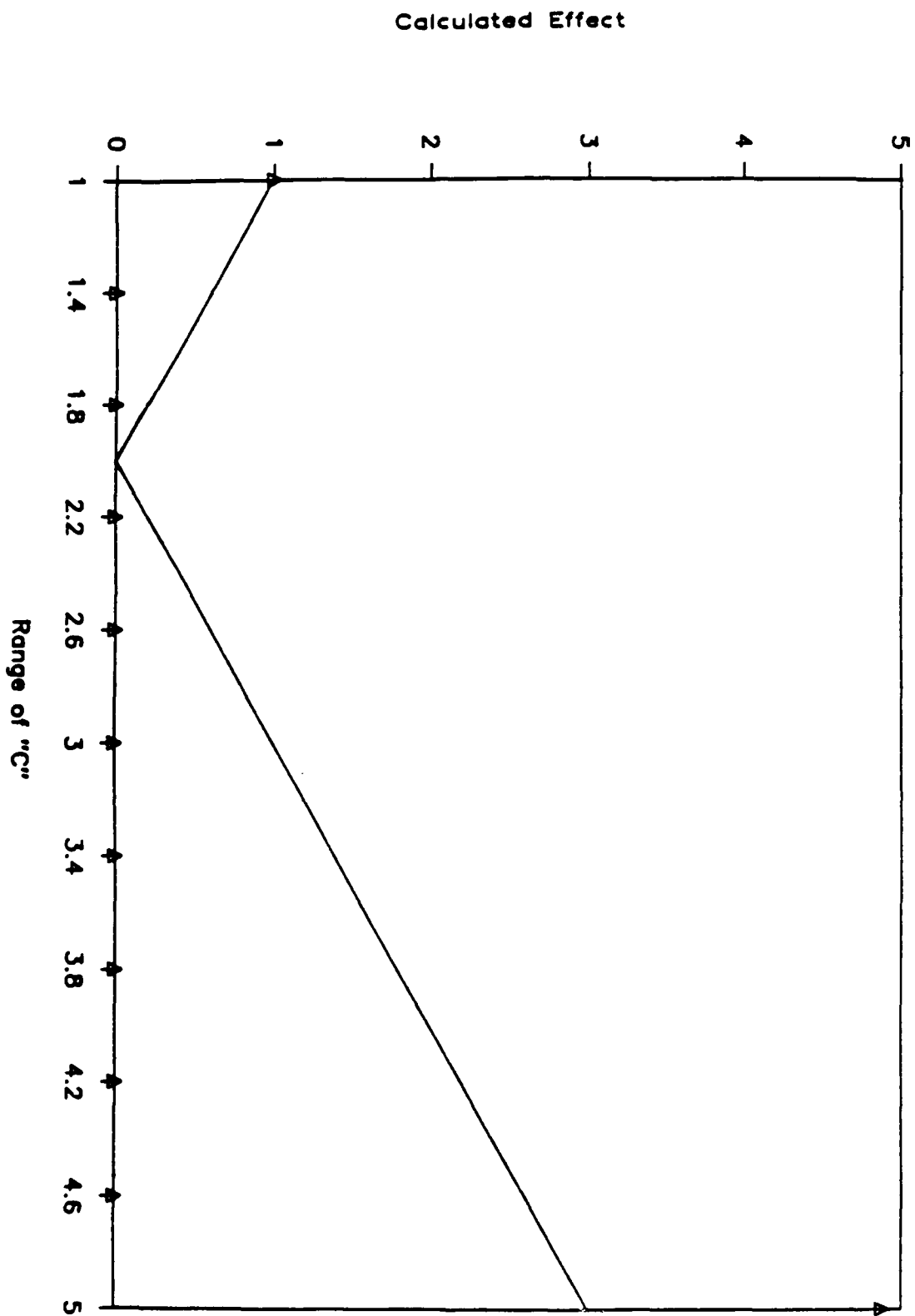
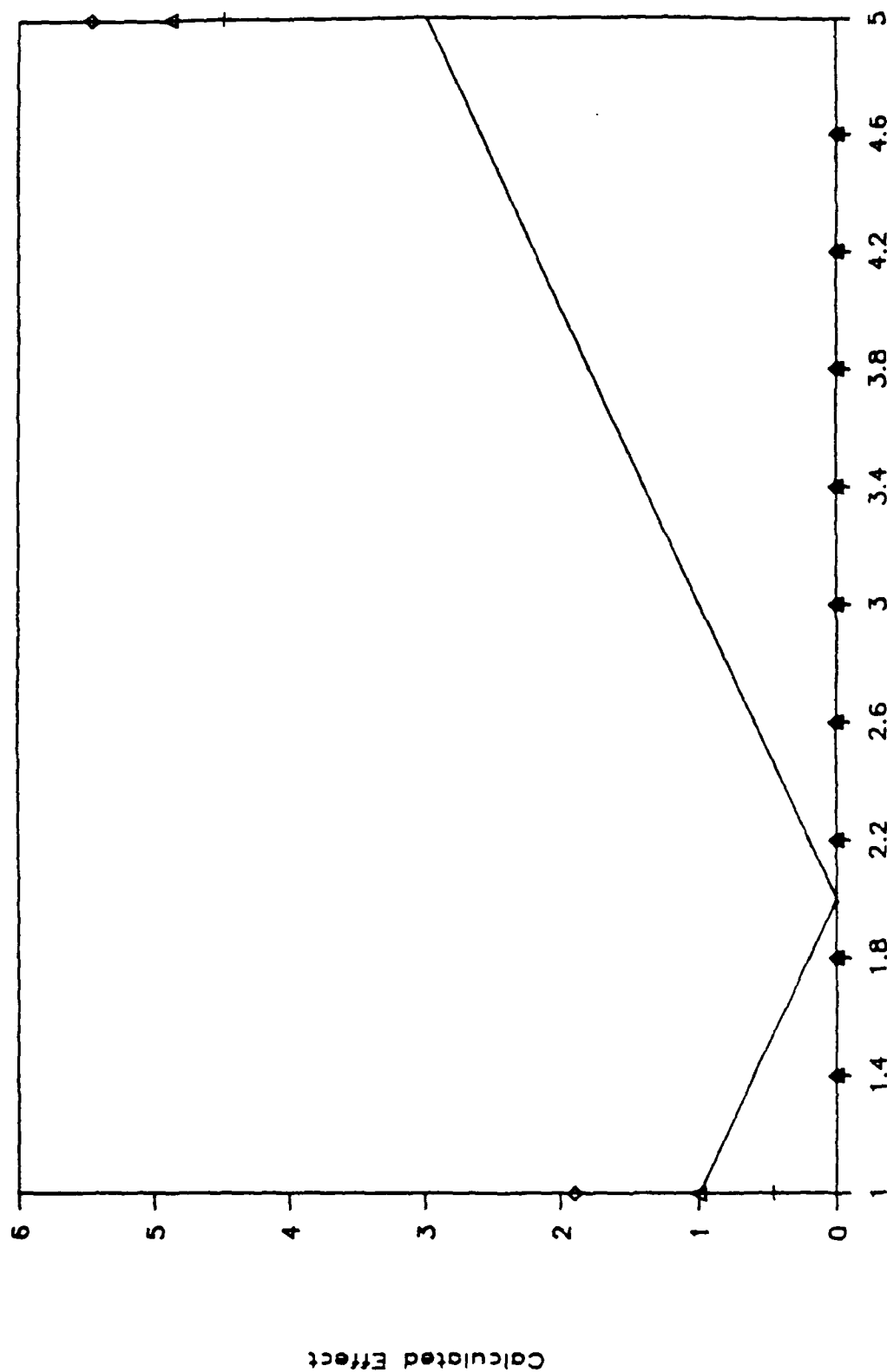


Figure 2.11 Effect of cross terms on solutions for parameter C.

C, X-terms + noise



Range of "C"

Figure 2.12 All modifiers affecting solutions for parameter C: levels and measurement error and cross terms.

E, Cross Term Effects

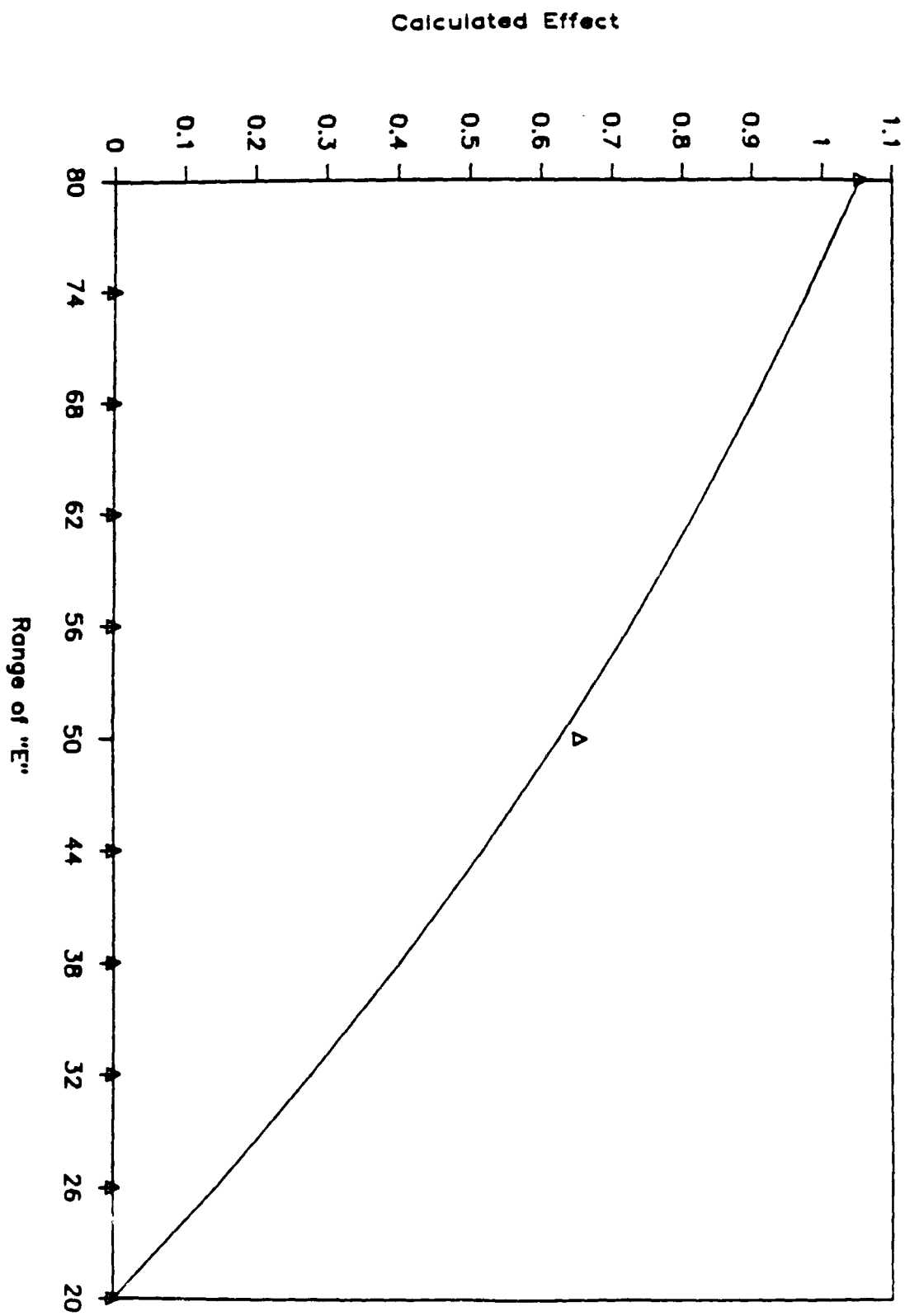


Figure 2.13 Solutions for parameter E as affected by cross terms.

F; Cross terms ON or OFF

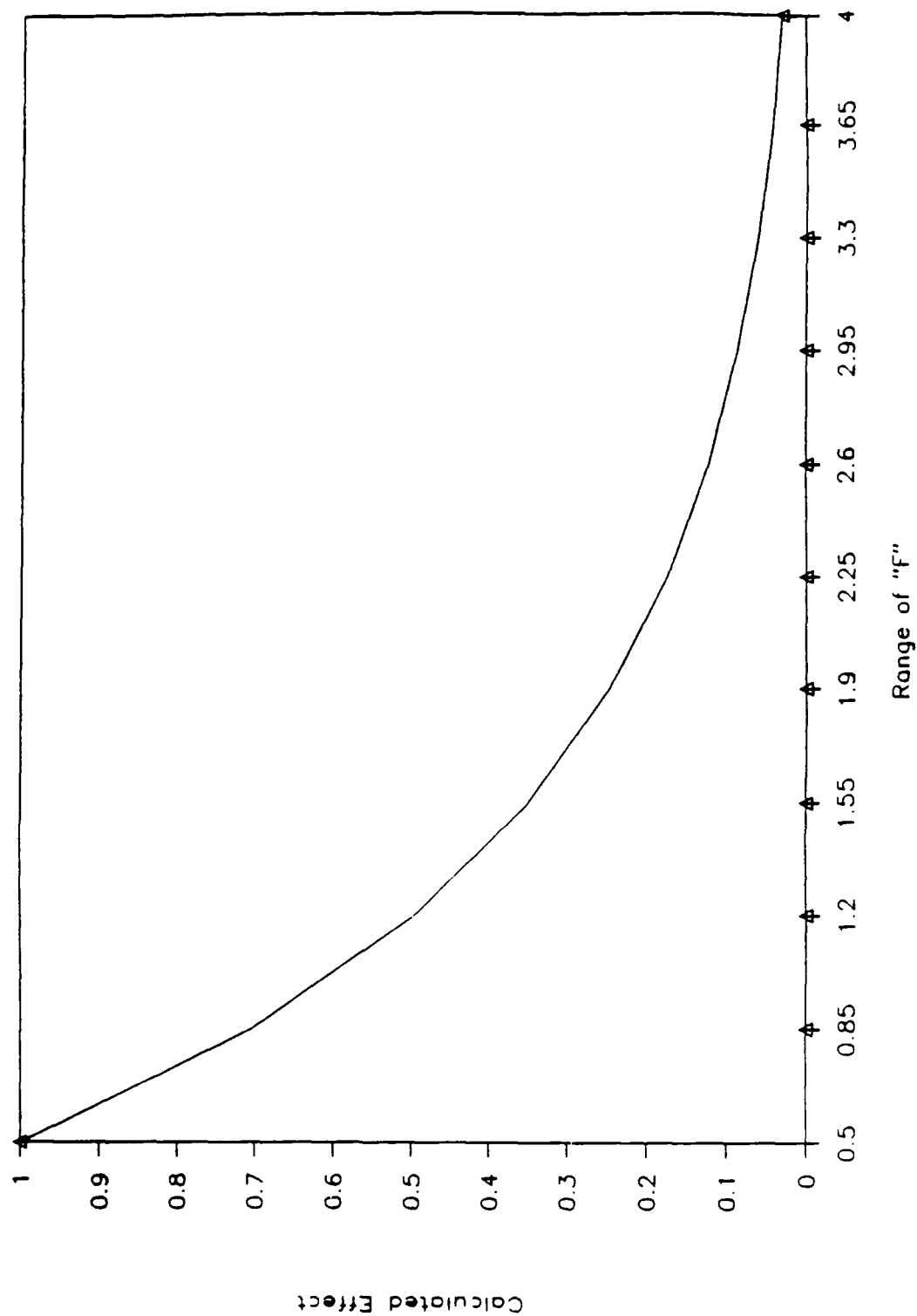


Figure 2.14 Solutions for parameter F with or without cross terms.

A; All Effects

Weak function of A

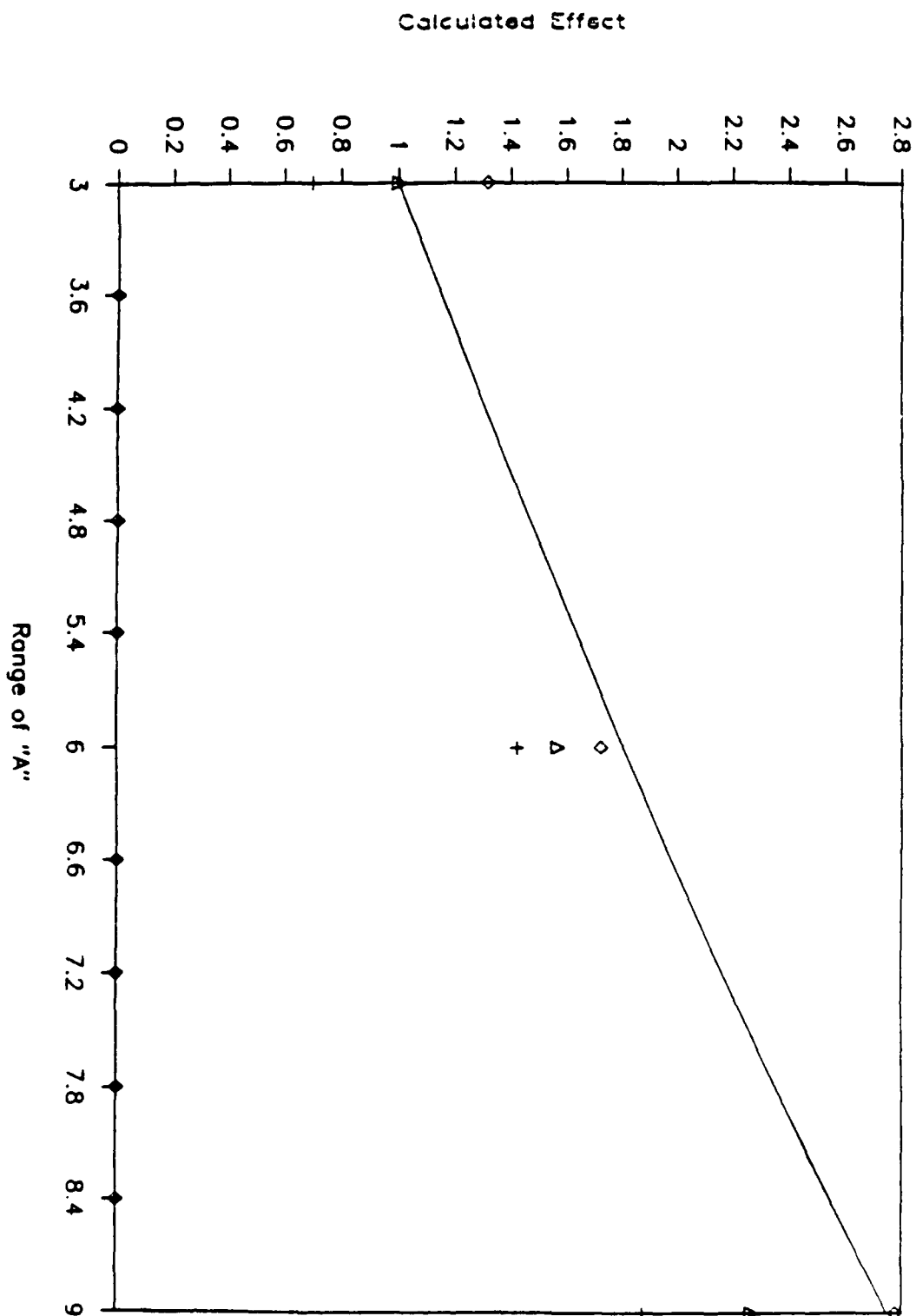


Figure 2.15 Range of solutions for parameter A due to all modifiers; weak function of A.

A; All Effects

Strong function of A

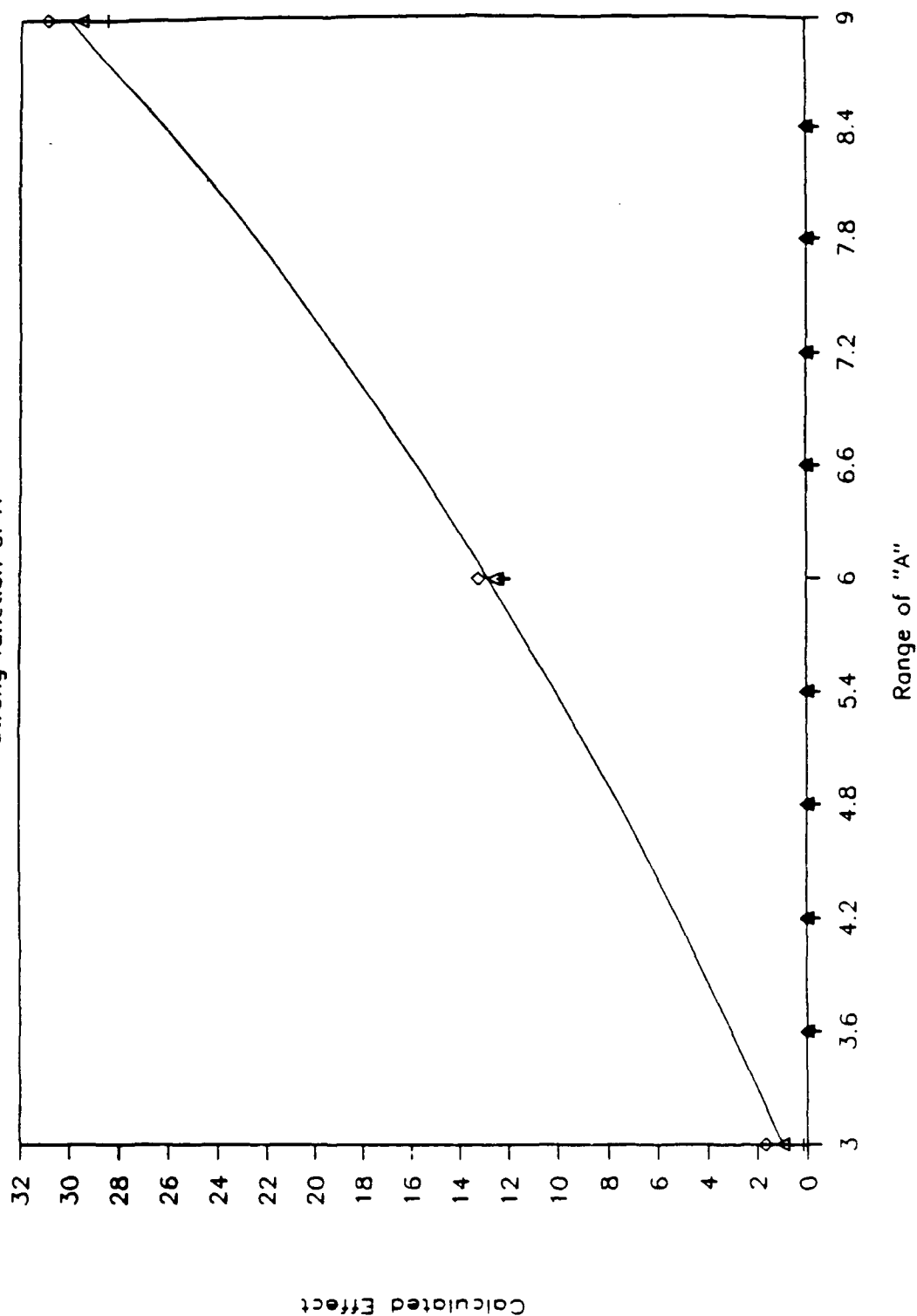


Figure 2.16 Range of solutions for parameter A due to all modifiers; strong function of A.

F; Levels and Measurement Error

Weak function of A

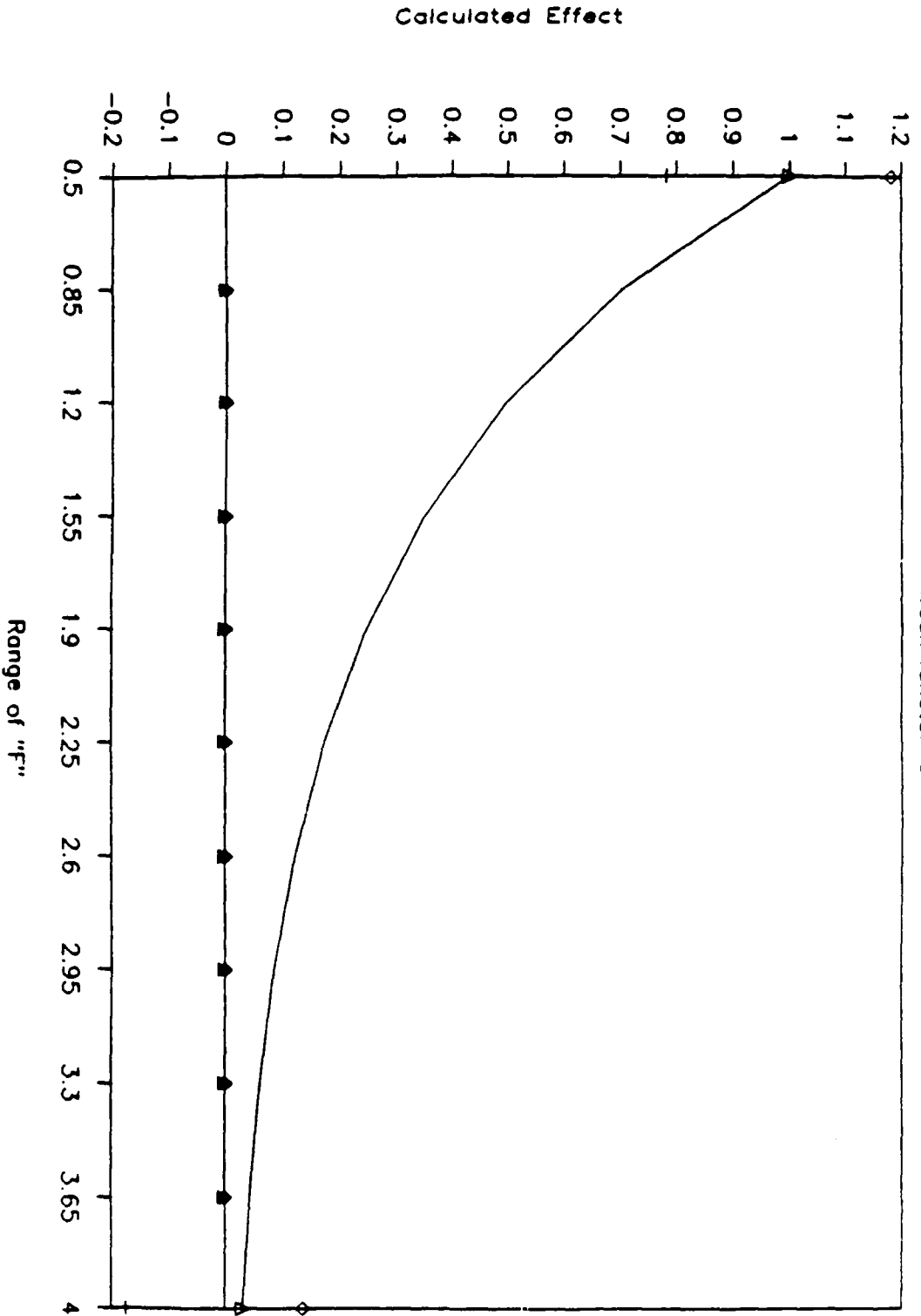


Figure 2.17 Range of solutions for parameter F with all modifiers; weak function of A.

F; Levels and Measurement Errors

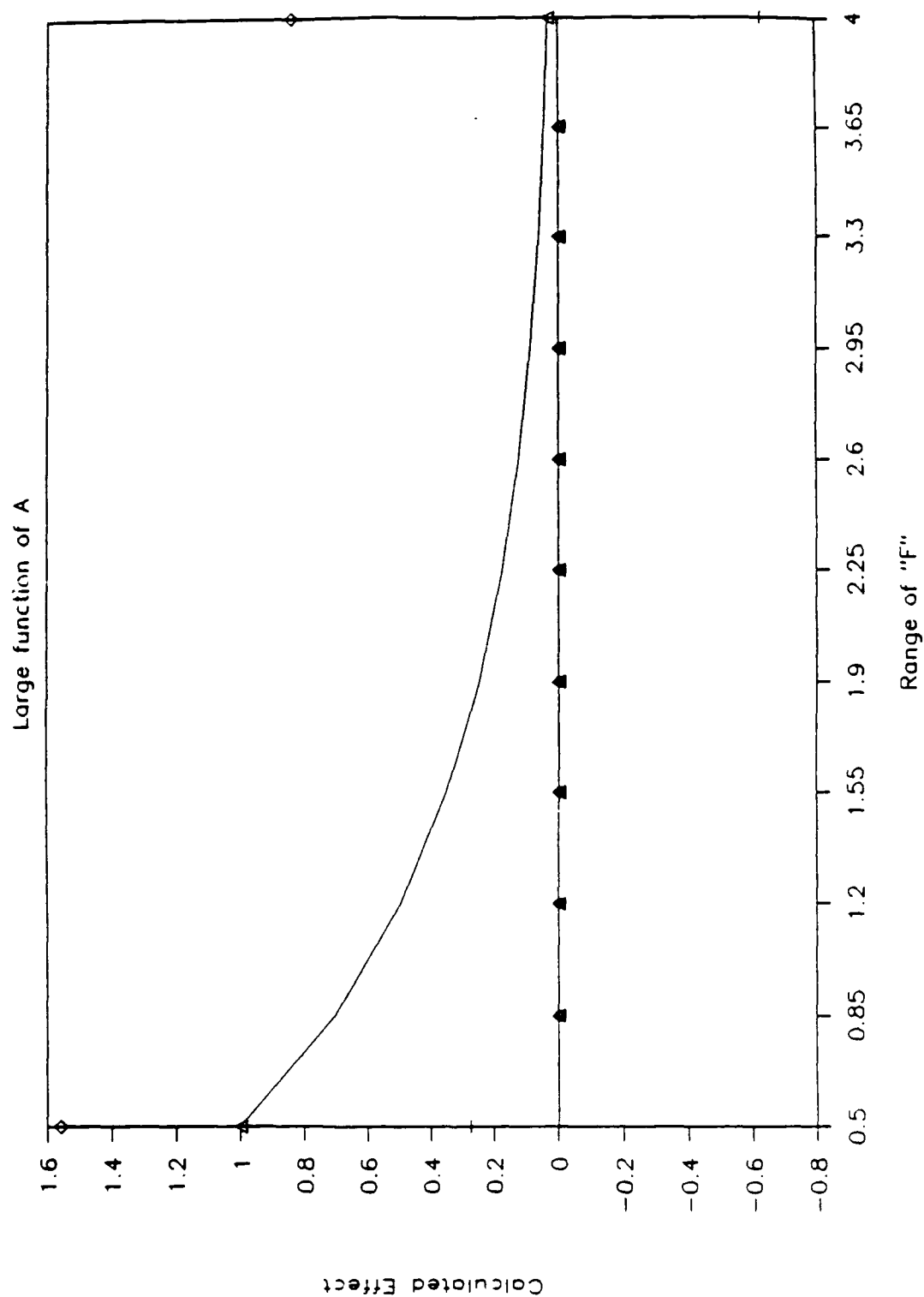


Figure 2.18 Range of solutions for parameter F with all modifiers; strong function of A.

B; All Effects

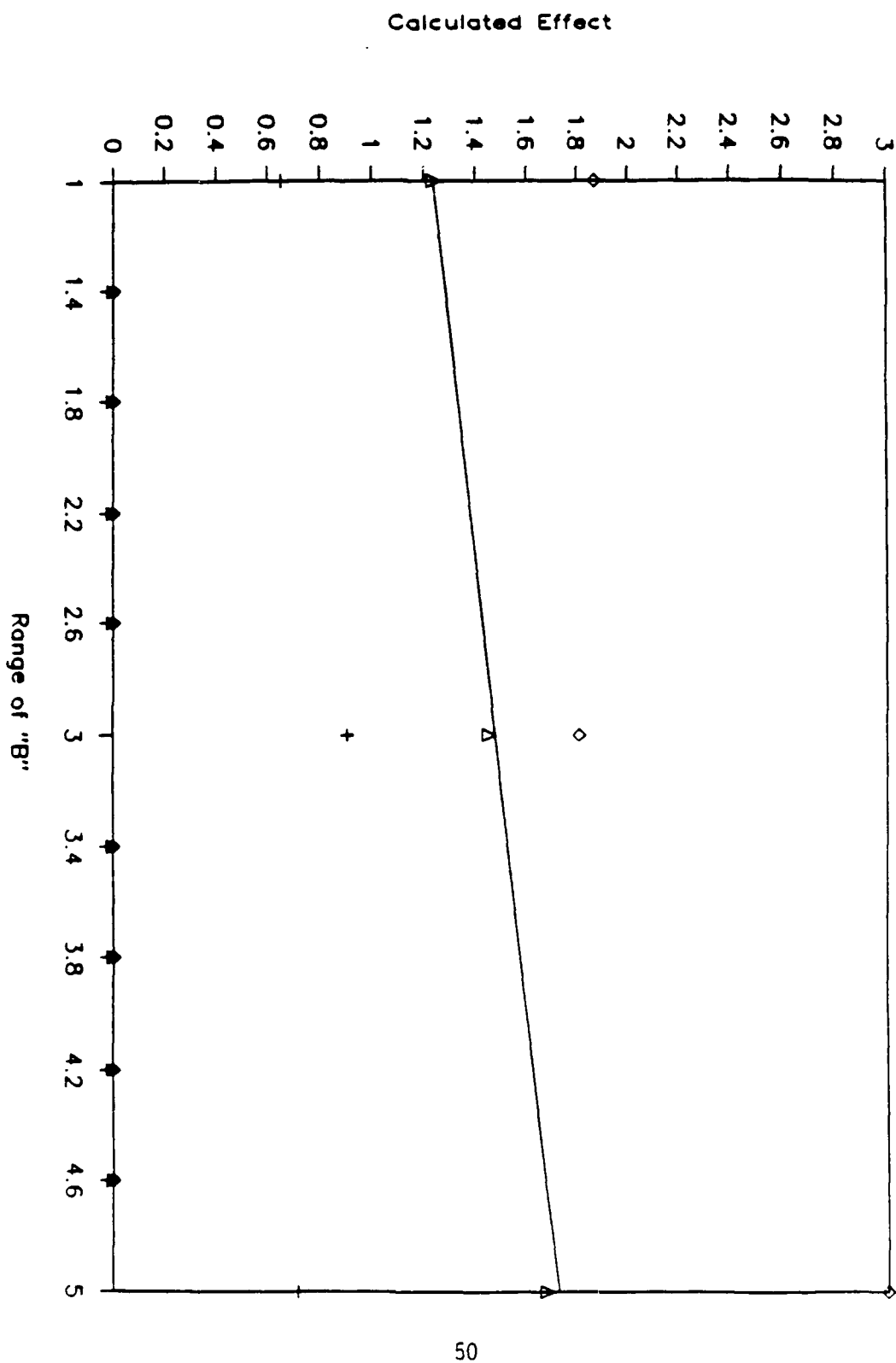


Figure 2.19 Range of solutions for B due to all modifiers.

CHAPTER 3

PREFORM DESIGN

Previous studies have indicated that several fabrication parameters play a role in determining the radiation sensitivity of optical fibers [1]. Some of these parameters, such as phosphorus doping in the core and/or clad, have been shown to exhibit a large effect, while the effects of other parameters, such as germanium concentration in the core and clad, fluorine doping, and oxygen stoichiometry during deposition, are not as well-defined. The objective of this program is to systematically vary these parameters in order to quantitatively determine the role that each plays in determining the radiation sensitivity of optical fibers. As a baseline, all fibers in this study have a matched clad design capable of operating single-mode at 1.3 microns.

For this study the preform fabrication parameters under investigation include the dopant levels of germanium in the core, the dopant levels of germanium or phosphorus in the clad (down doped with an appropriate amount of fluorine to maintain a matched-clad condition), and the stoichiometric flow of oxygen in the core and clad. The levels of the parameters investigated are intended to encompass the range used in commercial fabrication of fibers. Using this parameter space of variation, the orthogonal matrix analysis (OMA) technique was applied to predict the effect of each parameter on the radiation response of a given fiber. A more detailed description of the OMA technique and its limitations is given in Chapter 2.

In order to accurately distinguish the effect of each parameter on the radiation response, two phases of the study have been developed. Phase 1 includes those parameters which are expected to exhibit more subtle contributions to the radiation-induced loss, such as Ge concentration in the

core and clad, F doping, and oxygen stoichiometry in the core and clad. Also included in the scope of this study are fiber draw parameters, i.e. draw speed and draw tension. Phase 1 parameter levels are given in Table 3.1. Using the OMA technique, an experimental design table was developed for Phase 1 and is given in Table 3.2. The left-hand column, designated n, of this table indicates the preform/fiber number, and the so called "recipe" for each of the 16 preforms is specified by each row. The recipes used in conjunction with the parameter levels shown in Table 3.1 designate the fabrication parameters to be used for each preform and fiber. For example, preform n=1 should have 6.5 wt% GeO₂ in the core, pure SiO₂ clad, and low oxygen flow in both the core and clad; the fiber should be drawn at 0.5 m/sec with a tension of 80 grams. The orthogonal matrix requires several preform parameters to be changed simultaneously for each case, thus limiting to 16 the number of preforms required for Phase 1.

Phase 2 of this study was designed mainly to observe the effect of phosphorus doping on the radiation-induced loss. Mies and Soto [2] have reported a one-dimensional study of the effect of only phosphorus variations on radiation response. Phase 2 expands this work to include the effects of other fabrication parameters and possible cross correlations. Since phosphorus has been shown to have a large effect on the radiation response, it has been isolated to this second phase so as not to mask the effects of the other parameters. The parameters for Phase 2 include phosphorus concentration in the clad, oxygen stoichiometry in the clad, draw speed, and draw tension. Phase 2 parameter levels are given in Table 3.3, and the corresponding parameter values are given in Table 3.4. The number of preforms required for Phase 2 has been decreased to 8 due to limiting the number of experimental parameters. It should be noted that the core composition for Phase 2 remained constant at 6.5 wt% Ge with low oxygen flow during deposition.

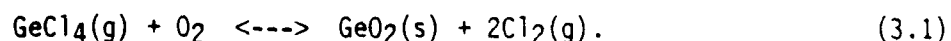
The two phases of this study are connected through a common preform, $n=1$. Since the parameter levels and fabrication conditions for both phases are similar, the radiation data obtained from both phases is assumed to be compatible. The information gathered from both phases is then combined into a model capable of predicting the radiation response of matched clad single mode optical fibers given the proper parameter input values, such as dopant levels, stoichiometry, and draw conditions.

PREFORM FABRICATION

The modified chemical vapor deposition (MCVD) process, which is widely used in the fiber optics industry, was used to fabricate the preforms for this study. The process involves the homogeneous chemical reaction of gaseous halide reagents with oxygen inside a rotating silica substrate tube heated with an external oxy-hydrogen torch. A schematic of the process is shown in Figure 3.1. The reagents are entrained in the gas stream by either bubbling oxygen through the liquid dopant sources (SiCl_4 , GeCl_4 , and POCl_3), or by using a gaseous dopant source (SiF_4). The vapors and gases are inserted into the substrate tube, and oxidation occurs in the hot zone of the torch. Small glassy particles with large surface areas are formed in the gas stream as a low density "soot" and are carried to the walls of the tube by the thermophoretic forces arising from the temperature gradient between the hot gas stream and the cold tube wall. After they deposit on the inside walls of the tube downstream from the torch, the deposited soot layer is fused into a thin glassy layer as the torch traverses over that point. Successive glassy layers are deposited inside the substrate tube to construct the desired fiber geometry. The composition of each layer is determined by the reagent gas flow, oxygen flow, and deposition temperature. A more detailed description of the MCVD process can be found in ref. 2.

Cladding layers are deposited first, which serve not only as an optical cladding for the light guided in the fiber core, but also as a barrier to impurities found in the substrate tube. Since a fraction of the waveguide's power travels in the clad it is important that the radius of the deposited cladding be > 5 times the radius of the core [3]. This ensures that excess loss does not arise due to impurities that have diffused into the deposited cladding from the substrate tube, or from the fraction of the evanescent wave which might extend out of the deposited cladding into the substrate tube. The cladding compositions that were used in this study include pure SiO_2 , SiO_2 co-doped with Ge and F, and SiO_2 co-doped with P and F. All preforms were fabricated so that the index of refraction of the clad was equal to that of the silica tube.

Deposition of the core directly follows the clad. The deposition rate of the core is decreased from that of the clad to allow greater control over the volume of glass deposited. All cores were doped with Ge to raise the index of the glass. It was observed that the Ge deposition efficiency was highly dependent on the flow of oxygen during deposition. As the oxygen flow decreased, the Ge efficiency decreased tremendously. At high oxygen flows (15 times stoichiometry), 30 mg/min of GeCl_4 was sufficient to obtain the level 1 parameter. However, at low oxygen (5 times stoichiometry) 170 mg/min of GeCl_4 was required to achieve the same Ge content. This decrease in Ge efficiency with decreasing oxygen can be explained by the following equilibrium reaction [4]:



The equilibrium constant for equation 3.1 is less than 1.0 at high temperatures; therefore at equilibrium GeCl_4 and GeO_2 coexist, and an increase in Cl_2 or a decrease in O_2 will favor the back reaction, which forms GeCl_4 .

After the deposition was completed, the torch temperature was increased

and the tube collapsed into a solid rod. Two separate collapse conditions were used for the preforms in this study. For preforms having low stoichiometry in the core, a mixture of oxygen and helium was flowed down the tube during collapse to minimize the volatilization of GeO_2 from the core. For preforms with high oxygen stoichiometry in the core, only oxygen was flowed down the tube during the collapse. During the course of the collapse, Ge volatilizes from the innermost layers, leaving a layer of silica-rich glass on the inside of the tube. A final etch of this layer is performed by passing Freon 12 and oxygen down the tube while transversing the torch; this procedure strips the innermost layer of glass from the tube, thus decreasing the index dip due to Ge burnout, which is commonly found in Ge-doped silica cores.

For this study the following materials and fabrication parameters were held constant:

1. General Electric 25mm x 19mm type 982WG fused quartz substrate tubes.
2. Synthatron fiber optic grade SiCl_4 , GeCl_4 , and POCl_3 .
3. Matheson Gas Products SiF_4 (99.99%)
4. Research grade O_2 for the carrier gas for the liquid reagents.
5. Deposition torch translation speed (2.5 mm/sec).
6. Diameter control (fabricated in-house, ± 0.1 mm)
7. Etch conditions: Freon 12 and O_2 .
8. Combined O_2 and He flow of approximately 1 l/m for the core deposition.
9. Core deposition rate: SiCl_4 = 0.26 g/min.
10. Combined O_2 and He flow of approximately 2 l/m for the clad deposition.
11. Clad deposition rate: SiCl_4 = 1.5 g/min.
12. Collapse conditions.

The preform fabrication parameters that were varied include:

1. Core and clad dopant levels.
2. The O₂:He ratio in the core and clad.
3. Deposition temperature for the clad ranged from 1790 to 1965 C depending on the dopant levels.
4. Deposition temperature for the core ranged from 1880 to 1910 C depending on the dopant levels.

Preforms were fabricated following the guidelines laid out in the experimental design Tables 3.2 and 3.4. However, it was found to be quite difficult to obtain precisely the required level of each parameter level. Variances in the parameter levels, in particular the Ge in the core, arose as a result of inconsistencies in the fabrication process. As a result, the yield of preforms with acceptable properties and parameter levels was quite low. In general, 4 to 5 preforms were fabricated for each one which was acceptable for the study.

All preforms in Phase 1 have been fabricated, drawn, and irradiated. The data corresponding to these fibers is given in Table 3.5. All preforms in Phase 2 have been fabricated, with the preform data given in Table 3.6.

ELECTRON PROBE MICROANALYSIS

The cross-sectional composition of each fiber was determined using an electron probe microanalyzer (EPMA). The EPMA is a non-destructive method of obtaining quantitative compositional information. The interaction of a focused electron beam with the sample produces x-rays characteristic of each element with a spatial resolution on the order of 1 μ m. The x-rays may be detected by using either an energy dispersive spectrometer (EDS) or a wavelength dispersive spectrometer (WDS). The EDS detector is often used for fast, qualitative analysis, whereas the WDS detector has higher energy

resolution and increased sensitivity for use in quantitative analysis. Material standards are also required for accurate quantitative analysis. The measured x-ray intensities of an element were compared to those of a standard, whose chemical content is known. Computer programs are available that convert the x-ray intensities into chemical composition.

The cross-sectional composition of each fiber was determined by stepping an 8 kV 15nA electron beam, with a 1 μm spot size, across the fiber in 1 μm steps. Figure 3.2 shows a typical data set obtained from the EPMA. The chemical compositions for each fiber can be found in Tables 3.5 and 3.6.

REFERENCES

1. C.G. Askins, C.M. Shaw, and E.J. Friebele, SPIE Vol. 721 (1986) 57.
2. W.C. French, R.E. Jaeger, J.B. MacChesney, S.R. Nagel, K. Nassau, A.D. Pearson, "Fiber Preform Preparation", Chapter 8 in Optical Fiber Telecommunications, S.E. Miller, A.G. Chynoweth, eds, Academic Press, New York 1979.
3. B.J. Ainslie, K.J. Beales, C.R. Day, and J.D. Rush, IEEE J. Quant. Elect., Vol QE-18, No. 4, (1982) 514.
4. D.L. Wood, K.L. Walker, J.B. McChesney, J.R. Simpson, and R. Csencsits, J. Lightwave Tech., Vol. LT-5, No. 2, (1987) 277.

Table 3.1

Parameters for Phase I of the Matched Clad Design

Parameter	Levels	1	2	3	
A. Ge in Core		6.5	10	14	wt%
B. Ge in Clad (balance F for matched clad)		0	2.4	3.8	wt%
C. Stoichiometry in Core		5x	15x		
D. Stoichiometry in Clad		5x	10x		
E. Draw Tension		80	50	20	grams
F. Draw Speed		0.5	4.0		m/sec

Table 3.2

Parameters for Phase 2 of the Matched Clad Design

Parameter	Levels	1	2	3	4	
A. P in Clad (balance F for matched clad)		0	0.5	1.0	2.0	wt%
B. Stoichiometry in Clad		5x	10x			
C. Draw Tension		80	20			grams
D. Draw Speed		0.5	4.0			m/sec

*All preforms in phase 2 have the core composition that is given for n=1 in phase 1 (GeO_2 = 6 wt%, low oxygen).

Table 3.3

Experimental Factors for Phase 1 of the Matched Clad Design

A _i = [Ge] in Core (no F)	i = 1, 2, 3
B _i = [Ge] in Clad, F to Match Clad	i = 1, 2, 3
C _i = Stoichiometry in Core	i = 1, 2
D _i = Stoichiometry in Clad	i = 1, 2
E _i = Draw Tension	i = 1, 2, 3
F _i = Draw Speed	i = 1, 2

Experimental Design Table for 6 Factors

n	A	B	C	D	E	F	R _i
1	1	1	1	1	1	1	R ₁
2	2	1	2	2	1	2	R ₂
3	1	2	2	2	2	2	R ₃
4	2	2	1	1	2	1	R ₄
5	2	1	1	1	2	2	R ₅
6	1	1	2	2	2	1	R ₆
7	2	2	2	2	1	1	R ₇
8	1	2	1	1	1	2	R ₈
9	2	2	2	1	2	1	R ₉
10	3	2	1	2	2	2	R ₁₀
11	2	3	1	2	3	2	R ₁₁
12	3	3	2	1	3	1	R ₁₂
13	3	2	2	1	3	2	R ₁₃
14	2	2	1	2	3	1	R ₁₄
15	3	3	1	2	2	1	R ₁₅
16	2	3	2	1	2	2	R ₁₆

Table 3.3 (cont.)

The significance of each control parameter can be obtained as follows:

$$\bar{A}_1 = 1/4 (R_1 + R_3 + R_6 + R_8) + W_A$$

$$\bar{A}_2 = 1/8 (R_2 + R_4 + R_5 + R_7 + R_9 + R_{11} + R_{14} + R_{16})$$

$$\bar{A}_3 = 1/4 (R_{10} + R_{12} + R_{13} + R_{15}) - W_A$$

$$W_A = 1/8 (R_9 + R_{11} + R_{14} + R_{16} - R_2 - R_4 - R_5 - R_7)$$

$$\bar{B}_1 = 1/4 (R_1 + R_2 + R_5 + R_6) + W_B$$

$$\bar{B}_2 = 1/8 (R_3 + R_4 + R_7 + R_8 + R_9 + R_{10} + R_{13} + R_{14})$$

$$\bar{B}_3 = 1/4 (R_{11} + R_{12} + R_{15} + R_{16}) - W_B$$

$$W_B = 1/8 (R_9 + R_{10} + R_{13} + R_{14} - R_3 - R_4 - R_7 - R_8)$$

$$\bar{C}_1 = 1/8 (R_1 + R_4 + R_5 + R_8 + R_{10} + R_{11} + R_{14} + R_{15})$$

$$\bar{C}_2 = 1/8 (R_2 + R_3 + R_6 + R_7 + R_9 + R_{12} + R_{13} + R_{16})$$

$$\bar{D}_1 = 1/8 (R_1 + R_4 + R_5 + R_8 + R_9 + R_{12} + R_{13} + R_{16})$$

$$\bar{D}_2 = 1/8 (R_2 + R_3 + R_6 + R_7 + R_{10} + R_{11} + R_{14} + R_{15})$$

$$\bar{E}_1 = 1/4 (R_1 + R_2 + R_7 + R_8) + W_E$$

$$\bar{E}_2 = 1/8 (R_3 + R_4 + R_5 + R_6 + R_9 + R_{10} + R_{15} + R_{16})$$

$$\bar{E}_3 = 1/4 (R_{11} + R_{12} + R_{13} + R_{14}) - W_E$$

$$W_E = 1/8 (R_9 + R_{10} + R_{15} + R_{16} - R_3 - R_4 - R_5 - R_6)$$

$$\bar{F}_1 = 1/8 (R_1 + R_4 + R_6 + R_7 + R_9 + R_{12} + R_{14} + R_{15})$$

$$\bar{F}_2 = 1/8 (R_2 + R_3 + R_5 + R_8 + R_{10} + R_{11} + R_{13} + R_{16})$$

Table 3.4

Experimental Factors for Phase 2 of the Matched Clad Design

A_i = [P] in Clad, F to Match Clad $i = 1, 2, 3, 4$
 B_i = Stoichiometry in Clad $i = 1, 2$
 C_i = Draw Tension $i = 1, 2$
 D_i = Draw Speed $i = 1, 2$

Experimental Design Table for 6 Factors

n	A	B	C	D	R _i
17	1	1	1	1	R ₁₇
18	1	2	2	2	R ₁₈
19	2	1	1	2	R ₁₉
20	2	2	2	1	R ₂₀
21	3	1	2	1	R ₂₁
22	3	2	1	2	R ₂₂
23	4	1	2	2	R ₂₃
24	4	2	1	1	R ₂₄

The significance of each control parameter can be obtained as follows:

$$\bar{A}_1 = 1/2 (R_{17} + R_{18}) \quad \bar{A}_3 = 1/2 (R_{21} + R_{22})$$

$$\bar{A}_2 = 1/2 (R_{19} + R_{20}) \quad \bar{A}_4 = 1/2 (R_{23} + R_{24})$$

$$\bar{B}_1 = 1/4 (R_{17} + R_{19} + R_{21} + R_{23})$$

$$\bar{B}_2 = 1/4 (R_{18} + R_{20} + R_{22} + R_{24})$$

$$\bar{C}_1 = 1/4 (R_{17} + R_{19} + R_{22} + R_{24})$$

$$\bar{C}_2 = 1/4 (R_{18} + R_{20} + R_{21} + R_{23})$$

$$\bar{D}_1 = 1/4 (R_{17} + R_{20} + R_{21} + R_{24})$$

$$\bar{D}_2 = 1/4 (R_{18} + R_{19} + R_{22} + R_{23})$$

Table 3.5a Matched Clad Single Mode Fibers

FIBERFORM	CORE		SiCl ₄		GeCl ₄		F		O ₂		He		TEMP C
	g/m	wt %	g/m (Volts)	wt %	wt %	lpm	Ratio	lpm	C				
	NRL 870914 #63, N=1	0.26	92.4	0.190 (.792)	7.5	0.018	0.28	5X	0.72	1900-1910			
	NRL 870224 #15, N=2	0.26	90.5	0.07 (.3)	9.4	0.021	0.64	15X	0.36	1890-1900			
	NRL 870416 #25, N=3	0.26	92.5	0.03 (.14)	7.4	0.022	0.56	15X	0.44	1890			
	NRL 870615 #40, N=4	0.26	89.5	0.26 (1.07)	10.3	0.017	0.32	5X	0.68	1890			
	NRL 870714 #48, N=5	0.26	89.7	0.285 (1.173)	10.2	0.036	0.33	5X	0.67	1890			
	NRL 870302 #17, N=6	0.26	93.4	0.03 (.14)	6.2	0.013	0.56	15X	0.36	1890-1900			
	NRL 870421 #27, N=7	0.26	88.4	0.07 (.3)	11.4	0.033	0.64	15X	0.36	1890			
	NRL 870611 #39, N=8	0.26	93.7	0.153 (0.64)	6.2	0.140	0.26	5X	0.74	1900			
	NRL 870602 #36, N=9	0.26	87.8	0.065 (.275)	12.0	0.013	0.64	5X	0.36	1890			
	NRL 870511 #31, N=10	0.26	84.5	0.365 (1.5)	15.2	0.041	0.38	5X	0.62	1890			
	NRL 870506 #29, N=11	0.26	90.0	0.255 (1.05)	9.8	0.260	0.32	5X	0.68	1890			
	NRL 870716 #49, N=12	0.26	84.3	0.14 (0.58)	15.4	0.270	0.76	15X	0.24	1880			
	NRL 870617 #41, N=13	0.26	83.8	0.125 (.53)	16.0	0.190	0.74	15X	0.24	1880			
	NRL 870504 #28, N=14	0.26	91.6	0.248 (1.0)	8.6	0.160	0.32	5X	0.68	1890			
	NRL 870513 #32, N=15	0.26	84.6	0.357 (1.47)	15.0	0.280	0.38	5X	0.62	1880			
	NRL 870625 #43, N=16	0.26	88.0	0.65 (.272)	11.8	0.260	0.64	15X	0.36	1890			
	NRL 870914 #63, N=17	0.26	92.4	0.190 (.792)	7.5	0.018	0.28	5X	0.72	1900-1910			
	NRL 870805 #52, N=18	0.26	92.6	0.173 (.715)	7.4	0.028	0.27	5X	0.73	1900			
	NRL 870820 #56, N=19	0.26	92.4	0.174 (.72)	7.5	0.120	0.27	5X	0.73	1900			
	NRL 870824 #57, N=20	0.26	91.8	0.172 (.712)	8.0	0.011	0.27	5X	0.73	1900			
	NRL 870817 #54, N=21	0.26	93.4	0.17 (.7)	6.5	0.022	0.27	5X	0.73	1900			
	NRL 870818 #55, N=22	0.26	92.6	0.175 (.725)	7.4	0.110	0.27	5X	0.73	1900			
	NRL 870910 #62, N=23	0.26	92.7	0.173 (.72)	7.3	0.050	0.27	5X	0.73	1900			
	NRL 870924 #67, N=24	0.26	93.3	0.172 (.715)	6.6	0.008	0.27	5X	0.73	1900			

Table 3.5b Matched Clad Single Mode Fibers

FIBER	CLADDING				SLP4				O2		TEMP C
	g/m	SI/CL4 wt %	g/m (Volts)	wt %	geom (Volts)	wt %	μm	ratio	μm		
NRU, 870914 #63, N=1	1.5	100.0					1.00	5X	1.00	1950-1970	
NRU, 870224 #15, N=2	1.5	100.0					2.00	10X	0.00	1940-1960	
NRU, 870416 #25, N=3	1.5	97.0	0.10 (.425)	2.5	6	0.55	2.10	10X	0.00	1925-1940	
NRU, 870615 #40, N=4	1.5	97.1	0.24 (1.0)	2.4	7	0.50	1.15	5X	0.85	1925-1950	
NRU, 870714 #48, N=5	1.5	100.0					1.00	5X	1.00	1945-1965	
NRU, 870302 #17, N=6	1.5	100.0					2.00	10X	0.00	1940-1960	
NRU, 870421 #27, N=7	1.5	97.0	0.10 (.425)	2.5	6	0.51	2.10	10X	0.00	1925-1940	
NRU, 870611 #39, N=8	1.5	97.2	0.24 (1.0)	2.3	7	0.53	1.15	5X	0.85	1925-1950	
NRU, 870602 #36, N=9	1.5	97.0	0.24 (1.0)	2.5	7	0.49	1.15	5X	0.85	1925-1950	
NRU, 870511 #31, N=10	1.5	97.0	0.10 (.424)	2.4	6	0.54	2.10	10X	0.00	1925-1940	
NRU, 870506 #29, N=11	1.5	95.2	0.25 (1.025)	3.8	31 (30.5)	0.87	2.30	10X	0.00	1900-1920	
NRU, 870716 #49, N=12	1.5	95.3	0.465 (1.93)	3.9	33 (32.6)	0.84	1.27	5X	0.73	1900-1935	
NRU, 870617 #41, N=13	1.5	97.0	0.24 (1.0)	2.3	7	0.53	1.15	5X	0.85	1925-1950	
NRU, 870504 #28, N=14	1.5	97.1	0.10 (.424)	2.4	6	0.50	2.10	10X	0.00	1925-1940	
NRU, 870513 #32, N=15	1.5	95.3	0.25 (1.025)	3.9	30 (2.96)	0.83	2.30	10X	0.00	1900-1935	
NRU, 870625 #43, N=16	1.5	95.2	0.462 (1.91)	4.0	33 (32.6)	0.82	1.27	5X	0.73	1900-1935	

FOCL3		
g/m (Volts)	wt %	
NRU, 870914 #63, N=17	1.5	100.0
NRU, 870805 #52, N=18	1.5	100.0
NRU, 870820 #56, N=19	1.5	99.5
NRU, 870824 #57, N=20	1.5	99.4
NRU, 870817 #54, N=21	1.5	98.6
NRU, 870818 #55, N=22	1.5	98.3
NRU, 870910 #62, N=23	1.5	97.8
NRU, 870924 #67, N=24	1.5	97.6

Table 3.5c Matched Clad Single Mode Fibers

PREFORM	PREFORM PARAMETERS					COMMENTS		FIBER DRAW		
	MA	OD mm	CD mm	CLAD FD @ 1.2 μ m	PROL #	PROL VOL		Tens g	Speed m/sec	Loc
NRL 870914 #63, N=1	0.106	17.3	1.05	141	13-14	8/27/87	Very round preform.	42	0.47	NRL
NRL 870224 #15, N=2	0.124	16.5	0.95	122	20-22	12/21/86	Monitor Ge flow with voltmeter.	72	4.00	ERC 2
NRL 870416 #25, N=3	0.100	17.0	1.18	132	38-40, 1	2/27/87, 4/17	O2 during collapse.	50	4.00	ERC
NRL 870615 #40, N=4	0.124	17.1	0.93	135	18-20	6/9/87	Two etches, O2/He collapse.	52	0.50	NRL
NRL 870714 #48, N=5	0.126	17.1	0.95	131	11-12	7/8/87	Two etches, O2/He collapse.	50	4.00	ERC
NRL 870302 #17, N=6	0.100	16.3	1.18	127	1-2	2/27/87		50	0.50	NRL
NRL 870421 #27, N=7	0.130	16.9	1.00	119	4-5	4/17/87	Very round, O2 collapse.	80	0.46	NRL
NRL 870611 #39, N=8	0.100	17.1	1.28	122	14-15	6/9/87	Two etches, O2/He collapse.	87	4.00	ERC
NRL 870602 #36, N=9	0.134	17.0	0.93	124	30-31	4/17/87	Two etches, O2 collapse.	50	0.52	NRL
NRL 870511 #31, N=10	0.160	17.0	0.80	122	12-13	4/17/87	Four etches. He/O2 collapse.	56	4.00	ERC
NRL 870506 #29, N=11	0.123	17.0	1.05	121	8-9	4/17/87	He/low O2 collapse.	24	4.00	ERC
NRL 870617 #41, N=13	0.152	17.4	0.95	110	13-14	7/8/87		20	0.50	ERC
NRL 870504 #28, N=14	0.124	17.1	1.10	115	21-	6/9/87		21	4.00	ERC
NRL 870513 #32, N=15	0.157	17.0	0.79	126	6-7	4/17/87	He/LOW O2 COLLAPSE.	20	0.50	ERC
NRL 870625 #43, N=16	0.127	17.0	0.93	132	15-16	4/17/87	Three etches. He/O2 collapse.	50	0.45	NRL
					30-31	6/9/87		50	4.00	ERC
NRL 870914 #63, N=17	0.106	17.3	1.05	141	13-14	8/27/87	Very round preform.	42	0.47	NRL
NRL 870805 #52, N=18	0.103	16.9	1.13	133	29-30	7/8/87		20	4.00	ERC
NRL 870820 #56, N=19	0.114	17.5	1.25	113	44-45	7/8/87		50	4.00	ERC
NRL 870824 #57, N=20	0.115	17.3	1.20	115	46-47	7/8/87		17.5	0.50	NRL
NRL 870817 #54, N=21	0.100	17.5	1.28	126	37-40	7/8/87		19	0.50	NRL
NRL 870818 #55, N=22	0.106	17.5	1.35	112	41-43	7/8/87	GE Special dep tube used	50	4.00	ERC
NRL 870910 #62, N=23	0.108	17.6	1.35	111	11-12	8/27/87	Slightly dep clad (.25)	15	4.00	ERC
NRL 870924 #67, N=24	0.104	17.3	1.25	122	20-21	8/27/87		42	0.50	NRL

Table 3.5d Etched Clad Single Mode Fibers

PREFORM	FIBER PARAMETERS				COMMENTS			
	CD μm	CD μm	Ellip a/b	CLAD DIA μm	CUTOFF λ_c (μm)	dB/km @ 1.39 μm	dB/km @ 1.3 μm	POWER DISTRIBUTION % CORE % CLAD
NRU 870914 #63, N=1	90	5.63	1.00	42.5	1.24	10.0	8.20	60 40 A long sloping cutoff.
NRU 870224 #15, N=2	112	7.23	0.68	62.1	1.24	5.5	0.75	83 17 Second draw from preform, 300m.
NRU 870416 #25, N=3	135	7.64	0.77	62.0	1.27	7.0	0.79	68 32 348.5m
NRU 870615 #40, N=4	128	6.96	0.91	56.1	1.29	6.7	0.56	76 24 670 m
NRU 870714 #48, N=5	113	6.15	0.93	49.5	1.26	15.0	0.89	66 34 286.75m
NRU 870302 #17, N=6	110	7.49	0.85	54.5	1.13	5.0	0.62	70 30 Min loss at 1.2, 385.8 m.
NRU 870421 #27, N=7	115	5.95	0.93	49.0	1.20	5.0	0.44	72 28 268m.
NRU 870611 #39, N=8	130	9.26	0.90	61.5	1.37	10.0	1.00	83 17 1.3 loss from OTDR measurement
NRU 870602 #36, N=9	117	5.31	0.91	54.3	1.23	10.0	1.30	65 35 346 m, OTDR 1.3 loss=0.69
NRU 870511 #31, N=10	110	4.69	0.83	46.1	1.24	4.0	0.90	66 34 348.5
NRU 870506 #29, N=11	120	6.03	0.92	52.5	1.23	4.0	0.99	81 19 298.8m
NRU 870716 #49, N=12	107	5.10	0.88	42.1	1.35	3.5	0.54	69 31 1.3 loss from OTDR measurement
NRU 870617 #41, N=13	105	5.29	0.89	50.0	1.29	4.0	0.41	67 33 347m
NRU 870504 #28, N=14	118	6.70	0.85	44.5	1.37	5.3	0.96	67 33 1.3 loss from OTDR measurement
NRU 870513 #32, N=15	115	4.32	1.00	50.0	1.10	4.0	0.65	61 39 372m
NRU 870625 #43, N=16	131	6.36	0.89	52.0	1.35	4.0	0.59	77 23 1.3 loss from OTDR measurement.
NRU 870914 #63, N=17	90	5.63	1.00	42.5	1.24	10.0	8.20	60 40 A long sloping cutoff.
NRU 870805 #52, N=18	125	7.87	0.88	62.1	1.28	13.0	0.63	75 25
NRU 870820 #56, N=19	100	6.83	0.97	42.1	1.15	8.0	0.80	73 27
NRU 870824 #57, N=20	118	7.38	0.93	46.1	1.27	5.5	0.41	70 30
NRU 870817 #54, N=21	125	7.26	0.93	45.9	1.33	5.8	0.64	63 37 Loss from OTDR measurement.
NRU 870818 #55, N=22	100	7.54	1.00	43.0	1.29	5.0	0.60	74 26
NRU 870910 #62, N=23	116	7.86	0.91	46.6	1.27	7.4	0.78	72 28 Loss from OTDR measurement.
NRU 870924 #67, N=24	90	6.84	0.91	43.2	1.35	10.0	1.35	70 30 Loss from OTDR measurement. Very long tail from main cutoff hump.

Table 3.5e Matched Clad Single Mode Fibers

PREFORM	NORMALIZED DOPANT CONCENTRATION				TENS		RECOVERY PARAMETERS				
	GeCl4 core	GeCl4 clad	FC13 clad	F core	F clad	NOM mg/cm ²	n	t(1/2)	Ao	Af	Std. Dev.
NRL 870914 #63, N=1	4.50	0.00	0.00	0.01	0.00	6.6	1.8	12	420.0	10.0	4.95
NRL 870224 #15, N=2	7.80	0.00	0.00	0.02	0.00	7.3	2.0	15	260.0	10.0	3.18
NRL 870416 #25, N=3	5.03	0.80	0.00	0.01	0.18	3.5	4.0	70	12.2	0.3	0.51
NRL 870615 #40, N=4	7.83	0.58	0.00	0.01	0.12	4.0	3.0	100	1.9	1.5	0.24
NRL 870714 #48, N=5	6.73	0.00	0.00	0.02	0.00	5.0	2.0	20	60.0	7.0	1.51
NRL 870302 #17, N=6	4.34	0.00	0.00	0.01	0.00	5.3	2.3	22	243.0	0.0	2.12
NRL 870421 #27, N=7	8.21	0.70	0.00	0.02	0.14	7.7	4.0	25	7.0	0.0	0.25
NRL 870611 #39, N=8	5.10	0.39	0.00	0.12	0.09	6.6	4.0	350	9.1	6.9	0.27
NRL 870602 #36, N=9	7.80	0.88	0.00	0.01	0.17	4.7	4.0	75	4.9	0.1	0.15
NRL 870511 #31, N=10	10.03	0.82	0.00	0.03	0.18	5.9	10.0	60000	4.8	0.0	0.12
NRL 870506 #29, N=11	7.90	0.72	0.00	0.21	0.17	2.1	4.0	20000	5.7	2.6	0.26
NRL 870716 #49, N=12	10.63	1.21	0.00	0.19	0.26	2.2	4.0	80	4.0	0.6	0.22
NRL 870617 #41, N=13	10.72	0.76	0.00	0.13	0.17	2.4	4.0	70	4.5	0.0	0.58
NRL 870504 #28, N=14	5.76	0.79	0.00	0.11	0.17	1.8	4.0	2000	11.4	7.2	0.23
NRL 870513 #32, N=15	9.15	1.52	0.00	0.17	0.32	4.8	4.0	100	5.1	4.7	0.22
NRL 870625 #43, N=16	9.05	0.92	0.00	0.20	0.19	3.7	3.5	15	3.7	0.0	0.22
NRL 870914 #63, N=17	4.50	0.00	0.00	0.01	0.00	6.6	1.8	12	420.0	10.0	4.95
NRL 870605 #52, N=18	5.55	0.00	0.00	0.02	0.00	1.6	2.3	28	237.0	0.5	2.30
NRL 870820 #56, N=19	5.48	0.00	0.09	0.09	0.05	6.4	4.0	300	8.0	1.0	0.67
NRL 870824 #57, N=20	5.60	0.00	0.14	0.01	0.05	1.6	4.0	50	4.3	2.8	0.10
NRL 870817 #54, N=21	4.10	0.00	0.44	0.01	0.09	1.5	4.0	60	5.6	2.6	0.27
NRL 870818 #55, N=22	5.48	0.00	0.39	0.08	0.07	6.4	3.0	20	7.5	4.5	0.75
NRL 870910 #62, N=23	5.26	0.00	0.53	0.04	0.10	1.4	3.0	25	5.2	3.7	0.19
NRL 870924 #67, N=24	4.62	0.00	0.66	0.01	0.10	6.6	2.0	25	6.5	2.8	0.86

This page unintentionally blank

SCHEMATIC OF MCVD

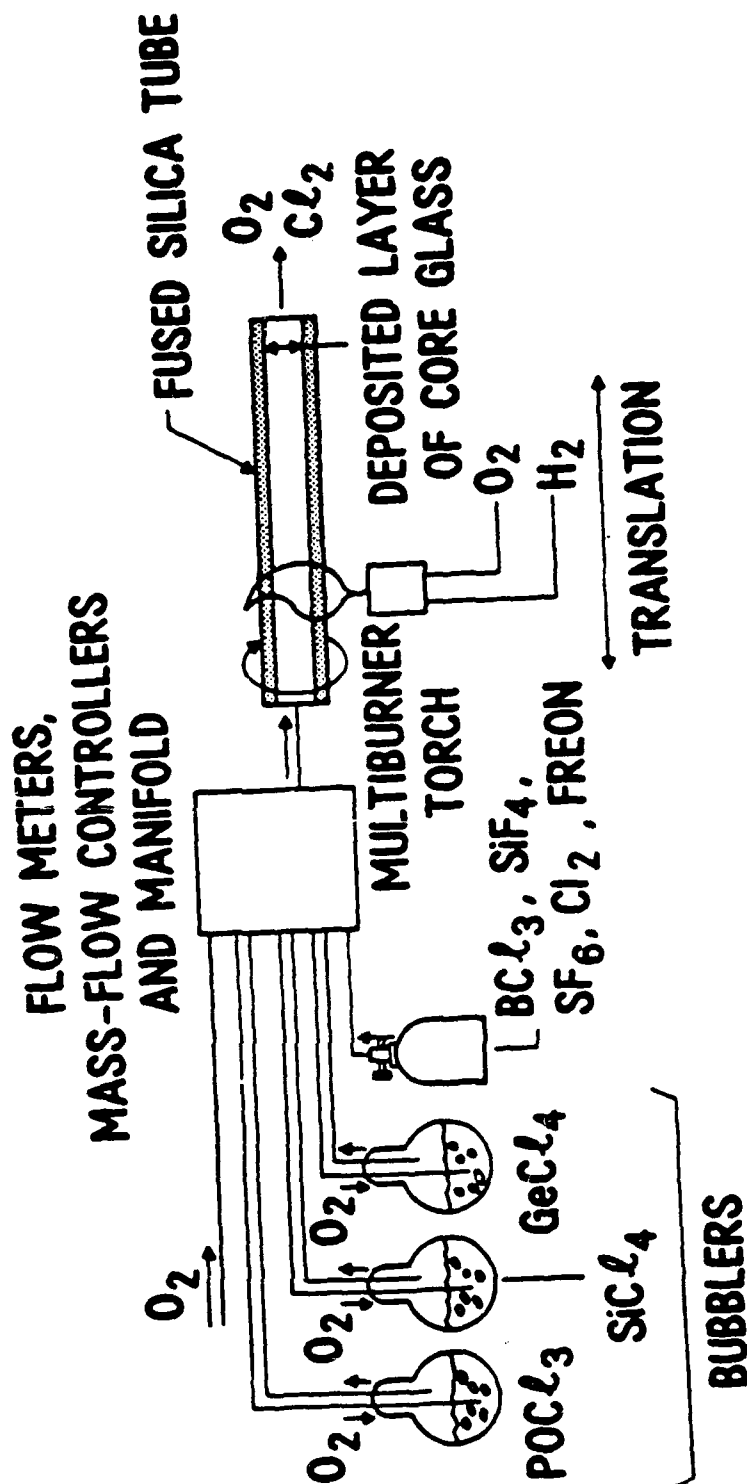


Figure 3.1 Schematic of a typical MCVD apparatus. Not shown are the controls for maintaining accurate temperature of the reaction zone and tube dimension by providing back pressure.

AK FIBER

1 UM SPOT/1 UM STEPS

DATE: 9-2-87

EPMA 126-87#5

FILE # 2552

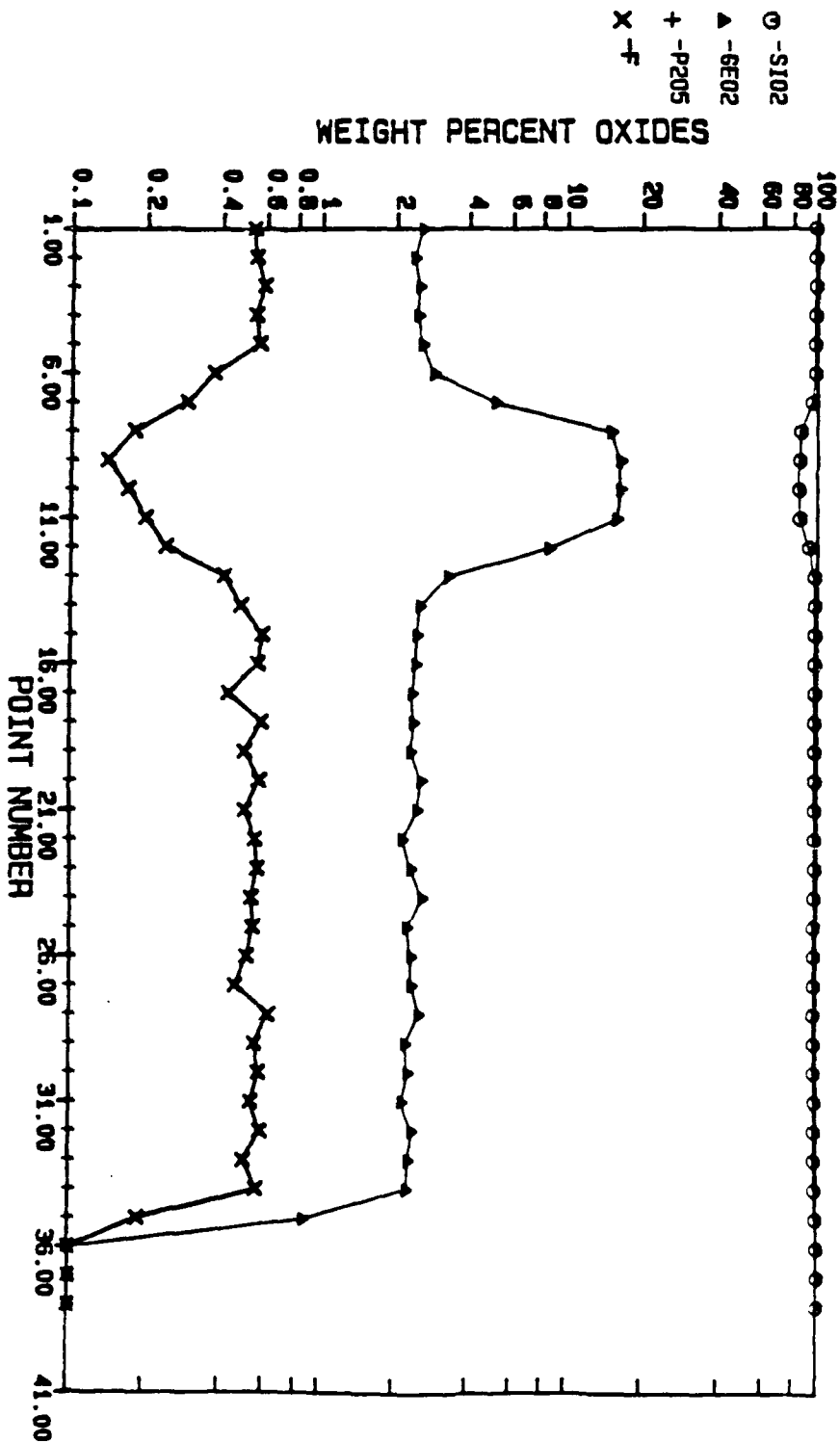


Figure 3.2 Typical results of electron microprobe analysis showing weight percents of GeO₂, SiO₂, P₂O₅ and F across the fiber core (centered 7.5 microns) and cladding.

CHAPTER 4

OPTICAL CHARACTERIZATION

The preforms and fibers in this study were characterized optically to assure that they had appropriate transmission characteristics and state-of-the-art intrinsic properties. The waveguide parameters determined by our measurements were the numerical aperture, core diameter, second mode cutoff wavelength, spectral intrinsic attenuation, and distribution of optical power in the core and clad at 1.3 μm .

The numerical aperture and core and clad diameter of the preform were determined by measuring the index of refraction of the preform across its diameter. A preform profile also provides the core/cladding diameter ratio of the eventual fiber and the degree of cylindrical symmetry of the preform. From this information, one can determine a target outer (clad) diameter of the fiber which will result in a core of the appropriate diameter to provide a second mode cutoff near 1.2 μm .

The numerical aperture is defined as half the acceptance angle of the light that can be injected into the fiber and is related to the indices of refraction of the core and cladding:

$$\text{N.A.} = \sqrt{n_1^2 - n_2^2} = \sin \theta \quad (4.1)$$

where n_1 and n_2 are core and cladding indices, respectively, and θ is the half angle.

The preform profiler used for this study was the P101 Preform Analyzer manufactured by York Technology Limited. The profiler works on the principle of dynamic spatial filtering, as illustrated in Figure 4.1. The refraction of a ray of light transversing the preform is measured as the preform is stepped through the beam with an increment of approximately 15 μm . The resultant deflection function is then numerically integrated to give the index

profile.[1]

Once the fiber was drawn from the preform, the cutoff wavelength of the second mode and the spectral attenuation were measured. Perhaps the most critical parameter is the cutoff wavelength, i.e. that wavelength where higher order modes cease to propagate as guided modes in the fiber. The target cutoff wavelength chosen for this study was $1.25\text{ }\mu\text{m}$ to assure that the fibers were single mode (i.e. propagating only the first mode) at the operational wavelength of $1.3\text{ }\mu\text{m}$, and that the first mode bending edge (cutoff) was not yet apparent. If the second mode cutoff wavelength were much less than $1.3\text{ }\mu\text{m}$, the fiber would have high bend sensitivity, and if the cutoff wavelength were greater than $1.3\text{ }\mu\text{m}$, the fiber would operate in the multimode regime.

The standard bend-induced loss method was used to measure the cutoff wavelength.[2] The apparatus is shown in Figure 4.2. A fiber length of 1.5 meters was used with a single, one-inch radial bend to induce high order mode attenuation. The fiber was mode-stripped at the output end so that any weakly guided modes in the cladding or jacketing were not considered. The transmission of the fiber was measured from 0.4 to $1.7\text{ }\mu\text{m}$, and the cutoff wavelength was determined by comparing the transmission of a relaxed, straight fiber to that with an induced bend.

The cutback method was used to determine the spectral attenuation. The apparatus is the same as the one used for the cutoff measurement (Figure 4.2). The technique consists of measuring the transmission of a long fiber sample (200 - 300 meters), and then repeating the measurement for the first 2 meters of the sample without disturbing the launching conditions. The fiber was again mode-stripped at the output end to avoid measuring power guided through the short length in leaky modes, in the cladding, or in the jacketing. The spectral attenuation measurements were used to determine the optical loss per

unit length of the fiber over the transmission spectrum of 0.4 to 1.7 μm :

$$\text{dB/km} = 10/l \log I_0/I, \quad (4.2)$$

where I_0 and I are the power transmissions of the short and long piece, respectively, and l is the length of the long fiber minus the short length, in kilometers.

We have recently measured the mode cutoff wavelength and spectral attenuation of a fiber which has been measured at NBS-Boulder and is being used as a "standard" for calibrating measurement equipment. Our results were identical within experimental error.

The spectral attenuation of the fibers is a sensitive probe of the consistency from sample to sample. This qualitative survey of impurity content, Rayleigh and large scale scattering provides assurance that the starting MCVD chemicals are consistently pure, that collapse and deposition conditions are correct, and that the fiber draw conditions are acceptable. Equally important to this study is the confirmation that the quality and characteristics of the waveguides fabricated at NRL are representative of industrial samples, in terms of water content (< 1 ppm), low intrinsic loss (≤ 1 dB/km at 1.3 μm), and background scattering losses. The theoretical intrinsic transmission at 1.3 μm is 0.3 dB/km, determined by Rayleigh scattering and the infrared multiphonon edge. If the measured attenuation at this wavelength is significantly greater, or if there are anomalies in the spectral transmission, one can infer glass properties that could potentially obscure the results of the study.

The impurities that contribute to a significant amount of loss in the wavelength range of 0.4 to 1.7 μm are primarily the transition metals and water; the former absorbs in the wavelength range of 0.6 to 1.0 μm (although Fe^{2+} has a broad absorption centered near 1.1 μm), while the latter, in the form of SiOH , has a strong second vibrational overtone band at 1.39 μm and a

combination band with Si-O at $1.24\text{ }\mu\text{m}$. The absorption at $1.39\text{ }\mu\text{m}$ is the strongest in the $0.9 - 1.6\text{ }\mu\text{m}$ range; as little as 1 ppm of water will add 40 dB/km excess loss at $1.39\text{ }\mu\text{m}$. Our typical excess loss of 3 - 10 dB/km at $1.39\text{ }\mu\text{m}$ indicates an OH content of $< 0.25\text{ ppm}$. The incorporation of transition metals into our samples has been essentially undetectable both by optical spectroscopic measurements and by spark source mass spectroscopy (Table 4.1).

The diameter of the fiber core and the mode field diameter were used to determine the fraction of the power guided in the fiber core and the cladding. A major concern with the power distribution is that if a significant amount is guided at distances greater than a few core diameters in the cladding, the radiation response may be dominated by the damage in the much more radiation sensitive substrate tube, which is fabricated from fused natural quartz.

The distribution of optical power in the single mode fiber was measured by the near field technique.[3] The near field measurement is, in theory, the simplest and most direct method and therefore the most reliable for fibers operating over a wide range of "V" numbers. This method is illustrated in Figure 4.3. The test fiber was coupled to a single mode fiber pigtailed $1.3\text{ }\mu\text{m}$ laser diode modulated at 1 kHz. The output end of the fiber was accurately cleaved so that the cleave angle was less than 2 degrees. This face was imaged onto a detection plane by a 60X objective lens placed approximately 72 cm from the detector. The detector was scanned across the diameter of the image to obtain the power distribution of the at the face of the fiber. The fiber was waxed into a V groove, to assure that there was no induced stress that will distort the guided mode. The fiber was mode stripped just before the V groove, which was mounted on a high precision XYZ translational stage to enable focusing and alignment of the fiber's center on the detector.[4] The detector scan rate, modulation frequency, and lock-in amplifier time

constant were optimized to minimize power fluctuations and drift errors. The system's spatial resolution, which is a function of the numerical aperture and operational wavelength of the fiber, was limited to 3 - 5 μm . The data were recorded as intensity vs. radius; a numerical integration gives the core/clad power ratio based on the fiber core diameter measured either from the fiber index profile or from a scanning electron microscope image.

The fiber index profiler operates on the refractive near field technique,[5] which is the direct measurement of the local index of refraction at the face of a cleaved fiber, in contrast to the transverse method used for profiling the preform. The basic principles and apparatus are illustrated in Figure 4.4. This technique utilizes the light refracted out of the fiber, neglecting the guided and leaky modes in the fiber. The index of refraction is determined by measuring the exit angles of the refracted cone of light from a 100X oil immersion objective focused on the fiber face. A dilation of the cone of light occurs when the index of the fiber at that point is lower in relation to the index matching oil. A contraction of the light cone corresponds to an increase in the index. The refracted power from the fiber face, located at one focus of an elliptical reflector, is imaged onto a detector, located at the other focus of the ellipse.[6] The refractive index at the scan point is proportional to power. The index is then plotted as a position of the fiber face with a resolution of 0.3 - 1 μm , dependent upon focusing accuracy. From this index profile one can determine the absolute size and index of refraction of the core and cladding and the latter can be used to determine the numerical aperture of the fiber, as shown in equation 4.1.

REFERENCES

1. York Technology Limited, Model P101 Preform Analyzer Handbook, York

Technology Limited, 1981.

2. Jeumhomme, Luc S. Single Mode Fiber Optics--Principles and Applications, Marcel Dekker Inc., New York (1983).
3. Kim, Ernest M., Douglas L. "Measurements of Far-Field and Near-Field Radiation Patterns from Optical Fibers," U.S. Dept. of Commerce, National Bureau of Standards, Washington D.C. (1981).
4. Anderson, William T., Philen Dan L. "Spot Size Measurements for Single-Mode Fibers - A Comparison of Four Techniques," J. Lightwave Tech, LT-1 (1): 20-26 (1983).
5. White K.I., "Practical Application of the Refracted Near-Field Technique for the Measurement of Optical Fibre Refractive Index Profiles," Opt. Quant. Elec. 11: 185-196 (1979).
6. Stewart W.J. "Optical Fiber and Preform Profiling Technology," IEEE J. Quantum Electronics, QE-18 (10): 1451-1466 (1982)

Table 4.1

Mass Spectrographic Analysis (ppmw) of Synthetic Silica Samples
 Elements Not Reported < 0.02 ppma

Element	SS2	Mitsubishi	SSW2	SS 300	NRL MCVD
Li	< 0.1	≤ 0.1	7.0	20.0	0.007
Be			0.5	0.2	
B	0.05	4.0	0.2	6.0	0.2
F				0.3	0.2
Na	1.0	5.0	0.2	0.2	0.2
Mg	≤ 1.0	2.0	2.0	≤ 2.0	4.0
Al	1.0	3.0	7.0	3.0	5.0
P	0.1	0.1	≤ 0.3	0.3	0.8
S	< 1.0	< 2.0	12.0	7.0	3.0
Cl	30.0	3600.0	25.0	1000.0	470.0
K	0.4	4.0	6.0	6.0	10.0
Ca	10.0	20.0	4.0	4.0	2.0
Sc			0.5	≤ 0.5	
Ti	≤ 0.05	≤ 0.01			≤ 2.0
V	≤ 0.05	≤ 0.05	0.08	0.2	≤ 0.3
Cr	0.2	0.4	3.0	5.0	< 5.0
Mn	0.2	0.2	0.6	0.8	0.3
Fe	≤ 3.0	≤ 3.0	≤ 15.0	≤ 15.0	6.0
Co	≤ 0.1	< 0.1	≤ 0.2	≤ 0.6	
Ni	< 2.0	< 2.0	2.0	6.0	2.0
Cu	≤ 0.2	≤ 0.7	0.9	0.9	0.9
Zn	≤ 0.3	≤ 0.3	0.3	2.0	0.3
Ga			≤ 0.2	≤ 0.2	
Ge				≤ 0.3	
As	3.0	1.0	≤ 0.2	0.4	
Se				≤ 2.0	
Br				≤ 0.4	
Sr	15.0	1.0		0.9	
Y				0.1	
Zr	1.0	5.0		0.3	
Nb				0.1	
Ba				0.3	
La				1.0	
Ce				1.0	
Pr				0.3	

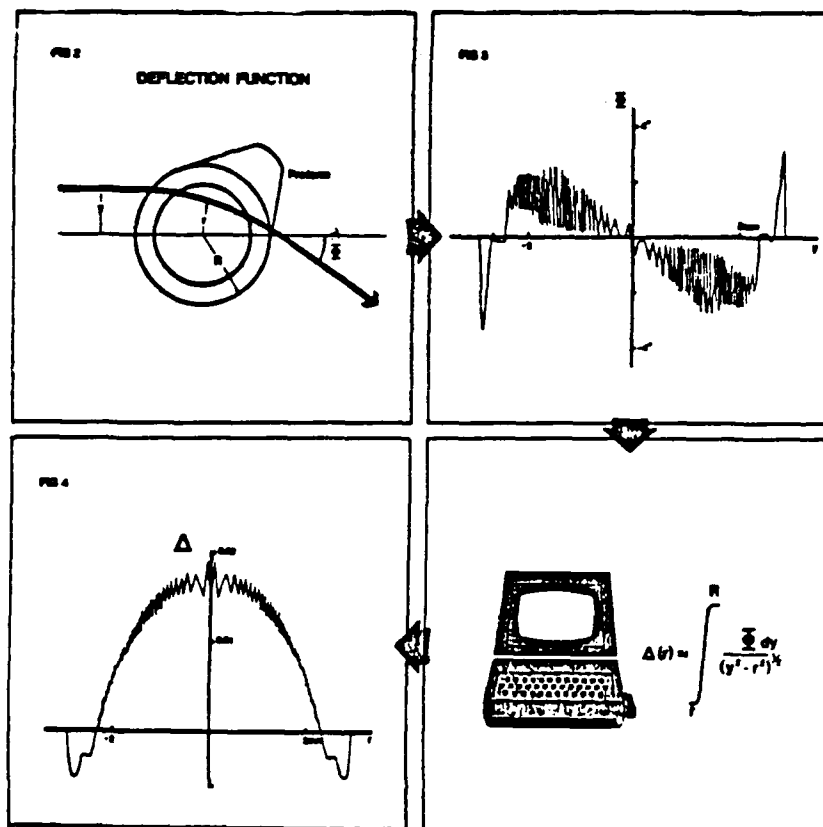
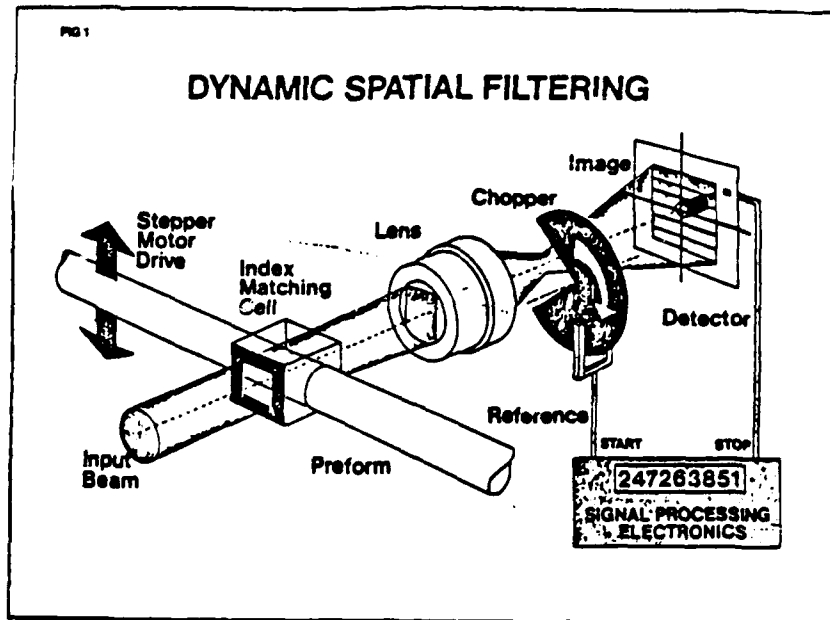


Figure 4.1 Dynamic spatial filtering technique for determining refractive index profile of fiber preforms. The deflection of the beam was measured with a 10 μm step (2) to give the deflection function (3), which was then integrated by computer, resulting in the profile (4).

Spectral Transmission Measurement

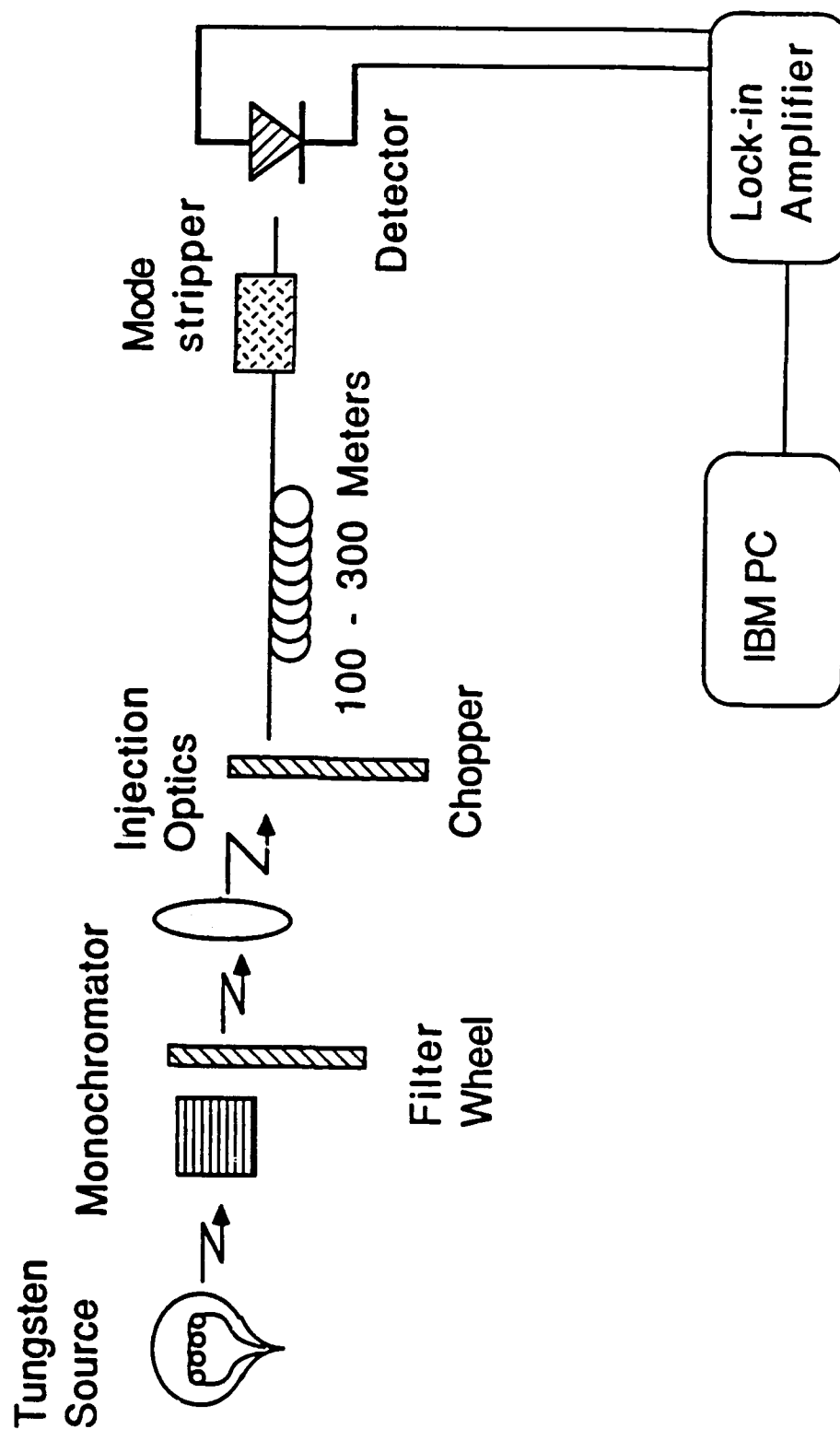


Figure 4.2 Apparatus for measuring single mode cutoff wavelength and spectral transmission of single mode fibers. For the cutoff measurement a 1.5 m length of fiber was used, and a comparison was made between the transmission when loosely coiled and when tightly bent (see text).

Near-Field Measurement

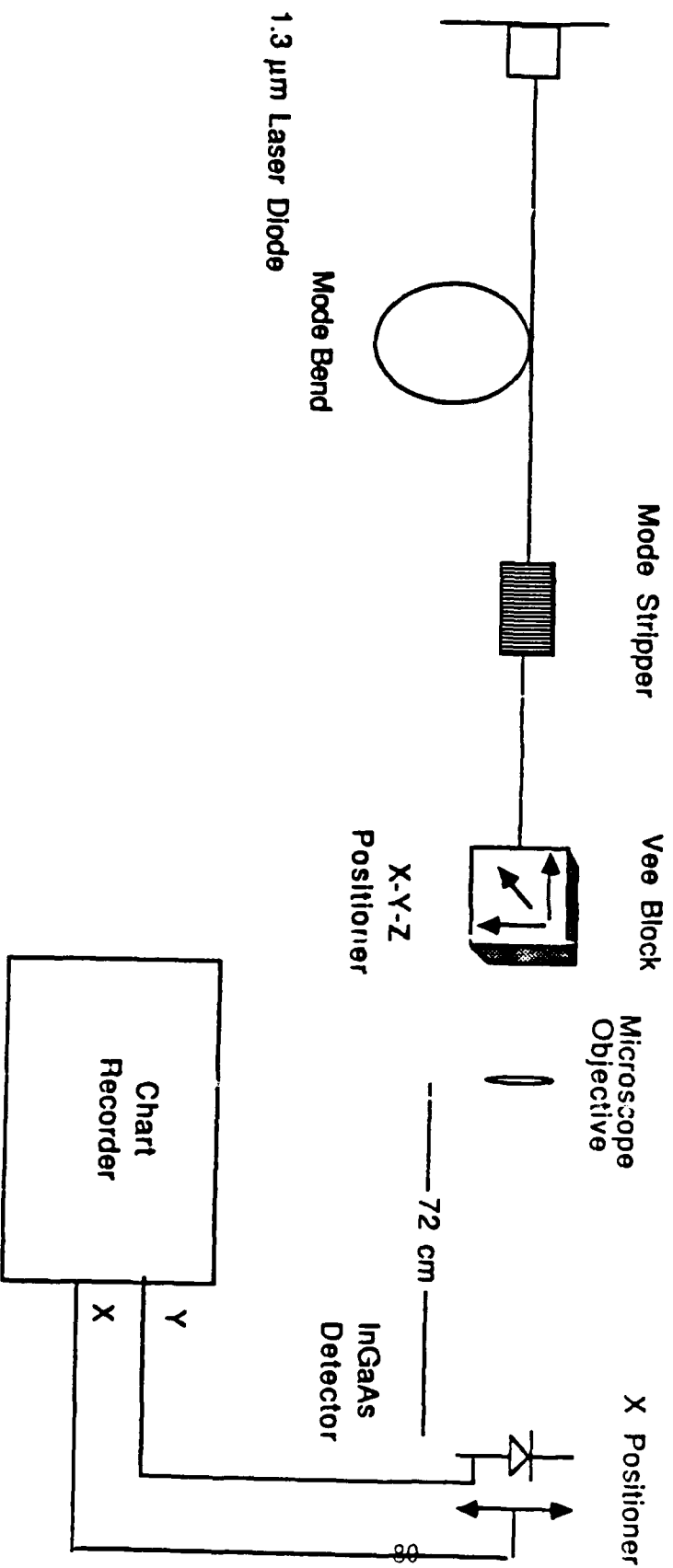


Figure 4.3 Apparatus for near-field measurement of the mode field diameter in the single mode fiber.

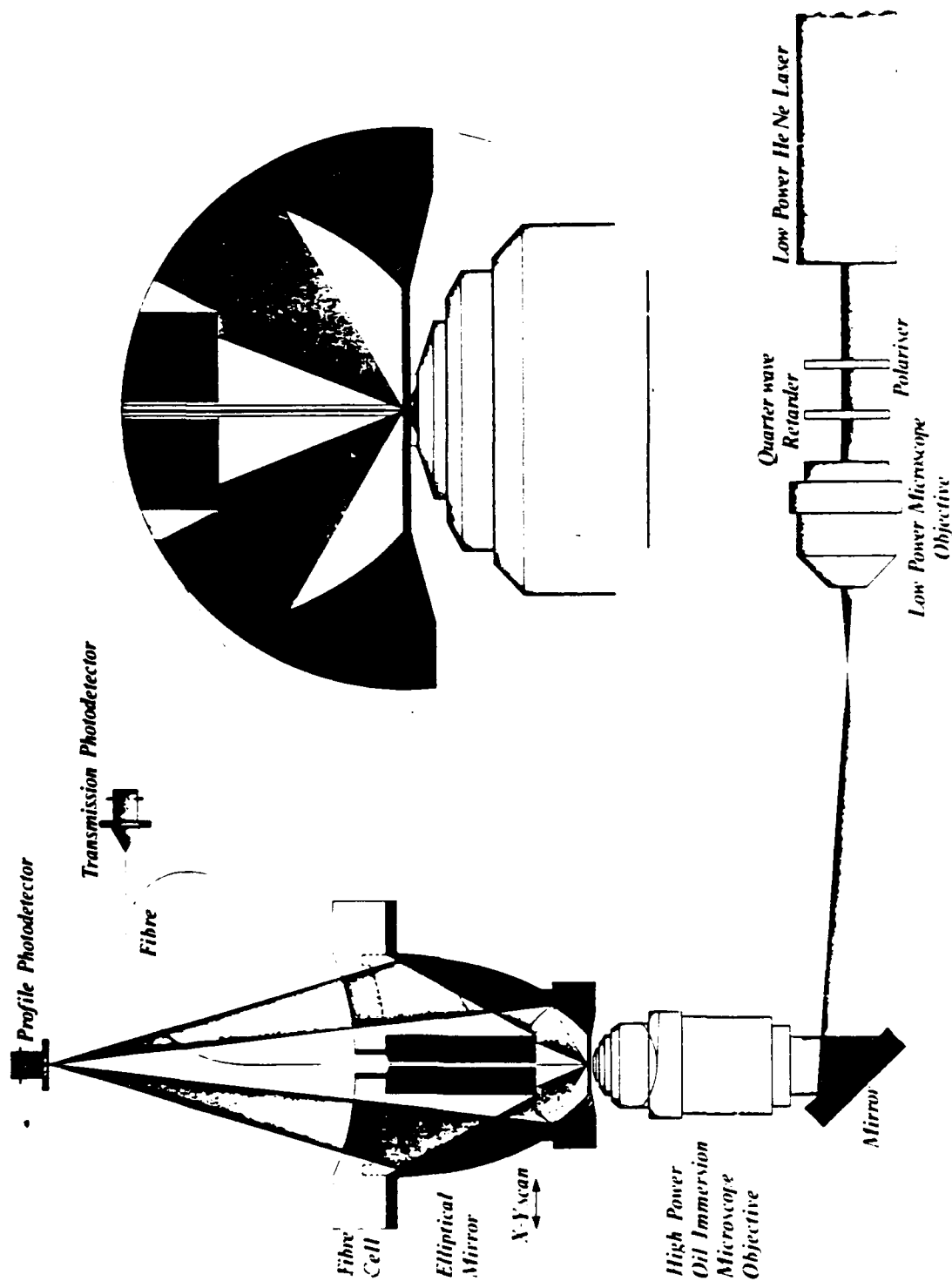


Figure 4.4 Refracted near field technique for measuring the fiber index profile. The fiber is placed at one focus of an elliptical reflector. The variations in index cause a change in the angle at which the light is refracted from the fiber. Appropriate blocking apertures cause this to change the light intensity falling on the photodetector located at the other focus of the ellipse.

Measurement: 0012, at 19:23 on 77 777 77
Sample code: NRL 070714, N=5, 15um, 0 DEG

Naval Research
Laboratory

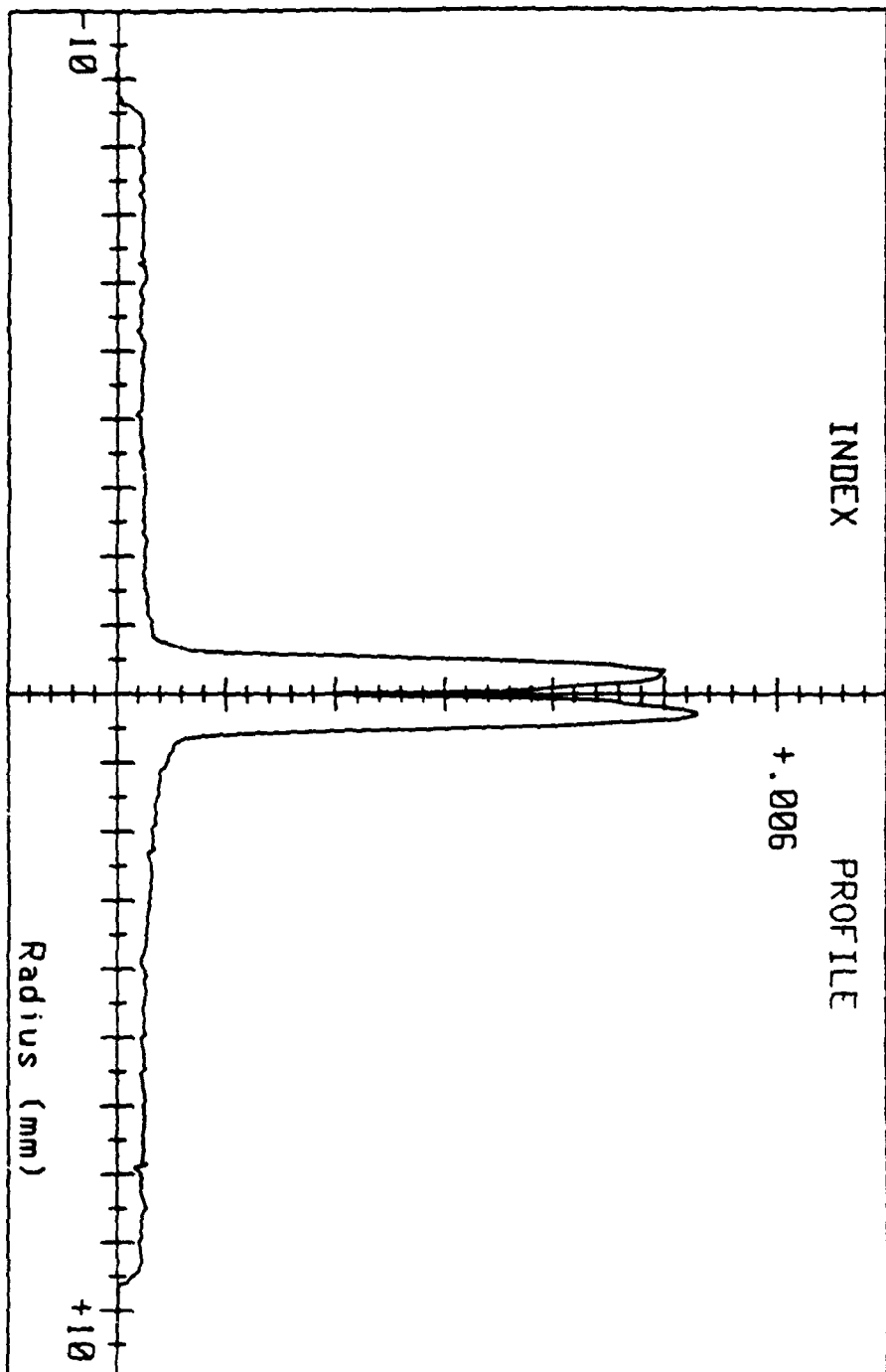


Figure 4.5 Refractive index profile of a typical matched clad single mode fiber preform made in this study.

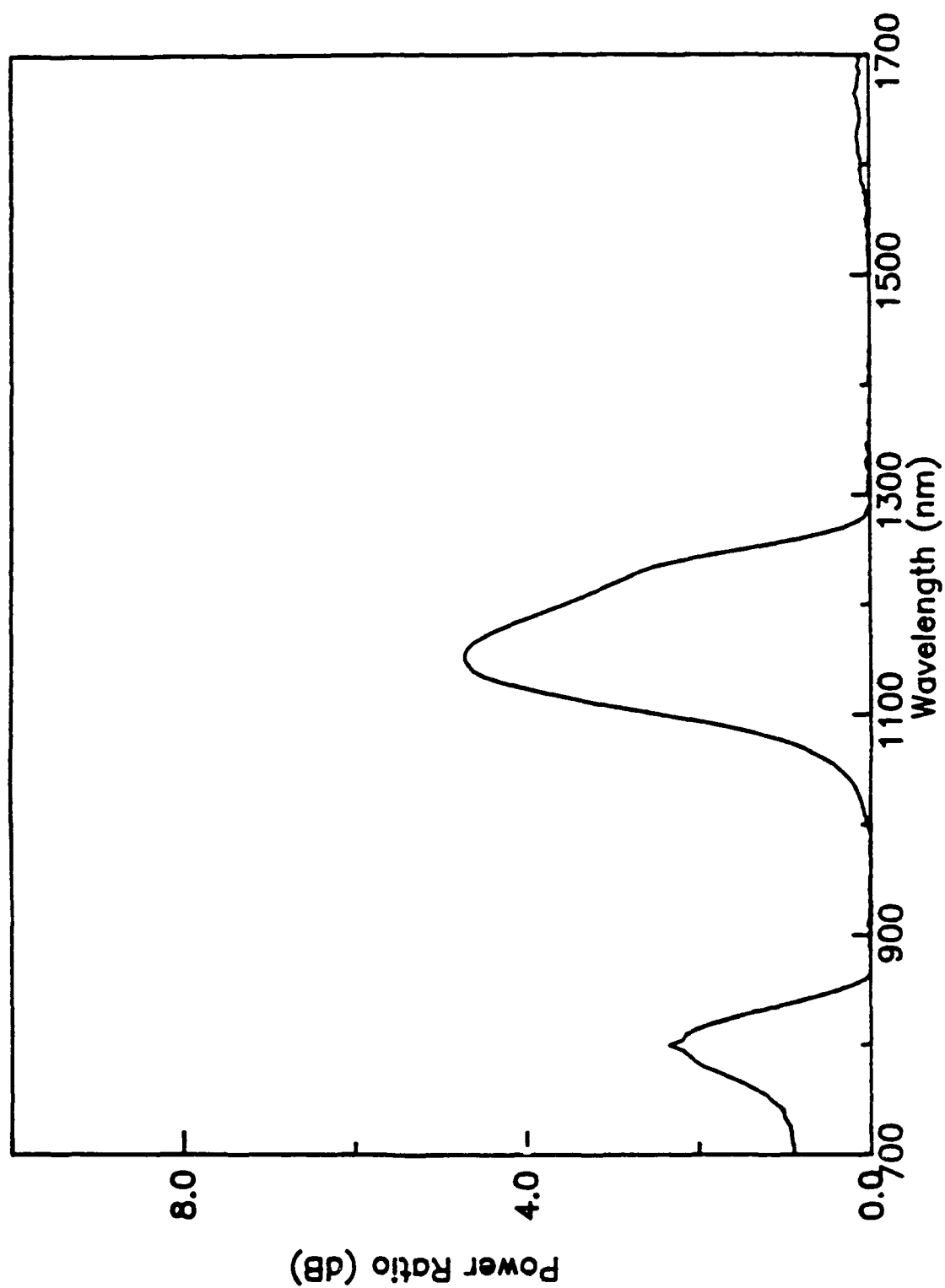


Figure 4.6 Spectral transmission ratio of bent and straight single mode fiber showing the large second mode cutoff and the location of the cutoff wavelength at 1.27 μm

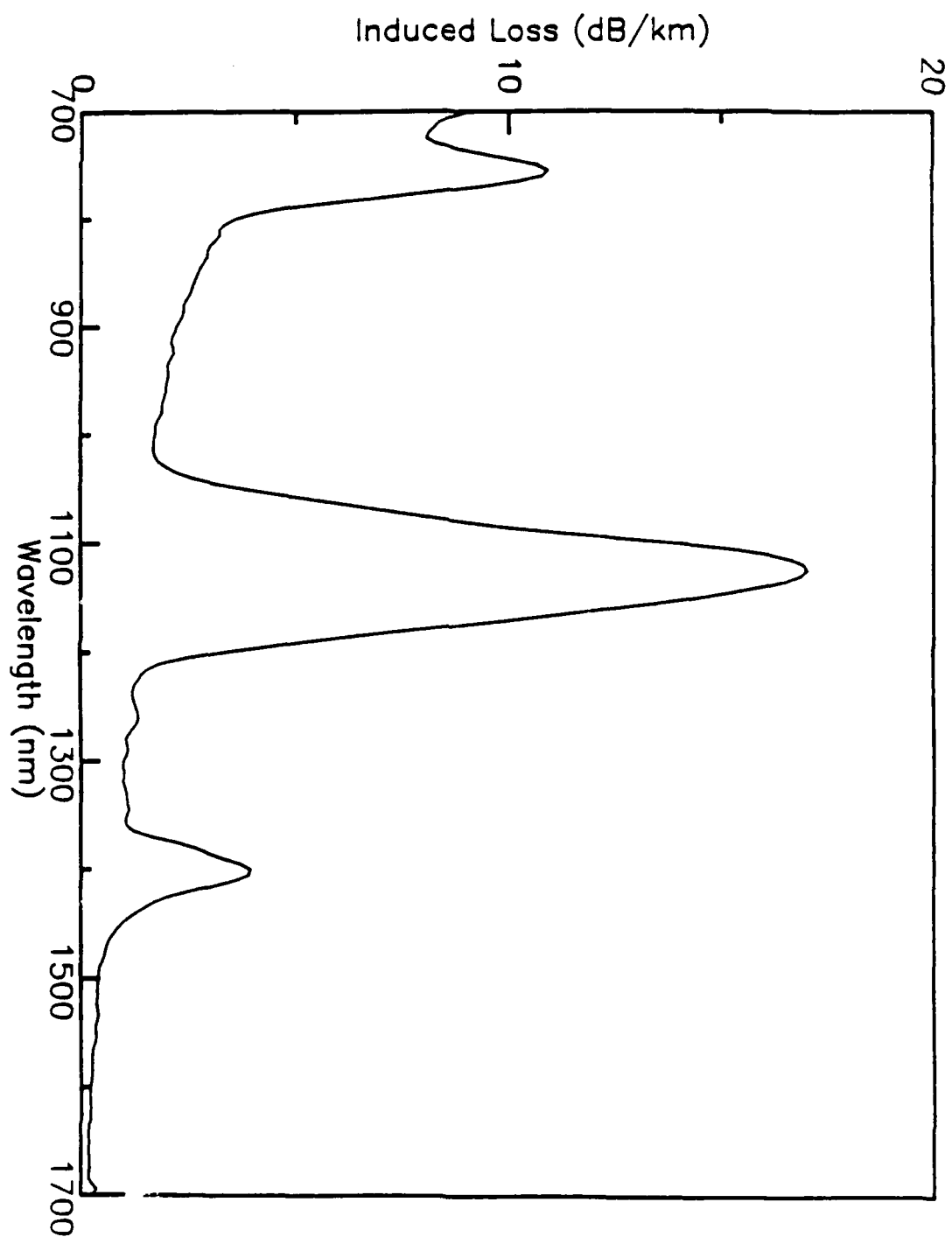


Figure 4.7 Typical spectral attenuation data for single mode fibers fabricated in this study. The large peak near $1.1 \mu\text{m}$ is the second mode cutoff; the weak peak near $1.4 \mu\text{m}$ is due to OH impurities at levels less than 1 ppm.

CHAPTER 5

RADIATION DAMAGE MEASUREMENTS

TEST PROCEDURE

The ultimate concern of this project is the magnitude and time evolution of the attenuation induced in single mode fibers by a radiation environment. As described in Chapter 1, radiation parameters chosen for the study consisted of a total dose of 2000 rads and a temperature of -35 C. Although the MIL-SPEC temperature range is -55 to 80 C, a higher temperature of -35 C was selected as being the minimum for a telecommunications system in the continental US. The total dose of 2000 rads was a compromise between lower doses that might be experienced in actual prompt gamma or fallout scenarios and the ability to achieve measurable induced attenuation in a practical length of fiber, 50-100 m. The dose was delivered at a rate of approximately 4500 rads/min, which mimics the delayed gamma component.

The responses of the most radiation-resistant, state-of-the-art single mode fibers are in the 0.001 dB/km-rad range at 1.3 μm . [1] Therefore, if a 50 m length of fiber is tested, a 2000 rad dose would induce a loss of 0.1 dB. This loss was considered to be the minimum required for accuracy and sufficient signal-to-noise. However, since fibers in real deployments may be exposed to lower delayed gamma or fallout doses, it is important to establish whether irradiations at 2000 rads can accurately extrapolate to lower doses. (Extrapolation to higher doses will always give the worst-case and may significantly over-estimate the incremental loss if saturation occurs with increasing dose.) To determine whether extrapolation to lower dose was feasible, one fiber was irradiated at both 2000 and 400 rads in lengths of 50 and 200 m, respectively. As shown in Fig. 5.1, where the two data sets have been scaled by their respective doses, both the magnitudes of the initial loss

and the recovery behaviors were independent of dose in this range. Since saturation with dose is typically observed at doses $\geq 10^4$ rads, the data obtained in the present study is applicable in the 0-10,000 rad range.

Figure 5.2 is a schematic of the apparatus used to measure the radiation-induced loss in the fibers as it has evolved over the life of the program. A 1.3 μm single mode laser diode with a single mode fiber pigtail was used as the light source, and the diode was modulated at 1 kHz with a 50% duty cycle so that phase sensitive detection could be used on the output. The pigtail was fusion-spliced to the test fiber, which had 10 m leads into and out of the ^{60}Co pool. The 50 m sample coil was maintained at -35 ± 0.5 C by means of a variable temperature chamber. Gaseous N_2 was passed through a heat exchanger coil immersed in a liquid nitrogen dewar attached to the sample cell. The gas then entered the sample can and was reheated to the desired -35 C temperature; the heater current was controlled by a Eurotherm temperature controller above the surface of the water.

Initially, the laser diode was fused directly to the test fiber without the splitter and reference fiber. Although adequate stability was usually obtained, thermal cycling of the room air conditioner during the summer caused significant long term fluctuations in the test fiber output power I . An example is shown in Fig. 5.3. The difficulty in reducing these data is obvious, so a portion of the laser diode output was used to provide a reference I_0 . The voltage outputs of the two detectors were processed by lock-in amplifiers whose outputs were fed to a log ratio amplifier to provide the attenuation $A = \log(I_0/I)$ to the computer, and the induced loss in dB/km was then calculated as $A(\text{dB/km}) = 10A/1(\text{km})$. The improvement in long term drift is obvious in comparing Fig. 5.3 and 5.4. (The hump in the data of Fig. 5.4 near 2000 sec is due to a temporary instability in the temperature and is not evident in data sets where better temperature control is maintained.)

Microbending noise was found to be most noxious on fibers with small cores and small numerical apertures, causing an excessive amount of handling noise and offsets when the fibers were inserted and removed from the source. To solve this problem, several measures were implemented: Lengths of commercial single mode fiber were used as the pigtailed spliced to the test fiber just outside the sample can. A sheet metal trough was fabricated to support the fiber between the optical table and the entrance to the source during the exposure and for an hour's recovery. In all cases, bend radii were kept to >6 cm by supporting the fiber. When the irradiation was completed, the fiber was not withdrawn fully from the pool since it was found that the handling involved in this maneuver induced a large amount of noise and offsets in the data. Rather, the sample can was raised approximately 4 feet to a position where the additional dose was negligible, and it was supported there for approximately one hour. Then, the can was raised to the surface, and whatever offset was induced at this point was clearly recognizable and could be removed from the data.

Early in the program the log ratio output was input to a chart recorder, and the attenuation values at selected times were calculated by hand and transferred to computer files for further plotting and processing. This procedure resulted in some smoothing of the data as the offsets and glitches were taken out during data reduction. Subsequently, computer data acquisition was implemented, and large data sets of 1500-2500 points could be recorded for each fiber. (As in the case of the chart recorder, both the growth of the attenuation during exposure and the recovery following irradiation were recorded. The recovery data were then used for further analysis.) The use of the reference arm obviated the necessity to massage the data; rather, a more manageable series of 30-50 points was selected from the full data set for input to the kinetic analysis. Fig. 5.5 is an example of such a reduced data

set and indicates the fidelity of this procedure.

COMMERCIAL FIBERS

A set of commercially-available single mode fibers was obtained for evaluation through FiberTrak, Inc. Corning provided two commercially-available fibers: Corning 1521 (a matched clad fiber optimized for 1.3 μm operation) and Corning 1524 (a segmented core, dispersion-shifted fiber for 1.55 μm), and a prototype Ce-doped Corning fiber, which was unfortunately single mode at 0.85 μm so that the mode field penetrated well into the cladding at 1.3 μm . Although the radiation response of the Ce-doped fiber was evaluated, because it was a laboratory prototype not optimized for 1.3 μm , the results will not be reported. Other fibers provided through FiberTrak included a standard Northern Telecom waveguide, and standard Ge-doped silica and pure silica core Sumitomo waveguides. Additionally, measurements were made on fibers provided by other manufacturers, including AT&T standard and radiation-hardened fibers, Lightwave Technologies, Inc. commercial and prototype fibers, a Schott fiber fabricated by the plasma impulse chemical vapor deposition (PICVD) technique, and a Philips fiber fabricated by the plasma chemical vapor deposition (PCVD) process. Two MCVD fibers fabricated at NRL were also included in this early study.

The results are shown in Figs. 5.6-5.11 and in Table 5.1, which contains the core and cladding dopants and the results of fitting the recovery data to kinetic analyses, as described in Chapter 6.

It was immediately apparent that there was a wide variation in the radiation responses of the fibers. For radiation hardening, there are basically two points to consider with the recovery data: the loss remaining 10 minutes following the radiation exposure is an indication of the system loss following a weapons detonation, and the loss (and slope) after 10^5 sec is

indicative of the response to low dose rate fallout exposure. In the first case, the fiber losses at 600 sec varied from 7.4-7.7 dB/km for the Philips and Corning 1521 fibers (Figs. 5.11 and 5.7) to 0.5-0.8 dB/km for the Schott and Spectran Rad Hard fibers (Figs. 5.10 and 5.6). Since the intrinsic loss of high quality single mode fibers is 0.5 dB/km, the incremental losses of > 7 dB/km in the Corning 1521 and Philips fibers represent a significant degradation, while losses < 1 dB/km could likely be incorporated in the budget. However, the incremental attenuations in the Corning 1521 and Philips fibers are known to be less at higher temperatures, and these waveguides continue to recover even at this low temperature. If the system is operating nearer to ambient or if the downtime following weapons detonation can be extended, the behavior of these fibers would be acceptable.

The long term (permanent or low dose rate) response of the fibers likewise varies between 2.3 dB/km for the standard Spectran fiber and essentially 0 dB/km for the AT&T commercial, Schott, and Spectran Rad Hard waveguides. Also of importance is the slope at 10^5 sec, which is indicative of long term recovery processes. It is generally true that the fibers with the higher permanent losses have flatter slopes and would therefore experience greater damage under low dose rate fallout exposure. About half of the fibers studied have at least 1.5 dB/km permanent loss at this dose; this will have to be incorporated into the design loss margin of the system.

It should be emphasized again that the loss data shown in these figures are for a worst case radiation exposure of 2000 rads, which would be the maximum expected for a buried cable under either prompt or heavy fallout conditions. It is important to establish whether these measurements can be extrapolated to other doses, and in particular to the substantially lower doses which might be experienced outside the heavy exposure region. The data shown in Fig. 5.1 establish that extrapolations from the 2000 rad measurements

to much lower doses are valid.

It is possible to derive some qualitative understanding of the relationship of fiber dopants and radiation response by sorting the data in Table 5.1 with respect to each recovery parameter. The obvious goals for a radiation hard fiber are: 1) low order of recovery kinetics (n), which will provide the steepest recovery curve, 2) low values of τ so that the recovery occurs in the shortest interval, 3) low A_0 to minimize the fiber's radiation response to prompt gamma exposure, and 4) small A_f so that the permanent damage and fallout response will be minimal.

Examination of the data in Table 5.2 shows that the fibers with the lowest values of n are the Sumitomo fibers fabricated by the VAD method and the LTI commercial fiber; both the LTI and Sumitomo Z fibers have pure silica cores. The Schott fiber also has a pure silica core, but it has an n value of 3. It should be mentioned, however, that the fitting procedure is not particularly sensitive to changes in n of ± 0.5 so that the difference between the Schott fiber and the other silica core fibers may not be significant. As discussed in Chapter 6, the physical interpretation of recovery with $n=2$ is diffusion-limited bimolecular recombination, and there is ample evidence that it is molecular hydrogen which is diffusing in irradiated silica.[2] Note also that with the exception of the LTI Prototype 2 fiber and NRL 860814, those fibers with the highest values of n have both Ge and F in the core.

As shown in Table 5.3, the fibers with the lowest values of the "half-life" τ are likewise found to be those with undoped silica cores and fluorine-doped silica clads. The exceptions here are the Spectran Rad-Hard and Corning 1521 fibers, which both have Ge-doped silica cores.

As shown in Table 5.4, the lowest values of initial loss A_0 are found in the 5 fibers which contain P doped into the cladding. This result is not unexpected since P doping has been shown in extensive prior studies to

decrease the radiation response of fibers at low temperatures.[1] Interestingly, the 5 fibers with the lowest initial losses are made by the MCVD process, and with the exception of the LTI Prototype 1 fiber, the 10 fibers with the lowest values of A_0 are made by either the MCVD or VAD process. Those fibers with the largest initial losses are made by the outside, PCVD or PICVD process.

The value of the permanent loss A_f is indicative of the response of the fiber to low dose rate fallout exposure. As shown in Table 5.5, except for the Schott and AT&T commercial fibers and NRL 860815, the 7 fibers with the values of $A_f \leq 0.3$ dB/km were all doped with both Ge and F in the core, indicating a potential benefit of F for decreasing permanent damage. Note that this benefit obtains in spite of the large values of n noted for these waveguides.

One observation apparent from the data in Table 5.2 is that when P is doped into the claddings of fibers, the effect is to raise the recovery kinetics to third or fourth order, while the concentration of P has been shown to determine the value of A_f . [1,3] Although the A_f values of the P-containing fibers are in some cases no greater than those of fibers whose clads do not contain P (Table 5.5), the slope of the data of the P-doped waveguides at 10^5 sec is near zero. Of course, the value of A_f and the slope at long times ultimately will determine the fallout sensitivity.

The discussion in this section gives ample evidence that the variations in radiation response found in single mode fibers cannot be attributed to core and/or clad composition alone. In some cases, multiply-clad structures have been developed by the manufacturers to improve radiation performance or shift the zero dispersion wavelength, further complicating the interpretation. Although some generalizations have been attempted above, it can be said that except for the larger values of A_0 measured for the OVD, PCVD and PICVD

fibers, no relationship between fabrication technique and radiation response is evident. Thus, carefully selected fibers made by any of the common methods such as MCVD, OVD, PCVD, or PICVD should be acceptable for fallout environments, provided sufficient budget is allowed for the radiation-induced loss.

An important final note concerns the development of "radiation-hardened" single mode fiber. In most cases the radiation hardening has been accomplished for a specific scenario or for a limited temperature range. For example, AT&T has adjusted the structure and dopant concentrations in their rad-hard fiber for improved radiation resistance over the full -55 to 80 C temperature range. Since the irradiations in this study were made only at an intermediate temperature of -35 C, some of the fibers, such as those with pure silica cores, which have decreased radiation response at room temperature may not appear to be superior to standard commercial products.

NRL PROTOTYPE FIBERS

The matched clad single mode fibers which were fabricated in the present study to investigate the dependence of radiation response on fiber and fabrication parameters were all measured using the apparatus described above. Although a series of measurements was performed without the reference detector shown in Fig. 5.2, these were repeated in order to maintain consistency among all the samples. The agreement between the sets of data was good, except in the cases where excessive long term drift or extraneous noise rendered the data obtained without the reference invalid. Examples of the data and their subsequent reduction to 30-50 points are shown in Figs. 5.4 and 5.5. Additional examples are shown in Figs. 5.12-5.19.

One problem which was encountered during this study is apparent from Table 3.5d where the second mode cutoff wavelengths for some of the fibers

were found to be greater than $1.3\text{ }\mu\text{m}$. In addition, the shape of the cutoffs were pathological in some cases, as noted in the comments column. Because many of these fibers had been drawn at high tension and/or high speed under contract at AT&T Engineering Research Center, time constraints and a limit on the funds available for out-of-house fiber drawing prevented redrawing to smaller diameters.

Radiation damage measurements of the fibers with second mode cutoff wavelengths $>1.3\text{ }\mu\text{m}$ required that steps be taken to insure that the fibers were transmitting only the low-order mode. This was accomplished by wrapping the fiber over a 25 mm diameter glass tube and then removing the higher order modes (which were now coupled into the cladding) using high index matching oil in a cladding mode stripper.

It is apparent from the data of the NRL prototype fibers that use of the reference detector results in data with low noise which can be used without further manipulation for input to the kinetic analyses. The sharp spikes evident in some of the unreduced data are due to switching transients when the automatic fill of the liquid nitrogen is activated. These have been removed for clarity. Also note that the digital resolution of the analog-to-digital converter causes the step-like response of the fiber shown in Fig. 5.18. Nevertheless, high quality data have been obtained for all the fibers of the present study; the results are presented in detail in Chapter 7.

REFERENCES

1. E.J. Friebele, K.J. Long, and M.E. Gingerich, Appl. Opt. 22, 1754 (1983).
2. D.L. Griscom, J. Non-Cryst. Solids 68, 301 (1984); in Structure and Bonding in Noncrystalline Solids, A.G. Revesz and G.E. Walrafen, Eds. (Plenum, New York, 1986).
3. E.W. Mies and L. Soto, Proc. ECOC '85 (Venice).

Table 5.1

Fiber Core and Cladding Dopants and Recovery Parameters

Fiber	Core		Clad		Recovery n t(1/2)	Parameters			Std Dev	Meth	% Rec
	Ge	F	Ge	P		F	Ao	Af			
ATI Commercial	X		X	X	4	65	5.0	0.1	0.12	MCVD	98
ATI RH Proto	X		X		4	55	8.4	1.2	0.23	MCVD	86
Corning 1521	X		X	X	4	23	28.5	2.2	0.78	OVD	92
Corning 1524	X		X		4	80	17.5	1.5	0.46	OVD	91
LTI Commercial					2	2	140.0	2.0	1.85	Outside	99
LTI Proto 1	X				5	200	8.4	0.9	0.26	Outside	89
LTI Proto 2	X	X			5	90	20.2	0.0	0.37	Outside	100
No. Telecom	X			X	3	100	4.4	2.2	0.05	MCVD	51
NRL 860814	X	X		X	2	110	12.1	0.1	0.19	MCVD	99
NRL 860815	X		X		3	40	2.6	0.3	0.08	MCVD	88
Phillips	X	X		X	5	200	17.7	0.2	0.45	PCVD	99
Schott 2282			X		3	2	23.0	0.0	0.24	PCVD	100
Spectran RH	X	X	X		4	9	10.0	0.0	0.31	MCVD	100
Spectran Std.	X		X	X	3	40	5.9	2.3	0.26	MCVD	61
Sumitomo Std.	X			X	2	40	8.8	2.2	0.23	VAD	75
Sumitomo Z				X	2	28	9.3	1.5	0.08	VAD	84

Table 5.2
Fiber Core and Cladding Dopants and Recovery Parameters
Sorted by Order of Recovery Kinetics n

Fiber	Core		Clad		Recovery Parameters					Meth	% Rec
	Ge	F	Ge	P	n	t(1/2)	Ao	Af	Std Dev		
LTI Commercial					2	2	140.0	2.0	1.85	Outside	99
NRL 860814	X	X	X		2	110	12.1	0.1	0.19	MCVD	99
Sumitomo Std.	X				2	40	8.8	2.2	0.23	VAD	75
Sumitomo Z					2	28	9.3	1.5	0.08	VAD	84
No. Telecom	X			X	3	100	4.4	2.2	0.05	MCVD	51
NRL 860815	X			X	3	40	2.6	0.3	0.08	MCVD	88
Schott 2282					3	2	23.0	0.0	0.24	PICVD	100
Spectran Std.	X			X	3	40	5.9	2.3	0.26	MCVD	61
AT&T Commercial	X		X	X	4	65	5.0	0.1	0.12	MCVD	98
AT&T RH Proto	X		X	X	4	55	8.4	1.2	0.23	MCVD	86
Corning 1521	X				4	23	28.5	2.2	0.78	OVD	92
Corning 1524	X		X		4	80	17.5	1.5	0.46	OVD	91
Spectran RH	X	X	X		4	9	10.0	0.0	0.31	MCVD	100
LTI Proto 1	X				5	200	8.4	0.9	0.26	Outside	89
LTI Proto 2	X	X			5	90	20.2	0.0	0.37	Outside	100
Philips	X	X	X		5	200	17.7	0.2	0.45	PCVD	99

Fiber Core and Cladding Dopants and Recovery Parameters
Sorted by Half-Life of Recovery $t(1/2)$

Table 5.3

Fiber	Core		Clad		n	Recovery Parameters		Std Dev	Meth	% Rec	
	Ge	F	Ge	P		t(1/2)	Ao				Af
LTI Commercial					2	2	140.0	2.0	1.85	Outside	99
Schott 2282					3	2	23.0	0.0	0.24	PICVD	100
Spectran RH	X	X			4	9	10.0	0.0	0.31	MCVD	100
Corning 1521	X		X		4	23	28.5	2.2	0.78	OVC	92
Sumitomo Z					2	28	9.3	1.5	0.08	VAD	84
NRL 860815	X			X	3	40	2.6	0.3	0.08	MCVD	88
Spectran Std.	X			X	3	40	5.9	2.3	0.26	MCVD	61
Sumitomo Std.	X			X	2	40	8.8	2.2	0.23	VAD	75
ATI RH Proto	X		X	X	4	55	8.4	1.2	0.23	MCVD	86
ATI Commercial	X		X	X	4	65	5.0	0.1	0.12	MCVD	98
Corning 1524	X		X	X	4	80	17.5	1.5	0.46	OVD	91
LTI Proto 2	X	X			5	90	20.2	0.0	0.37	Outside	100
No. Telecom	X			X	3	100	4.4	2.2	0.05	MCVD	51
NRL 860814	X	X		X	2	110	12.1	0.1	0.19	MCVD	99
LTI Proto 1	X		X		5	200	8.4	0.9	0.26	Outside	89
Phillips	X	X		X	5	200	17.7	0.2	0.45	PCVD	99

Table 5.4
Fiber Core and Cladding Dopants and Recovery Parameters
Sorted by Initial Induced Attenuation A₀

Fiber	Core		Clad		Recovery Parameters				Std Dev	Meth	% Rec
	Ge	F	Ge	P	F	n	t(1/2)	A ₀			
NRL 860815	X			X	X	3	40	2.6	0.08	MCVD	88
Mo. Telecom	X			X	X	3	100	4.4	0.05	MCVD	51
AT&T Commercial	X			X	X	4	65	5.0	0.12	MCVD	98
Spectran Std.	X		X	X	X	3	40	5.9	0.26	MCVD	61
AT&T RH Proto	X		X	X	X	4	55	8.4	0.23	MCVD	86
LTI Proto 1	X					5	200	8.4	0.26	Outside	89
Sumitomo Std.	X				X	2	40	8.8	0.23	VAD	75
Sumitomo Z					X	2	28	9.3	0.08	VAD	84
Spectran RH	X	X	X		X	4	9	10.0	0.31	MCVD	100
NRL 860814	X	X	X		X	2	110	12.1	0.19	MCVD	99
Corning 1524	X		X		X	4	80	17.5	0.46	OVD	91
Philips	X	X	X		X	5	200	17.7	0.45	PCVD	99
LTI Proto 2	X	X			X	5	90	20.2	0.37	Outside	100
Schott 2282					X	3	2	23.0	0.24	PICVD	100
Corning 1521	X					4	23	28.5	0.78	OVD	92
LTI Commercial					X	2	2	140.0	1.85	Outside	99

Table 5.5

Fiber Core and Cladding Dopants and Recovery Parameters
Sorted by Final or Permanent Induced Attenuation Af

Fiber	Core		Clad		Recovery n t(1/2)	Parameters			Std Dev	Meth	% Rec
	Ge	F	Ge	P		Ao	Af				
Spectran RH	X	X	X	X	4	9	10.0	0.0	0.31	MCVD	100
LTI Proto 2	X	X		X	5	90	20.2	0.0	0.37	Outside	100
Schott 2282				X	3	2	23.0	0.0	0.24	PICVD	100
MRL 860814	X	X	X	X	2	110	12.1	0.1	0.19	MCVD	99
AT&T Commercial	X		X	X	4	65	5.0	0.1	0.12	MCVD	98
Philips	X	X	X	X	5	200	17.7	0.2	0.45	PCVD	99
MRL 860815	X		X	X	3	40	2.6	0.3	0.08	MCVD	88
LTI Proto 1	X			X	5	200	8.4	0.9	0.26	Outside	89
AT&T RH Proto	X		X	X	4	55	8.4	1.2	0.23	MCVD	86
Sumitomo Z				X	2	28	9.3	1.5	0.08	VAD	84
Corning 1524	X		X		4	80	17.5	1.5	0.46	OVD	91
LTI Commercial				X	2	2	140.0	2.0	1.85	Outside	99
No. Telecom	X			X	3	100	4.4	2.2	0.05	MCVD	51
Sumitomo Std.	X			X	2	40	8.8	2.2	0.23	VAD	75
Corning 1521	X			X	4	23	28.5	2.2	0.78	OVD	92
Spectran Std.	X			X	3	40	5.9	2.3	0.26	MCVD	61

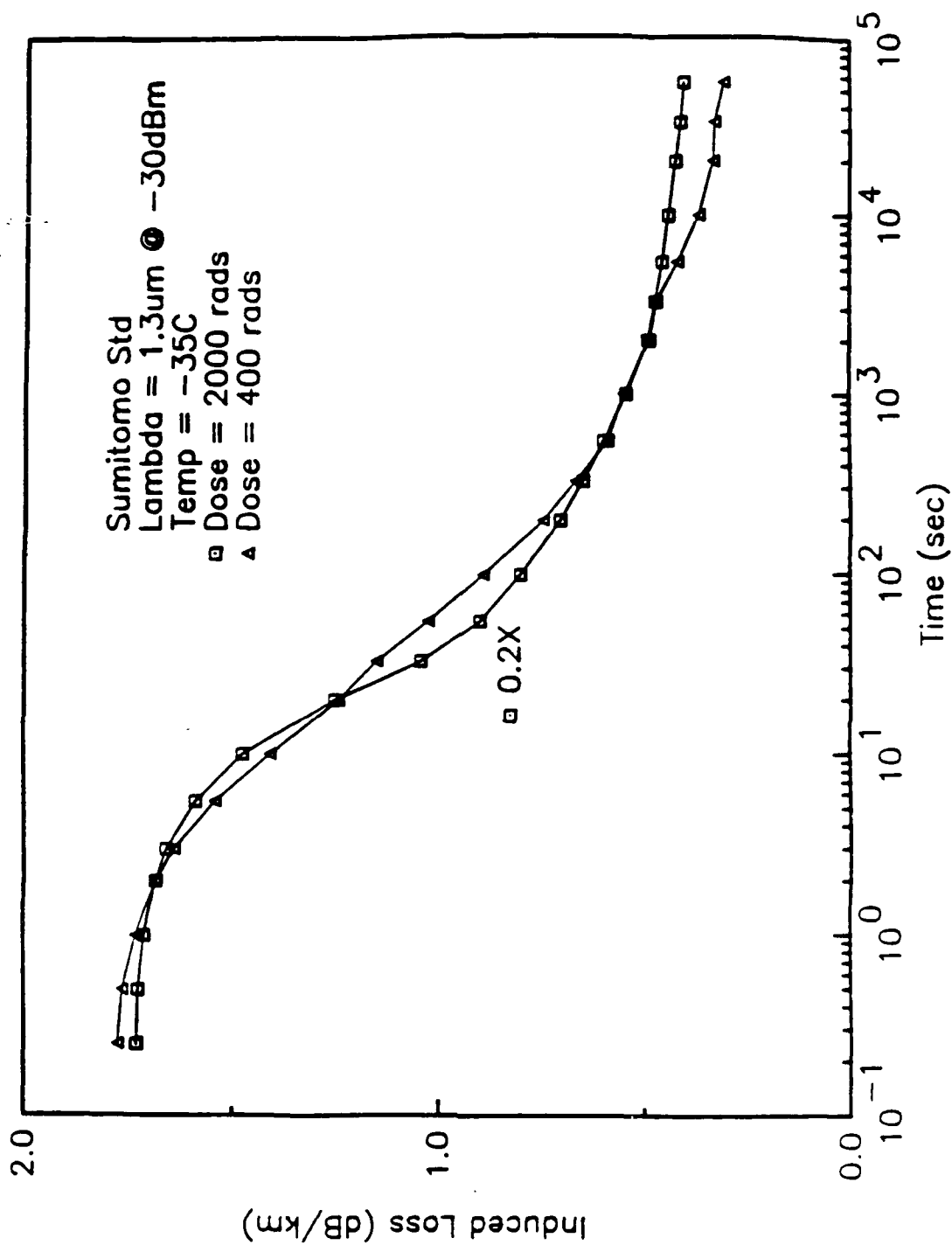


Figure 5.1 Recovery of the attenuation induced in a Sumitomo single mode fiber by doses of 2000 and 400 rads. The correspondence between the data sets indicates the independence of total dose.

The diagram illustrates the experimental setup for measuring the temperature dependence of the ^{60}Co NMR signal. The setup includes the following components and connections:

- 1.3 μm Source**: The primary light source.
- Modulated Power Source**: Connected to the 1.3 μm Source.
- 3 dB Splitter**: Splits the light into two paths.
- Second Mode Expander**: Expands the light beam.
- Mode Stripper**: Strips the light mode.
- Reference Detector**: Receives one path of the split light.
- Sample Detector**: Receives the other path of the split light.
- Lock-In Amp**: Two lock-in amplifiers are connected to the Reference Detector and the Sample Detector, respectively.
- Detector I/O Interface**: Connects the lock-in amplifiers to the IBM PC.
- IBM PC**: The computer system for data acquisition and processing.
- Sample Cell & Fiber Coil**: The sample cell is submerged in water, with a **10 ft** distance indicated between the source and the sample cell. The fiber coil is connected to the sample cell.
- Temperature Controlled Sample Cell & Fiber Coil**: The sample cell is temperature-controlled.
- ^{60}Co Source Pellets**: The sample cell contains ^{60}Co source pellets.
- Water Level**: The water level is indicated by an arrow.

100

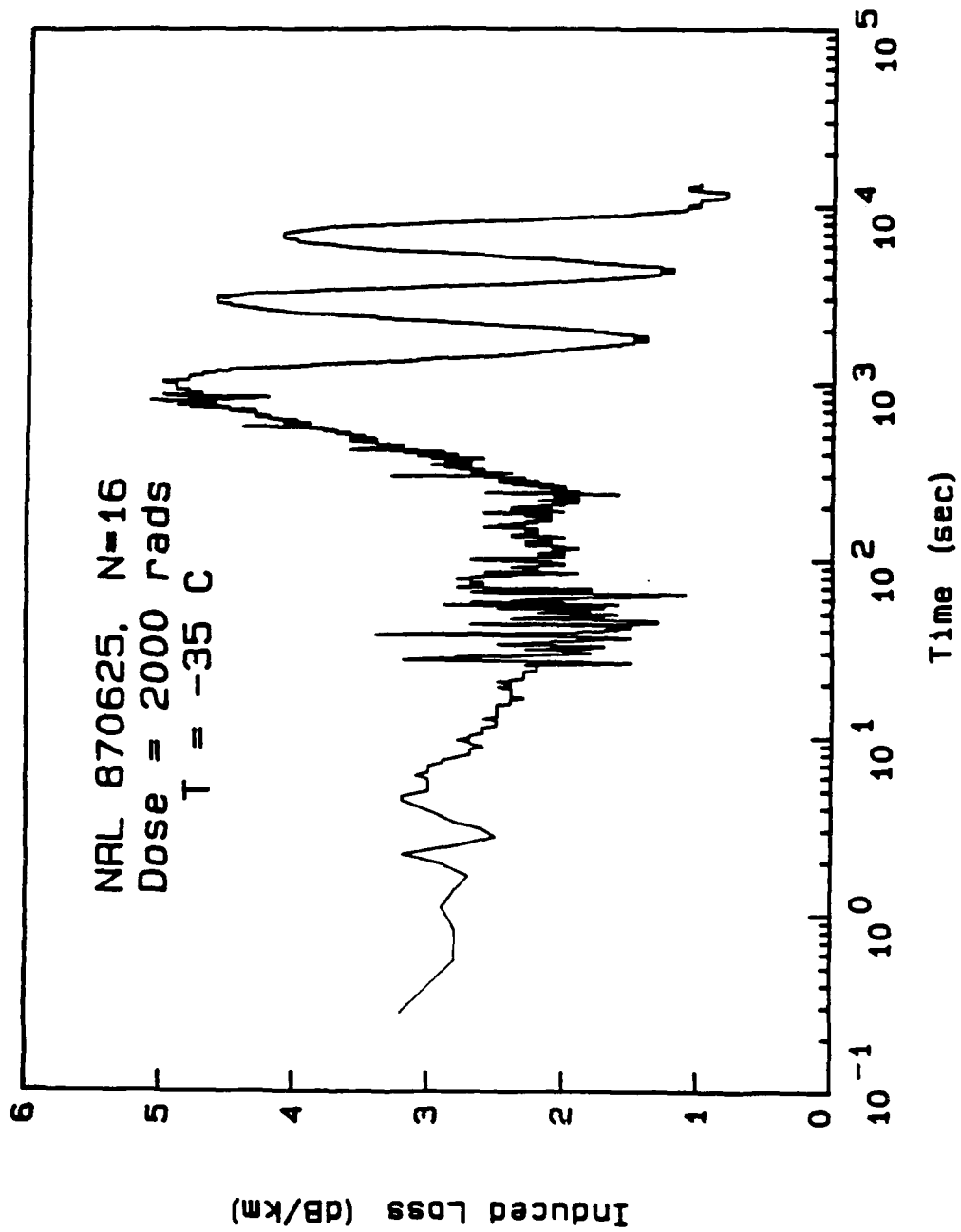


Figure 5.3 Raw recovery data of N=16 obtained without use of the reference fiber and detector.

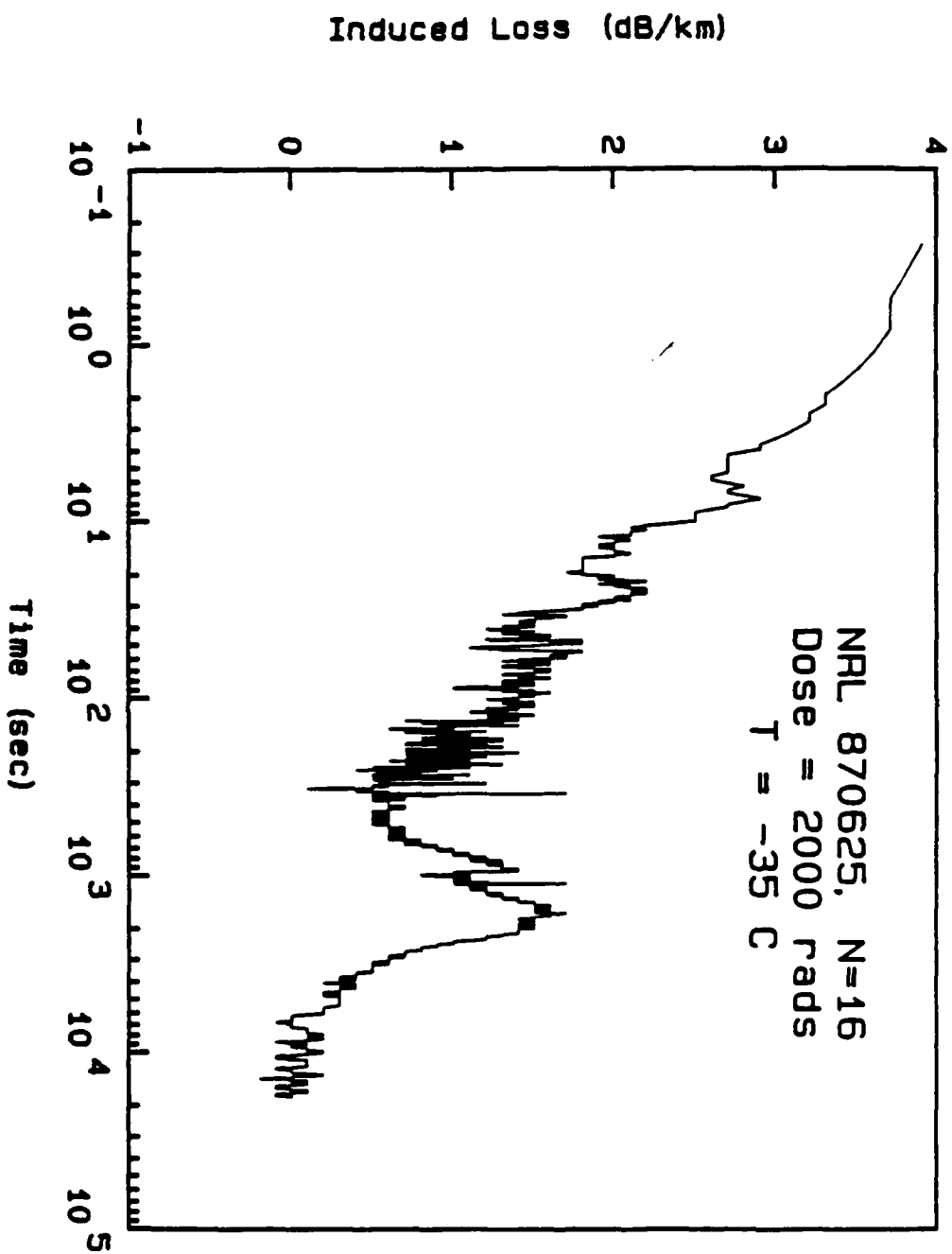


Figure 5.4 Recovery data of N=16 obtained using the reference fiber and detector to reduce long term drifts in the laser diode output. The hump near 2000 rads is due to a temperature instability.

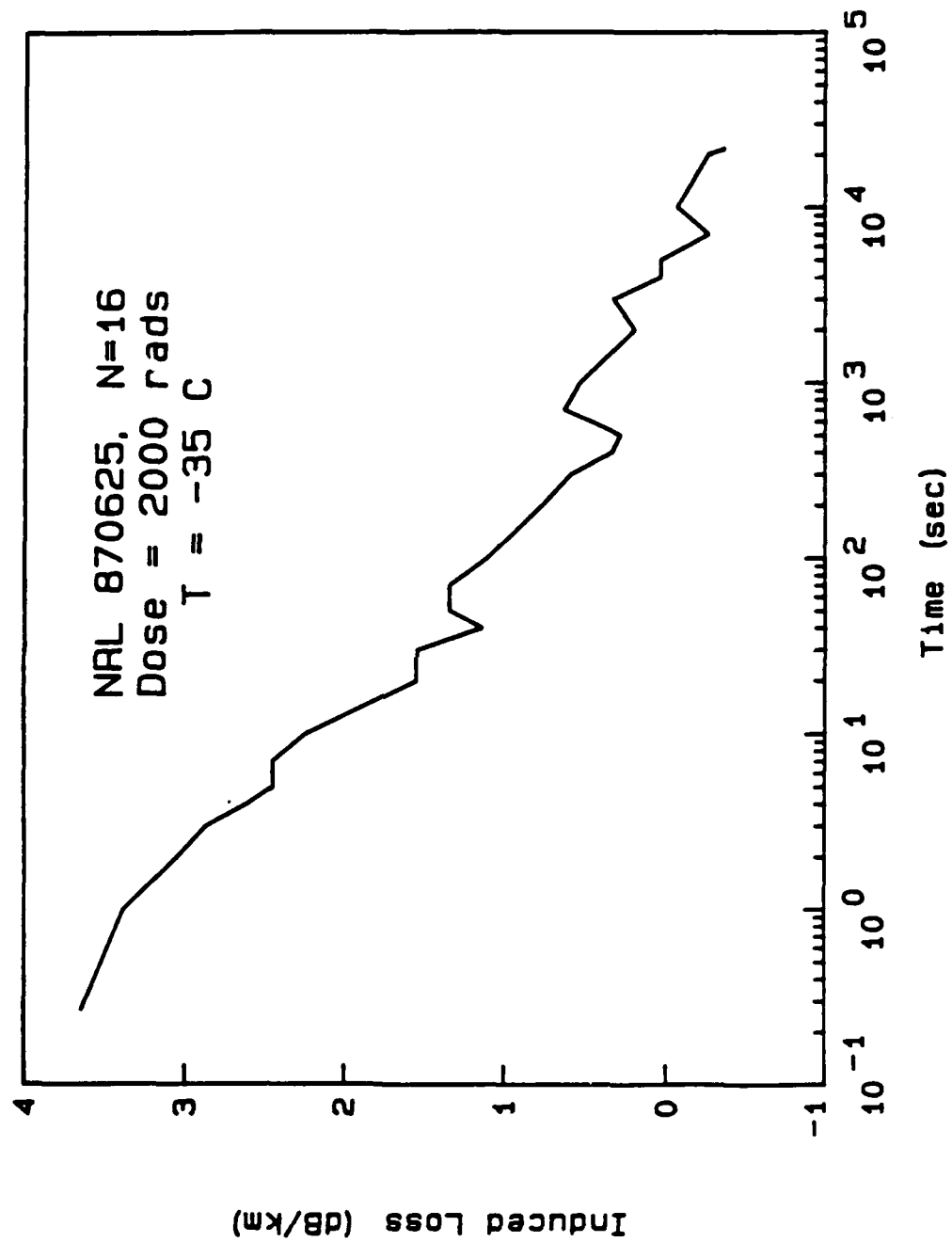


Figure 5.5 Data set of N=16 obtained by selection of 30 data points from the set at logarithmic intervals.

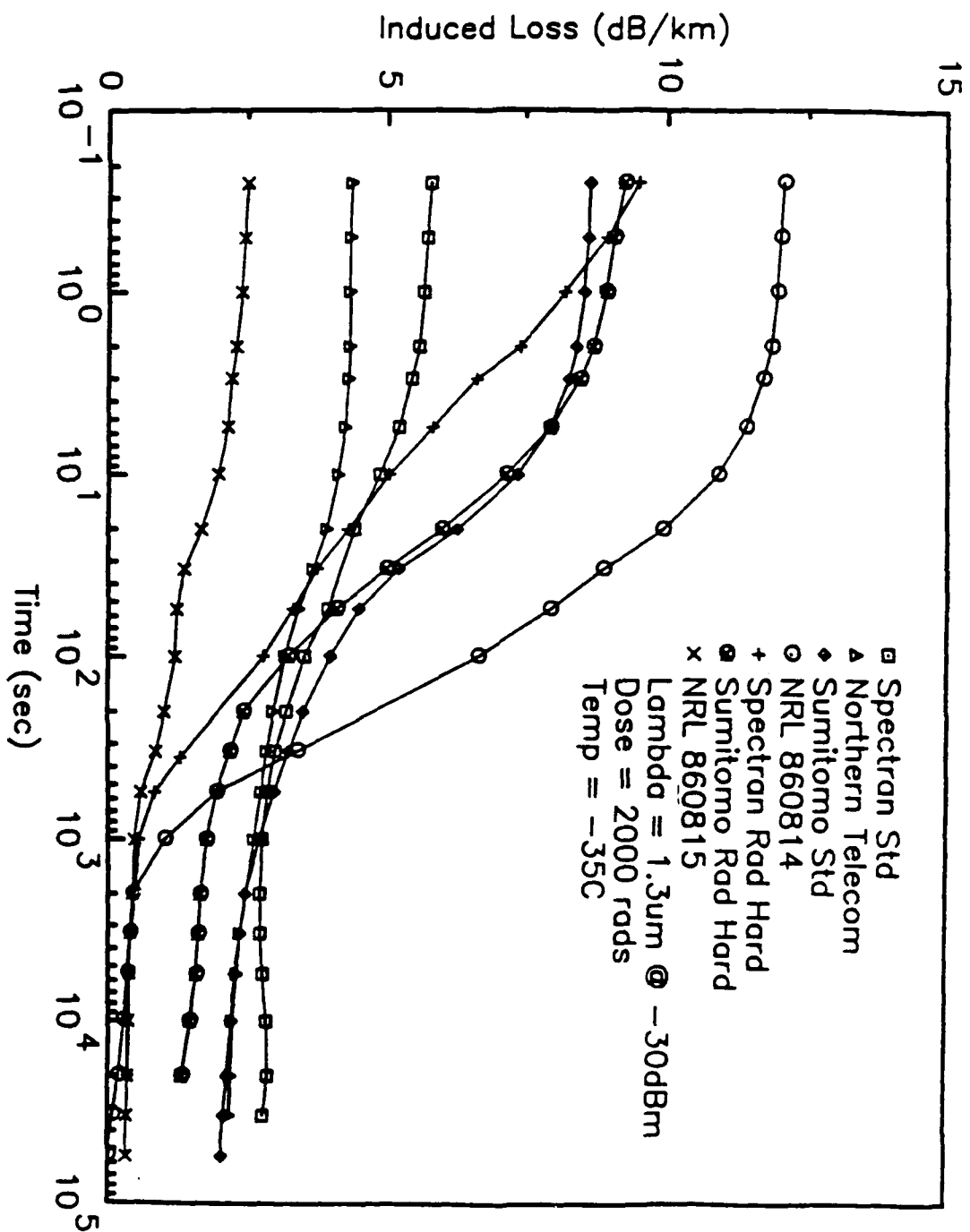


Figure 5.6 Recovery data of Northern Telecom, NRL, Spectran, and Sumitomo single mode fibers and two NRL prototype fibers.

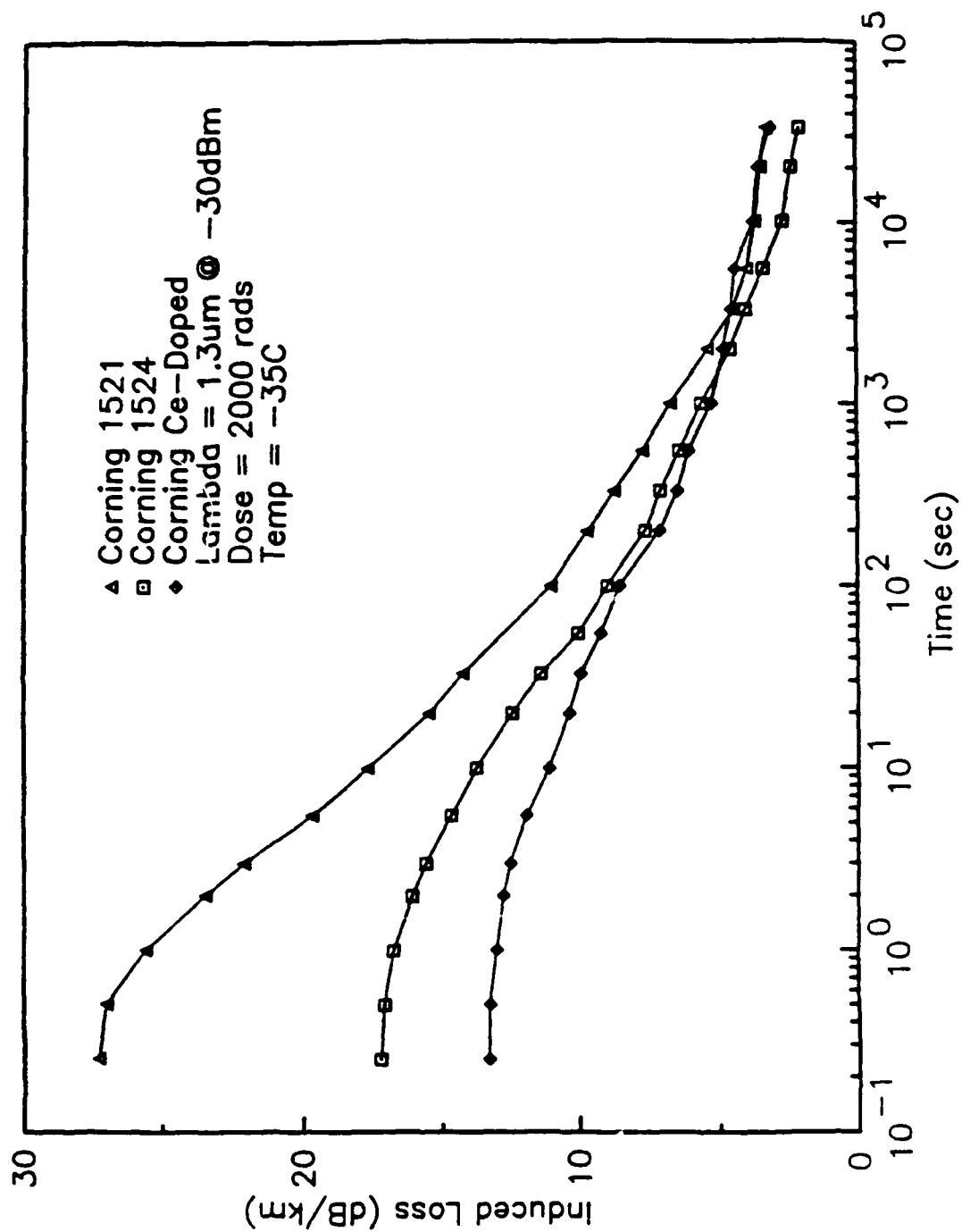


Figure 5.7 Recovery data of Corning commercial single mode fibers.

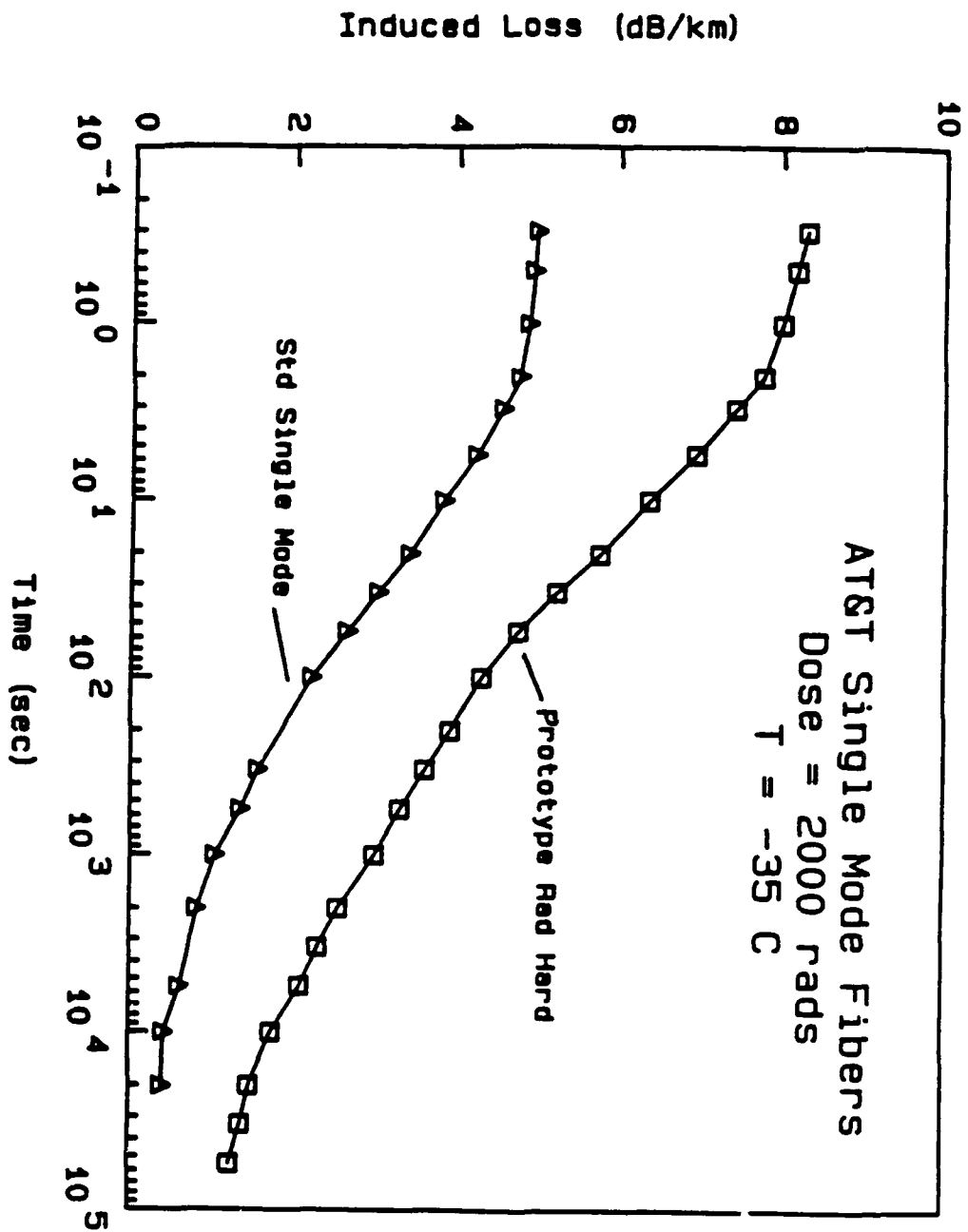


Figure 5.8 Recovery data of AT&T standard and rad-hard single mode fibers.

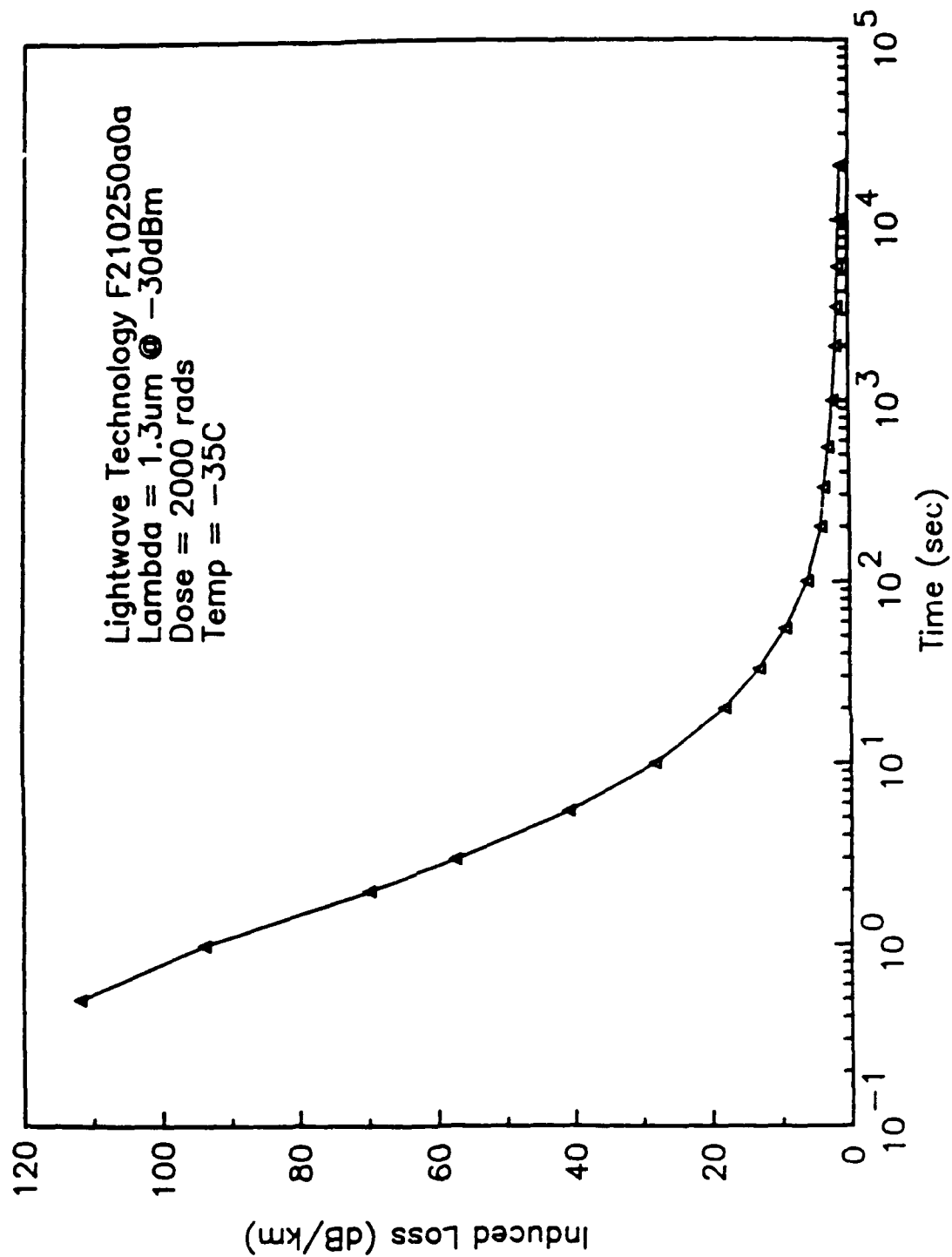


Figure 5.9 Recovery data of a Lightwave Technologies, Inc. commercial single mode fiber.

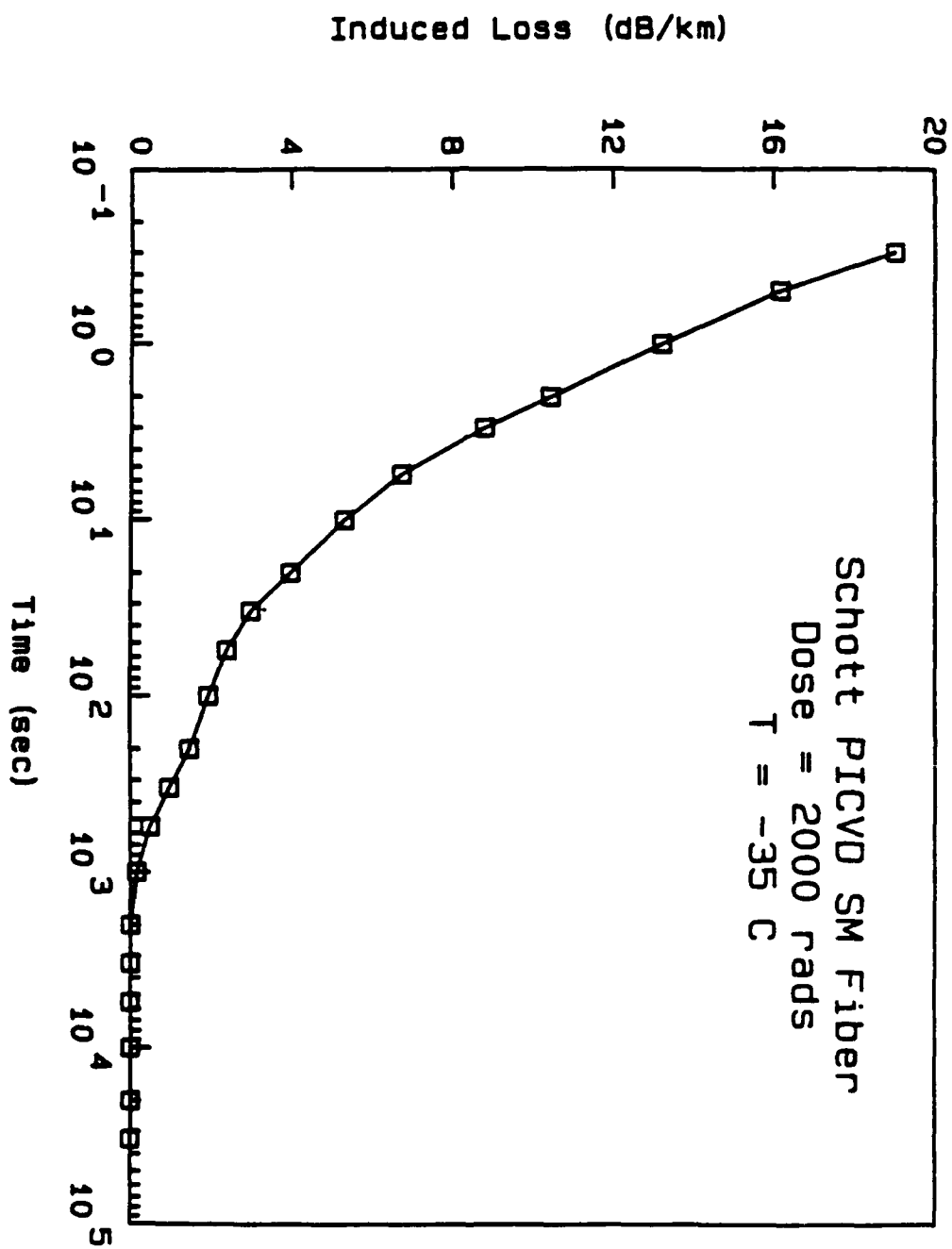


Figure 5.10 Recovery data of a Schott commercial single mode fiber made by the plasma impulse chemical vapor deposition (PICVD) process.

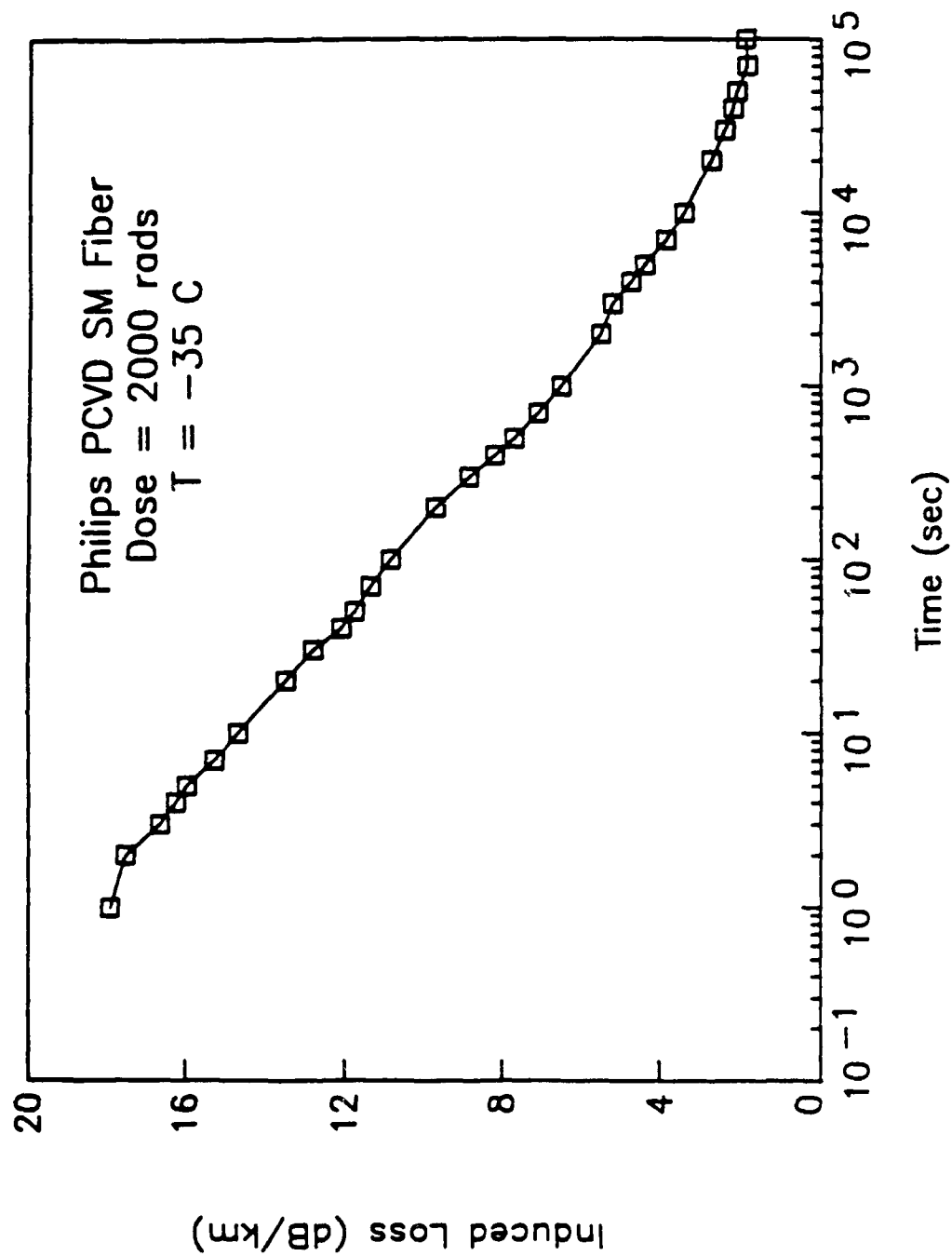


Figure 5.11 Recovery data of a Philips single mode fiber made by the plasma chemical vapor deposition (PCVD) process.

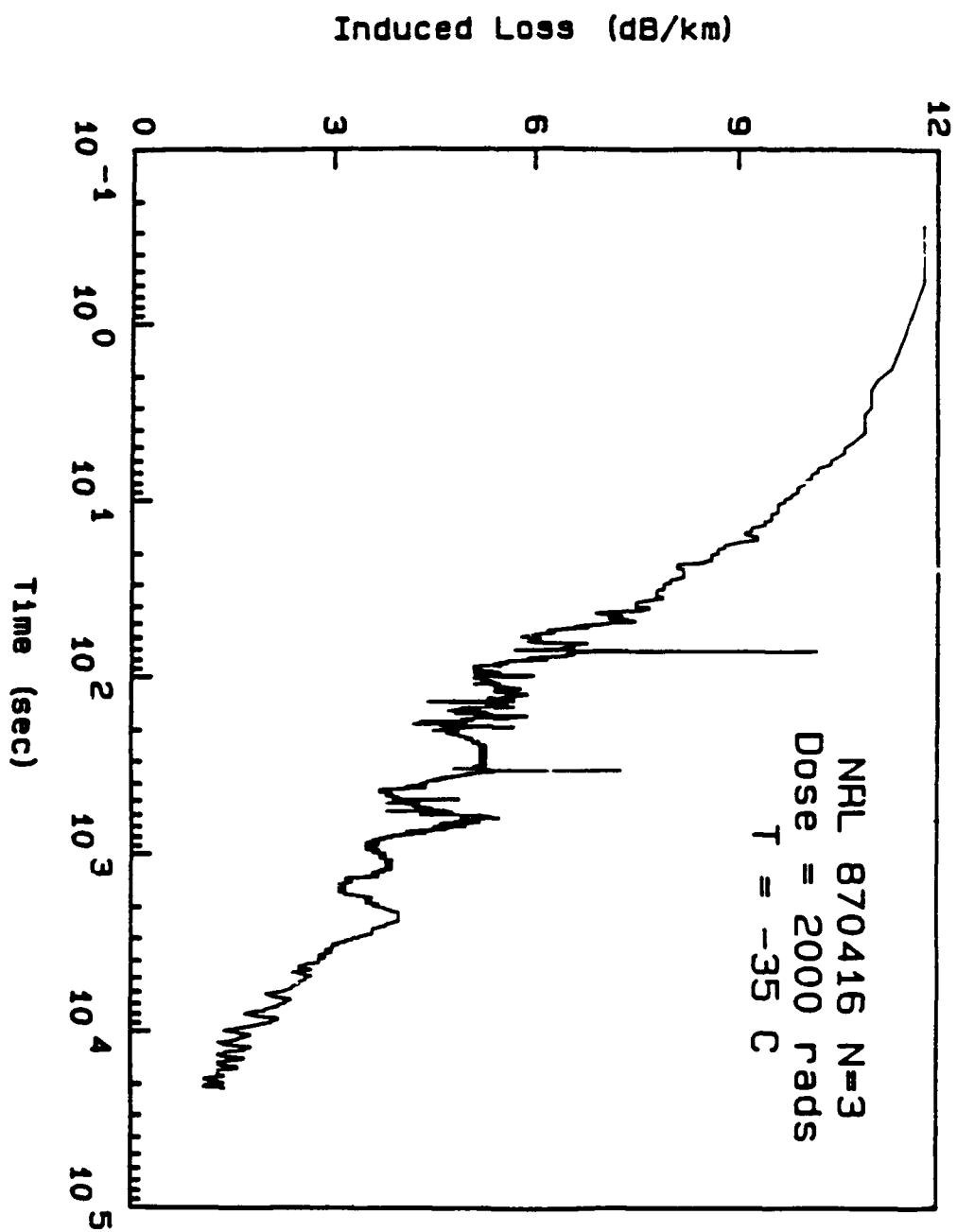


Figure 5.12 Raw recovery data for N = 3.

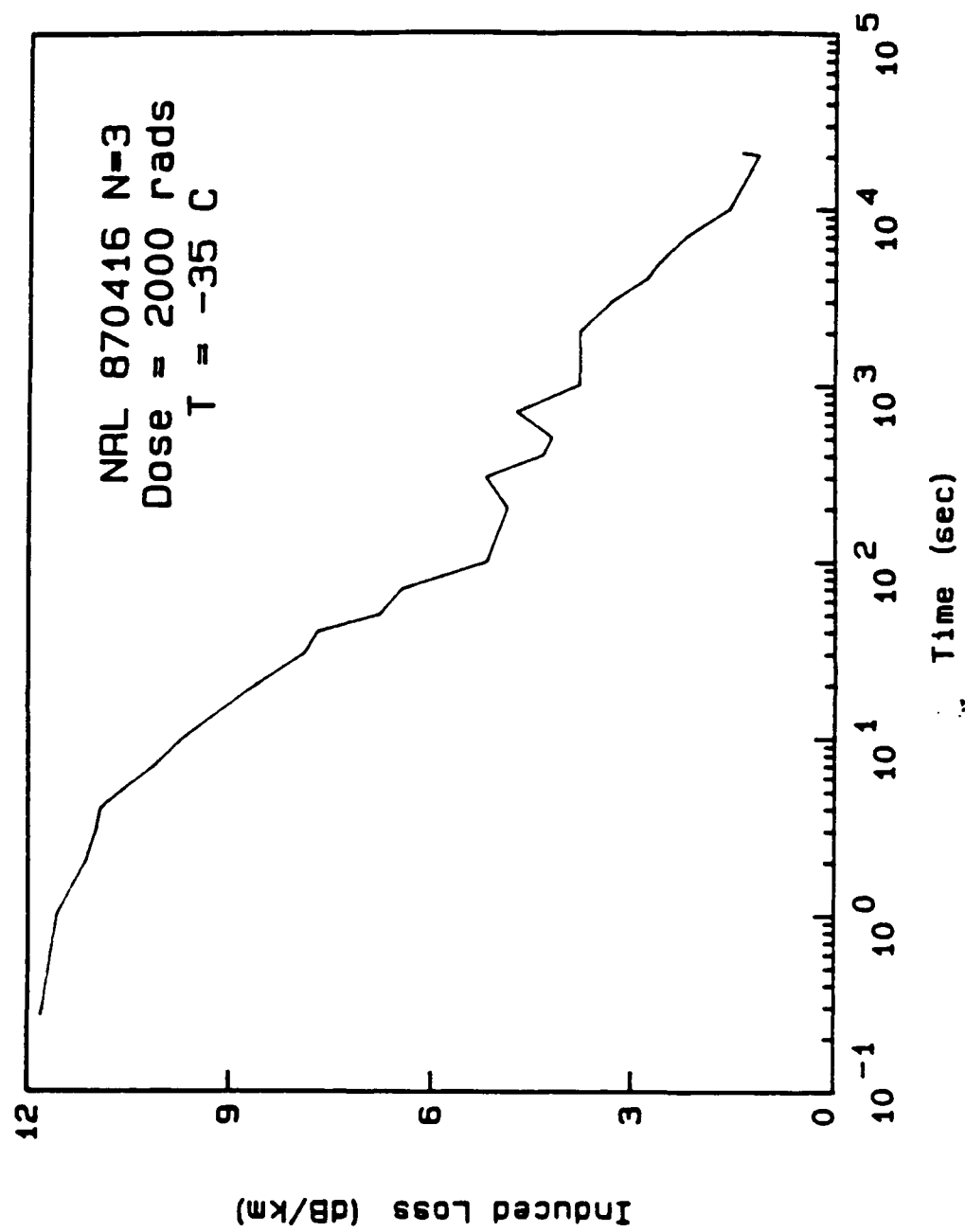


Figure 5.13 Reduced and selected recovery data for N = 3.

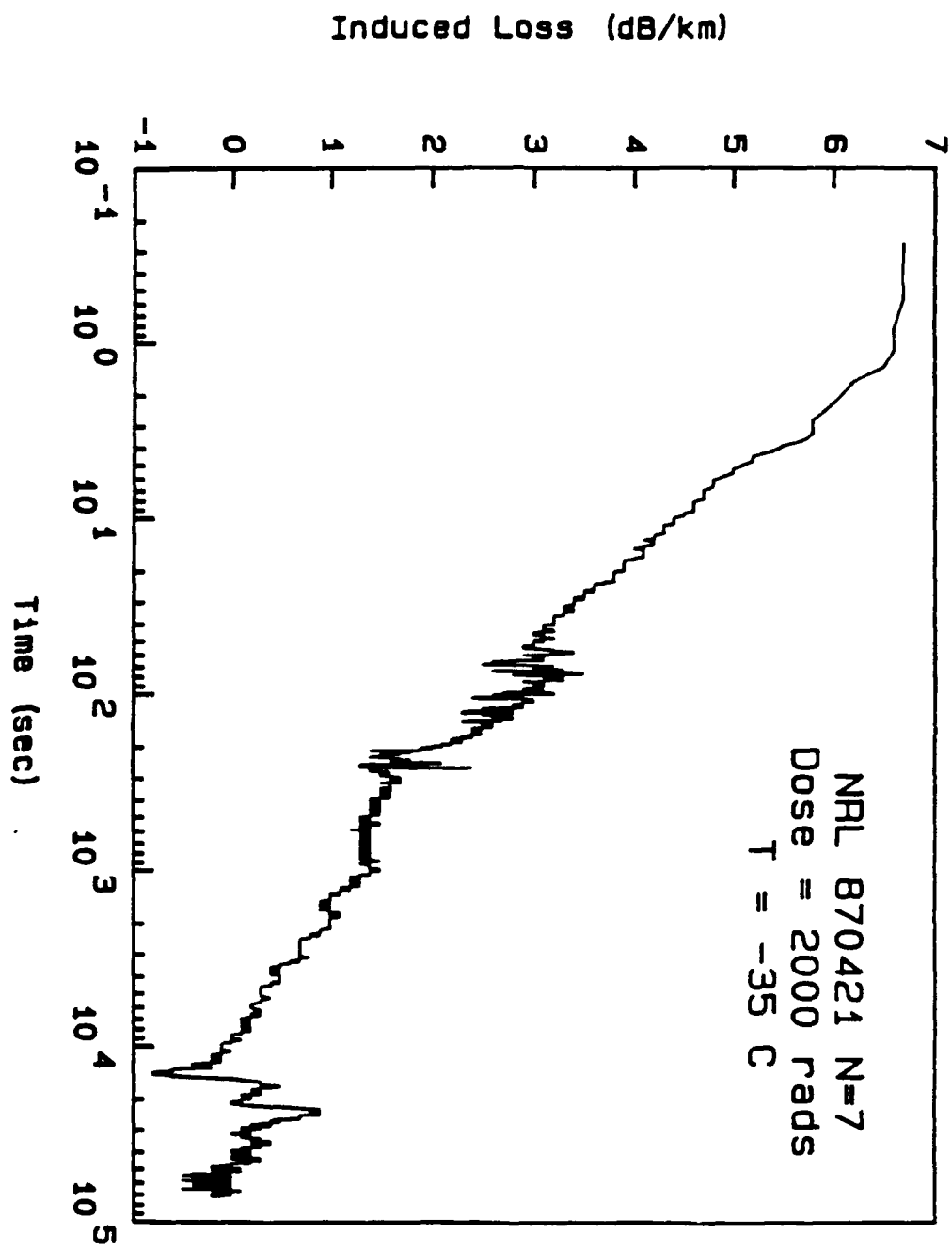


Figure 5.14 Raw recovery data for N = 7.

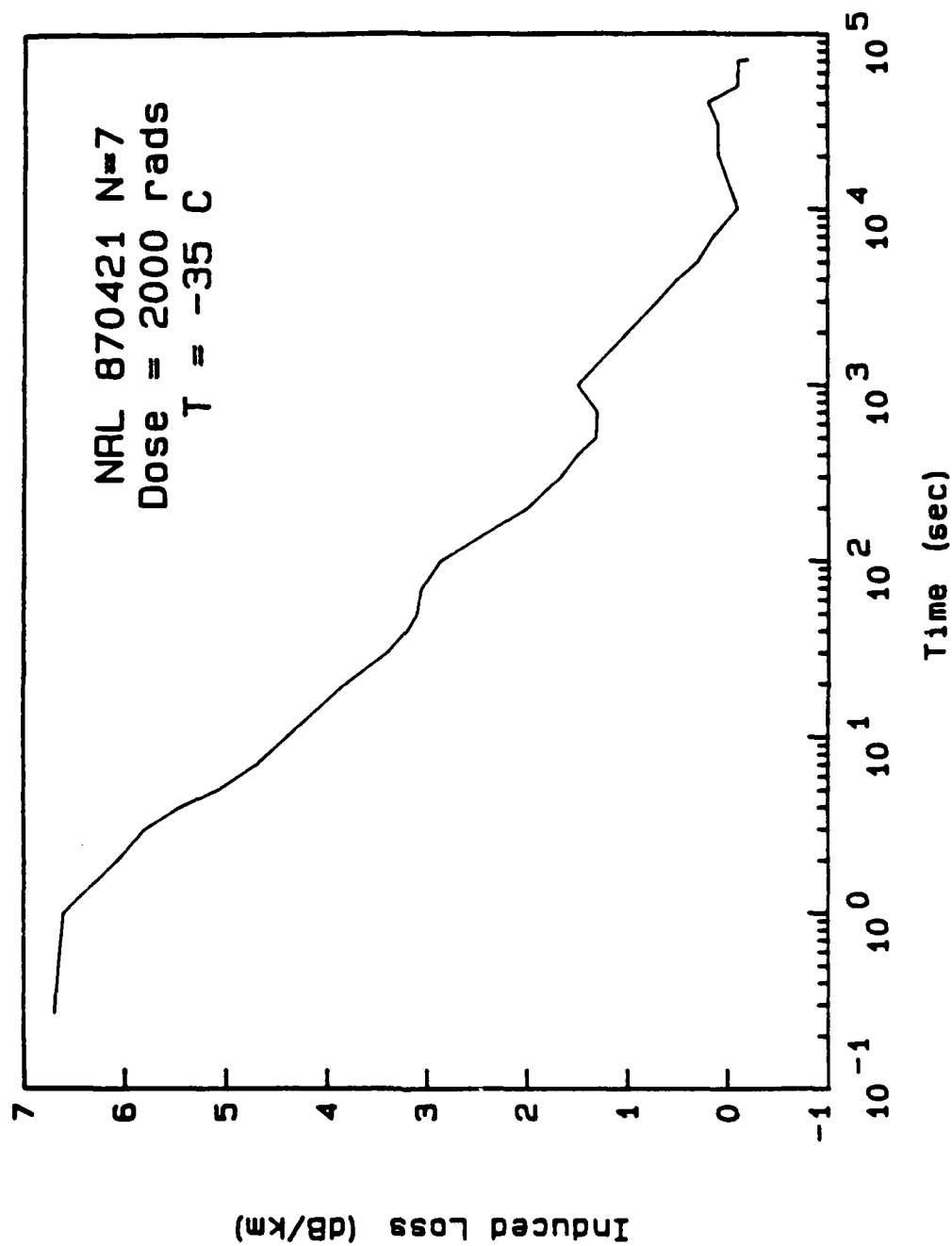


Figure 5.15 Reduced and selected recovery data for $N = 7$.

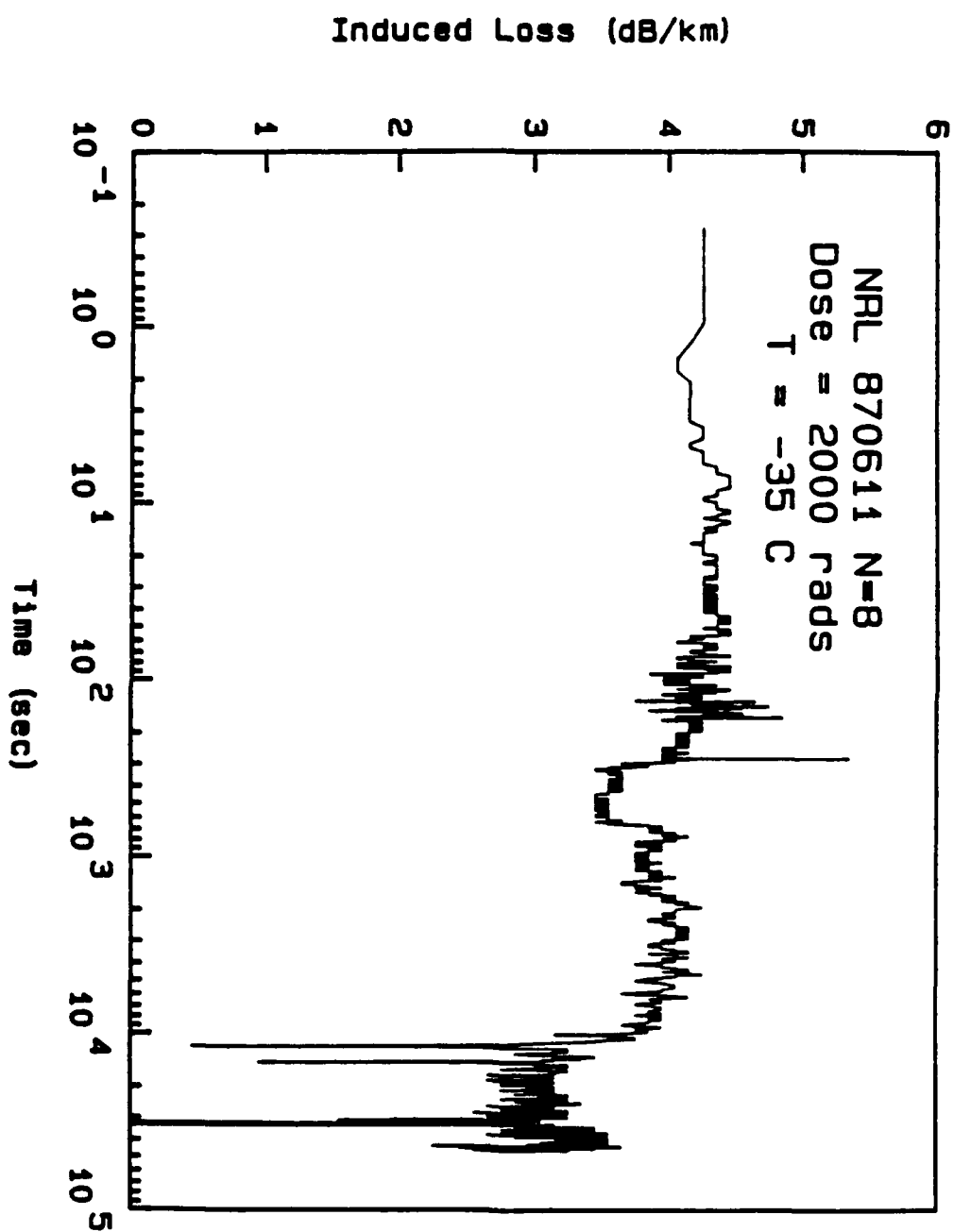


Figure 5.16 Raw recovery data for N = 8.

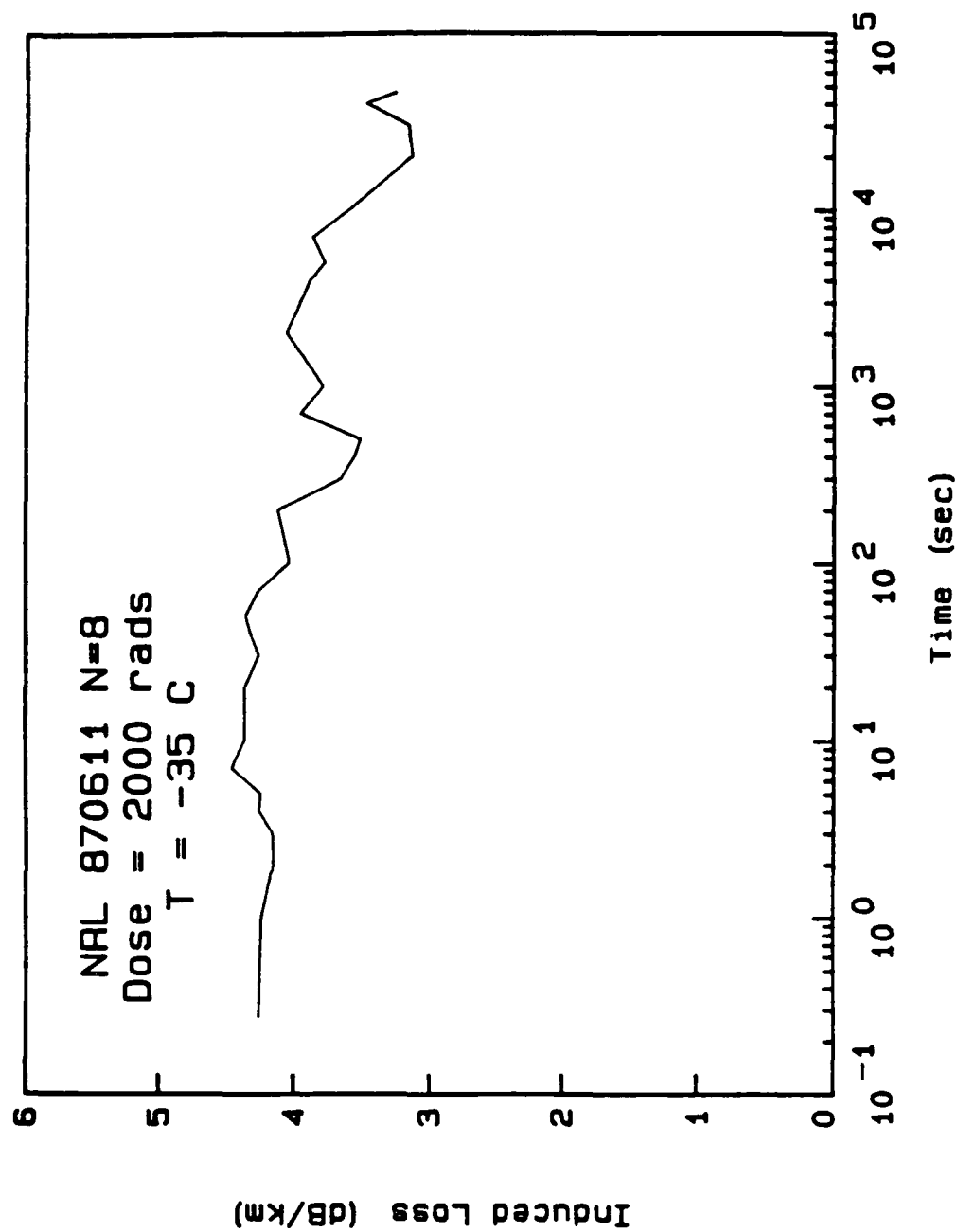


Figure 5.17 Reduced and selected recovery data for N = 8.

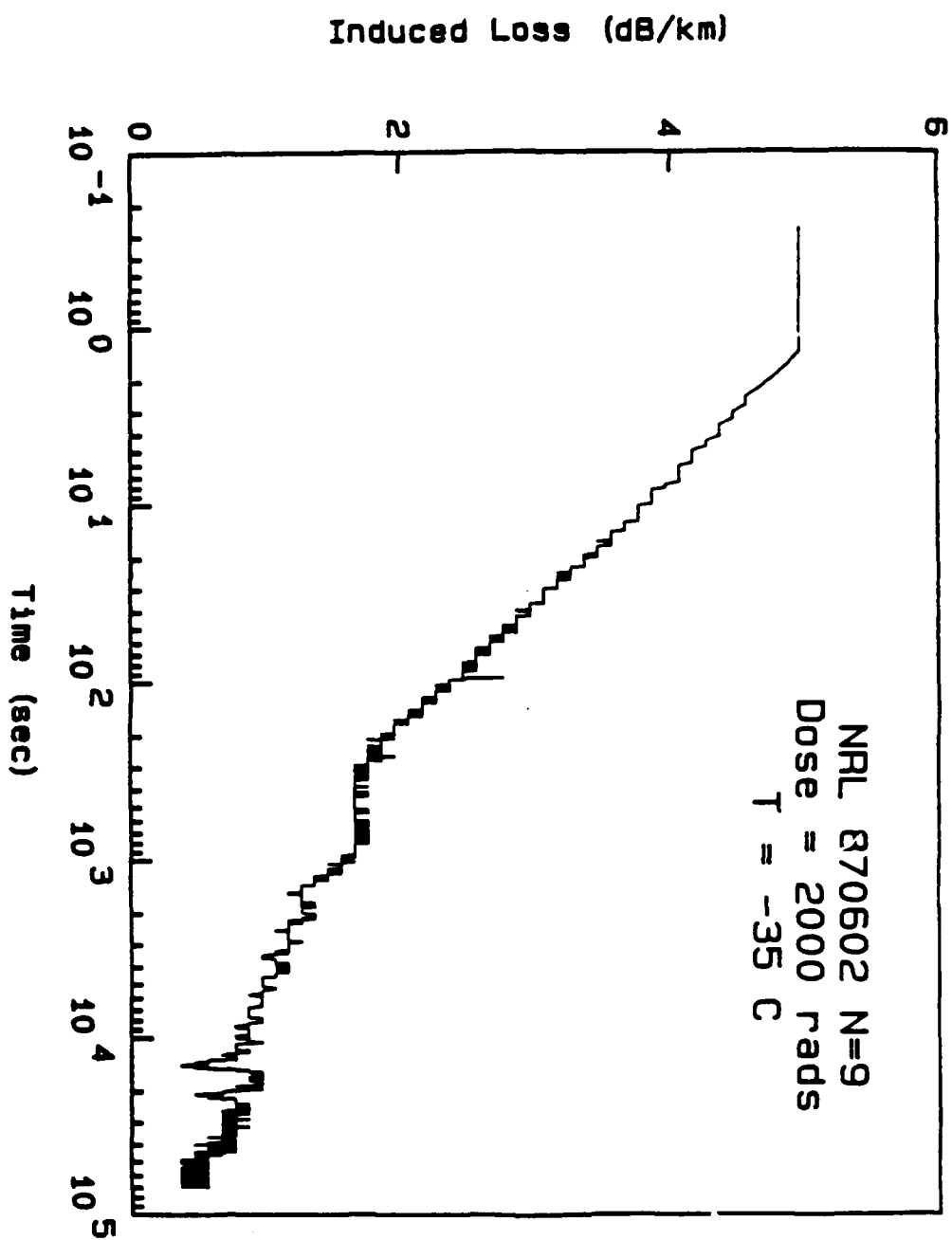


Figure 5.18 Raw recovery data for N = 9.

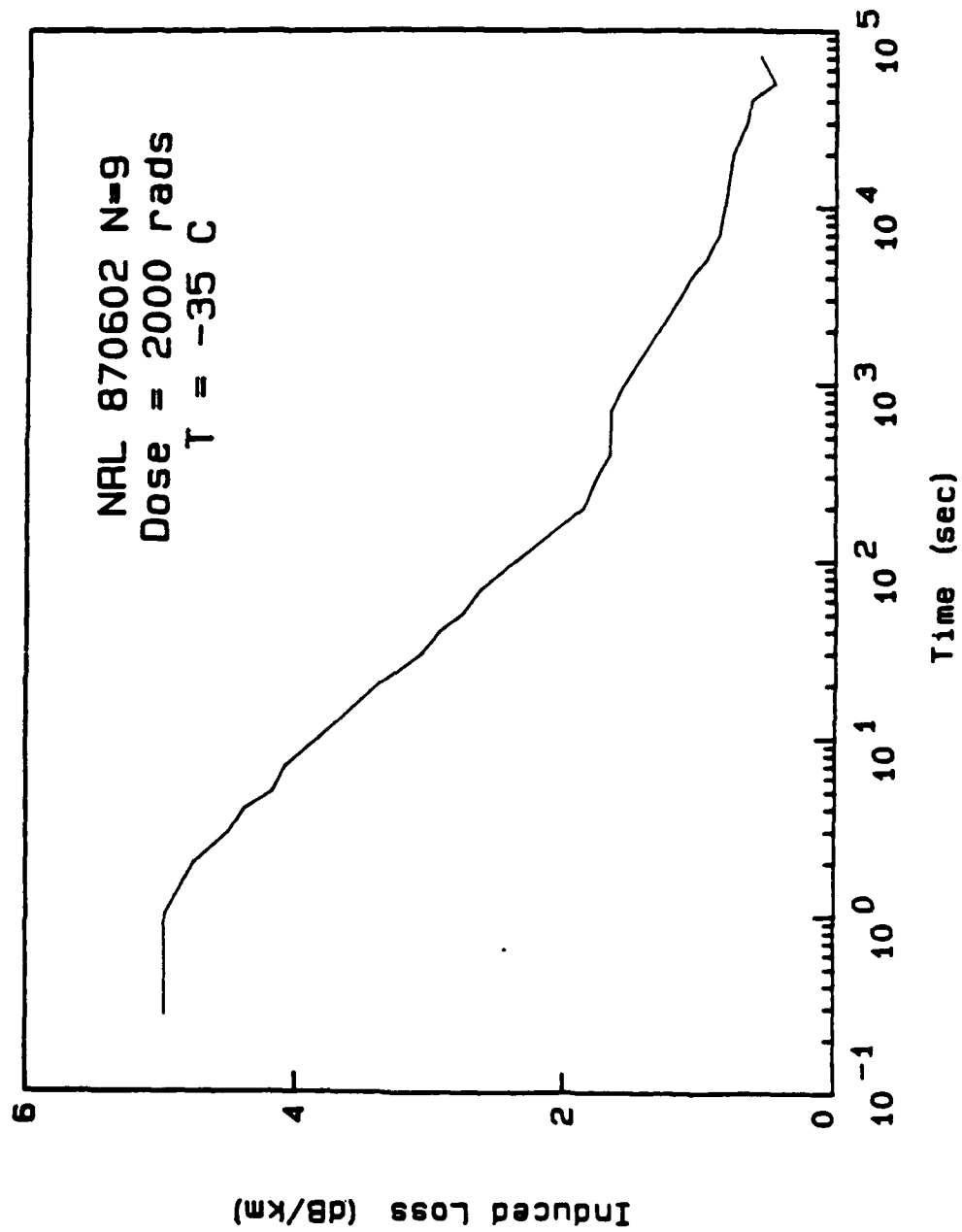


Figure 5.19 Reduced and selected recovery data for N = 9.

CHAPTER 6

KINETIC ANALYSIS

Chemical kinetics is the branch of physical chemistry concerned with the study of systems whose properties are time-dependent, particularly the subgroup of those systems whose chemical composition is changing with time [1]. When a mass of solid material is exposed to energetic radiations, its net chemical composition is essentially unaffected. However, important changes can be wrought in the physical chemistry of local regions of the material: Atoms can be displaced and electrons and holes can become trapped at defect sites which were either pre-existing in the material or created by the radiation itself. Of course, these changes are metastable since in their lowest energy states most of the displaced atoms would be returned to their original positions, and all electrons would be paired. If the system does not relax to its initial state immediately upon removal from the radiation field, this is because there are energy barriers which stand between the damaged state and the relaxed state. To the extent that these barriers may be surmounted with the assistance of lattice phonons, the radiation-induced damage will thermally bleach at finite temperatures. Thus, thermally-activated bleaching of radiation damage, such as color centers in optical fibers, can be formally described in terms of standard chemical rate theory.

It is possible to write the general kinetic equation in the form

$$-\frac{dq}{dt} = \lambda q^n, \quad (6.1)$$

where q is the concentration of the reactant, t is the time, λ is a constant, and n is the order of the reaction. For purposes of analyzing isothermal data, Eq. (6.1) can be integrated giving:

$$q = q_0 [1 + (n-1)q_0^{n-1}\lambda t]^{1/(1-n)} \quad \text{for } n \neq 1, \quad (6.2)$$

or

$$q = q_0 e^{-\lambda t} \text{ for } n=1. \quad (6.3)$$

In reaction processes, the rate constant λ is usually given by the Arrhenius expression

$$\lambda = \lambda_0 e^{-E/kT}, \quad (6.4)$$

where E is the activation energy, k is Boltzmann's constant, and T is the absolute temperature.

Equations (6.2) and (6.3), in conjunction with Eq. (6.4), provide quite general solutions for simple kinetic processes characterized by well-defined values of n and E . Other possible situations may be only approximately describable by these equations. For example, the bimolecular reaction of two reactants, A and B, is precisely described by Eq. (6.2) with $n=2$ only for the special case when $[A]_0 = [B]_0$. Clearly, when $[A]_0 > [B]_0$, a portion of reactant A ($= [A]_0 - [B]_0$) will never be consumed. By the same token, it has been remarked that for $[A]_0 > [B]_0$ the time evolution of the concentration of reactant B might be approximately described by Eq. (6.2) for an appropriately selected noninteger value of $n < 2$ [2]. Certainly, in the limit $[A]_0 \gg [B]_0$, the decay of reactant B is accurately represented by the first-order solution, Eq. (6.3).

The physics of the situation might be further clouded by the existence of a statistical distribution of activation energies E , as is a common occurrence in amorphous materials. Indeed, it is impossible to determine concurrently both the order of the reaction and the distribution of activation energies through analysis of a single set of isothermal (or isochronal) data [3]. Nevertheless, Eqs. (6.2) and (6.3) provide a useful frame of reference for any preliminary analysis of isothermal bleaching data.

In the case of radiation-induced optical absorption bands in optical fiber waveguides, little or no a priori information is available as to the

natures of the chemical reactants, their initial concentrations, or any distributions in activation energies. Unless this information is laboriously uncovered through other experiments such as electron spin resonance (ESR), a fiber under test must be considered as something of a "black box" from the standpoint of the underlying physical chemistry. Nevertheless, for many purposes it may be useful to fit isothermal recovery data to standardized mathematical expressions which may later be related to physical theory. It seems desirable to use the fewest possible parameters in any such fit and also to use mathematical forms which can eventually be related to the fundamental kinetic theory laid out above. The parameters which have been selected here are A_0 , the initial induced attenuation, A_f , the final induced attenuation (the component which does not decay in practical laboratory times), τ , the time required for the decaying component to fall to half of its initial value, and n , the apparent order of the kinetics. The following relation can be derived from Eq. (6.2) by adding a constant term (A_f) and subsuming a number of time independent terms into a single new constant, c :

$$A = (A_0 - A_f)[1 + ct]^{-x} + A_f, \quad (6.5)$$

where

$$x = 1/(n-1) \quad (6.6)$$

and

$$c = (1/\tau)[(2)^{1/x} - 1]. \quad (6.7)$$

Figure 6.1 is a plot of Eq. (6.5), showing that it is relatively straightforward to determine values of A_0 and A_f from a set of recovery data. The half-life τ is found from the value of time for which the attenuation $A = 0.5(A_0 + A_f)$. Figure 6.1 contains plots showing the effect of various values of n on the recovery curve.

All fading data for the radiation-induced attenuation in the fibers of the present study were successfully fitted by means of Eq. (6.5). These fits

were accomplished on an electronic spread sheet by an "eyeball" method. Several examples of the fits of data from both commercial single mode fibers and fibers of the present study are shown in Figs. 6.2 through 6.9. As described in Chapter 5, the data of these fibers were recorded on a chart recorder, and selected times were transferred to computer files for subsequent analysis. This procedure resulted in much less noise in the data (and much less information as to the reliability of the data). Later measurements on NRL fibers were directly recorded by computer at much higher data densities; Examples of the results of this procedure and the resultant fits are presented in Chapter 7.

The derived values of A_f , A_0 , τ , and n for the fibers of Figs. 6.2-6.9 are listed in Table 6.1. It is apparent that in all cases except for the Lightwave Technologies waveguide, which has an extremely large initial loss, and Corning 1521, the standard deviation of the fit is < 0.5 dB/km.

The values of n determined in the fitting process were all in the range 2 to 5. In general, the fits have been constrained to integer values of n , although in some cases non-integer values would significantly improve the fit. For example, a value of $n = 2.3$ instead of 2 for the commercial Lightwave Technologies fiber shown in Fig. 6.4 reduces the standard deviation by a factor of 2.

The values of $n=2$ almost certainly indicate bimolecular fading processes. For such cases a non-zero value of A_f may be a consequence of the concentration of the diffusing (but optically unseen) reactant being lower than the concentration of optically absorbing centers or, alternatively, it may indicate the presence of a second optically absorbing center which is thermally stable on a laboratory time scale. For $A_f=0$, a value of $n=2$ would suggest that the concentrations of the absorbing and diffusing species are about equal. Values of $n>2$ might imply a either a broad distribution in

activation energies or a more complex, multi-step reaction chain. The two humps in the recovery behaviors of the AT&T rad-hard and 2 Corning fibers (Figs. 6.2 and 6.2), which have been fit with $n=4$, suggest the presence of such a multistep recovery mechanism, one contributing to the short time recovery for $t \leq 1$ sec, and the second operational for $t \geq 1000$ sec. Although invoking two or more mechanisms would improve the fits, the added complexity and the resultant inability to compare the recovery data of these fibers with others does not seem to justify the effort. Rather, we have chosen to simulate these multistep processes with values of $n > 3$.

There is also an obvious discrepancy between the data and the fit of the Spectran Standard fiber for times > 1000 sec, as shown in Fig. 6.8. The increase in radiation-induced attenuation which occurs after the radiation exposure has terminated is well-understood[4] as arising from the release of trapped holes from the phosphorus oxygen hole center and subsequent retrapping by a phosphorus-related color center whose absorption peaks at $1.65 \mu\text{m}$. [5] However, the fact that the Spectran fiber shows this behavior while the data of the Northern Telecom fiber shown in Fig. 6.5, which has virtually the same core and clad dopants (Table 6.1) and compositions do not is further evidence that there are processing variables in addition to composition which can have a significant effect on radiation response.

It is noteworthy, however, that the values of τ which were determined by the fitting procedure were quite similar for all the fibers investigated. This last observation suggests that the diffusing species may be the same in all cases.

Based on the known diffusion coefficients of various atoms and molecules in silica (and taking into account their relative chemical reactivities), the diffusing species accounting for the fading of the radiation-induced attenuation in the fibers is almost certainly molecular hydrogen. (This

supposition can be true even when the OH content of the fiber is as low as ~1 ppm, since the numbers of defect centers seldom exceeds one per million silicon atoms.) Evidence has been given that this hydrogen is the end result of radiolysis of silanol groups in the glass [6]. Thus, the initial effect of the irradiation is to fission the hydrogen-oxygen bond:



where the notation " \equiv " denotes three back bonds with oxygens in the glass network. At temperatures above ~130 K the atomic hydrogen dimerizes on a time scale <1 sec:



The nonbridging-oxygen hole center ($\equiv\text{Si-O}\cdot$) appearing on the right-hand side of Eq. (6.8) is known to have an optical absorption band centered at 630 nm. Thus, to the extent that this defect accounts for the induced attenuation at the wavelength of the measurement, the fading kinetics would be determined by the following diffusion-limited reaction:



It should be noted, however, that the induced attenuation at 1.3 μm appears to arise from a color center distinct from the nonbridging-oxygen hole center. Nevertheless, the fading kinetics observed in the present study are strongly suggestive that the diffusion of radiolytic molecular hydrogen may be the rate-limiting step at the latter wavelength as well.

REFERENCES

1. S.W. Benson, The Foundations of Chemical Kinetics, (Robert E. Krieger, Malabar, Florida, 1982).
2. D.L. Griscom, in Structure and Bonding in Noncrystalline Solids (Plenum

Press, New York, 1986).

3. P.H. Fang, Phys. Rev. B1, 932 (1970).

4. E.J. Friebele, C.G. Askins, M.E. Gingerich and K.J. Long, Nucl. Inst. Meth. in Phys. Res. B1, 355 (1984).

5. D.L. Griscom, E.J. Friebele, K.J. Long and J.W. Fleming, J. Appl. Phys. 54, 3743 (1983).

6. D.L. Griscom, J. Non-Cryst. Solids 68, 301 (1984).

Table 6.1
Fiber Core and Cladding Dopants and Recovery Parameters

Fiber	Core		Clad		n	Recovery Parameters			Std Dev	Meth	% Rec
	Ge	F	Ge	P		t(1/2)	Ao	Af			
AT&T Commercial	X		X	X	4	65	5.0	0.1	0.12	MCVD	98
AT&T RH Proto	X		X	X	4	55	8.4	1.2	0.23	MCVD	86
Corning 1521	X				4	23	28.5	2.2	0.78	OVD	92
Corning 1524	X		X		4	80	17.5	1.5	0.46	OVD	91
LII Commercial					2	2	140.0	2.0	1.85	Outside	99
LII Proto 1	X				5	200	8.4	0.9	0.26	Outside	89
LII Proto 2	X	X			5	90	20.2	0.0	0.37	Outside	100
No. Telecom	X	X	X	X	3	100	4.4	2.2	0.05	MCVD	51
NRL 860814	X	X	X	X	2	110	12.1	0.1	0.19	MCVD	99
NRL 860815	X	X	X	X	3	40	2.6	0.3	0.08	MCVD	88
Philips	X	X	X	X	5	200	17.7	0.2	0.45	PCVD	99
Schott 2282					3	2	23.0	0.0	0.24	PICVD	100
Spectran RH	X	X	X	X	4	9	10.0	0.0	0.31	MCVD	100
Spectran Std.	X			X	3	40	5.9	2.3	0.26	MCVD	61
Sumitomo Std.	X			X	2	40	8.8	2.2	0.23	VAD	75
Sumitomo Z				X	2	28	9.3	1.5	0.08	VAD	84

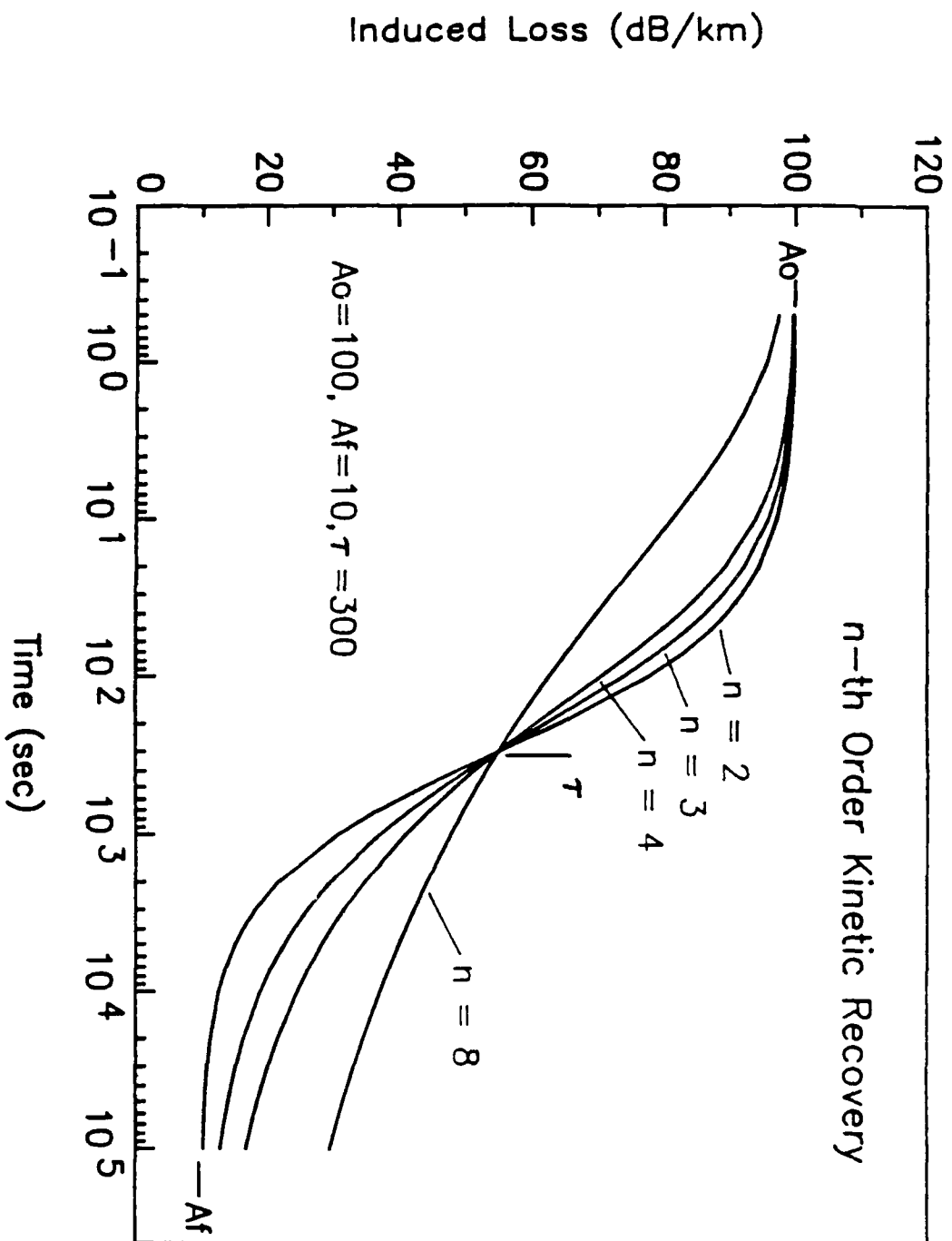


Figure 6.1 Plots of kinetic equation (6.5) used to fit the recovery data of the radiation-induced attenuation measured in fibers of this study, showing the effect of variations in n .

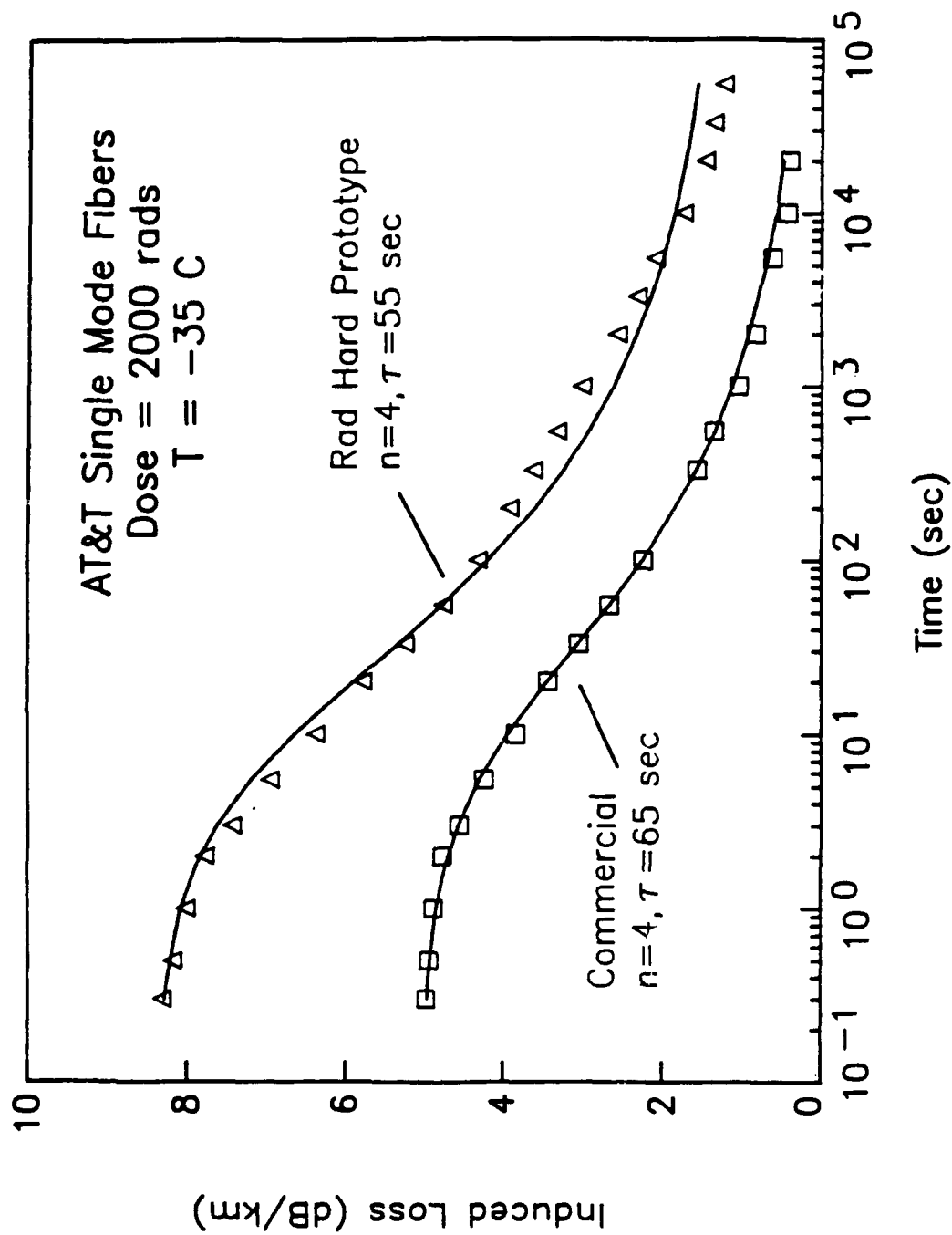


Figure 6.2 Recovery of radiation-induced attenuation (points) in AT&T radiation-hardened and commercial single mode fiber and fits to kinetic model (lines).

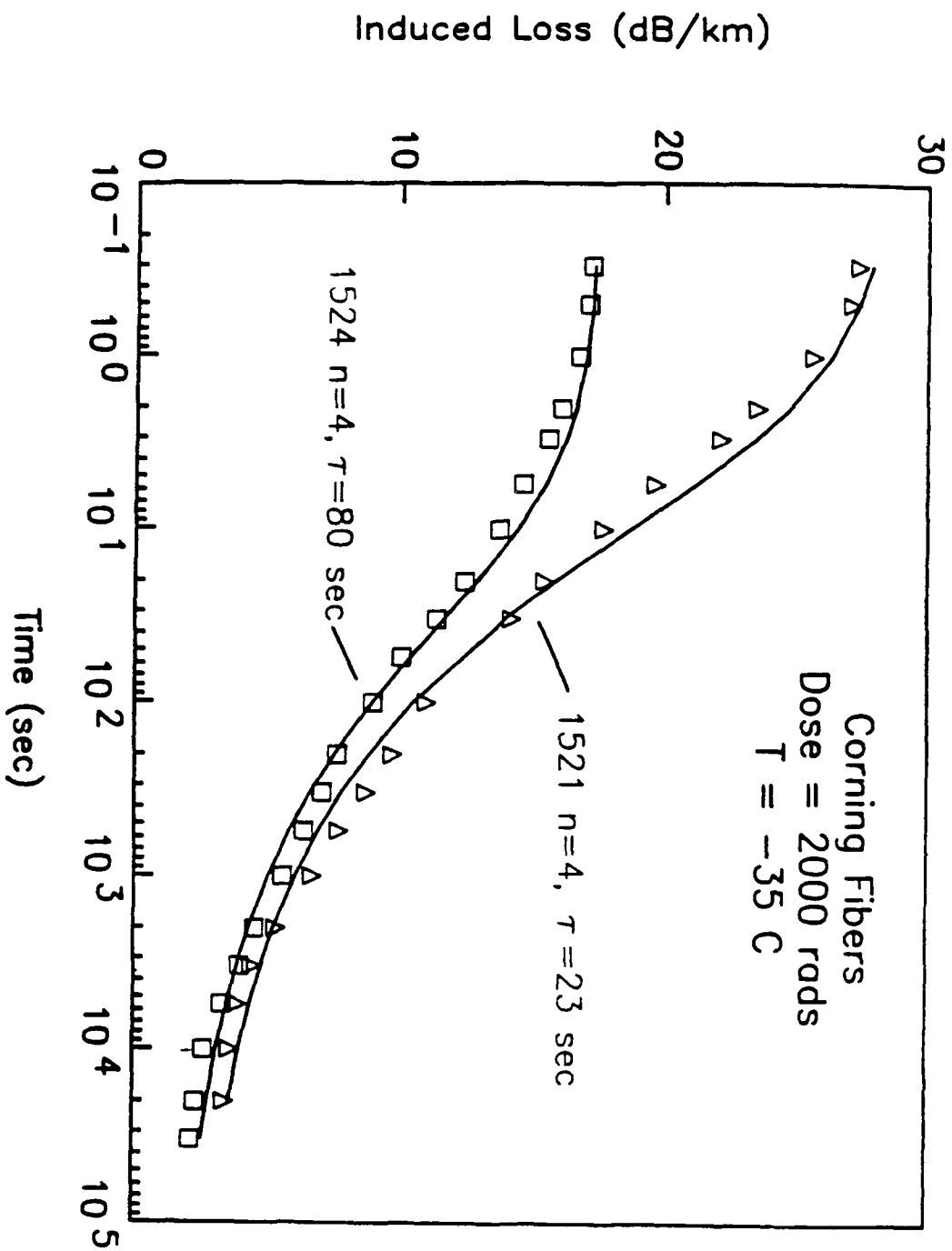


Figure 6.3 Recovery of radiation-induced attenuation (points) in commercially-available Corning 1521 and 1524 single mode fibers and fits to kinetic model (lines).

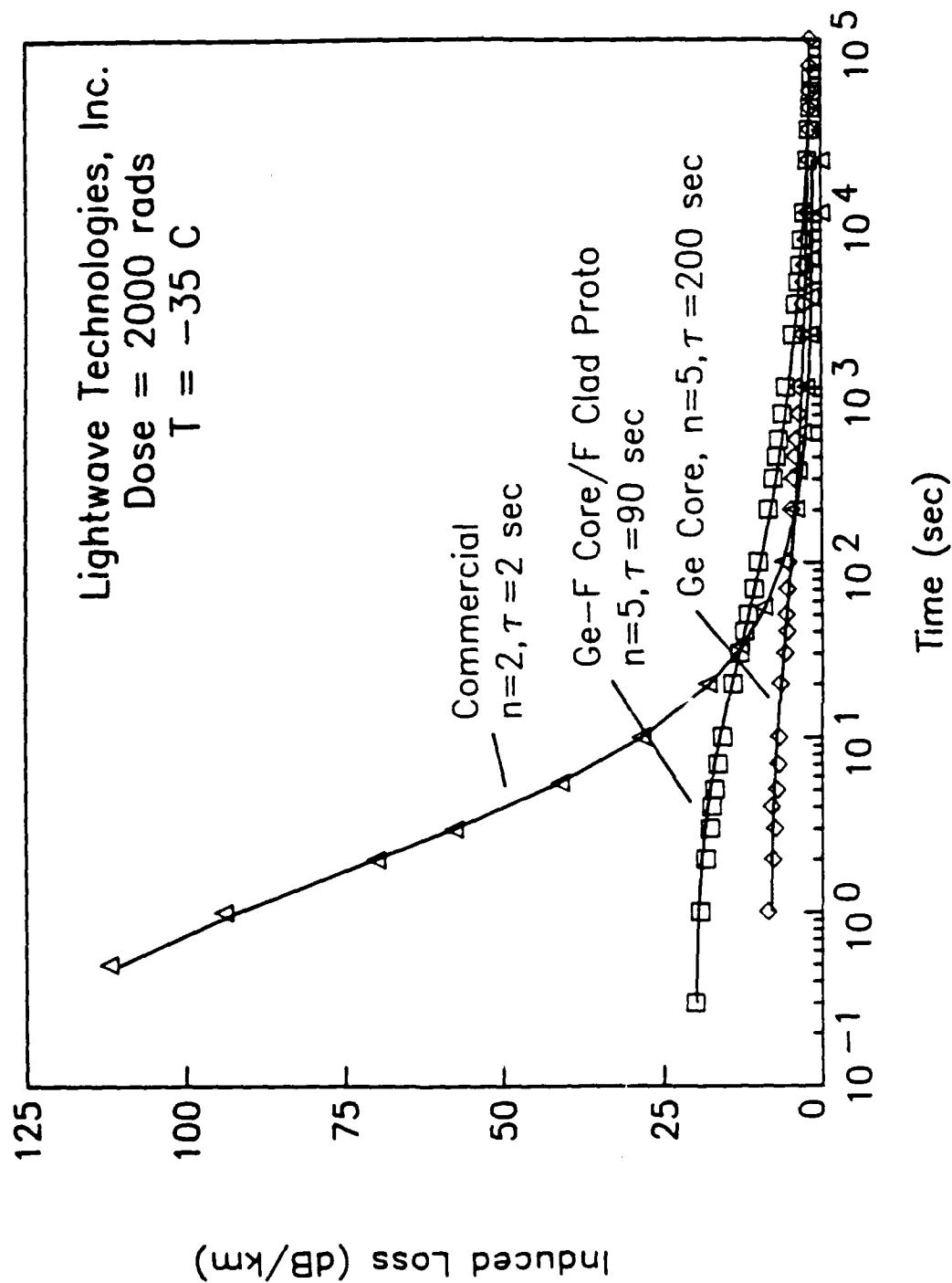


Figure 6.4 Recovery of radiation-induced attenuation (points) in commercially-available and prototype Lightwave Technologies, Inc. single mode fibers and fits to kinetic model (lines).

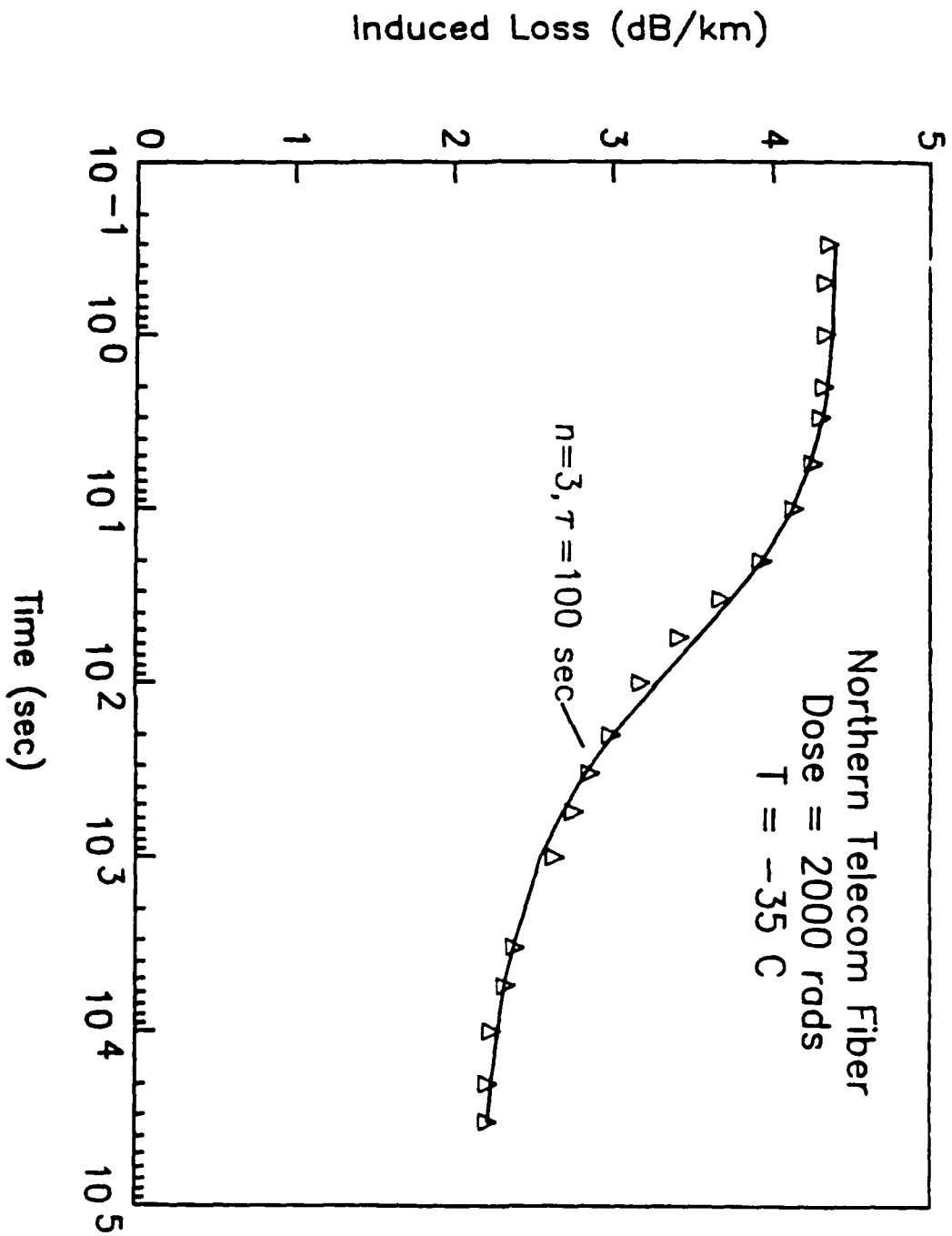


Figure 6.5 Recovery of radiation-induced attenuation (points) in a commercial Northern Telecom single mode fiber and fit to kinetic model (line).

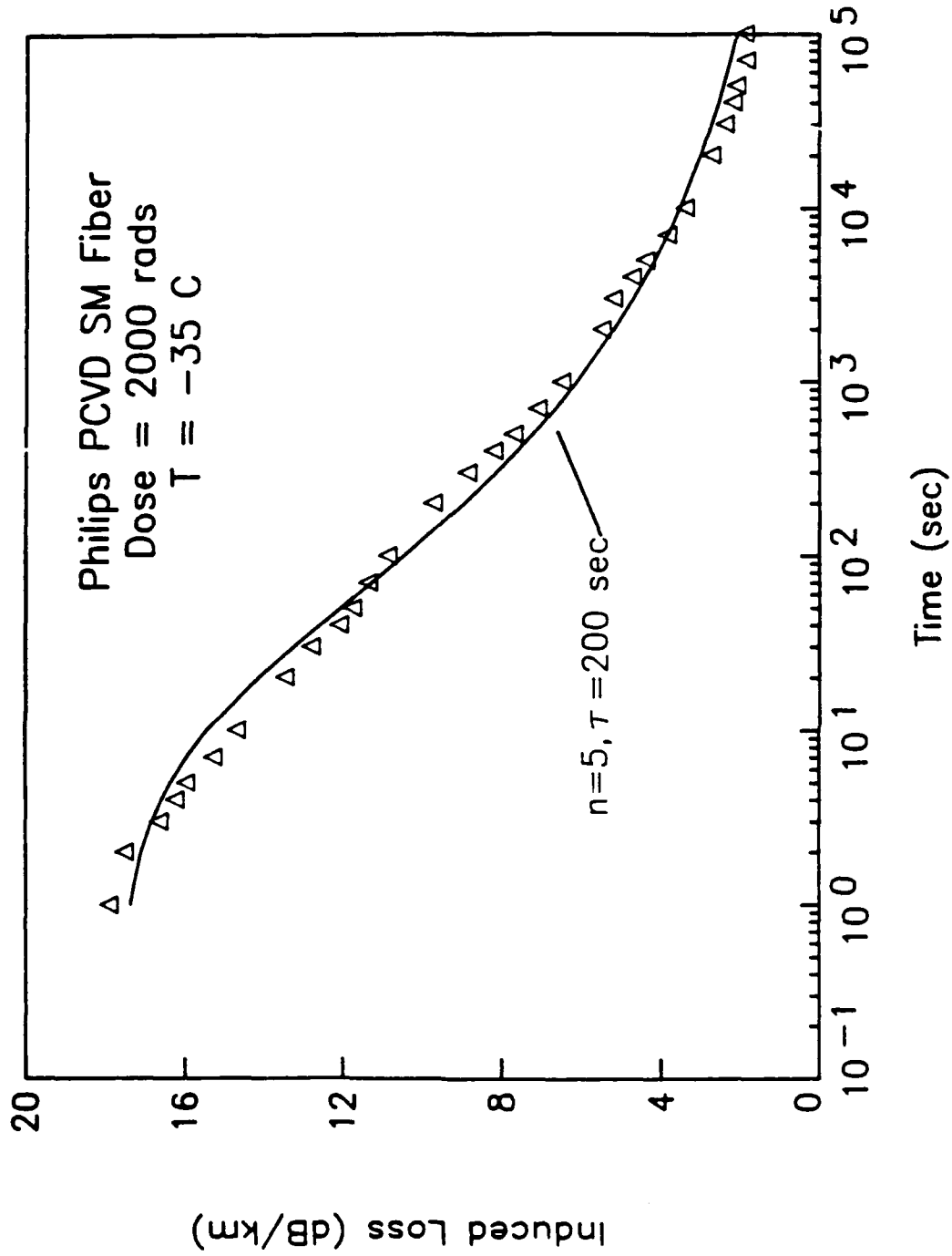
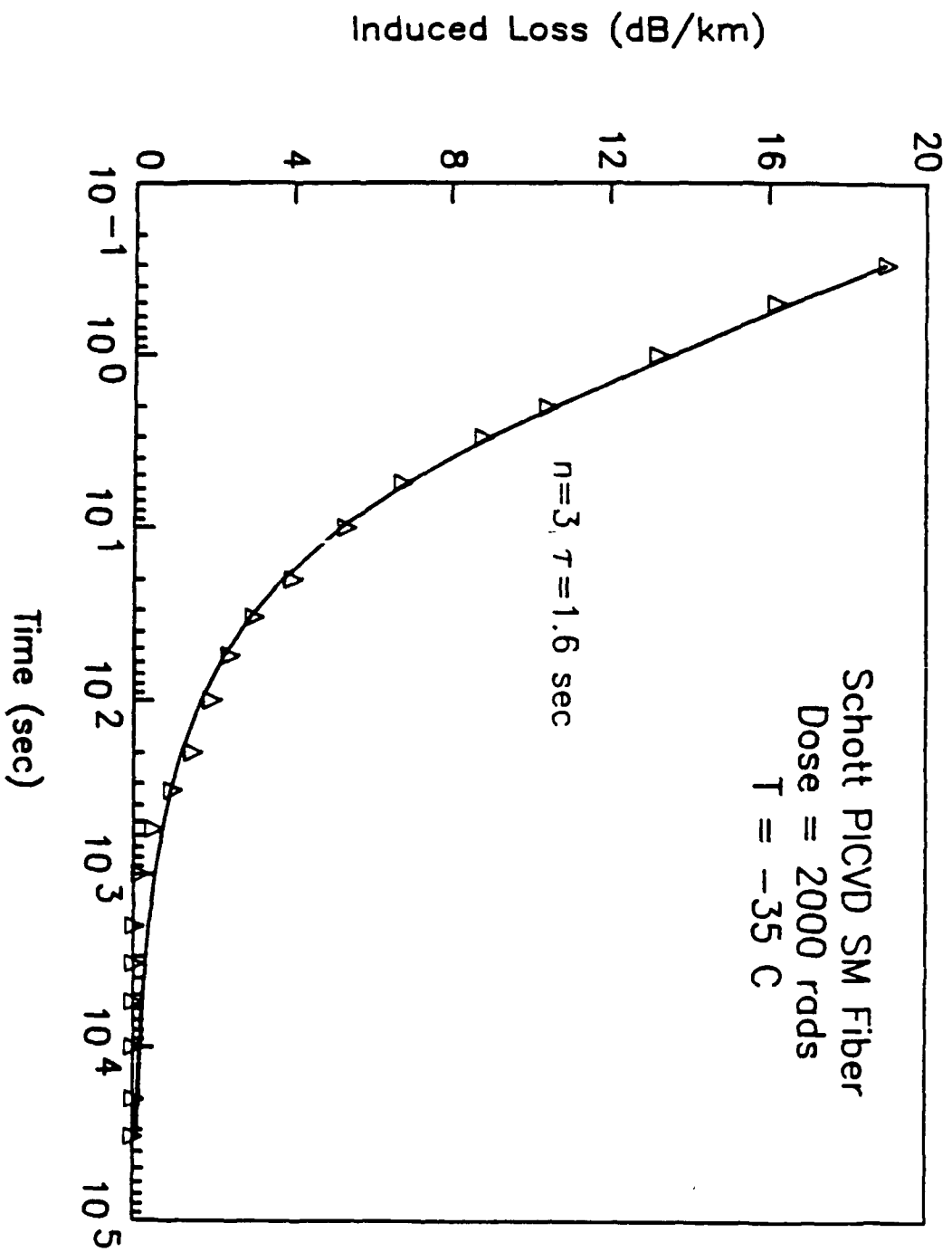


Figure 6.6 Recovery of radiation-induced attenuation (points) in a Philips single mode fiber made by the plasma CVD process and fit to kinetic model (line).

Figure 6.7 Recovery of radiation-induced attenuation (points) in a Schott single mode fiber made by the plasma-enhanced CVD process and fit to kinetic model (line).



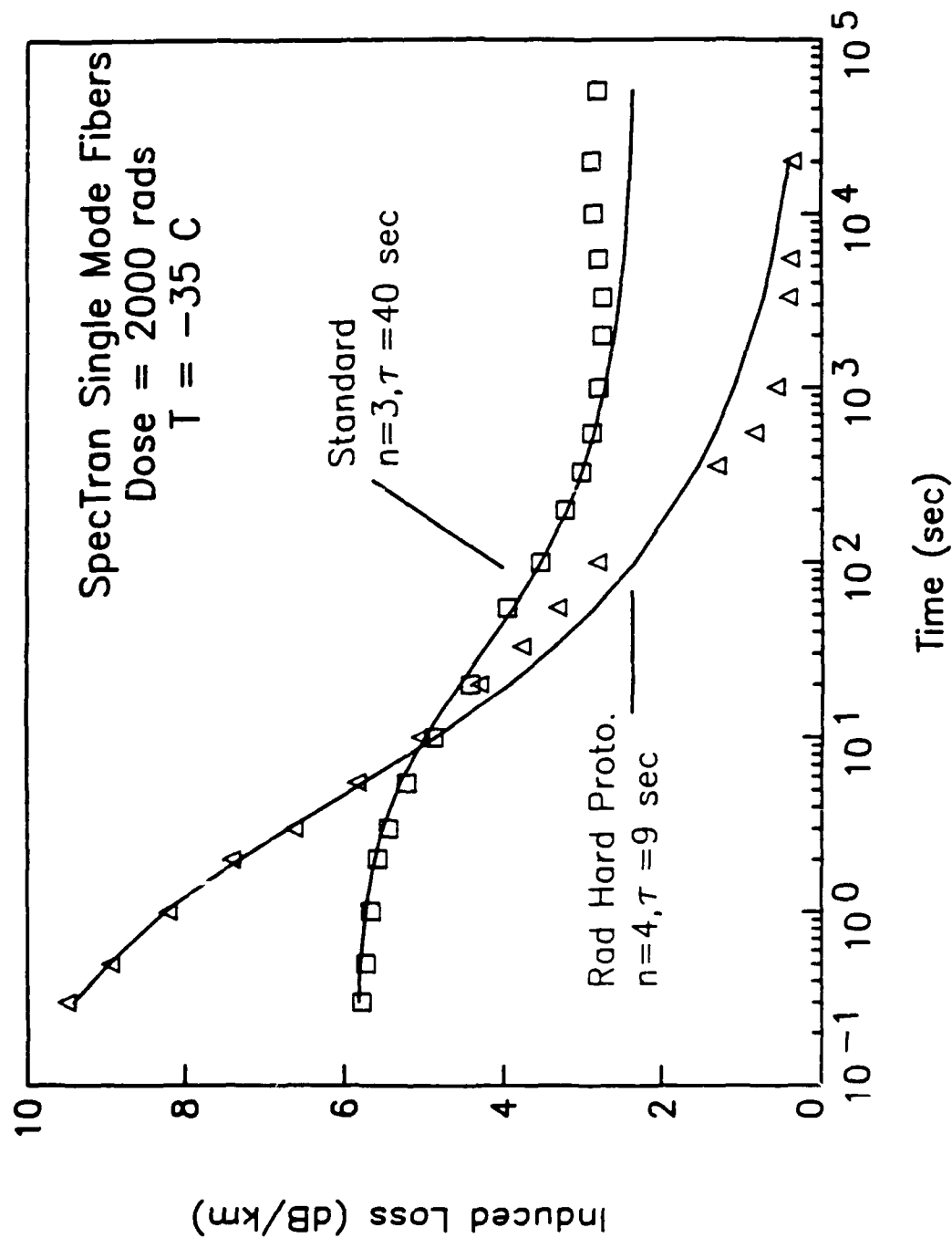


Figure 6.8 Recovery of radiation-induced attenuation (points) in commercial and rad-hard Spectran single mode fibers and fits to kinetic model (lines).

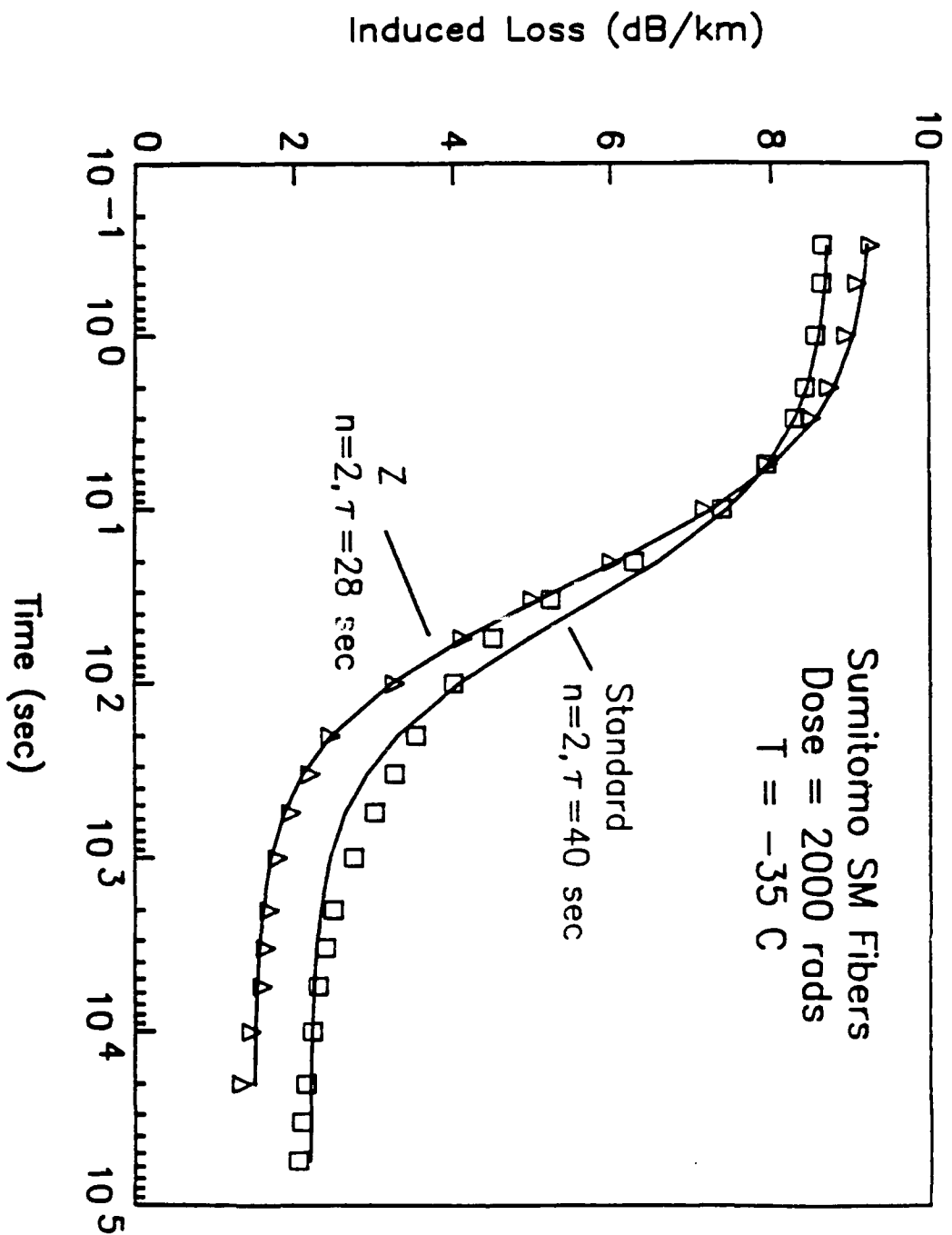


Figure 6.9 Recovery of radiation-induced attenuation (points) in Sumitomo standard Ge-doped silica and pure silica core (Z) single mode fibers and fits to kinetic model (lines).

CHAPTER 7

EXPERIMENTAL RESULTS AND MODEL DEVELOPMENT

The matched clad single mode fibers which have been designed and fabricated for this study have been all subjected to identical irradiation exposures, namely 2000 rads in a period of approximately 30 sec while maintained at -35 C. The recovery behavior following this exposure has been monitored for up to 10^5 sec, and the data have been processed as described in the previous chapters. All of the recovery curves have been fit to the kinetic model described in Chapter 6, and the resultant parameters, i.e. the initial and final ("permanent") induced attenuation, the order of the kinetics, and the "half-life" of the radiation damage, have each been used as responses in the orthogonal matrix model. In this way, it has been possible to develop relationships between fabrication parameters and each of the kinetic parameters.

RECOVERY DATA

The recoveries of the radiation-induced losses of the 24 fibers of the two matrices are shown in Figs. 7.1-7.7. They are grouped according to some common feature in their fabrication. As is evident by comparing the data, the behaviors span a broad range--the initial damages in the pure silica clad fibers are quite high, while those of the other waveguides are substantially lower. The apparent noise in the data is low in the pure silica clad fibers because of their large induced losses (Fig. 7.1), while it appears greater in the fibers with lower radiation response (Figs. 7.2-7.7).

It is interesting to note that the initial damage in the pure silica clad fibers shown in Fig. 7.1 varies considerably from sample to sample. Fiber #1 with the lowest [Ge] in the core shows the greatest damage, while #5 with the

second level of [Ge] shows the greatest. Unfortunately, there are no pure silica clad fibers with the third level of [Ge] in the core to ascertain if this trend of decreasing A_0 with increasing core [Ge] continues. However, in this sample the effect of oxygen stoichiometry is evident by comparing fiber #1 with #6, since the latter has the second level of oxygen to reagent ratio in both the core and clad (and the second level of draw tension). The agreement between the data of fibers #2 and #18 seems to indicate either an insensitivity to draw tension and core [Ge] or a cancelling of the effects of varying both parameters since #2 had a higher level of [Ge] while #18 was pulled at a lower tension.

Even in the case of doped claddings, there is a range of initial responses, and some fibers show good long term recovery while others do not. Of course, one would expect inhibited long term recovery and enhanced permanent attenuation in the P-doped clad fibers, and this is indeed the case, as shown in Figs. 7.5-7.7. However, some of the other fibers which do not contain P in the cladding show substantial long term attenuation, indicating that the measured radiation response results from a complex interaction of all the fabrication parameters.

Other than to note the large initial induced attenuation in the pure silica clad fibers, it is impossible to qualitatively relate the observed responses to fabrication parameters because of the fact that multiple parameters are changed between any two fibers.

Each of the recovery curves shown in Figs. 7.1-7.7 have been fit to the empirical kinetic model, and the parameters are shown in Table 7.1. The fits in general are quite good, as evidenced by the low standard deviations of < 0.86 dB/km for the fibers with low radiation response. Of course, the standard deviations are higher for those with large initial losses, but in all cases are $< 1\%$ of A_0 .

The dopant concentrations are required as input to both the orthogonal matrix analysis and multiple regression. Table 3.5 contains the analyzed core and cladding dopant concentrations of the fibers used for the study, and it is apparent that they were well controlled. The standard deviation of the core [Ge] is 8.5% for level 1, 12% for level 2 and only 1.8% for level 3. It is less than 3% within the 2 levels of [Ge] in the clad. The standard deviation of the [P] in the clads is 16% for levels 2 and 3 and 10% for level 4. The standard deviations are greater in these cases than for the core or clad [Ge] since there are only two P-doped samples at each level. Likewise, the [F] in the clads are well-controlled with standard deviations ranging from 0 to 4%.

ORTHOGONAL MATRIX ANALYSIS

Graphical results of exercising the orthogonal matrix analysis routine are shown in Figs. 7.8-7.34, grouped according to parameters of the kinetic model. As described previously, the numerical results of this technique for one factor are offset by the average contributions of all other parameters; for this reason, this offset has been removed and the data are plotted relative to the lowest induced attenuation within a given factor.

Initial Attenuation

Considering the effect of fabrication variables first on the initial damage level, examination of Figs. 7.8-7.15 results in some significant observations:

1. Increasing the Ge content in the core and cladding decreases the radiation response (Fig. 7.8). The effect is quite dramatic; fibers with the first level of [Ge] in the clad or core show initial induced attenuations of hundreds of dB/km, while the loss in those with second or third level [Ge] is < 10 dB/km. It appears that the effect is stronger in the clad than in the core, but the increased Ge in the clad is accompanied by appropriate increases in F from 0 to 0.87 wt%; similar codoping occurs in the core, but the increase

in F between levels 1 and 3 is only from 0.12 to 0.25 wt%. A similar effect is noted in Fig. 7.9 for the P-doped fibers, where the introduction of P is likewise accompanied by F-doping to maintain a clad of matched index of refraction. Apparently, the use of pure silica clads is not favored for initial radiation hardness, while doping with either Ge and/or F or P and/or F decreases the initial damage level.

2. The variations of the initial induced attenuation with oxygen stoichiometry shown in Figs. 7.10 and 7.11. Different behaviors are evident for the fibers of the two groups: increased oxygen flows in either the core or clad of the P-free fibers cause a slight increase in A_0 (Fig. 7.10), while substantial decreases in A_0 are measured when the clad oxygen flow in the P-doped clad fibers is increased (Fig. 7.11).

3. Similarly, draw tension seems to have an opposite effect on the fibers of the two groups: as shown in Fig. 7.12, the initial attenuations in the P-free group decrease slightly with changes between 20 and 50 g and then increase dramatically as the tension is raised to 80 g. In contrast, a substantial decrease in A_0 is evident in Fig. 7.13 as the draw tension in the P-doped clad fibers increases from 18 to 46 g.

4. Increased draw speed is seen to decrease the initial attenuation in both the P-free and P-doped clad fibers, as is evident in Figs. 7.14 and 7.15. Moderate tension and high draw speeds both tend to decrease the initial loss in both groups of fibers, and the effect is quite significant, amounting to as much as 50 dB/km for the tension and 45 dB/km for the speed. Fortunately, these requirements are not contradictory since high draw speed requires moderate-to-high draw tension. The manufacturer must therefore be careful control the draw tension in order to not increase the initial radiation-induced attenuation of the resultant fibers.

Final Attenuation

The effect of fabrication variables on the final, permanent attenuation is shown in Figs. 7.11-7.18. The precision of these data is much less because the final attenuations are small and the noise is comparatively greater. The effects appear to be generally similar to those described above for the initial induced attenuation.

1. Increasing the core [Ge] causes a slight increase in A_f while increasing the clad [Ge] and [F] significantly decreases A_f , as shown in Fig. 7.16. Although there is more scatter in the data, a similar decrease is noted in Fig. 7.17 with P/F doping in the clad. As expected, however, there remains substantial permanent induced attenuation in the P-doped clad fibers. Thus, for fallout applications, the use of Ge-F-doped clad fibers with higher doping levels appears attractive.

2. Increasing oxygen flows in the core and clad of both the Ge-F-doped (Fig. 7.18) and P-F-doped (Fig. 7.11) clad fibers results in decreases in A_f of at most 3 dB/km.

3. Draw tension does not seem to be a significant determinant of permanent attenuation in either group of fibers; only slight changes are evident for the Ge-F-doped clad waveguides (Fig. 7.12), and no dependence was found for the P-F-doped clad fibers (Fig. 7.13).

4. Increasing the draw speed from 0.5 to 4 m/sec seems to result in a slight increase in A_f in the Ge-F-doped clad fibers (Fig. 7.14) and a slight decrease in A_f in the P-F-doped fibers (Fig. 7.15). However, draw speed does not appear to be a significant determinant of the permanent attenuation in these waveguides.

Order of the Kinetics

As described in Chapter 6, a goal of increasing the radiation hardness of fibers to fallout is to decrease the order of the kinetics so that the long

term recovery occurs at a faster rate. However, it should be emphasized that the fits of the recovery data are relatively insensitive to the kinetic order parameter, and variations of ± 0.5 should not be considered significant. Furthermore, the recovery data of some of the fibers, such as #10, is distinctly different in shape from those of the others (see Figs. 7.2 and 7.3). These cases are not well-described by Eq. 6.5 and require large values of n and large half-lives to simulate their delayed recovery. When their value of n enters the response equations shown in Tables 3.3 and 3.4, the results are highly skewed.

The relationships between processing variables and the change in the order of the kinetics are shown in Figs. 7.19-7.26:

1. The dependence of n on the [Ge] concentration in the core and clad of the fibers of the first group (Fig. 7.19) has a maximum at the third level of core [Ge] due to the contribution of $n=10$ for fiber #10 to only this level for this factor (Table 3.3). Likewise, the maximum in second level of the clad [Ge] shown in Fig. 7.19 is due to the cumulative contributions of fibers #7-9 and #13-14, which all have $n=4$, together with #10 with $n=10$. The large maxima shown in Fig. 7.19 make it difficult to assess any distinct trends in the data, although it is apparent that without these anomalous points, there would be no dependence of n on [Ge] within experimental error.

The data for the effect of [P] on the order of recovery in Fig. 7.20 show that except for the pure silica core case, increasing P content decreases the order of recovery.

2. Figs. 7.21 and 7.22 indicate a relative insensitivity of n to oxygen stoichiometry within experimental error. The possible exception is the increase in kinetic order of +1 which occurs with an increase in Ge-F-clad oxygen ratio from 5 to 10.

3. Fibers from both the P-free and P-doped clad groups show an increase

in kinetic order with increasing draw tension (Figs. 7.23 and 7.24) and a similar increase with draw speed (Figs. 7.25 and 7.26). However, the effect is much less in the P-doped clad fibers than in their Ge-doped clad counterparts, as seen by comparing Figs. 7.24 and 7.26 with Figs. 7.23 and 7.25.

In general, it can be concluded that the dependence of kinetic order on variations in fabrication parameters remains unclear at this time due to the anomalous behavior of several fiber samples. It does appear that the changes are slight and within experimental error, with the exception of the P content in the clad and draw tension in the P-free clad fibers.

Half-Life of the Induced Attenuation

The final goal of hardening a fiber optic system against fallout is to decrease the "half-life" of the induced attenuation so that recovery occurs more quickly. Although the logic of this goal is apparent, consideration of the half-life should be second-order. If the initial and final losses are kept low via appropriate control of the fiber fabrication, the damage will be kept low. Adjustment of the half-life then represents a fine-tuning on an already radiation-resistant fiber. It is also important to note that similar to the case of kinetic order, the fitting procedure is insensitive to changes in τ of 10-20% and that the results will be skewed by fibers such as #10, #11, and #14, which have a large half-life ≥ 2000 sec.

Consideration of the parameter effects shown in Figs. 7.27-7.34 results in the following observations:

1. Increasing the Ge and F content in the clad decreases the half-life by a significant amount, as shown in Fig. 7.27. The large values of relative half-lives for the first and second level of clad [Ge] are due to the fact that fibers #10 and 14 with a half-lives of 60,000 and 2000 sec, respectively, contribute additively to the response of these levels, as shown in Table 3.3.

Increases in the core [Ge] seem to have the opposite effect of increasing half-life, due to the positive contribution of fiber #10 to only the third level of this factor. Interestingly, except for the pure silica core fiber, additions of P to the fiber clad cause a significant decrease in half-life, as shown in Fig. 7.28.

2. The data of the effect of oxygen stoichiometry on relative half-life contain anomalously large points for the first level in the case of the core and the second level in the case of the clad (Fig. 7.29) due to the additive contributions of fibers #10, 11 and 14 in the former and #10, 11 and 14 in the latter. Fig. 7.30 shows that increasing the oxygen flow in the P-doped clad core results in a slight decrease in the recovery time.

3. The draw tension data shown in Fig. 7.31 indicate a substantial increase in half-life with tension, but they likewise contain two anomalously large points. Figure 7.32 shows that a slight decrease in half-life with increased draw tension in the case of the P-doped clad fibers.

4. Increased draw speed seems to increase the half-life in both the Ge-F-doped clad (Fig. 7.33) and P-F-doped clad (Fig. 7.34) fibers. The effect is much greater in the former case because fibers #10 and 11 contribute to the result at the second level, while only fiber #14 contributes to the first level result.

It is apparent from the above discussion that the analysis of the initial and final induced attenuation on the basis of fabrication variables is consistent and reasonable based on prior studies of other fibers. However, inconsistencies are evident in the cases of the kinetic order and half-life due to the contributions of several fibers whose behavior cannot be well-described by the kinetic equation. Because the success of orthogonal matrix analysis depends on a complete averaging of the contributions of all factors other than the one under consideration, anomalous values of response for one

or two cases tend to be highly-weighted in the final result.

MULTIPLE REGRESSION ANALYSIS

Multiple regression analysis has been used to derive a predictive capability for determining the radiation response of matched clad single mode fibers from fabrication parameters. SPSS/PC+ was the computer code chosen for the analysis. Regressions were performed using each of the recovery parameters, A_0 , A_f , n and τ , shown in Table 7.1, which also contains the effective dopant concentrations, the normalized draw tension and the actual draw speed. These data form the input for the regressions, which included the full set of 24 fibers, and various subsets chosen to investigate a particular type of fiber: 1) including only the Ge-F-doped silica clad cases, 2) including only the P-F-doped silica clad cases, and various combinations.

In general, the first attempts at regression were made using the core and clad dopant concentrations determined from electron microprobe analysis (Tables 3.5a,b). Subsequent regressions were then performed where the dopant concentrations were weighted by the fraction of optical power being carried (Table 3.5e) once these data became available.

As discussed in Chapter 3, the best fit to the data is obtained by using as many fabrication parameters as possible. In the limit, a perfect fit would occur if there were 24 fabrication parameters affecting the radiation response of the 24 fibers of the study. Although the fit would be perfect in this case, there would be no predictive capability for samples outside the study. Rather than enter all the 6 factors of the first group (P-free clad) and the 4 factors of the second group (P-doped clad) into the regression, the stepwise technique was used. In this way only the minimum number of factors necessary to establish a significant predictive capability was included in the regression. The suggested criterion for inclusion of a factor is significance

at the 5% level, i.e. significance of an f- or t-test of 0.05, but since the f or t statistics are inversely proportional to the sample size, this constraint was deemed to be too severe for the limited population of fibers studied here. Indeed, we have found that relaxation of criterion to the 10% level results in a vastly improved fit without substantial reduction in the significance of the fit.

Initial Attenuation

Stepwise multiple regression of A_0 of all Ge-F-doped, P-F-doped and pure silica clad fibers of the study was first undertaken to determine if one equation could be developed to deal with all matched clad fibers. The regression of this case is shown in Table 7.2.

Table 7.2a can be used as an illustration of the regression output. The first three numbers are measures of the goodness of the fit to a linear model. The coefficient of determination R^2 is the square of the correlation coefficient R between A_0 and the effective [Ge] in the clad and may also be interpreted as the square of the correlation coefficient between the observed values of A_0 and the predicted values. If all observations lie on the regression line, $R^2 = 1$, while if there is no linear relationship between dependent and independent variables, $R^2 = 0$. Since the sample R^2 tends to be an optimistic estimate of how well the linear model fits the population, the adjusted R^2 attempts to correct R^2 to more closely reflect the goodness of the fit:

$$R_a^2 = R^2 - \{p(1 - R^2)\} / \{N - p - 1\} \quad 7.1$$

where N is the number of samples and p is the number of independent variables in the equation.

The analysis of variance table in the second section shows tests of the hypothesis of no linear relationship between dependent and independent variable. The total observed variability is divided into that attributed to

the regression and that which is not, i.e. the residual. In other words, a measured value of A_0 is composed to a part that is predicted by the regression and a part which is due to "noise" from whatever source. The latter part would be zero if the point was on the regression line. The mean square values are the sum of squares divided by the degrees of freedom, and the value of the f statistic is the ratio of the mean square regression to the mean square residual.

The value of f serves to test how well the regression model fits the data; a small significance associated with f (typically < 0.05 , i.e. 5%) rejects the null hypothesis that the observed values in A_0 are completely random.

The second section of the Table 7.2a contains the regression coefficients of the variables in the column labeled B. Thus, A_0 is predicted at this step of the regression from the effective clad $[Ge]$ from the population of all matched clad fibers from

$$A_0 \text{ (dB/km)} = -105.22 [Ge_{\text{clad}}]_{\text{eff}} + 104.04. \quad 7.2$$

The column labeled SE B contains the standard errors of the regression coefficients and indicate the 95% confidence interval. The standardized regression coefficient, labeled Beta in Table 7.2a, is a dimensionless representation of the regression coefficients and varies between 0 and 1. The t statistics support the hypothesis that A_0 is related to the effective $[Ge]$ in the core.

The final part of Table 7.2a contains information about the variables which have not been included in the regression equation at this step. Beta In is the standardized regression coefficient that would result if the variable were entered at the next step. The t test and significance of the t test are for the hypothesis that there is no dependence of A_0 on these variables. Obviously, the effective clad $[P]$ (EFPCLAD) is quite significant at the 0.7%

level and should be included in the regression equation. The low values of t and the high significance ($>>0.05$) of the other factors support the null hypothesis for them.

The second step of the regression, i.e. the addition of the effective clad $[P]$ to the equation, is shown in Table 7.2b. The "goodness of fit" parameters have improved, as expected, as have the f statistic and the significance of f , indicating an improved fit to the data and improved predictive capability based on these two factors:

$$A_0 = -170.00 [Ge_{clad}]_{eff} - 326.86 [P_{clad}]_{eff} + 164.44 \quad 7.3$$

where the units of A_0 are dB/km and $[Ge]$ and $[P]$ are wt%. However, note that a relatively large standard error is associated with the regression coefficient of the clad $[P]$. No other variables have a large enough significance to be included in the equation, and the stepwise procedure terminates.

The results of this regression seem strange from a physical standpoint since the only significant factors are associated with the fiber clad and none of the factors associated with the core are predictors. However, the regression results are consistent with the fact that A_0 is determined to a large extent by whether or not the clad of the fiber is pure silica or is doped with P or Ge. The anomalously large values of A_0 for the silica clad fibers have skewed the results significantly, and as shown in Fig. 7.35, the predictive capability of this model is not particularly good due to the outlying points.

When the the pure Si clad cases (fibers #1, 2, 5, 6, 17 and 18) are excluded from the population, the significant variable in the first step is the effective Ge concentration in the core, as shown in Table 7.3a. Two other variables, the effective clad $[Ge]$ and $[P]$ appear to be sufficiently significant to be included in further steps, and the former is entered on the

second step, as shown in Table 7.3b. Interestingly, it is now the draw speed which is the most significant variable not in the equation. After the third step, shown in Table 7.3c, no other variables are sufficiently significant to be included in the regression. The initial induced attenuation can now be predicted for the doped silica clad fibers from

$$A_0 = -1.44 [\text{Ge}_{\text{core}}]_{\text{eff}} + 4.77 [\text{Ge}_{\text{clad}}]_{\text{eff}} + 0.52 \text{ Speed} + 12.54 \quad 7.4$$

where the units of Speed are m/sec. A plot of the predicted vs. the observed values of A_0 for these fibers (Fig. 7.36) shows a substantial improvement in the predictive capability of the model through the elimination of the outlying points due to fibers with pure silica clads.

The population can be further narrowed by limiting the sample set to the 12 Ge-F-doped silica clad fibers. Stepwise regression of A_0 for this case is shown in Table 7.4. There is good evidence for a linear relationship between A_0 and the effective core [Ge] and clad oxygen stoichiometry,

$$A_0 = -1.13 [\text{Ge}_{\text{core}}]_{\text{eff}} + 0.41 \text{ OClad/Reag} + 12.22 \quad 7.5$$

where OClad/Reag stoichiometry is a dimensionless ratio. Likewise, there is no evidence to support a relationship between A_0 and any other fabrication parameters. A plot of the predicted vs. observed values is shown in Fig. 7.35. Note the good agreement.

Table 7.5 contains a similar regression of A_0 using only those fibers containing P in the clad. Although the f statistic is approximately the same as in the Ge-F-doped clad fibers (Table 7.4), the significance is less because of the smaller sample size of 6 fibers. It is interesting to note that the most significant predictor in this case is the draw tension, while one might expect that the [P] in the clad would be dominant. Nevertheless, at the 5% level A_0 for this class of fibers is fit to

$$A_0 = 0.45 T + 4.36 \quad 7.6$$

where T is the draw tension normalized by the fiber diameter in units of

mg/ μm^2 . Note that once again the oxygen stoichiometry in the clad is on the border of being significant enough to be included in a second step, while draw speed and effective core [Ge] are clearly not.

When the entry criterion is relaxed to include the clad oxygen factor (in this case 11%), the fit improves markedly. Note the large values of the goodness of fit parameters, the increase in f and decrease in the significance of f after the second step. Thus, good predictive capability for A_0 is found from the normalized draw tension and the clad oxygen stoichiometry during deposition:

$$A_0 = 0.54 T - 0.22 O_{\text{Clad/Reag}} + 5.72. \quad 7.7$$

Figure 7.37 contains a plot of the predicted values vs. the observed values of A_0 for these P-F-doped silica clad fibers, showing excellent agreement, which is not unexpected since the number of predictors (2) is a large fraction of the number of samples (6).

Regression was also attempted on the set of 5 pure silica clad fibers. However, no variables were entered at the 10% level, likely due to the small population of fibers and/or a lack of linear dependence of initial loss in these fibers on any of the fabrication parameters.

Final Attenuation

Table 7.4 contains the stepwise multiple regression of the final attenuation A_f for all matched clad single mode fibers of this study. The only variable entered in this case at the 10% level is the oxygen stoichiometry in the core, and examination of the variables not in the equation reveals that none of the others are significant. Because the core oxygen-to-reagent ratio is a bimodal function with values of either 5 or 15 times stoichiometry, the derived regression equation for A_f ,

$$A_f = -0.25 O_{\text{Core/Reag}} + 5.09, \quad 7.8$$

will give a poor fit to the data, as seen in Fig. 7.39. The regression results for this population indicate that a more thorough study of the relationship of core oxygen flow and A_f with multiple levels of the variable is in order.

Similar results obtain when the population excludes the doped silica clad fibers, as shown in Table 7.7. The core oxygen-to-reagent ratio is the only significant predictor of A_f ,

$$A_f = -0.32 \text{ OCore/Reag} + 4.95, \quad 7.9$$

and the bimodal nature of the core oxygen ratio results in a poor fit to the data, as shown in Fig. 7.40.

When the population is limited to fibers with Ge-F-doped silica clads, stepwise regression enters the core oxygen on the first step, as shown in Table 7.8a. The f statistic is slightly lower and the significance of f greater than in the case of all doped clads, most likely due to the smaller sample size. If the entrance criterion is 5% significance, the regression stops here with the same type of unsatisfactory fit to the data as seen in Fig. 7.40. However, it is apparent from Table 7.8a that the effective core [Ge] is also significant, and this variable is entered at the 10% level, as seen in Table 7.8b. The f statistic is slightly less, but the R^2 statistics increase and the significance of f improves slightly. Thus, a prediction of A_f for the the Ge-F-doped silica clad fibers can be accomplished through

$$A_f = -0.31 \text{ OCore/Reag} - 0.56 [\text{Ge}_{\text{core}}]_{\text{eff}} + 9.65. \quad 7.10$$

As seen in Fig. 7.41, the agreement between the predicted and observed values of A_f is not as good as in the case of A_0 shown in Figs. 7.37 and 7.38, but this is attributable to the fact that the measured A_f is more likely to be affected by long-term drift in the apparatus and measurement errors due to the much smaller values of loss.

Interestingly, a stepwise regression of A_f using analyzed rather than

effective core and clad compositions yielded somewhat different results. If carried out on the Ge-F-doped silica clad fibers, i.e. the same population as used above, only the core oxygen ratio is entered at the 10% level, and the fit is poor. However, if the pure silica clad fibers are also included with the Ge-F-doped silica fibers, the predictors are the analyzed clad [Ge] and the core oxygen-to-reagent ratio, as shown in Table 7.9. Figure 7.42 shows the relatively good agreement between predicted and measured values of A_f using the equation

$$A_f = -1.34 [\text{Ge}_{\text{clad}}]_{\text{any}} - 0.35 \text{ OCore/Reag} + 9.62. \quad 7.11$$

Note that the coefficient of the oxygen term and the constant are virtually identical, whether the regression is carried out on the effective or analyzed compositions (Eqs. 7.10 and 7.11). The fact that the analyzed clad [Ge] is an important term is apparent from Fig. 7.16, where the orthogonal analysis indicates that the Ge (and F) doping in the clad has a much more significant effect on the permanent induced attenuation than the [Ge] in the core. Since a much smaller fraction of the light is carried in the clad than in the core (typically 17-40% as shown in Table 3.5d), it is more proper to use the power-weighted compositions when performing an analysis of the radiation results. In this case, the effective core [Ge] becomes the more important predictor. It is encouraging, however, that in both regressions the core oxygen-to-reagent ratio was found to be significant and that none of the other variables was significant.

Regressions of A_f were also attempted on the P-F-doped clad fibers alone, but no variables were entered, even at the 10% level, so that no predictive capability can be established for this case at this time. It is anticipated that improved regression results will obtain with a larger population and decreased noise on A_f .

Order of Kinetics

Stepwise regressions of n were first attempted on the set of all fibers of the study; the results are shown in Table 7.10. Only one variable was entered, i.e. the effective clad $[Ge]$, yielding a limited predictive capability via

$$n = 1.10 [Ge_{clad}]_{eff} + 2.85. \quad 7.11$$

Figure 7.43 is a plot of the observed kinetic order vs. the predicted value. As mentioned above, the fits of the recovery data are not particularly sensitive to variations in n of 0.5, so within these error bars there is reasonable agreement between the regression results and the data.

The population was narrowed to only the Ge-F-doped silica clad fibers, and as shown in Table 7.11 there was a corresponding increase in the quality of the fit, as evidenced by the increase in the R^2 parameters and decrease in the significance of f . However, only the effective clad $[Ge]$ was entered; the regression equation is

$$n = 1.59 [Ge_{clad}]_{eff} + 2.39, \quad 7.12$$

and the fit is shown in Fig. 4.44. Once again, within the experimental error, there is reasonable agreement between the data and the fit.

A regression was attempted on the population of P-F-doped silica clad fibers, but no variables were entered at the 10% level.

Half-Life of Recovery

Regression of τ over the whole population of fibers resulted in the inclusion of the effective core $[Ge]$ and the core oxygen stoichiometry, as shown in Table 7.12. However, the fit is not particularly good, as evidenced by the small values of R^2 and the large significance of f , and as seen graphically in Fig. 4.45. It is obvious from the figure that the half-lives

of fibers #10 and 11 are so much larger than those of the other fibers that they form two groups and the regression attempts to solve for a line between them. Indeed, when these outlying points are removed from the population, the regression fails to enter any points, confirming that the results shown in Table 7.12 and Figure 4.45 are anomalous, and that no predictive capability for half-life exists from this study.

The fact that the regressions of n and τ were significantly less satisfactory than those of the initial and final loss can be attributed to the fact that these two fitting parameters are far less precise than A_0 and A_f , and that they often have to be artificially adjusted to fit recovery curves which do not behave in accord with Eq. 6.5. Fortunately, neither parameter is a significant determinant of the fallout response of the fibers, so the lack of predictive capability of these two parameters, although troublesome, is not considered a major drawback of the study.

The results of the multiple regression of the various recovery parameters are summarized in Table 7.12. In general, increases in core [Ge] and oxygen flow during core deposition decrease the initial and permanent induced attenuation. It is interesting to note that the oxygen flow during clad deposition has a different effect on the Ge-F-doped and P-F-doped silica clad fibers, increasing the initial induced attenuation in the former, and decreasing it in the latter. Except for the anomalous cases of A_0 regressed over all fibers and the regression of A_f using the unnormalized dopant concentrations, increases in the clad [Ge] increase the initial induced attenuation.

Several points should be made concerning the results of the regression analysis: First and foremost, the sample size of at most 24 fibers is extremely small for any statistical confidence in the results. This is especially true with the current experimental design derived from orthogonal

matrix analysis where many of the parameters are simultaneously varying from sample to sample. Such an experimental design also tends to heighten correlated effects between parameters, and these have not been explored here.

Second, the regression model assumes linear dependence between the variables and the responses. In the case where more than two levels of a factor were used, the regression attempts to derive a linear relationship, even if the data are clearly nonlinear, as in the case of core and clad [Ge] (Figs. 7.8 and 7.16). In the case of variables such as oxygen flow and draw speed (and draw tension in the P-F-doped silica clad fibers) which were examined at only two levels, the failure of the regression to include them into the equation may be interpreted as a lack of any dependence of the response on them.

Finally, the issue of the anomalously large initial induced attenuations in the silica clad fibers must be resolved since these results have such a dramatic effect on the regression. The origin of these large losses is not known at this time although the large A_0 of the LTI commercial silica core fiber shown in Table 5.1 supports the hypothesis that pure silica under some processing conditions can lead to large initial induced attenuations at low temperatures.

Table 7.1

Analyzed and Power-Weighted Core and Clad Dyeant Concentrations, Draw Conditions,
and Radiation Recovery Parameters

Fiber No.	Core				Clad				Draw		Recovery Parameters								
	Ge	Ge Eff	F	F Eff	O	Ge	Ge Eff	P	P Eff	F	F Eff	O	Temp	Spd	n	t(1/2)	No	At	Std. Dev.
1	7.50	4.50	0.07	0.01	5.00	0.00	0.00	0.00	0.00	0.00	0.00	5.00	6.6	0.5	1.8	12	420.0	10.0	4.95
2	9.40	7.80	0.06	0.02	15.00	0.00	0.00	0.00	0.00	0.00	0.00	10.00	7.3	4.0	2.0	15	260.0	10.0	3.18
3	7.40	5.03	0.10	0.01	15.00	2.50	0.80	0.00	0.00	0.55	0.18	10.00	3.5	4.0	4.0	70	12.2	0.3	0.51
4	10.30	7.83	0.20	0.01	5.00	2.40	0.58	0.00	0.00	0.50	0.12	5.00	4.0	0.5	3.0	100	1.9	1.5	0.24
5	10.20	6.73	0.10	0.02	5.00	0.00	0.00	0.00	0.00	0.00	0.00	5.00	5.0	4.0	2.0	30	60.0	7.0	1.51
6	6.20	4.34	0.04	0.01	15.00	0.00	0.00	0.00	0.00	0.00	0.00	10.00	5.3	0.5	2.3	22	243.0	0.0	2.12
7	11.40	8.21	0.24	0.02	15.00	2.50	0.70	0.00	0.00	0.51	0.14	10.00	7.7	0.5	4.0	25	7.0	0.0	0.25
8	6.20	5.10	0.14	0.12	5.00	2.30	0.39	0.00	0.00	0.53	0.09	5.00	6.6	4.0	4.0	350	9.1	6.9	0.27
9	12.00	7.80	0.18	0.01	15.00	2.50	0.88	0.00	0.00	0.49	0.17	5.00	4.7	0.5	4.0	75	4.9	0.1	0.15
10	15.20	10.03	0.26	0.03	5.00	2.40	0.82	0.00	0.00	0.54	0.18	10.00	5.9	4.0	10.0	60000	4.8	0.0	0.12
11	9.75	7.90	0.26	0.21	5.00	3.80	0.72	0.00	0.00	0.87	0.17	10.00	2.1	4.0	4.0	20000	5.7	2.6	0.26
12	15.40	10.63	0.27	0.19	15.00	3.90	1.21	0.00	0.00	0.84	0.26	5.00	2.2	0.5	4.0	80	4.0	0.6	0.22
13	16.00	10.72	0.19	0.13	15.00	2.40	0.76	0.00	0.00	0.53	0.17	5.00	2.4	4.0	4.0	70	4.5	0.0	0.58
14	8.60	5.76	0.16	0.11	5.00	2.40	0.79	0.00	0.00	0.50	0.17	10.00	1.8	0.5	4.0	2000	11.4	7.2	0.23
15	15.00	9.15	0.28	0.17	5.00	3.90	1.52	0.00	0.00	0.83	0.32	10.00	4.8	0.5	4.0	100	5.1	4.7	0.22
16	11.75	9.05	0.26	0.20	15.00	4.00	0.92	0.00	0.00	0.82	0.19	5.00	3.7	4.0	3.5	15	3.7	0.0	0.22
17	7.50	4.50	0.02	0.01	5.00	0.00	0.00	0.00	0.00	0.00	0.00	5.00	6.6	0.5	1.8	12	420.0	10.0	4.95
18	7.40	5.55	0.03	0.02	5.00	0.00	0.00	0.00	0.00	0.00	0.00	10.00	1.6	4.0	2.3	28	237.0	0.5	2.30
19	7.50	5.48	0.12	0.09	5.00	0.00	0.00	0.40	0.09	0.17	0.05	5.00	6.4	4.0	4.0	300	8.0	1.0	0.67
20	8.00	5.60	0.01	0.01	5.00	0.00	0.00	0.50	0.14	0.17	0.05	10.00	1.6	0.5	4.0	50	4.3	2.8	0.10
21	6.50	4.10	0.02	0.01	5.00	0.00	0.00	1.20	0.44	0.25	0.09	5.00	1.5	0.5	4.0	60	5.6	2.6	0.27
22	7.40	5.48	0.11	0.08	5.00	0.00	0.00	1.50	0.39	0.25	0.07	10.00	6.4	4.0	3.0	20	7.5	4.5	0.75
23	7.30	5.26	0.05	0.04	5.00	0.00	0.00	1.90	0.53	0.34	0.10	5.00	1.4	4.0	3.0	25	5.2	3.7	0.19
24	6.60	4.62	0.01	0.01	5.00	0.00	0.00	2.20	0.66	0.32	0.10	10.00	6.6	0.5	2.0	25	6.5	2.8	0.86

Table 7.2a
Stepwise Multiple Regression of A_0
All Fibers

Step 1: Effective Clad [Ge]

Multiple R .43864
R Square .19241
Adjusted R Square .15395
Standard Error 104.97626

Analysis of Variance

	DF	Sum of Squares	Mean Square
Regression	1	55136.10306	55136.10306
Residual	21	231420.30303	11020.01443

F = 5.00327 Signif F = .0363

----- Variables in the Equation -----

Variable	B	SE B	Beta	T	Sig T
EFGECLAD	-105.22270	47.04164	-.43864	-2.237	.0363
(Constant)	104.04770	30.08347		3.459	.0024

----- Variables not in the Equation -----

Variable	Beta In	Partial	Min Toler	T	Sig T
EFGECORE	.02424	.01827	.45873	.082	.9357
OCORE	.24278	.25353	.88072	1.172	.2549
EFPCCLAD	-.56946	-.55787	.77506	-3.006	.0070
OCLAD	.09272	.10315	.99974	.464	.6478
DRAWTENS	.19484	.21445	.97834	.982	.3379
DRAWSPED	-.13351	-.14665	.97446	-.663	.5149

Table 7.2b
Stepwise Multiple Regression of A_0
All Fibers

Step 2: Effective Clad [P]

Multiple R .66615
R Square .44375
Adjusted R Square .38813
Standard Error 89.27393

Analysis of Variance			
	DF	Sum of Squares	Mean Square
Regression	2	127159.70934	63579.85467
Residual	20	159396.69674	7969.83484

F = 7.97756 Signif F = .0028

----- Variables in the Equation -----

Variable	B	SE B	Beta	T	Sig T
EFGECLAD	-170.00999	45.44094	-.70873	-3.741	.0013
EFPCCLAD	-326.85955	108.72976	-.56946	-3.006	.0070
(Constant)	164.44499	32.52959		5.055	.0001

----- Variables not in the Equation -----

Variable	Beta In	Partial	Min Toler	T	Sig T
EFGECORE	-.12567	-.11191	.43662	-.491	.6291
OCORE	.11833	.14431	.72801	.636	.5326
OCLAD	.10117	.13562	.77469	.597	.5578
DRAWTENS	.11733	.15363	.74264	.678	.5061
DRAWSPED	-.22737	-.29648	.73699	-1.353	.1919

Table 7.3a
Stepwise Multiple Regression of A_0
Excluding Silica Clad Fibers

Step 1: Effective Core [Ge]

Multiple R .53960
R Square .29117
Adjusted R Square .24687
Standard Error 2.30241

Analysis of Variance

	DF	Sum of Squares	Mean Square
Regression	1	34.84063	34.84063
Residual	16	84.81715	5.30107

F = 6.57238 Signif F = .0208

----- Variables in the Equation -----

Variable	B	SE B	Beta	T	Sig T
EFGE CORE	-.65518	.25556	-.53960	-2.564	.0208
(Constant)	10.83881	1.89323		5.725	.0000

----- Variables not in the Equation -----

Variable	Beta In	Partial	Min Toler	T	Sig T
OCORE	.29950	.30980	.75839	1.262	.2262
EFGECLAD	.70731	.54594	.42229	2.524	.0234
EFPC LAD	-.54467	-.51438	.63219	-2.323	.0346
OCLAD	.32397	.38248	.98798	1.603	.1297
DRAWTENS	.16263	.19310	.99936	.762	.4577
DRAWSPED	.22043	.26181	.99992	1.051	.3101

Table 7.3b
Stepwise Multiple Regression of A_0
Excluding Silica Clad Fibers

Step 2: Effective Clad [Ge]

Multiple R .70883
R Square .50243
Adjusted R Square .43609
Standard Error 1.99228

Analysis of Variance

	DF	Sum of Squares	Mean Square
Regression	2	60.12019	30.06010
Residual	15	59.53759	3.96917

F = 7.57339 Signif F = .0053

----- Variables in the Equation -----

Variable	B	SE B	Beta	T	Sig T
EFGECORE	-1.30793	.34030	-1.07721	-3.843	.0016
EFGECLAD	3.99529	1.58312	.70731	2.524	.0234
(Constant)	13.23199	1.89288		6.990	.0000

----- Variables not in the Equation -----

Variable	Beta In	Partial	Min Toler	T	Sig T
OCORE	.19751	.23842	.40372	.919	.3739
EFPCCLAD	-.33781	-.32763	.31264	-1.298	.2154
OCLAD	.22453	.30684	.39456	1.206	.2477
DRAWTENS	.18752	.26538	.42110	1.030	.3205
DRAWSPED	.35674	.48985	.39619	2.102	.0541

Table 7.3c
Stepwise Multiple Regression of A_0
Excluding Silica Clad Fibers

Step 3: Draw Speed

Multiple R	.78856
R Square	.62182
Adjusted R Square	.54079
Standard Error	1.79785

Analysis of Variance

	DF	Sum of Squares	Mean Square
Regression	3	74.40614	24.80205
Residual	14	45.25164	3.23226

F = 7.67328 Signif F = .0028

----- Variables in the Equation -----

Variable	B	SE B	Beta	T	Sig T
EFGECORE	-1.43783	.31024	-1.18420	-4.590	.0004
EFGECLAD	4.76609	1.47492	.84377	3.231	.0060
DRAWSPED	.52559	.25000	.35674	2.102	.0541
(Constant)	12.53927	1.73964		7.208	.0000

----- Variables not in the Equation -----

Variable	Beta In	Partial	Min Toler	T	Sig T
OCORE	.17782	.24592	.37785	.915	.3770
EFPCCLAD	-.23210	-.25101	.27850	-.935	.3669
OCLAD	.24436	.38249	.37617	1.493	.1594
DRAWTENS	.15956	.25811	.39582	.963	.3530

Table 7.4a
Stepwise Multiple Regression of A_0
Ge-F-Doped Silica Clad Fibers

Step 1: Effective Core [Ge]

Multiple R	.78245
R Square	.61222
Adjusted R Square	.57345
Standard Error	2.06221

Analysis of Variance

	DF	Sum of Squares	Mean Square
Regression	1	67.14201	67.14201
Residual	10	42.52715	4.25272

F = 15.78803 Signif F = .0026

----- Variables in the Equation -----

Variable	B	SE B	Beta	T	Sig T
EFGECORE	-1.24797	.31408	-.78245	-3.973	.0026
(Constant)	16.30128	2.61303		6.238	.0001

----- Variables not in the Equation -----

Variable	Beta In	Partial	Min Toler	T	Sig T
OCORE	.15801	.24574	.93786	.761	.4664
EFGECLAD	.20111	.28023	.75290	.876	.4039
OCLAD	.34207	.53561	.95070	1.903	.0895
DRAWTENS	-.09734	-.15513	.98498	-.471	.6488
DRAWSPED	.10429	.16708	.99536	.508	.6234

Table 7.4b
Stepwise Multiple Regression of A_0
Ge-F-Doped Silica Clad Fibers

Step 2: Oxygen Stoichiometry in the Clad

Multiple R	.85057
R Square	.72347
Adjusted R Square	.66202
Standard Error	1.83566

Analysis of Variance

	DF	Sum of Squares	Mean Square
Regression	2	79.34234	39.67117
Residual	9	30.32682	3.36965

F = 11.77309 Signif F = .0031

----- Variables in the Equation -----

Variable	B	SE B	Beta	T	Sig T
EFGE CORE	-1.12683	.28673	-.70650	-3.930	.0035
OCLAD	.41365	.21739	.34207	1.903	.0895
(Constant)	12.21759	3.16481		3.860	.0038

----- Variables not in the Equation -----

Variable	Beta In	Partial	Min Toler	T	Sig T
OCORE	.28402	.49987	.85657	1.632	.1412
EFGECLAD	.07693	.11905	.65140	.339	.7432
DRAWTENS	-.12364	-.23268	.94057	-.677	.5177
DRAWSPED	.10951	.20775	.94606	.601	.5647

Table 7.5a
Stepwise Multiple Regression of A_0
P-F-Doped Silica Clad Fibers Only

Step 1: Normalized Draw Tension

Multiple R	.87740
R Square	.76983
Adjusted R Square	.71229
Standard Error	.75812

Analysis of Variance

	DF	Sum of Squares	Mean Square
Regression	1	7.68936	7.68936
Residual	4	2.29897	.57474

F = 13.37881 Signif F = .0216

----- Variables in the Equation -----

Variable	B	SE B	Beta	T	Sig T
DRAWTENS	.45558	.12455	.87740	3.658	.0216
(Constant)	4.36862	.58476		7.471	.0017

----- Variables not in the Equation -----

Variable	Beta In	Partial	Min Toler	T	Sig T
EFGEORE	-.03458	-.07091	.96798	-.123	.9098
EFPCCLAD	-.12587	-.26225	.99908	-.471	.6700
OCLAD	-.43094	-.83959	.87363	-2.677	.0752
DRAWSPED	.31976	.63542	.90890	1.425	.2493

Table 7.5b
Stepwise Multiple Regression of A_0
P-F-Doped Silica Clad Fibers Only

Step 2: Oxygen Stoichiometry in the Clad

Multiple R	.96544
R Square	.93208
Adjusted R Square	.88680
Standard Error	.47554

Analysis of Variance

	DF	Sum of Squares	Mean Square
Regression	2	9.30992	4.65496
Residual	3	.67842	.22614

F = 20.58455 Signif F = .0177

----- Variables in the Equation -----

Variable	B	SE B	Beta	T	Sig T
DRAWTENS	.53512	.08359	1.03059	6.402	.0077
OCLAD	-.22241	.08308	-.43094	-2.677	.0752
(Constant)	5.71984	.62395		9.167	.0027

----- Variables not in the Equation -----

Variable	Beta In	Partial	Min Toler	T	Sig T
EFGE CORE	.05642	.20799	.83293	.301	.7920
EFPC LAD	-.08528	-.32534	.86437	-.487	.6747
DRAW SPED	.14672	.46650	.66002	.746	.5335

Table 7.6
Stepwise Multiple Regression of Af
All Fibers

Multiple R .37179
R Square .13823
Adjusted R Square .09719
Standard Error 3.08446

Analysis of Variance		DF	Sum of Squares	Mean Square
Regression		1	32.04593	32.04593
Residual		21	199.79233	9.51392

F = 3.36832 Signif F = .0807

----- Variables in the Equation -----

Variable	B	SE B	Beta	T	Sig T
OCORE	-.24783	.13504	-.37179	-1.835	.0807
(Constant)	5.09250	1.31316		3.878	.0009

----- Variables not in the Equation -----

Variable	Beta In	Partial	Min Toler	T	Sig T
EFGE CORE	-.18969	-.18686	.83630	-.851	.4050
EFGE CLAD	-.21722	-.21959	.88072	-1.007	.3261
EFPC LAD	-.12048	-.12071	.86504	-.544	.5926
OCLAD	-.02543	-.02738	.99899	-.122	.9037
DRAW TENS	.30902	.33116	.98967	1.570	.1322
DRAW SPED	4.7567E-03	.00512	.99899	.023	.9820

Table 7.7
Stepwise Multiple Regression of Af
Excluding Only Pure Silica Clad Fibers

Multiple R .65969
R Square .43519
Adjusted R Square .39989
Standard Error 1.81801

Analysis of Variance			
	DF	Sum of Squares	Mean Square
Regression	1	40.74694	40.74694
Residual	16	52.88250	3.30516

F = 12.32830 Signif F = .0029

----- Variables in the Equation -----

Variable	B	SE B	Beta	T	Sig T
OCORE	-.31917	.09090	-.65969	-3.511	.0029
(Constant)	4.95417	.87031		5.692	.0000

----- Variables not in the Equation -----

Variable	Beta In	Partial	Min Toler	T	Sig T
FFGECORE	-.23219	-.26906	.75839	-1.082	.2964
GECLAD	.15872	.18384	.75766	.724	.4800
OCLAD	.05459	.07059	.94444	.274	.7877
DRAWTENS	-.07466	-.09934	.99982	-.387	.7044
DRAWSPED	-.08038	-.10696	1.00000	-.417	.6828

Table 7.8a
Stepwise Multiple Regression of A_f
Ge-F-Doped Silica Clad Fibers Only

Step 1: Core Oxygen Stoichiometry

Multiple R	.69222
R Square	.47917
Adjusted R Square	.42709
Standard Error	2.08427

Analysis of Variance

	DF	Sum of Squares	Mean Square
Regression	1	39.96750	39.96750
Residual	10	43.44167	4.34417

F = 9.20027 Signif F = .0126

----- Variables in the Equation -----

Variable	B	SE B	Beta	T	Sig T
OCORE	-.36500	.12034	-.69222	-3.033	.0126
(Constant)	5.64167	1.34539		4.193	.0018

----- Variables not in the Equation -----

Variable	Beta In	Partial	Min Toler	T	Sig T
EFGECORE	-.40263	-.54029	.93786	-1.926	.0862
EFGECLAD	5.1488E-03	.00707	.98170	.021	.9835
OCLAD	-.05690	-.07433	.88889	-.224	.8281
DRAWTENS	-.08461	-.11711	.99790	-.354	.7317
DRAWSPED	-.13592	-.18833	1.00000	-.575	.5792

Table 7.8b

Stepwise Multiple Regression of A_f
Ge-F-Doped Silica Clad Fibers Only

Step 2: Effective Core [Ge]

Multiple R .79449
R Square .63121
Adjusted R Square .54925
Standard Error 1.84874

Analysis of Variance

	DF	Sum of Squares	Mean Square
Regression	2	52.64849	26.32425
Residual	9	30.76067	3.41785

F = 7.70198 Signif F = .0112

----- Variables in the Equation -----

Variable	B	SE B	Beta	T	Sig T
OCORE	-.31208	.11022	-.59185	-2.831	.0197
EFGECORE	-.56004	.29075	-.40263	-1.926	.0862
(Constant)	9.64919	2.39849		4.023	.0030

----- Variables not in the Equation -----

Variable	Beta In	Partial	Min Toler	T	Sig T
EFGECLAD	.25456	.36369	.71914	1.104	.3016
OCLAD	-.12267	-.18822	.85657	-.542	.6025
DRAWTENS	-.13118	-.21435	.92548	-.621	.5521
DRAWSPED	-.16417	-.26966	.93321	-.792	.4512

Table 7.9a
Stepwise Multiple Regression of Af
Ge-F-Doped Silica Clad Fibers

Step 1: Analyzed [Ge] in Clad

Multiple R .52034
R Square .27076
Adjusted R Square .21867
Standard Error 3.37043

Analysis of Variance

	DF	Sum of Squares	Mean Square
Regression	1	59.04755	59.04755
Residual	14	159.03683	11.35977

F = 5.19795 Signif F = .0388

----- Variables in the Equation -----

Variable	B	SE B	Beta	T	Sig T
GECLAD	-1.37180	.60169	-.52034	-2.280	.0388
(Constant)	6.18207	1.56281		3.956	.0014

----- Variables not in the Equation -----

Variable	Beta In	Partial	Min Toler	T	Sig T
GECORE	-.20587	-.20546	.72630	-.757	.4626
OCORE	-.47565	-.55680	.99928	-2.417	.0311
OCLAD	-.02201	-.02577	1.00000	-.093	.9274
DRAWTENS	.06233	.06161	.71236	.223	.8273
DRAWSPED	.04107	.04809	.99992	.174	.8649

Case 1

Stepwise Multiple Regression of Y on

Self-Drawings of Faces and Features

Step 2: Oxygen Stoichiometry in Core

Multiple R .70487
R Square .49684
Adjusted R Square .41343
Standard Error 2.90533

Analysis of Variance

	DF	Sum of Squares	Mean Square
Regression	2	108.35289	54.17644
Residual	13	109.33289	8.40953

F = 6.41829 Significant = .0113

----- Variables in the Equation -----

Variable	B	SE B	Beta	Partial	Signif.
GECLAD	-1.33822	.51885	-.50740	-.42155	.0229
OCORE	-.35121	.14532	-.27565	-.27677	.0211
(Constant)	9.62075	1.95938		8.951	.0000

----- Variables not in the Equation -----

Variable	Beta In	Partial	Min. Toler.	Signif.
GECORE	-.12993	-.15455	.71122	.487
OCLAD	-.02201	-.03103	.99928	.978
DRAWTENS	.07194	.08559	.71164	.228
DRAWSPED	.04118	.05805	.99920	.977

Table 7.10
Stepwise Multiple Regression of n
All Fibers

Multiple R .61517
R Square .37844
Adjusted R Square .34736
Standard Error .69419

Analysis of Variance

	DF	Sum of Squares	Mean Square
Regression	1	5.86802	5.86802
Residual	20	9.63789	.48189

F = 12.17698 Signif F = .0023

----- Variables in the Equation -----

variable	B	SE B	Beta	T	Sig T
EFGECLAD	1.10247	.31594	.61517	3.490	.0023
(Constant)	2.84909	.19906		14.312	.0000

----- Variables not in the Equation -----

Variable	Beta In	Partial	Min Toler	T	Sig T
EFGECORE	-.22533	-.19536	.46723	-.868	.3961
OCORE	-.10589	-.12407	.85326	-.545	.5921
EFPCCLAD	.12219	.13718	.78346	.604	.5532
OCLAD	-.07954	-.10087	.99958	-.442	.6635
DRAWTENS	-.24908	-.31073	.96737	-1.425	.1704
DRAWSPED	.05670	.07042	.95887	.308	.7515

Table 7.11
Stepwise Multiple Regression of α
Ge-F-Doped Silica Clad Fibers

Multiple R .82617
R Square .68255
Adjusted R Square .65813
Standard Error .52038

Analysis of Variance			
	DF	Sum of Squares	Mean Square
Regression	1	7.56904	7.56904
Residual	13	3.52029	.27079

F = 27.95151 Signif F = .0001

----- Variables in the Equation -----

Variable	B	SE B	Beta	T	Sig.
EFGECLAD	1.58707	.30019	.82617	5.287	.0001
(Constant)	2.39253	.22906		10.445	.0000

----- Variables not in the Equation -----

Variable	Beta In	Partial	Min Toler	T	Sig.
EFGECORE	-.16435	-.22937	.61830	-.816	.4302
OCORE	.04644	.08203	.99053	.285	.7804
OCLAD	.05661	.10029	.99629	.349	.7330
DRAWTENS	-.07016	-.10659	.73260	-.371	.7168
DRAWSPED	.17224	.29823	.95172	1.082	.3004

Table 7.12a
Stepwise Multiple Regression of τ
All Fibers

Step 1: Effective Core [Ge]

Multiple R .35483
R Square .12591
Adjusted R Square .08428
Standard Error 12412.29559

Analysis of Variance

	DF	Sum of Squares	Mean Square
Regression	1	466032789.21912	466032789.21912
Residual	21	3235366718.69392	154065081.84257

F = 3.02491 Signif F = .0966

----- Variables in the Equation -----

Variable	B	SE B	Beta	T	Sig T
EFGECORE	2195.74475	1262.48354	.35483	1.739	.0966
(Constant)	-11328.05782	8980.72764		-1.261	.2210

----- Variables not in the Equation -----

Variable	Beta In	Partial	Min Toler	T	Sig T
OCORE	-.41826	-.40912	.83630	-2.005	.0587
EFGECLAD	-.09999	-.07243	.45873	-.325	.7487
EFPCCLAD	.02951	.02793	.78303	.125	.9018
OCLAD	.30331	.32291	.99070	1.526	.1427
DRAWTENS	.09427	.10072	.99778	.453	.6556
DRAWSPED	.22268	.23695	.98971	1.091	.2884

Table 1.11
Stepwise Multiple Regression of $Y = \text{Core}$
1. Filters

Step 2: Core 0

Multiple R .52174
R Square .27221
Adjusted R Square .19943
Standard Error 11605.69481

Analysis of Variance

	DF	Sum of Squares	Mean Square
Regression	2	100755646.92933	50377823.31466
Residual	20	2693843040.08192	134692152.00400

F = 3.74022 Signif. F = .0417

----- Variables in the Equation -----

Variable	B	SE B	Beta	t	Signif.
EFGECORE	3242.93354	1290.41382	.52404	2.511	.0217
OCORE	-1114.04021	555.60134	-.40424	-2.005	.0687
(Constant)	-9016.11119	8455.91681		-.064	.9501

----- Variables not in the Equation -----

Variable	Beta In	Partial	Wald	df	Signif.
EFGECLAD	-.05683	-.04438	43331	1, 26	.6466
EFPCCLAD	-.06945	-.07025	12002	1, 26	.7422
OCLAD	.30638	.35745	42031	1, 26	.0007
DRAWTENS	.14744	.17112	42177	1, 26	.0580
DRAWSPED	.19314	.22451	42322	1, 26	.0070

Table 7.13

Summary of Regression Coefficients for Matched Clad Fibers

Parameter	Fibers	Effective Core [Ge]	Core Oxygen	Effective Clad [Ge]	Effective Clad [P]	Clad Oxygen	Draw Tension	Draw Speed	Constant
AO	AlI			-170.00	-326.86				164.44
AO	Ex SiO2 Clad	-1.43		4.77				0.53	12.54
AO	Ge-F-Clad	-1.13				0.41			12.22
AO	P-F-Clad					-0.22	0.54		5.72
Af	AlI		-0.25						5.09
Af	Ex SiO2 Clad		-0.32						4.95
Af	Ge-F-Clad	-0.56	-0.32						9.65
Af	Ex P-F-Clad*		-0.35	-1.34					9.62
n	AlI			1.10					2.85
n	Ge-F-Clad			1.59					2.39
t(1/2)	AlI	3242.93	-1114.04						9016.11

* Composition by electron microprobe analysis not normalized by optical power

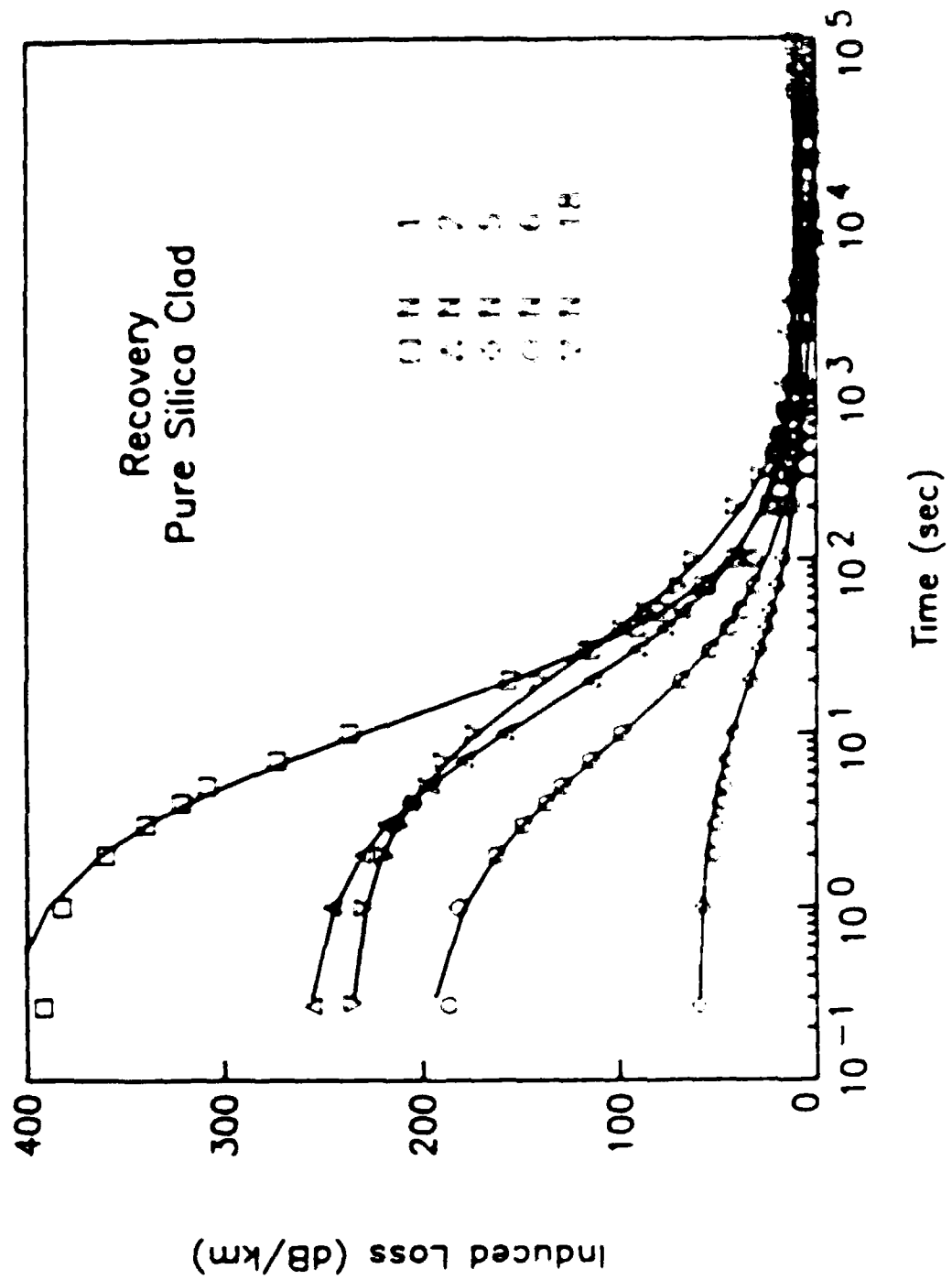


Figure 7.1 Recovery of radiation-induced attenuation in pure silica clad single mode fibers (points) and fits to the generalized kinetic recovery equation (lines).

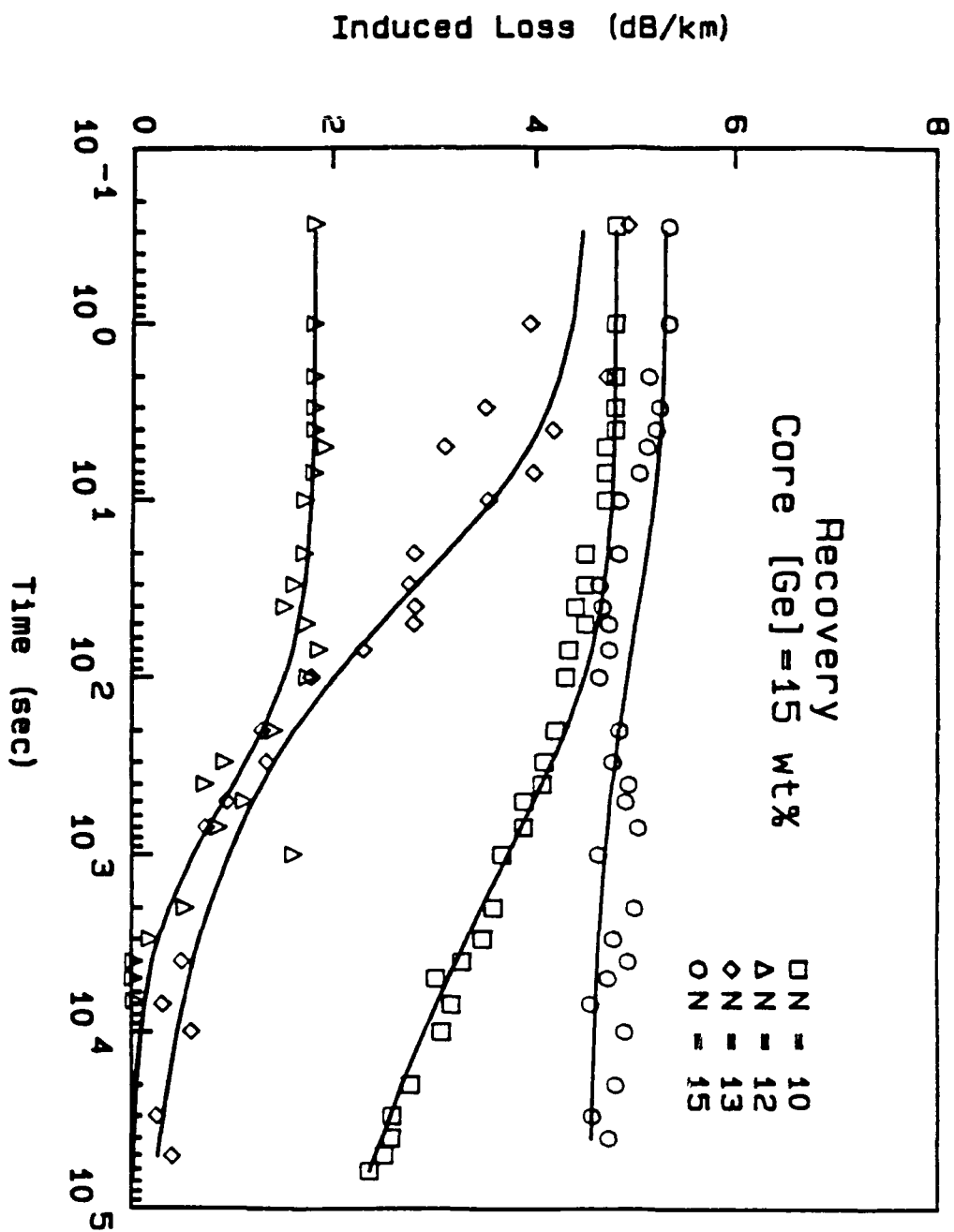


Figure 7.2 Recovery of radiation-induced attenuation in matched clad single mode fibers with level 3 Ge in the core (points) and fits to the generalized kinetic recovery equation (lines).

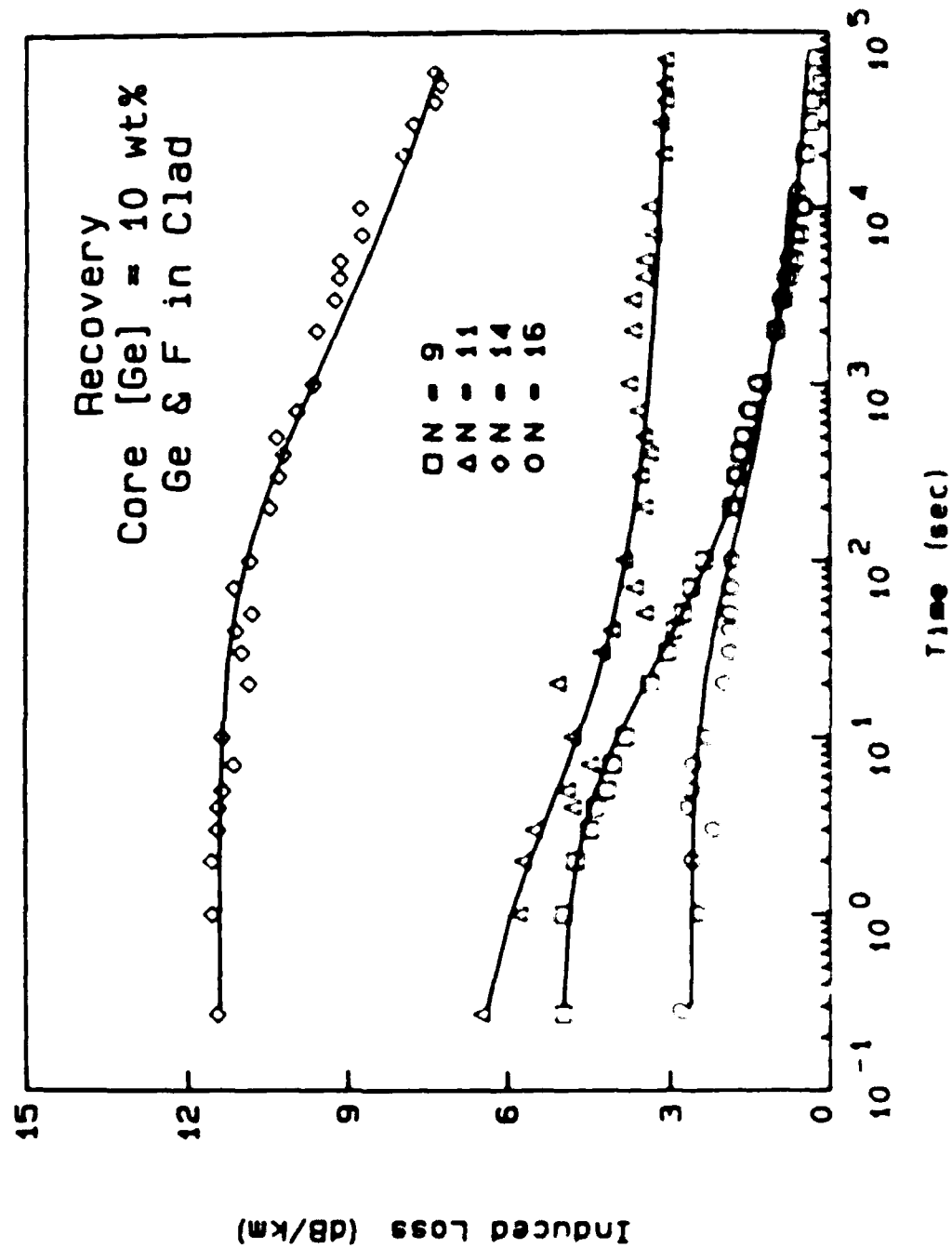


Figure 7.1 Recovery of radiation-induced attenuation in matched clad single mode fibers with level 2 Ge in the core (points) and fits to the generalized kinetic recovery equation (lines)

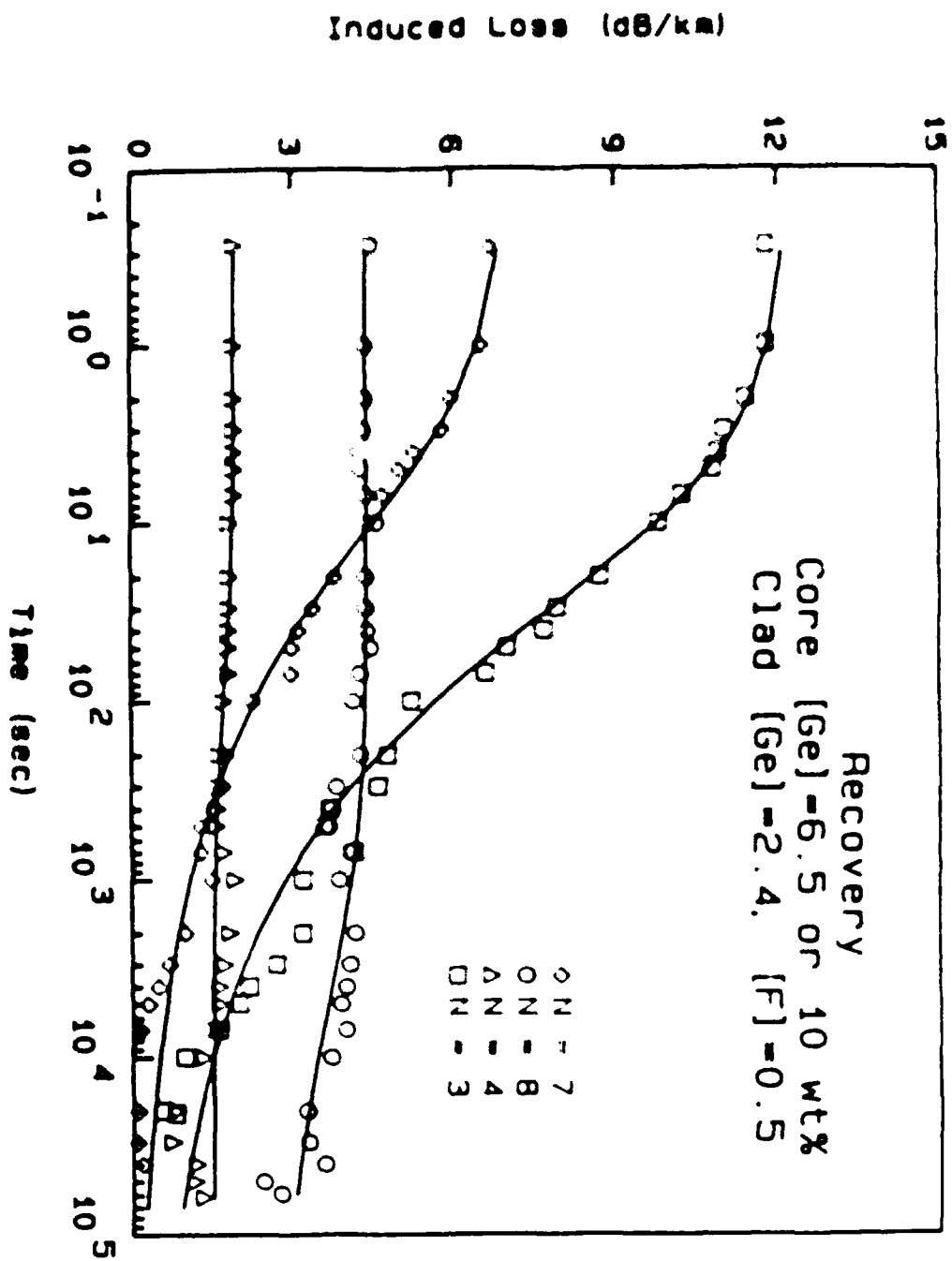


Figure 7.4 Recovery of radiation-induced attenuation in matched clad single mode fibers with levels 1 or 2 Ge in the core and level 2 Ge in the clad drawn doped with F to maintain the proper index (points) and fits to the generalized biexponential recovery equation (lines).

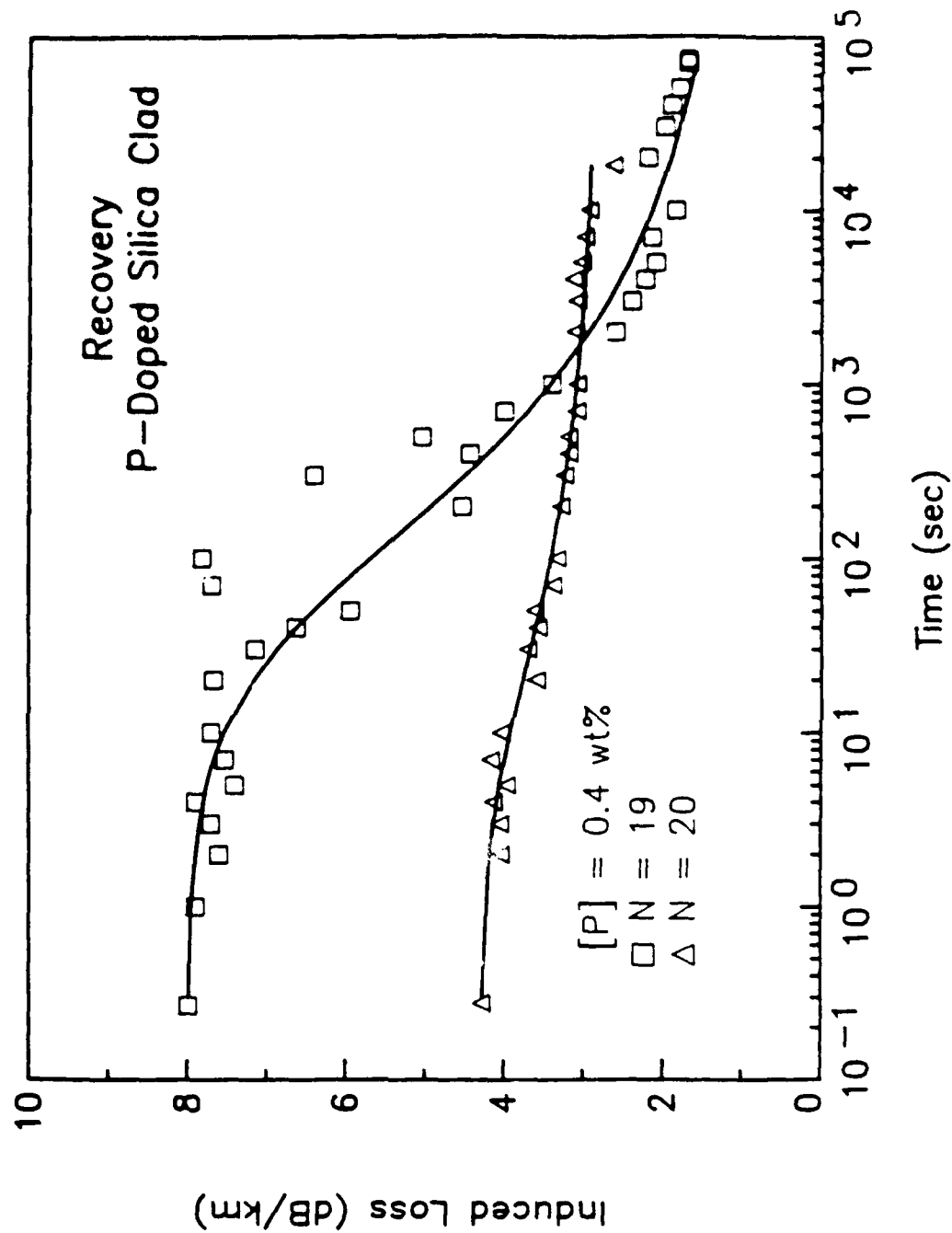


Figure 7.5 Recovery of radiation-induced attenuation in matched clad single mode fibers with level 1 P in the clad down doped with F to maintain the proper index (points) and fits to the generalized kinetic recovery equation (lines).

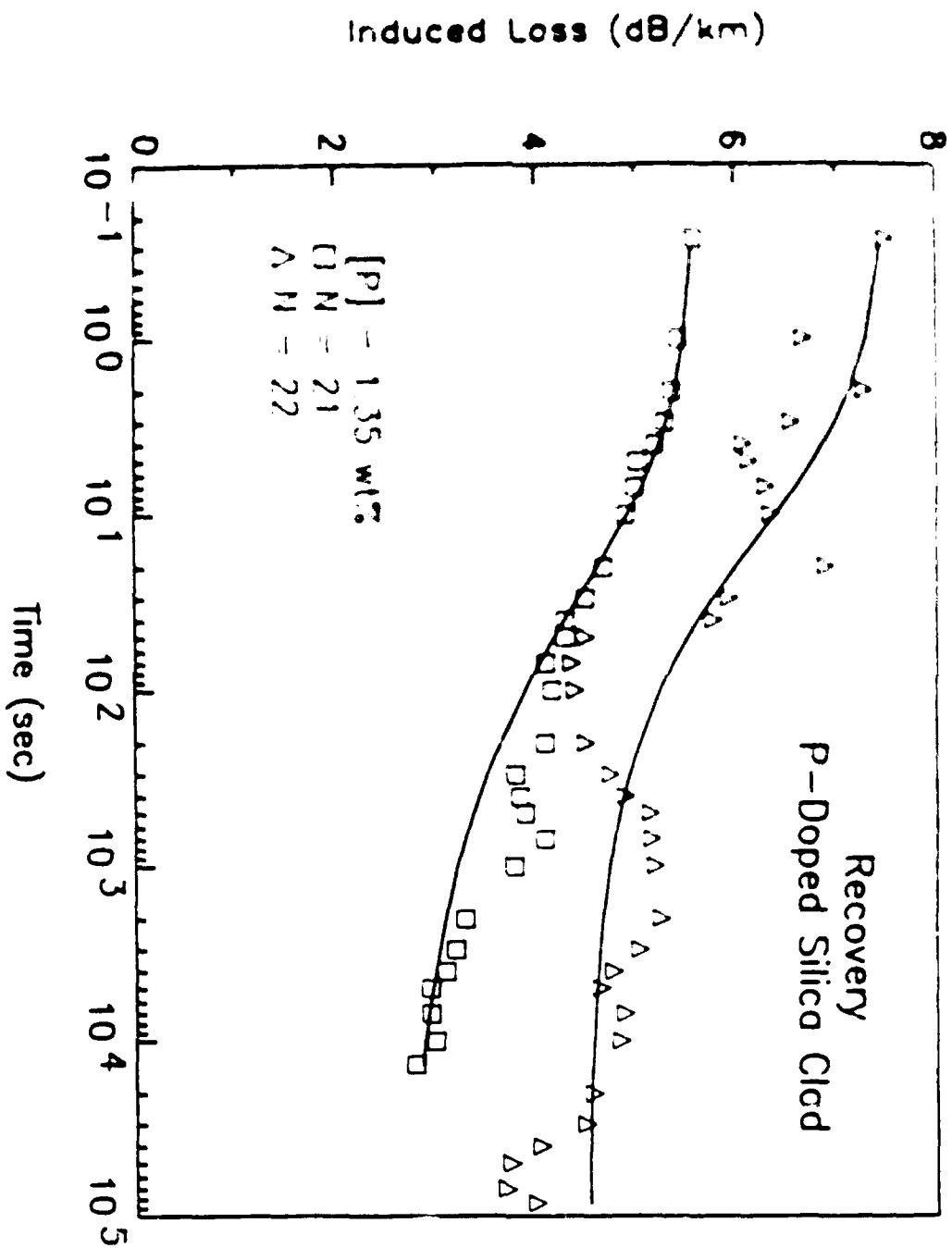


Figure 7.6 Recovery of radiation-induced attenuation in matched clad single mode fibers with level 2 P in the clad doped with F to maintain the proper index (points) and fits to the generalized kinetic recovery equation (lines).

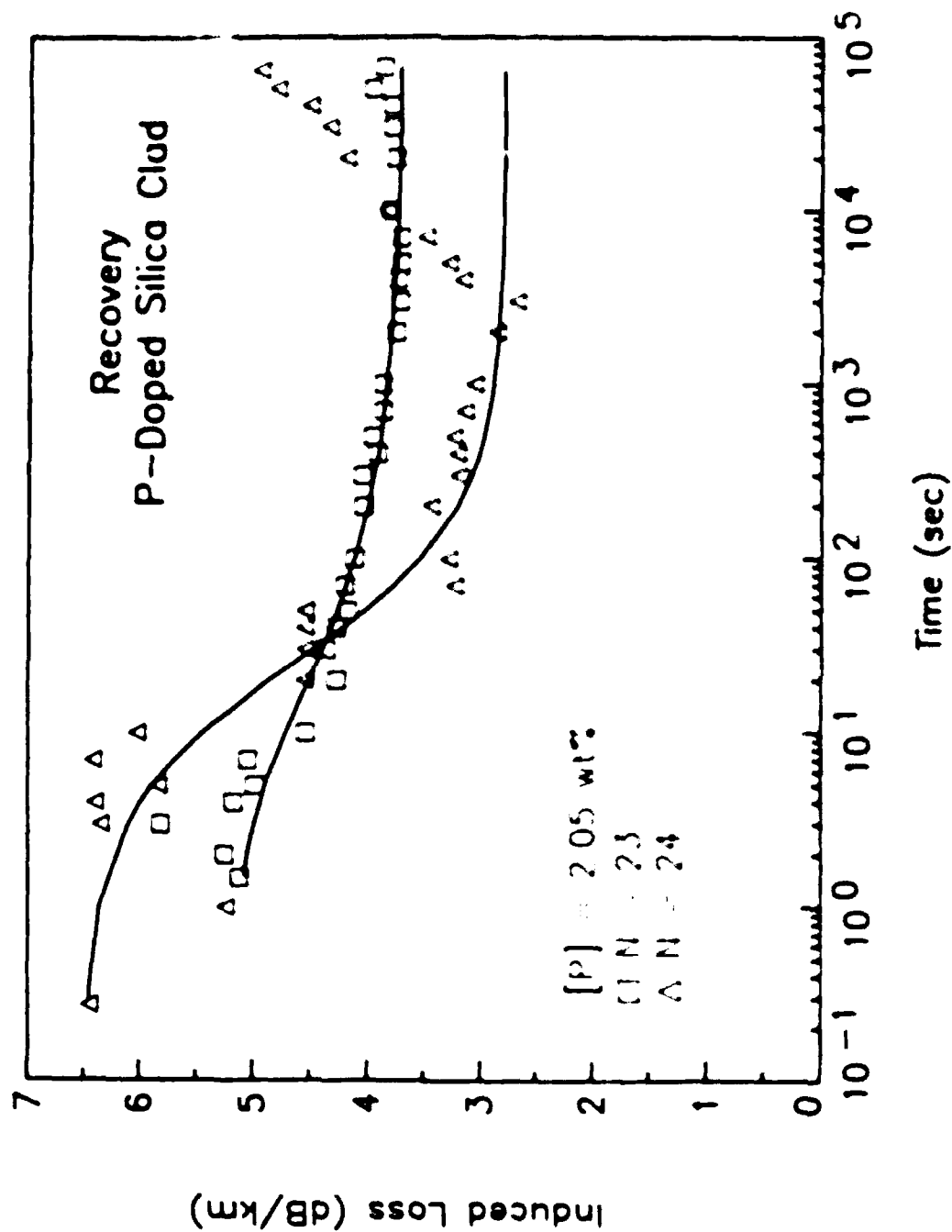


Figure 2.7. Recovery of radiation-induced attenuation in etched clad single mode fibers with level 3 P in the clad down doped with F to maintain the proper index (points) and fits to the generalized kinetic recovery equation (lines)

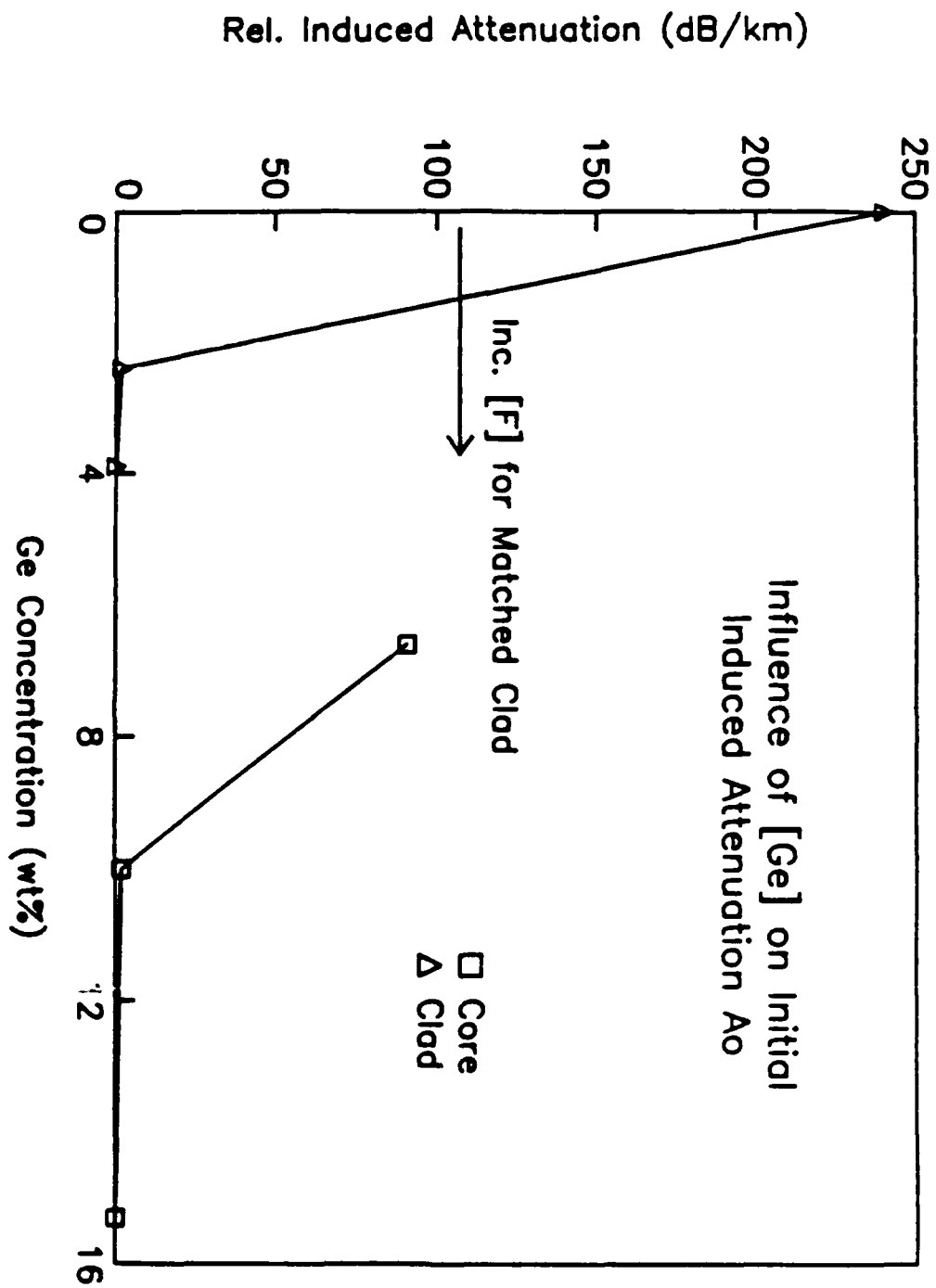


Figure 7.8 Effect of Ge concentration in the core and clad (down-doped with F) on the initial damage level A_0 of fibers of the first group.

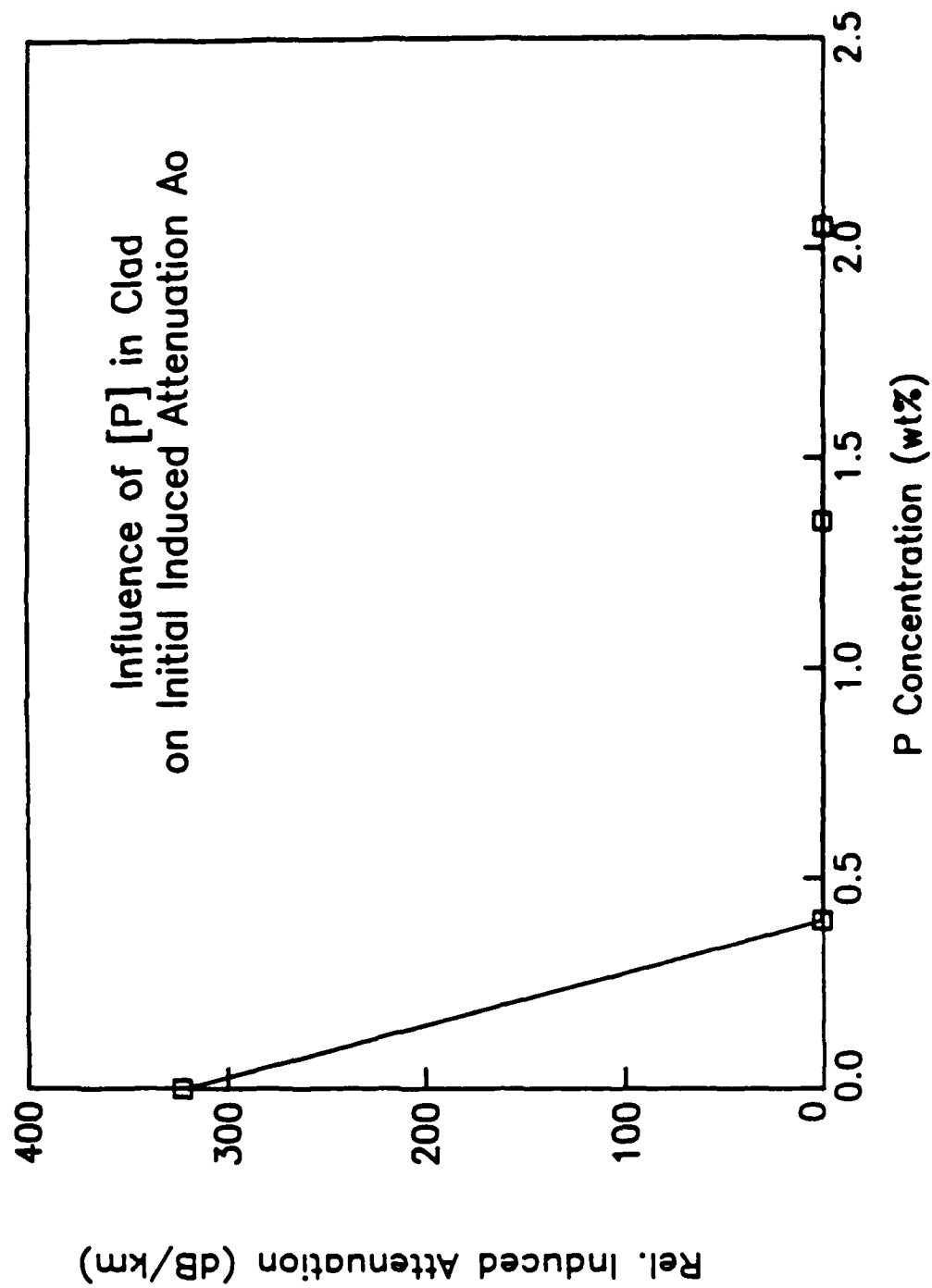


Figure 7.9 Effect of P concentration in the clad (down-doped with f) on initial damage level A_0 of fibers of the second group.

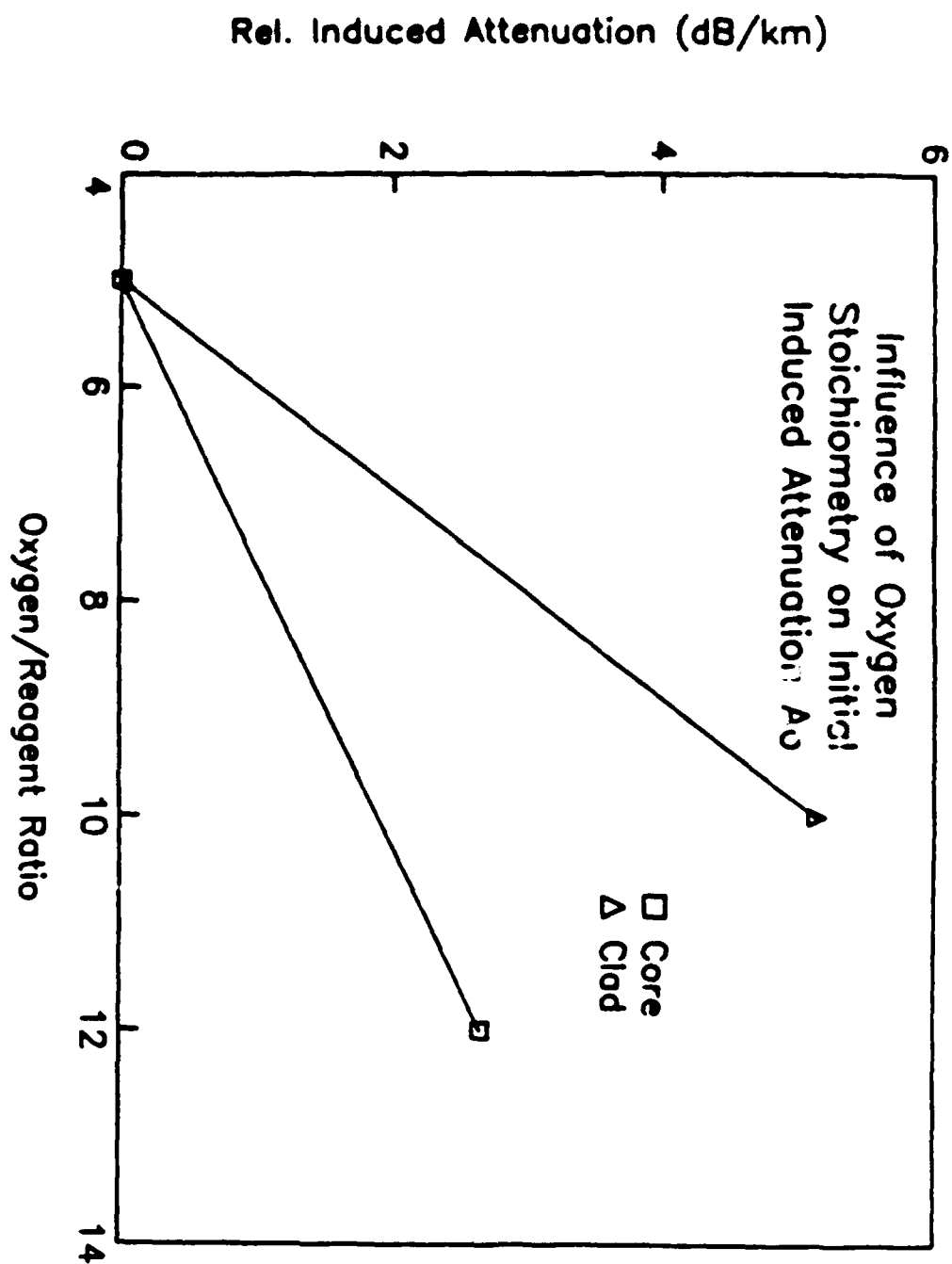


Figure 7.10 Effect of the ratio of oxygen carrier gas to reagent concentration during core and clad deposition on the initial damage level A_0 of fibers of the first group.

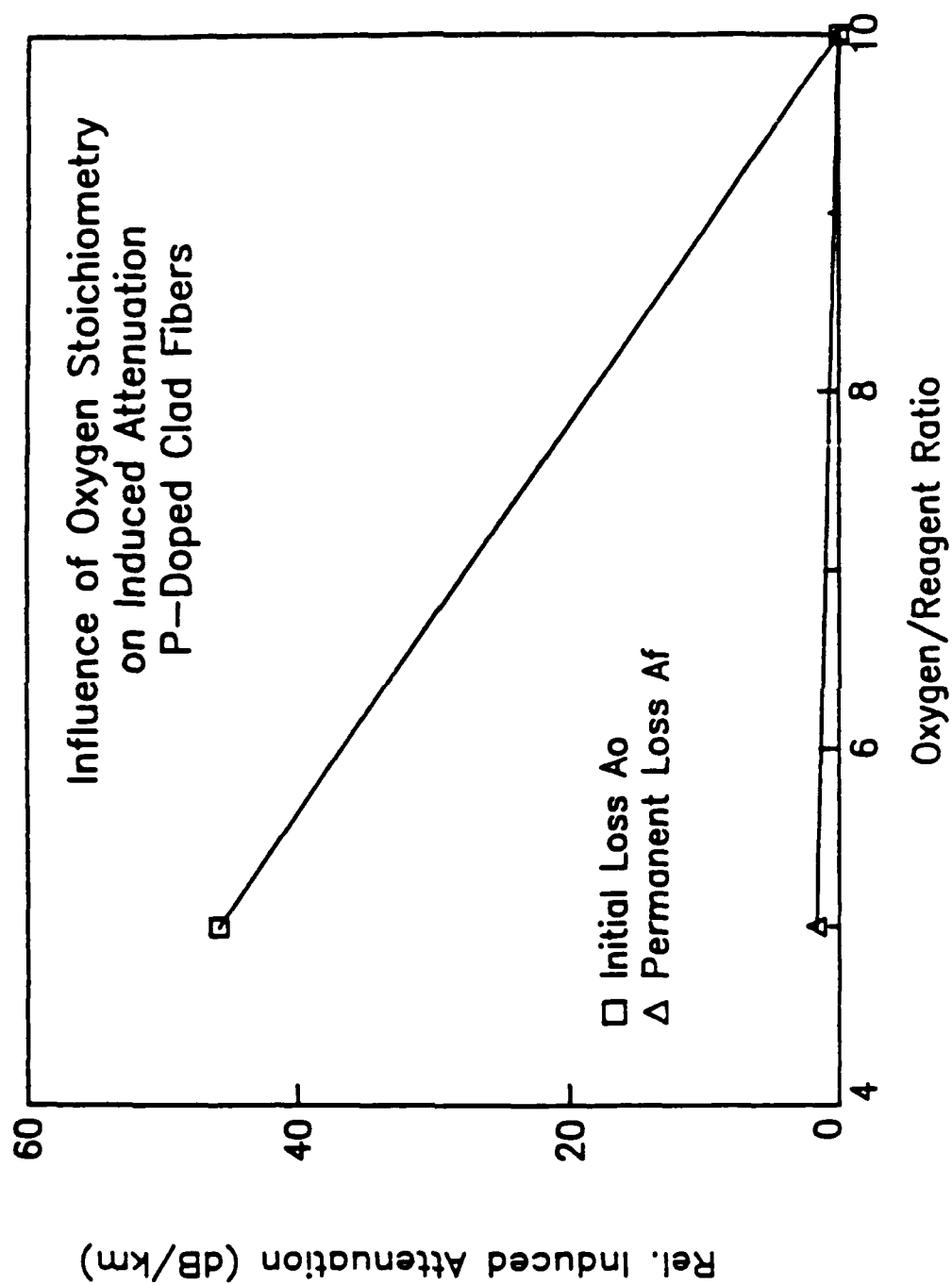


Figure 7.11 Effect of the ratio of oxygen carrier gas to reagent concentration during clad deposition on the initial damage level A_0 of fibers of the second group.

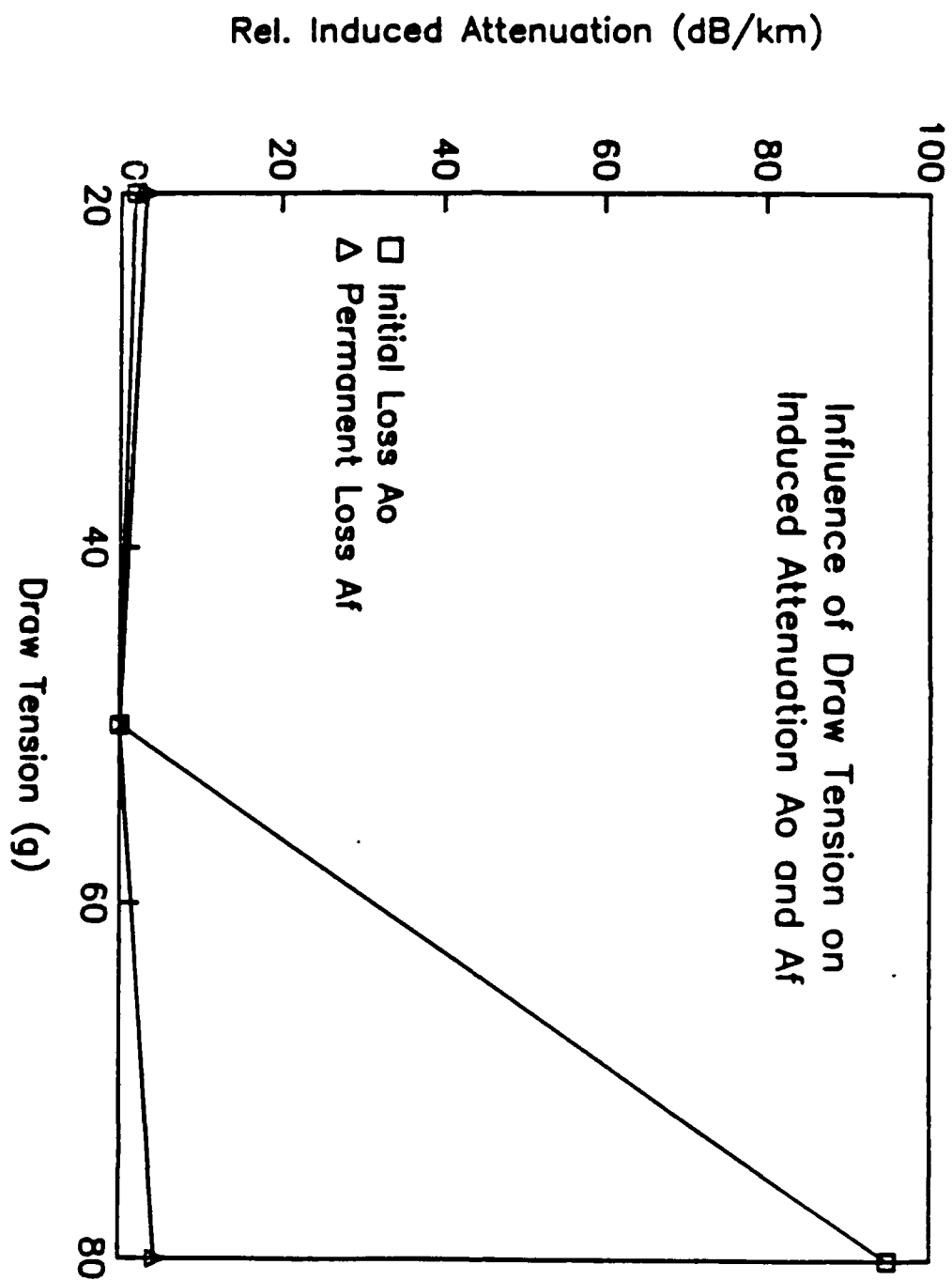


Figure 7.12 Effect of draw tension on initial damage level A_0 and permanent incremental loss A_f of fibers of the first group.

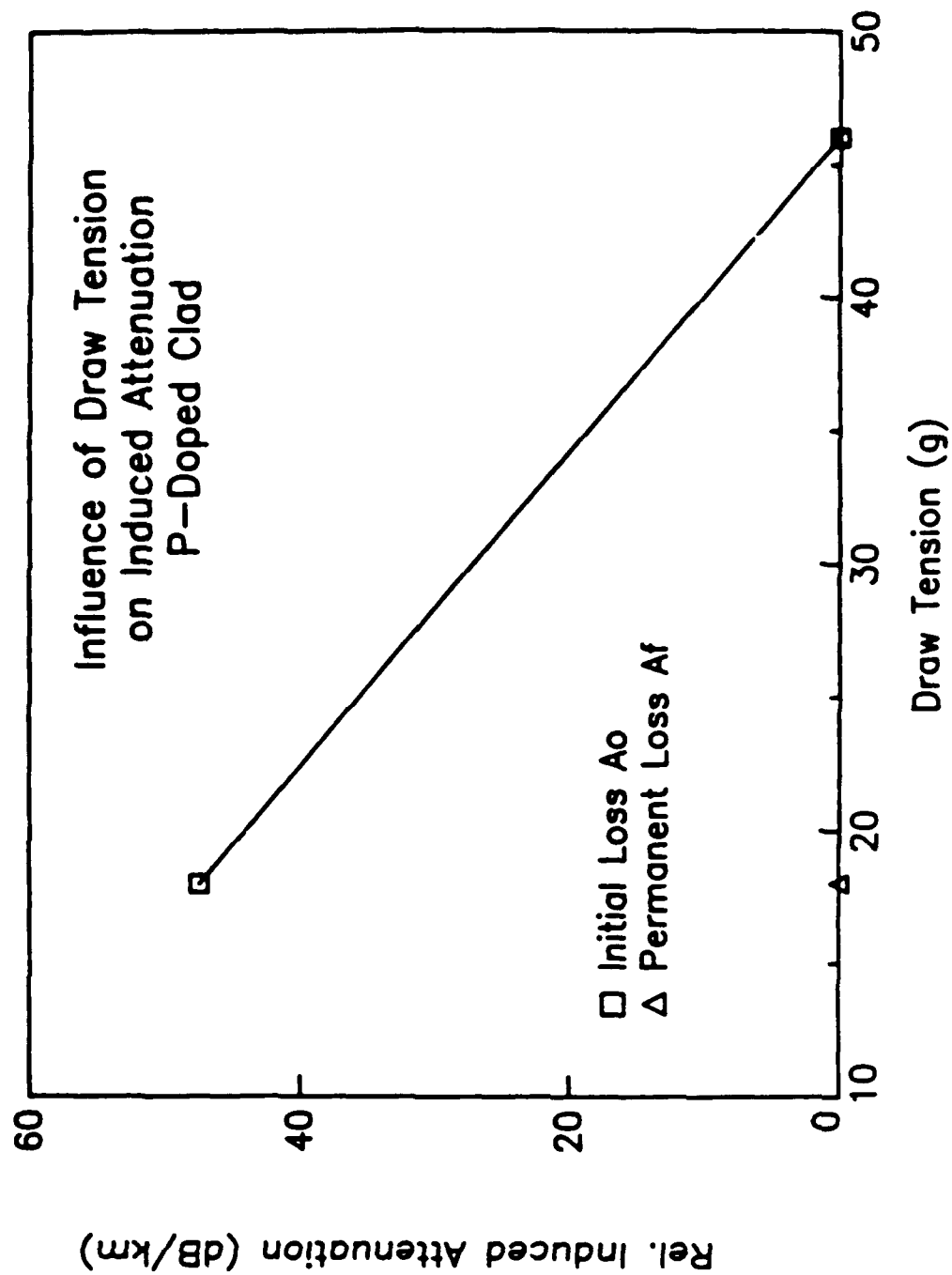
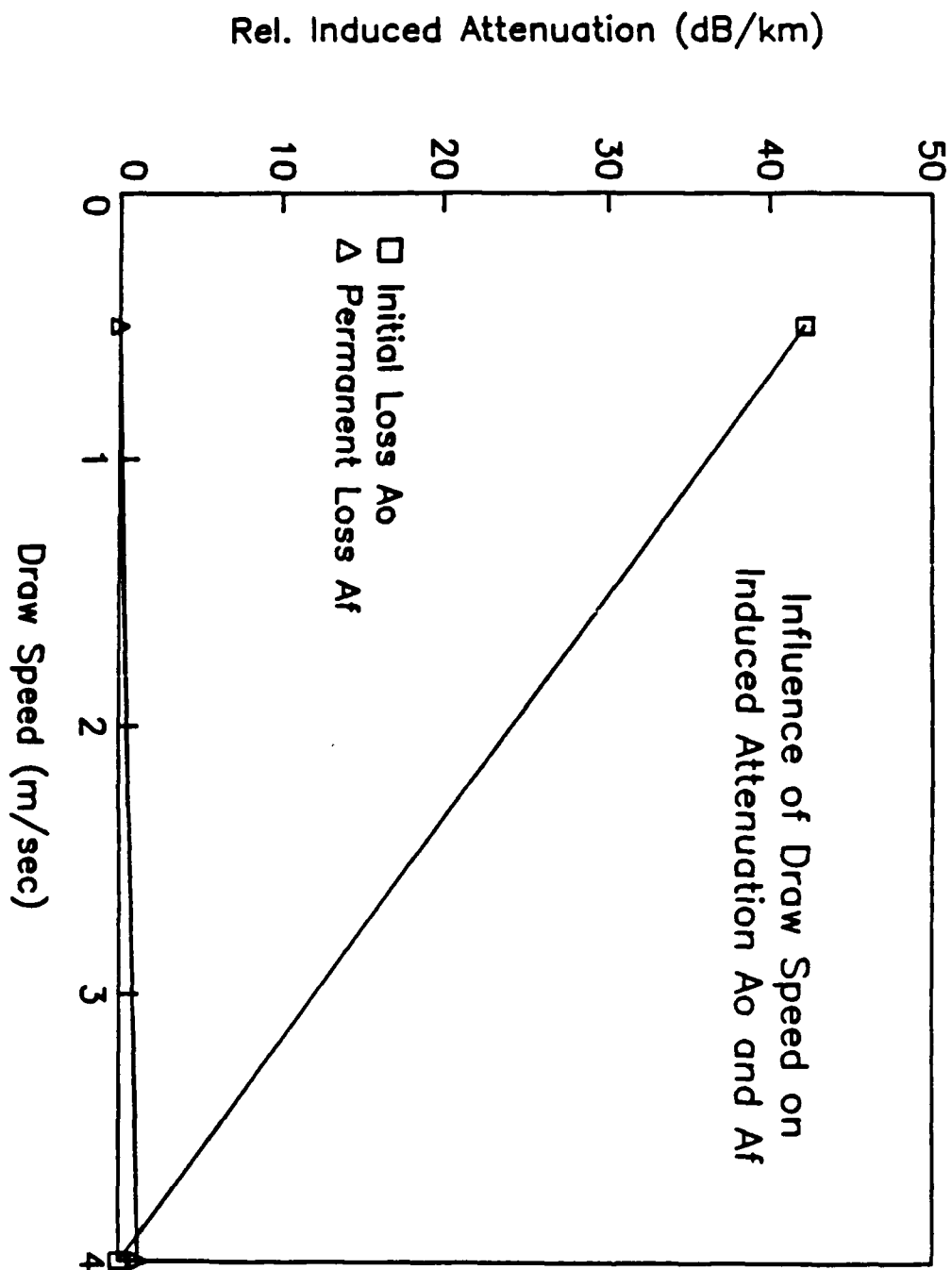


Figure 7.13 Effect of draw tension on initial damage level A_0 and permanent incremental loss A_f of fibers of the second group.

Figure 7.14 Effect of draw speed on initial damage level A_0 and permanent incremental loss A_f of fibers of the first group.



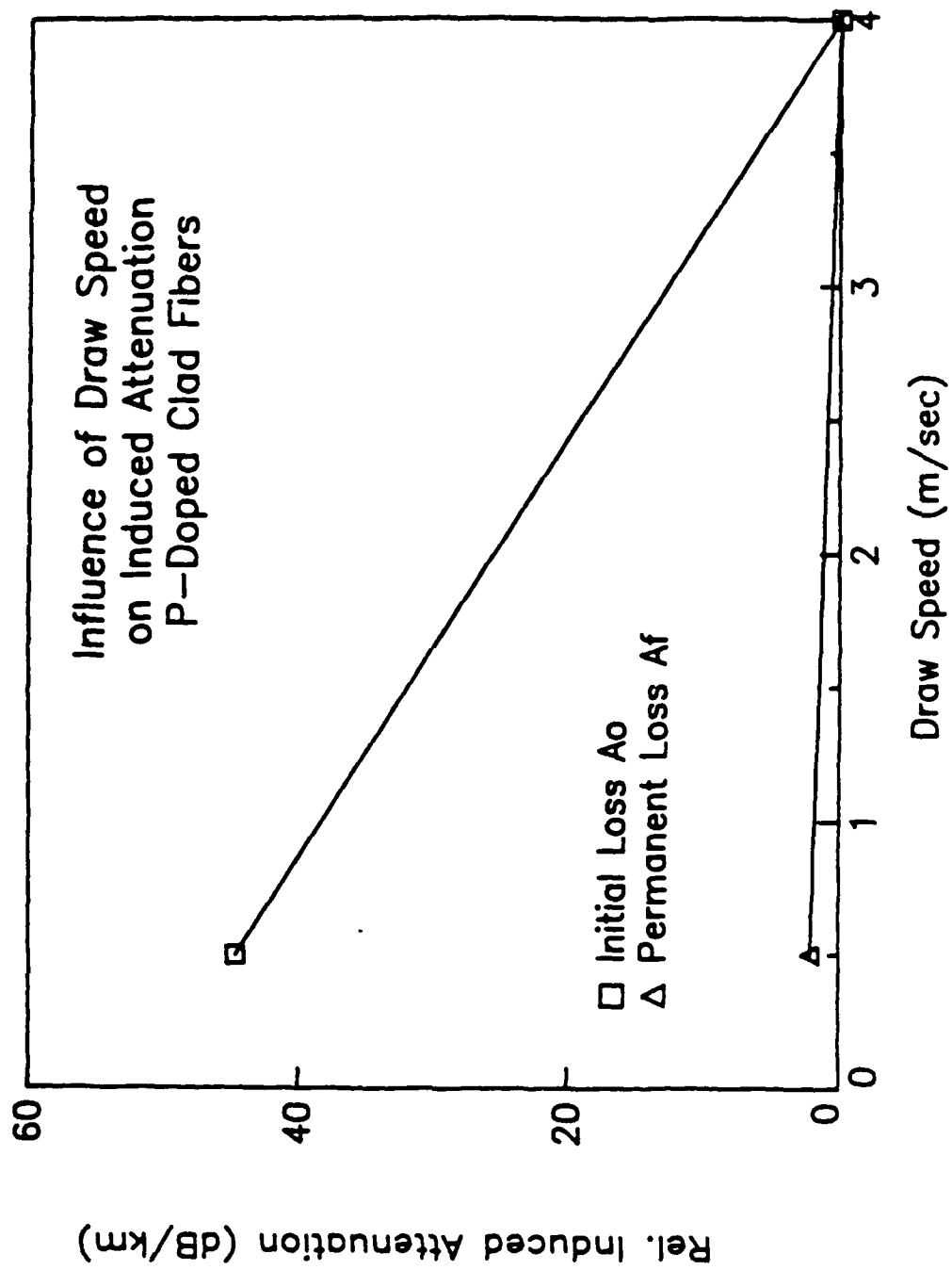


Figure 7.15 Effect of draw speed on initial damage level A_0 and permanent incremental loss A_f of fibers of the second group.

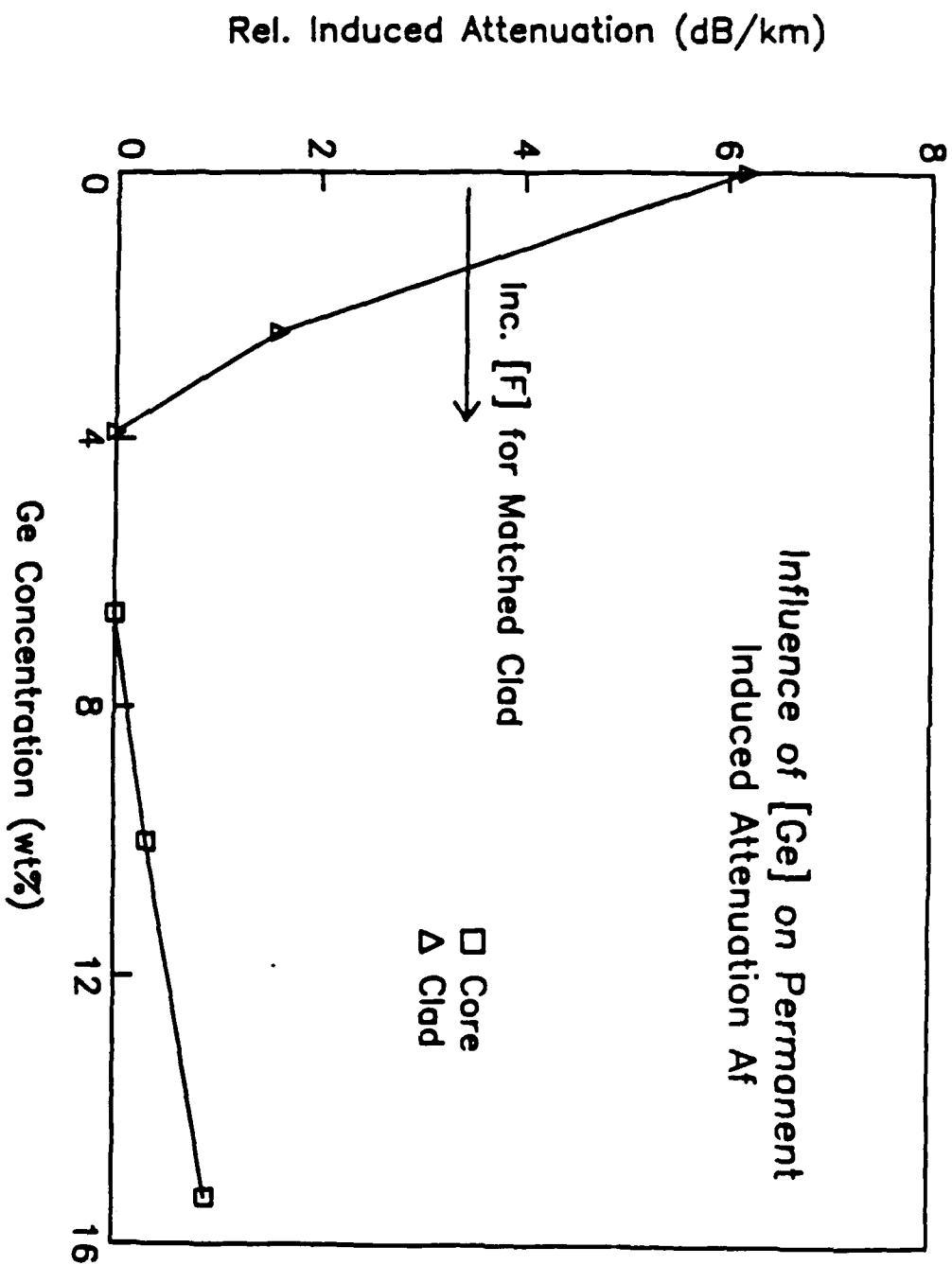


Figure 7.16 Effect of Ge concentration in the core and clad (down-doped with F) on the permanent induced attenuation A_f of fibers of the first group.

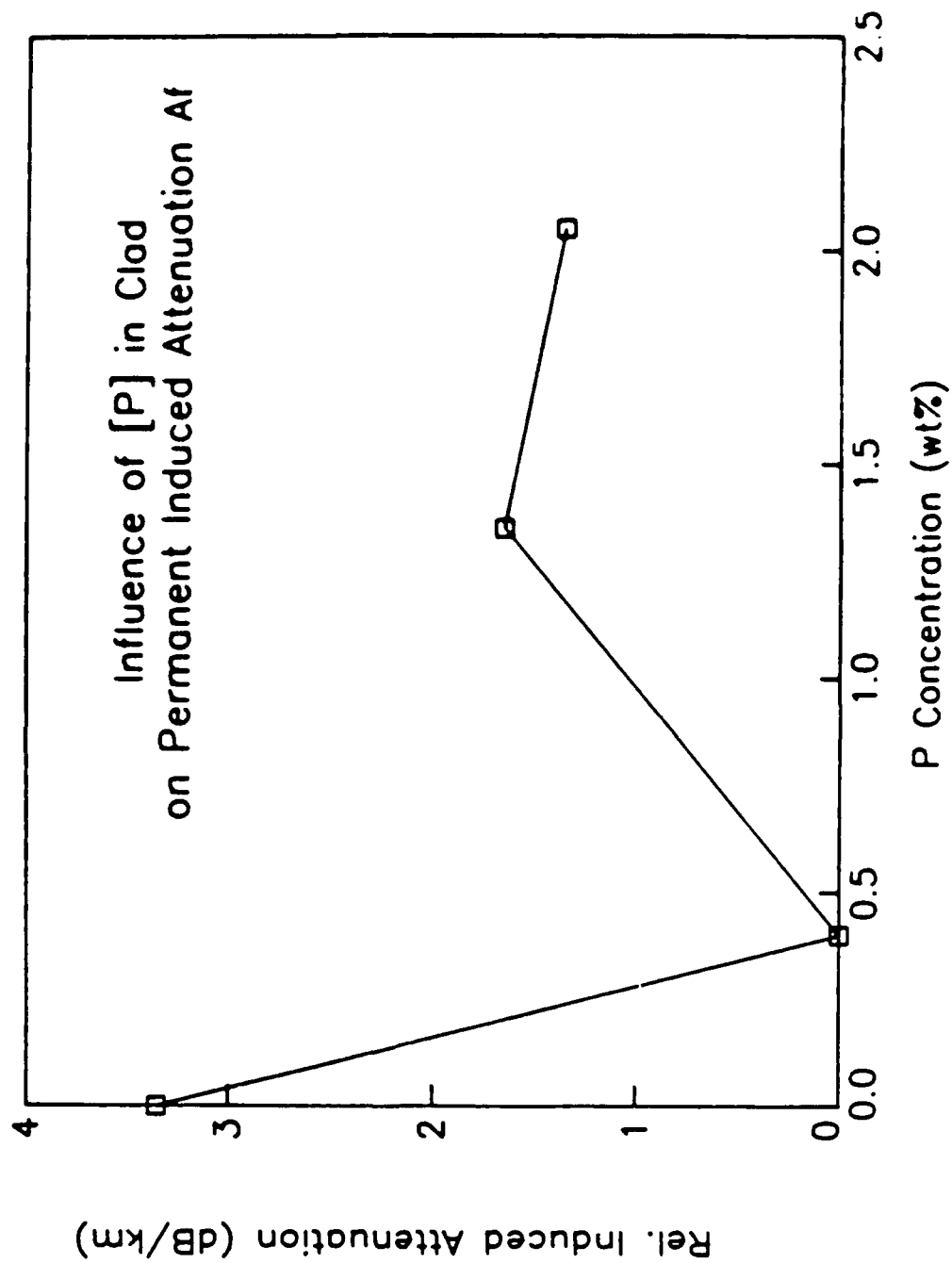


Figure 7.17 Effect of P concentration in the clad (down-doped with F) on the permanent induced attenuation A_f of fibers of the second group.

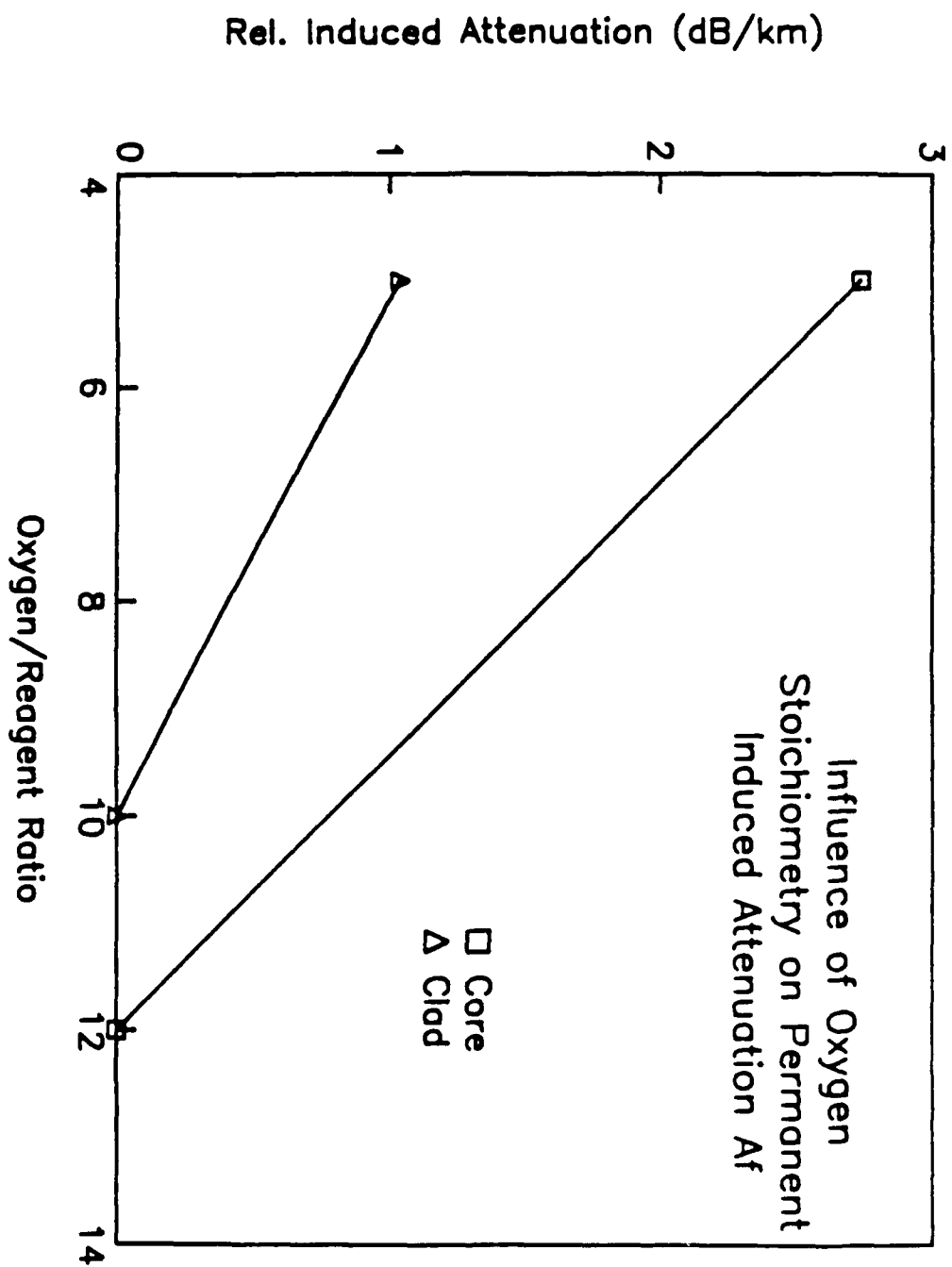


Figure 7.18 Effect of ratio of oxygen carrier to reagent concentration during core and clad deposition on permanent damage level A_f of fibers of the first group.

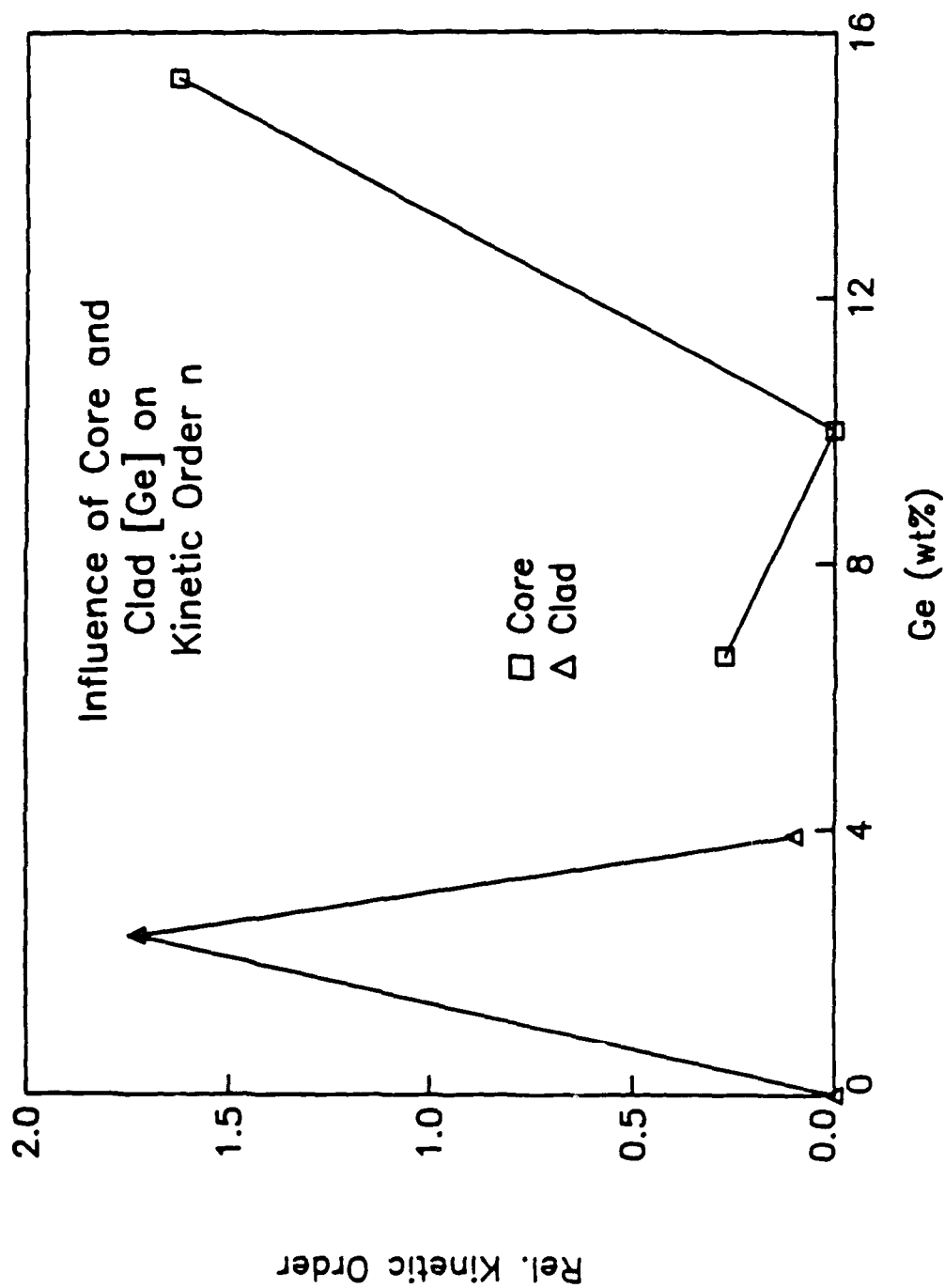


Figure 7.19 Effect of Ge concentration in the core and clad (down-doped with F) on the order of the kinetics n of fibers of the first group.

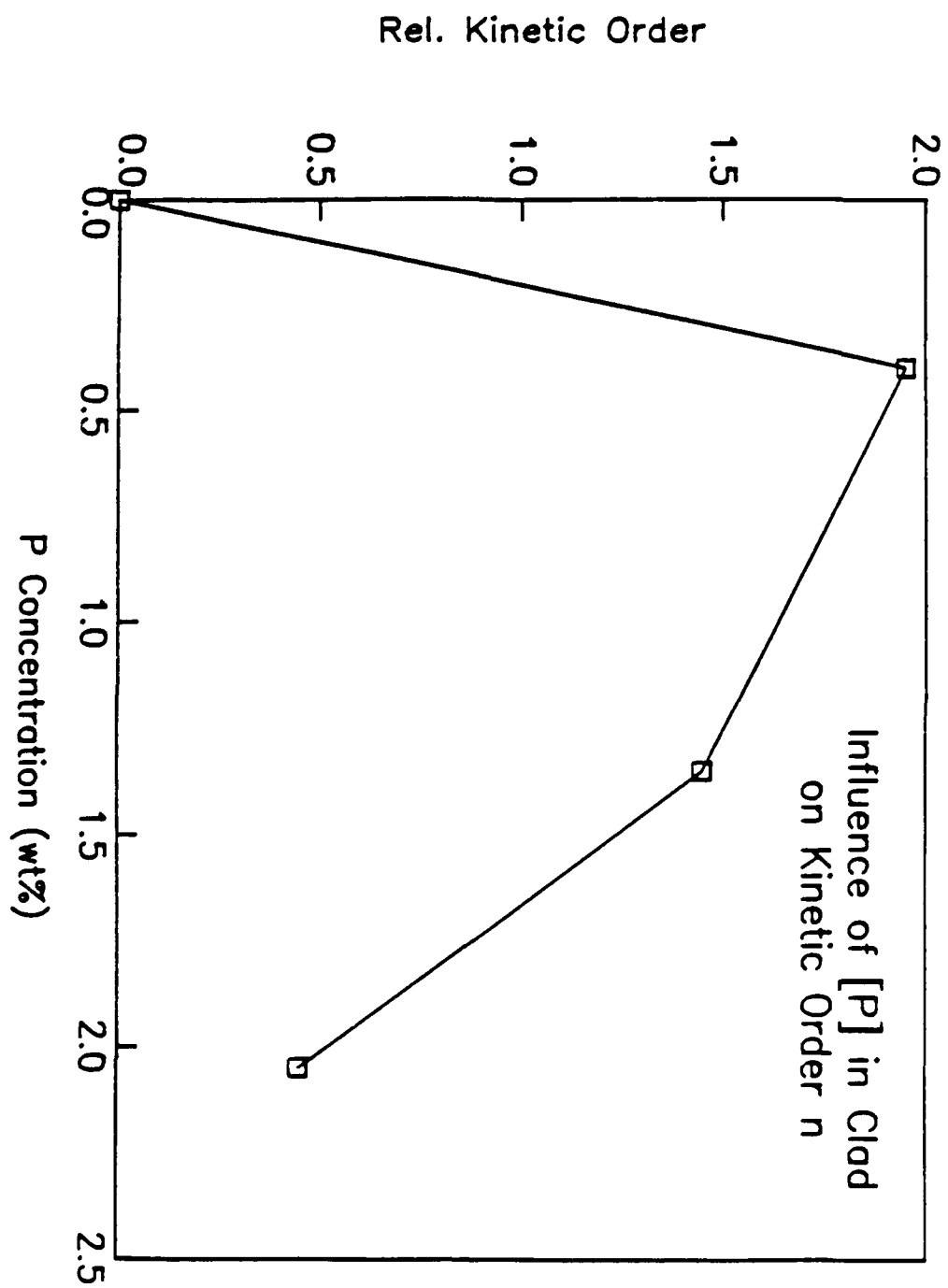


Figure 7.20 Effect of P concentration in the clad (down-doped with F) on the order of the kinetics n of fibers of the second group.

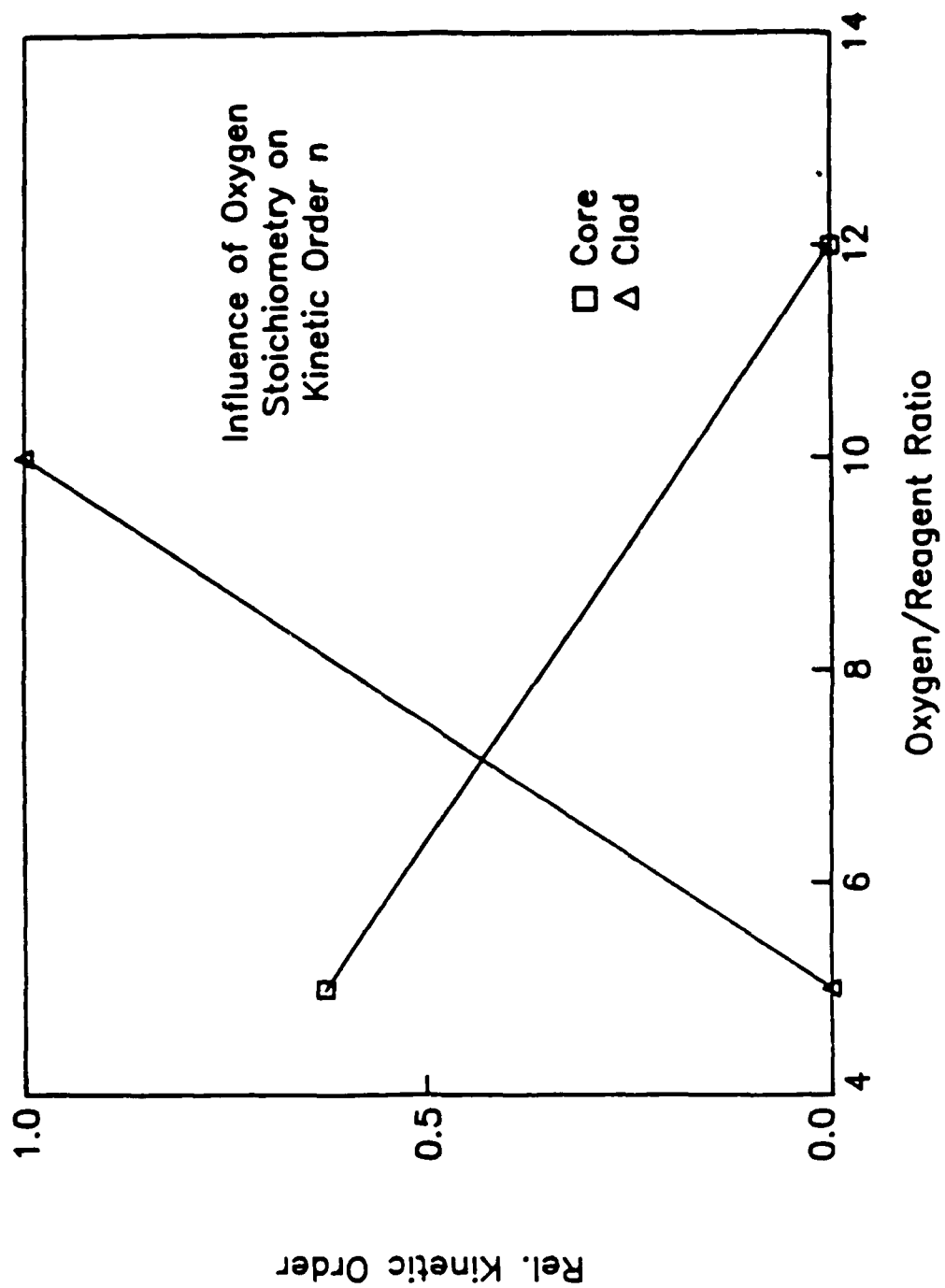


Figure 7.21 Effect of ratio of oxygen carrier to reagent concentration during core and clad deposition on the order of the kinetics n of Phase 1 fibers.

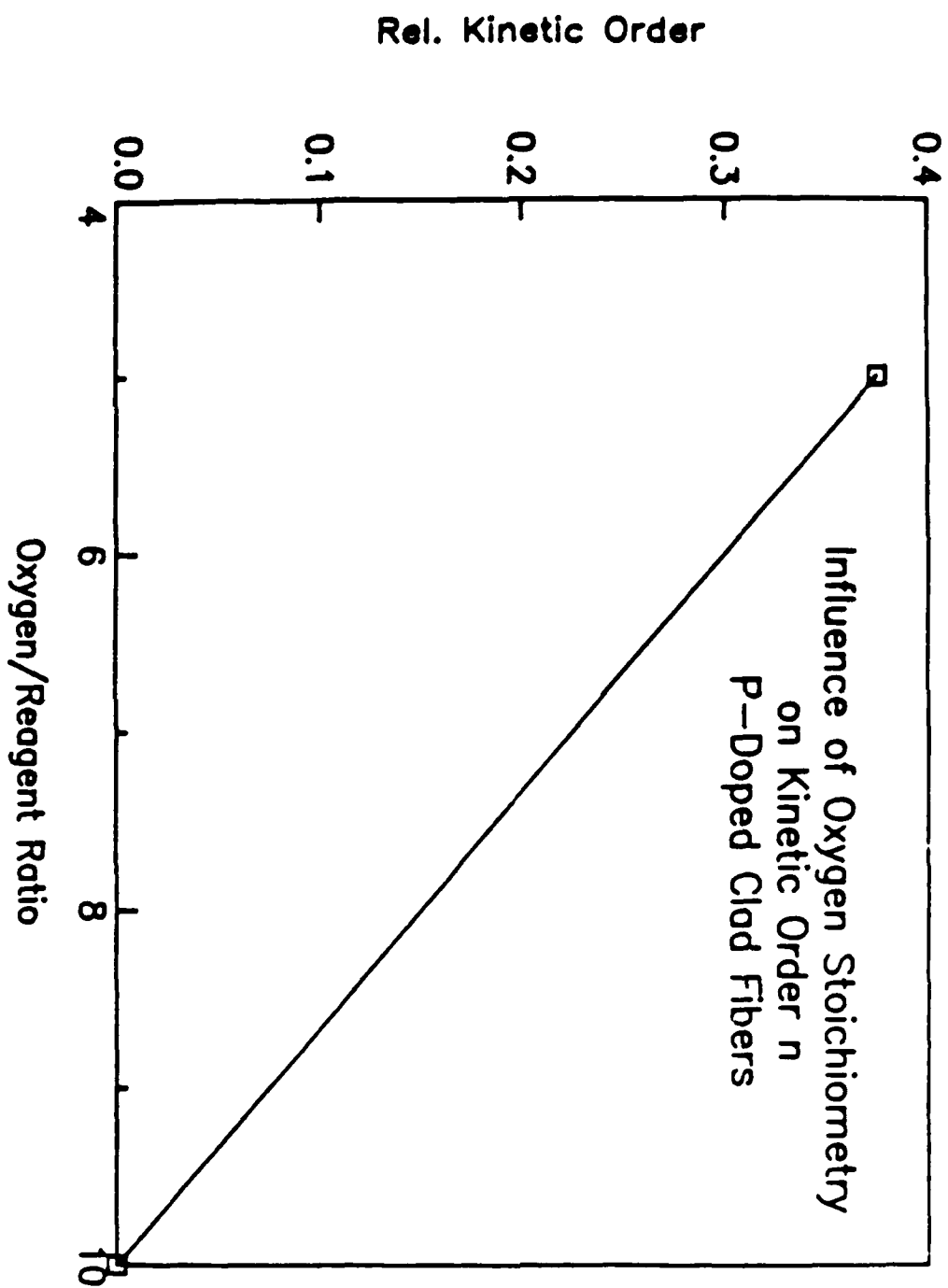


Figure 7.22 Effect of ratio of oxygen carrier to reagent concentration during cladding deposition on the order of the kinetics n of fibers of the second group.

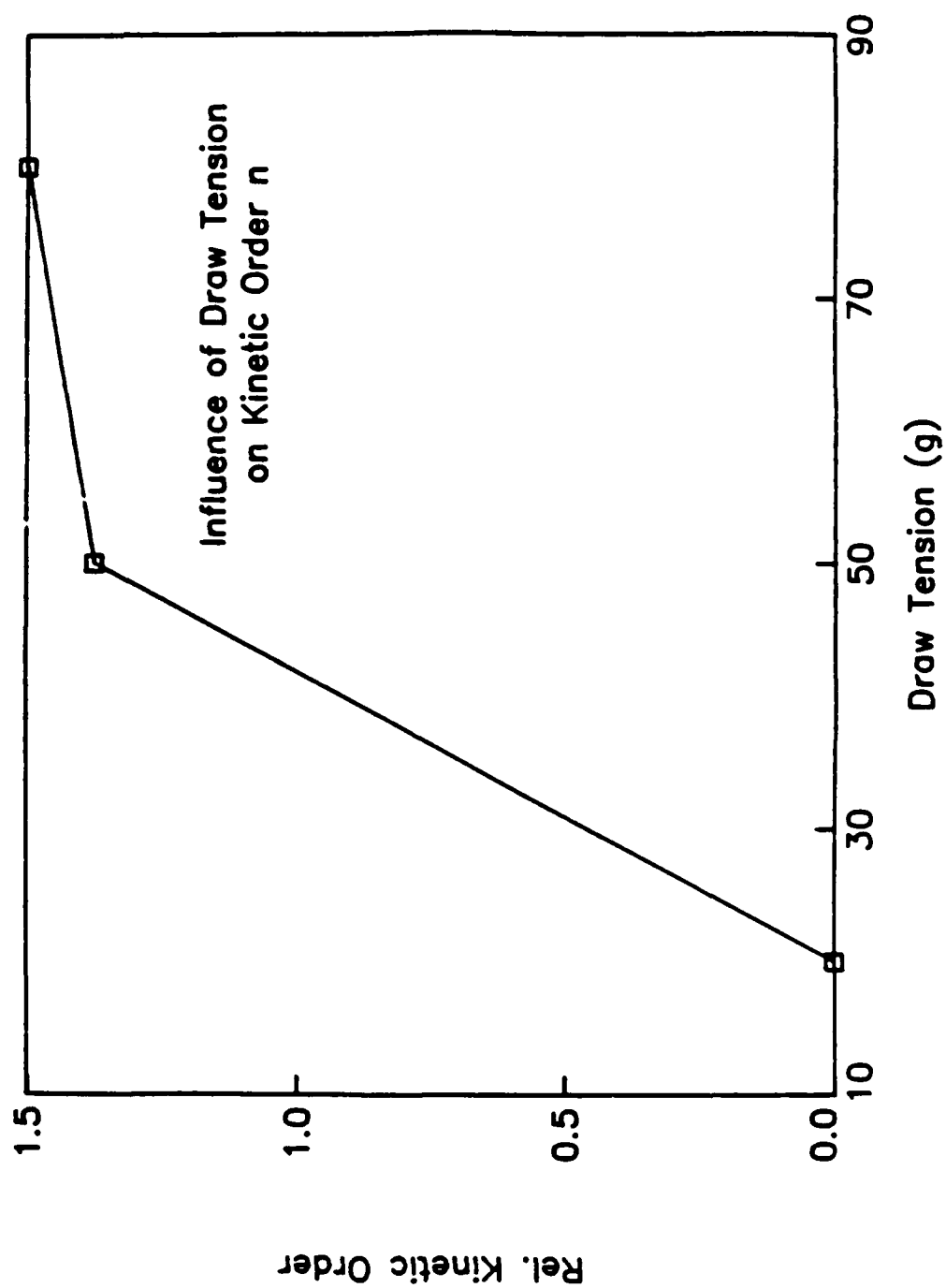


Figure 7.23 Effect of draw tension on the order of the kinetics n of Phase 1 fibers.

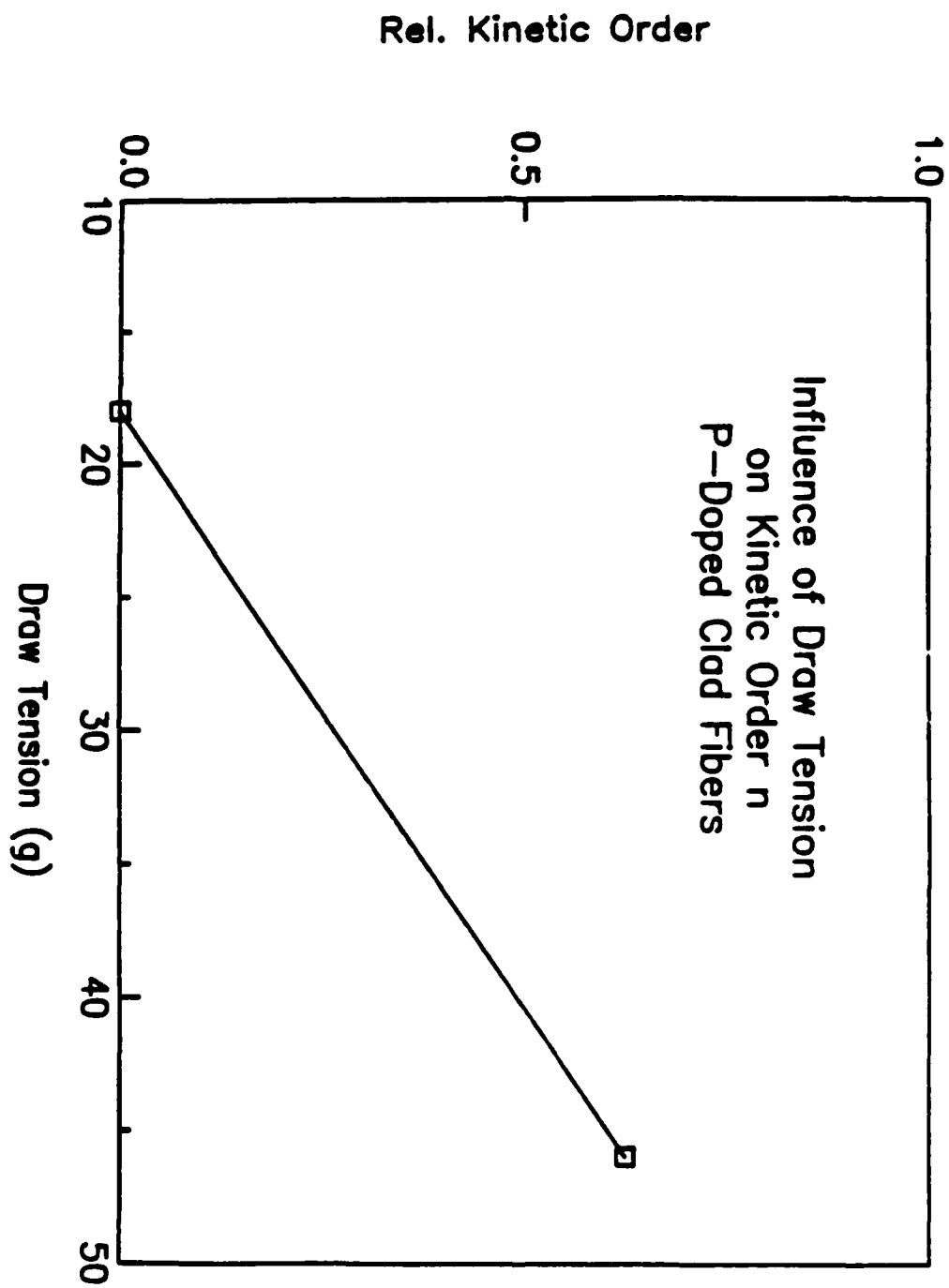


Figure 7.24 Effect of draw tension on the order of the kinetics n of fibers of the second group.

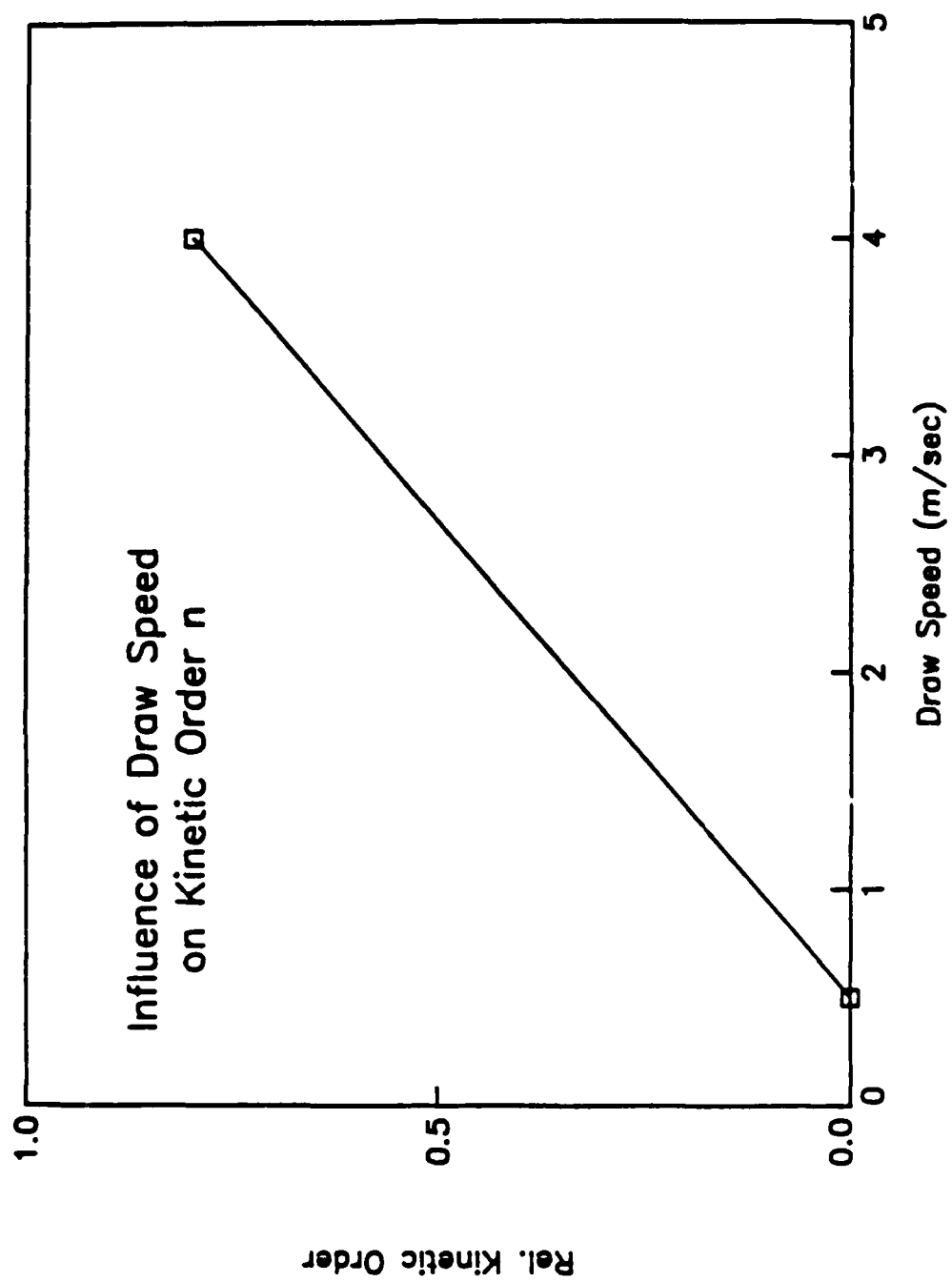


Figure 7.25 Effect of draw speed on the order of the kinetics n of fibers of the first group.

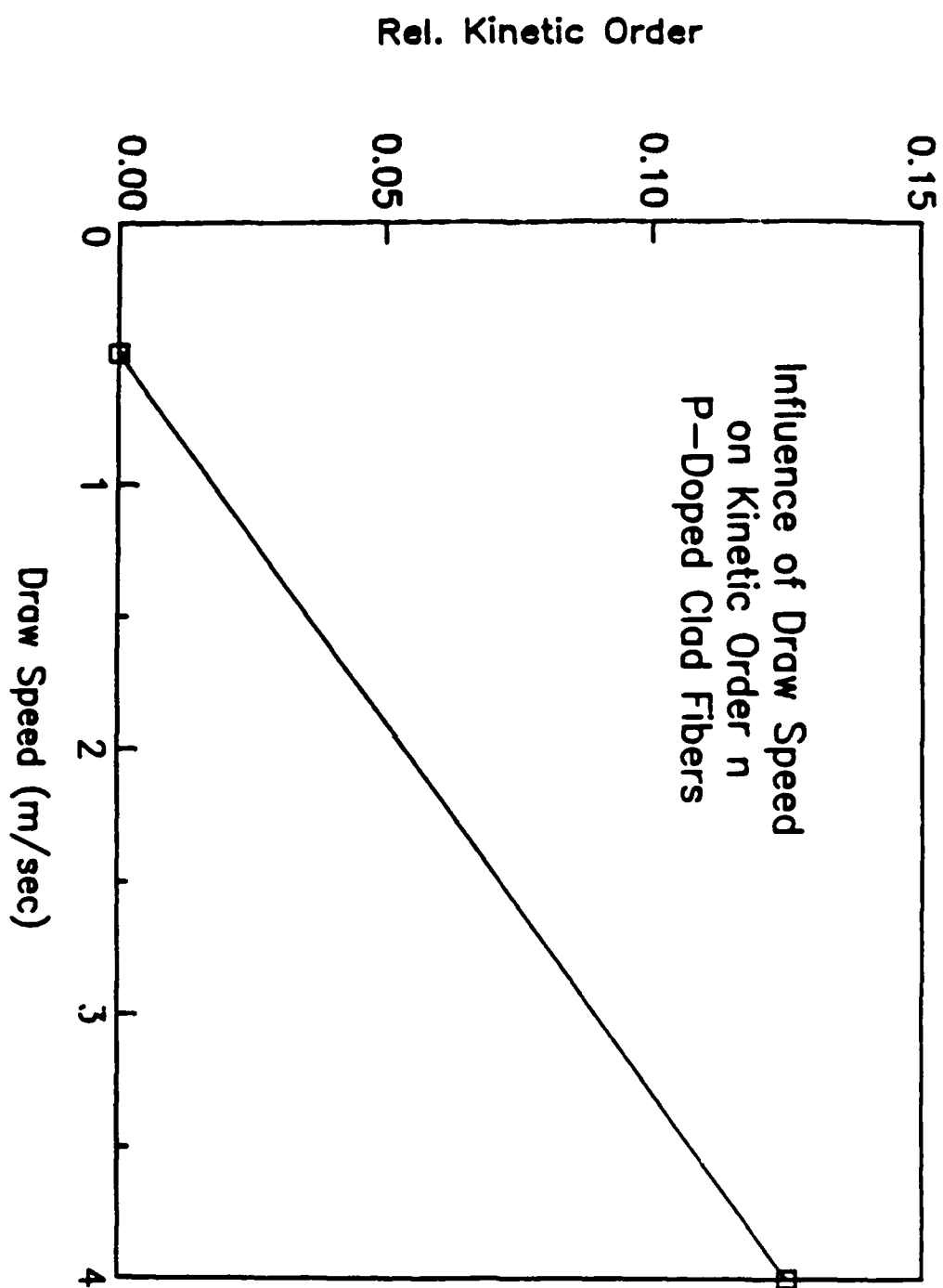


Figure 7.26 Effect of draw speed on the order of the kinetics n of fibers of the second group.

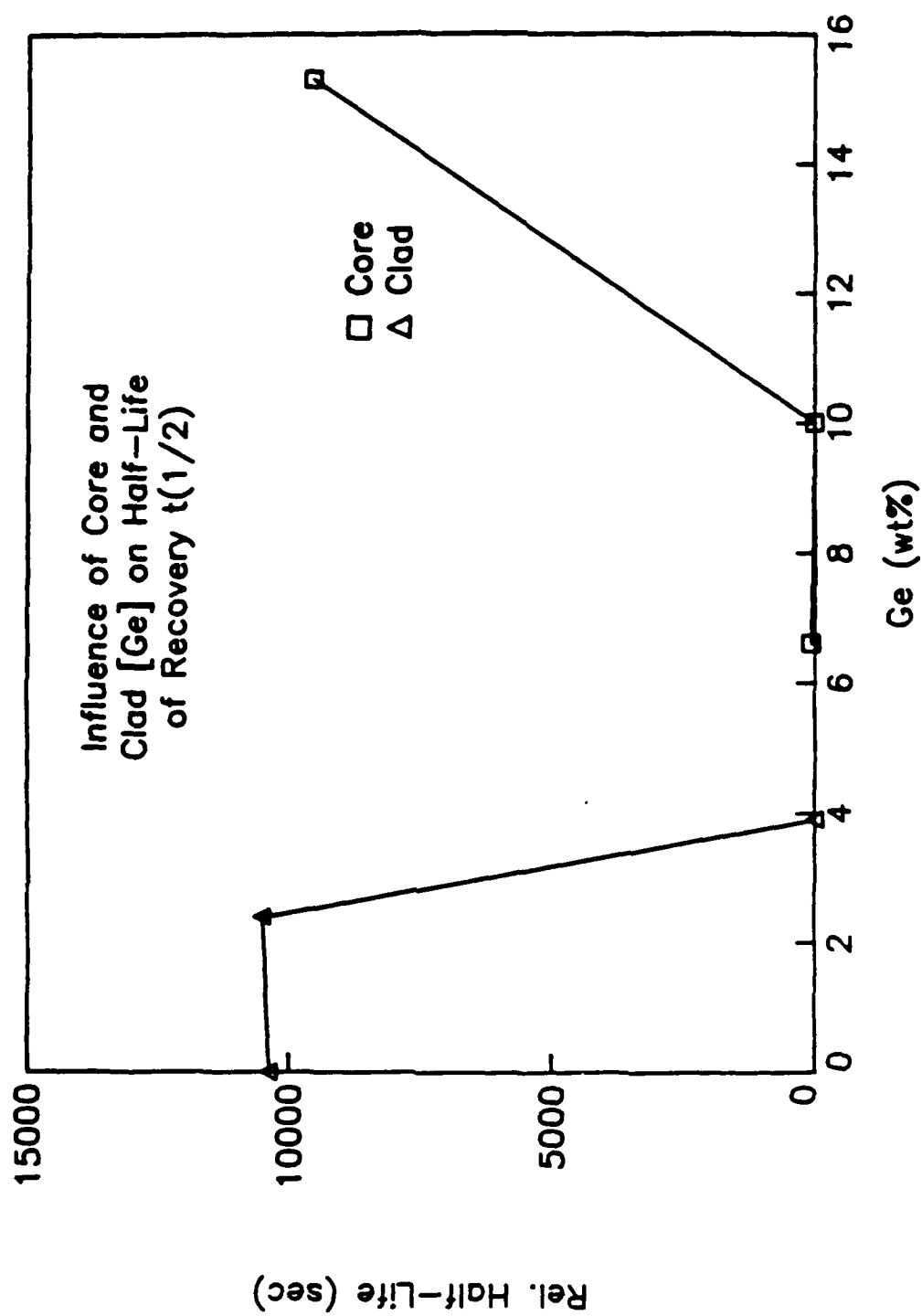


Figure 7.27 Effect of Ge concentration in the core and clad (down-doped with F) on the "half-life" τ of fibers of the first group.

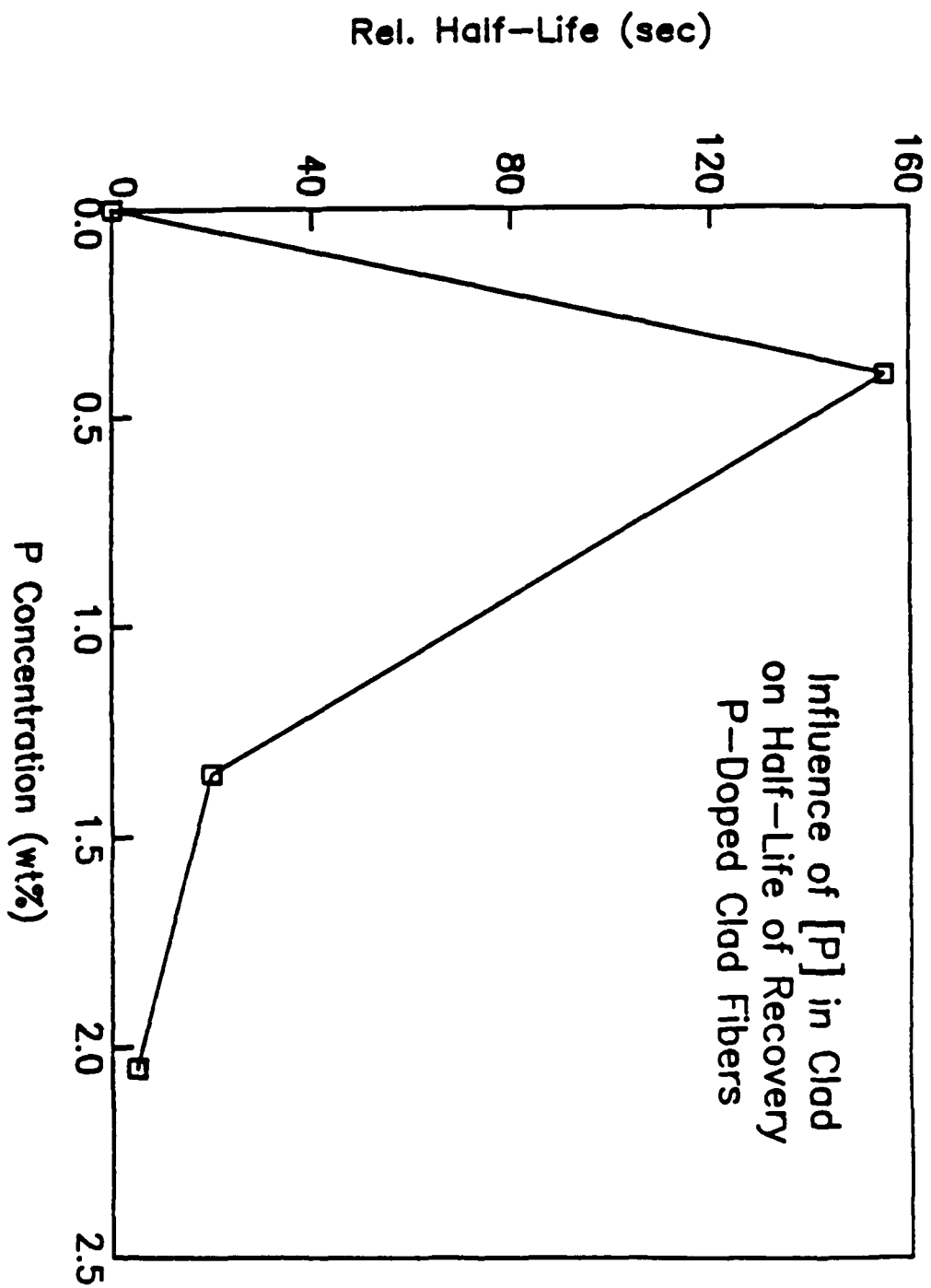


Figure 7.28 Effect of P concentration in the clad (down-doped with F) on the "half-life" τ of fibers of the second group.

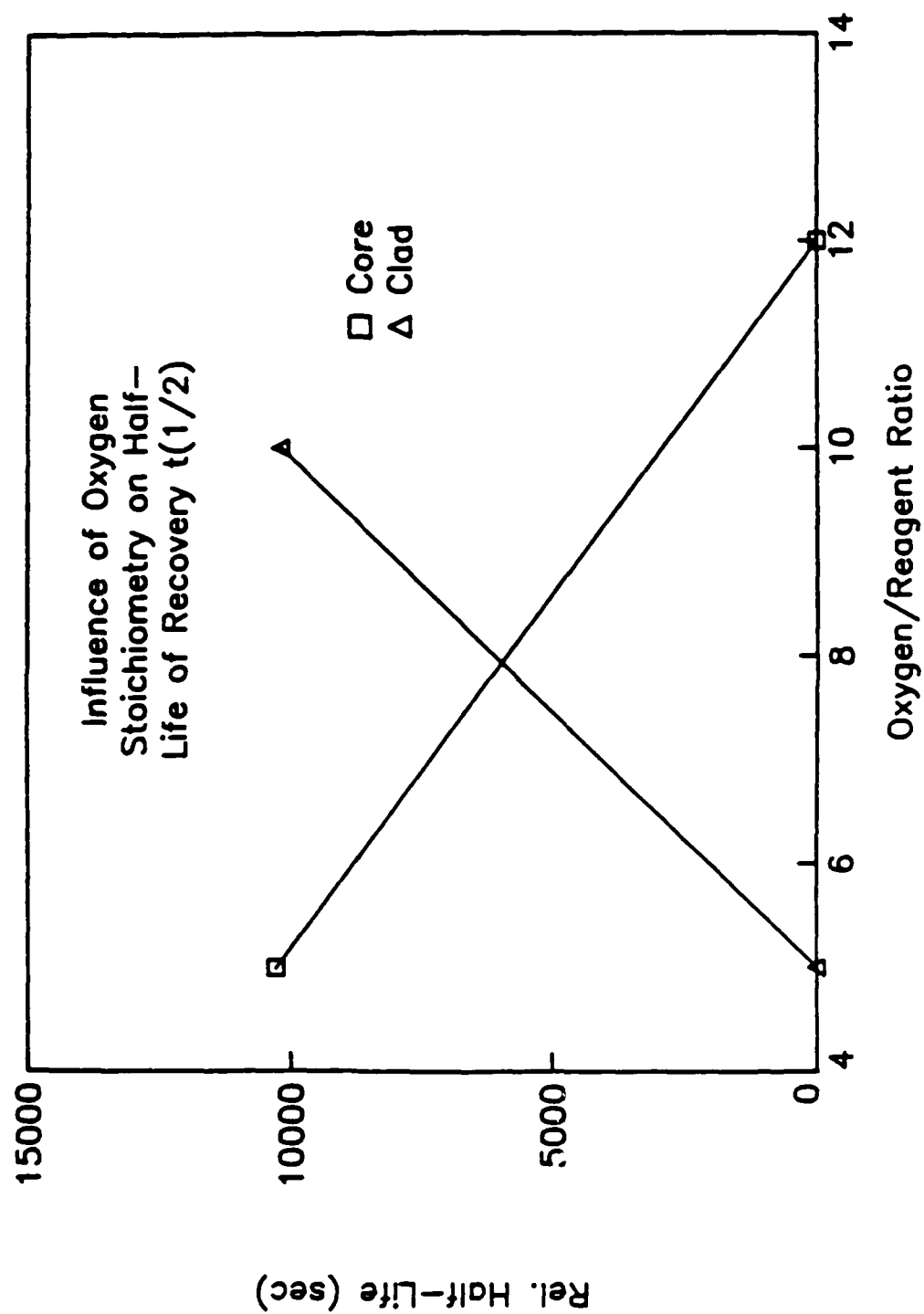


Figure 7.29 Effect of ratio of oxygen carrier to reagent concentration during core and clad deposition on the "half-life" τ of Phase I fibers.

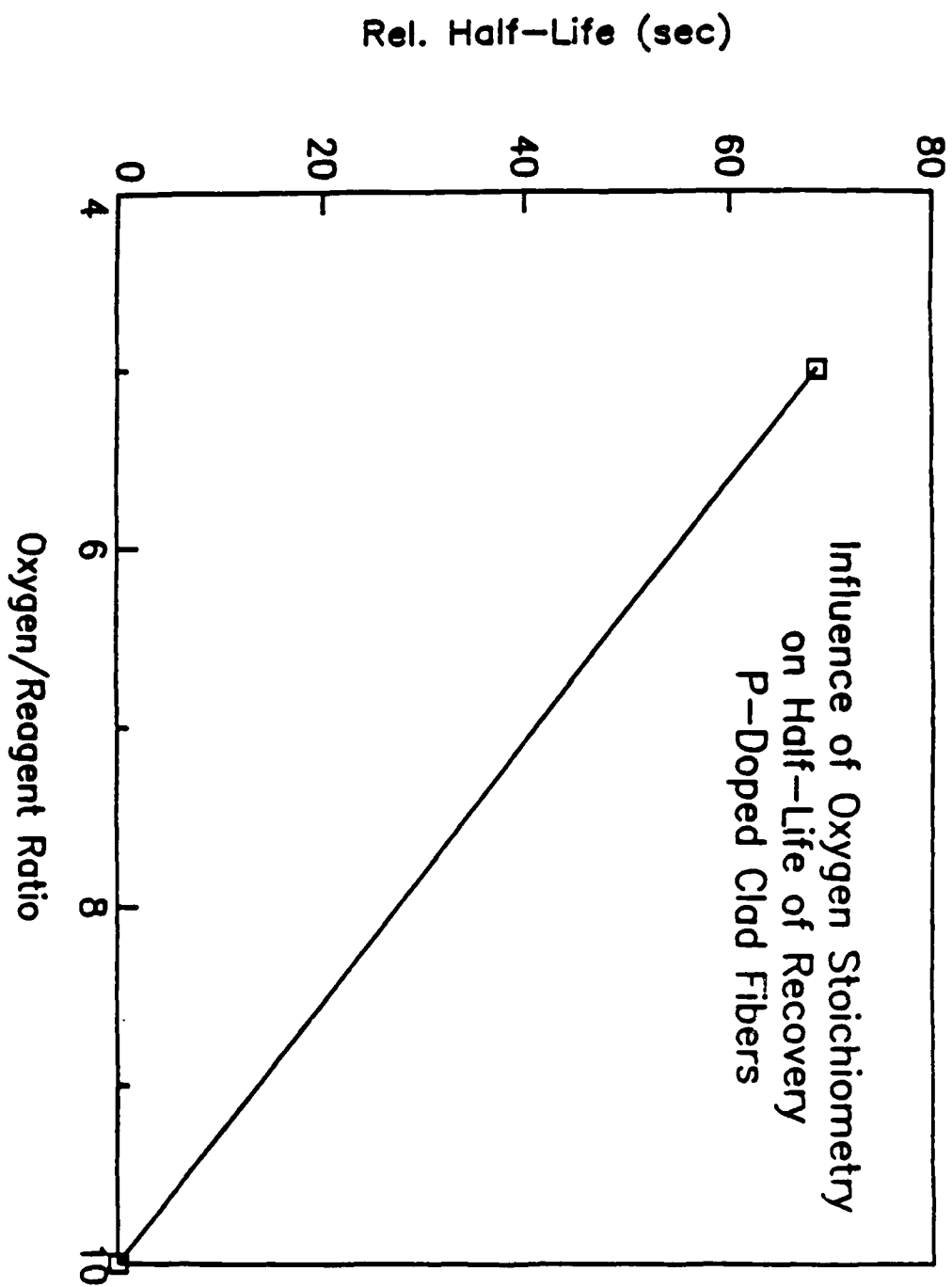


figure 7.30 Effect of ratio of oxygen carrier to reagent concentration during cladding deposition on the "half-life" τ of fibers of the second group.

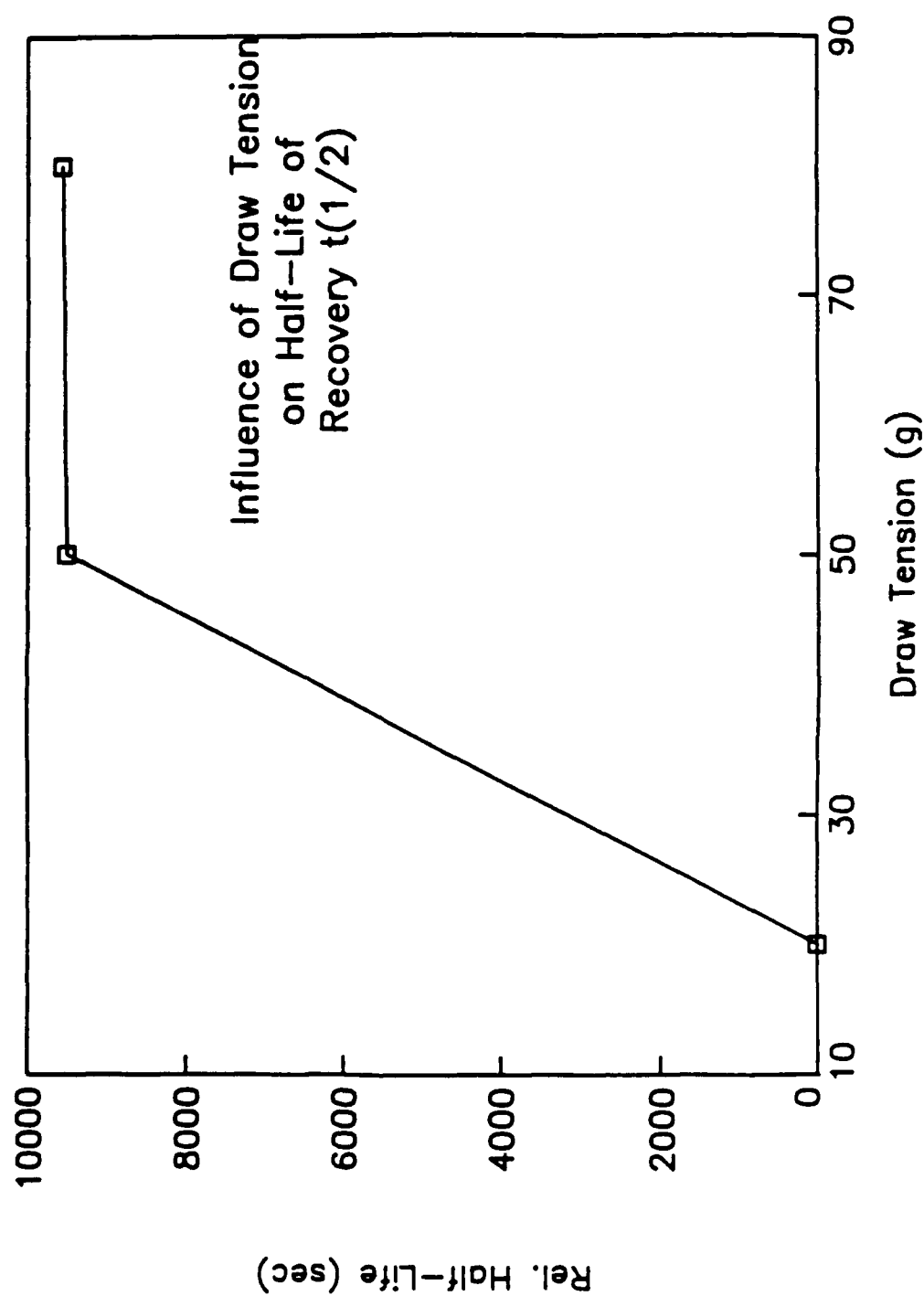


Figure 7.31 Effect of draw tension on the "half-life" τ of Phase 1 fibers.

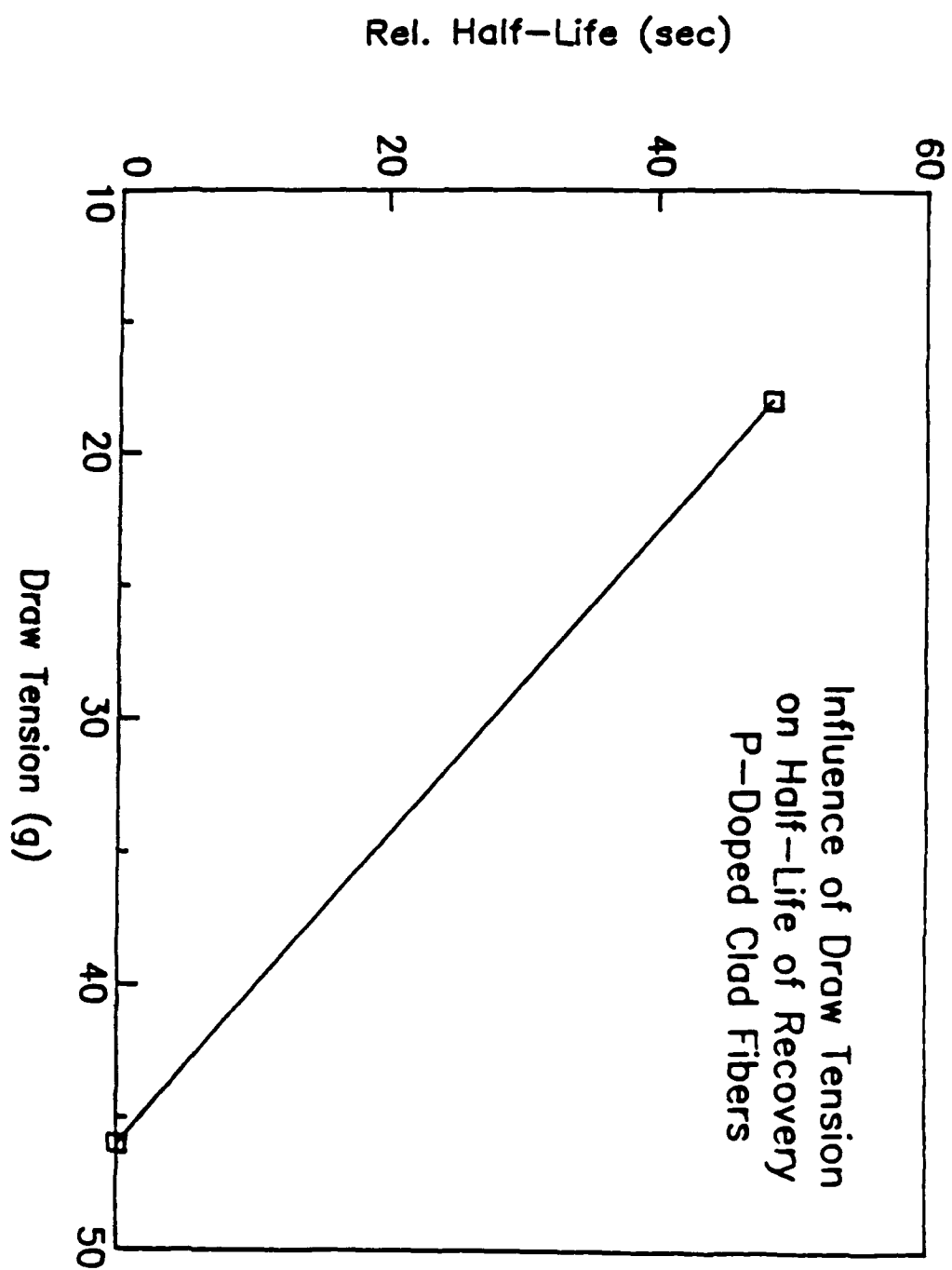


Figure 7.32 Effect of draw tension on the "half-life" τ of fibers of the second group.

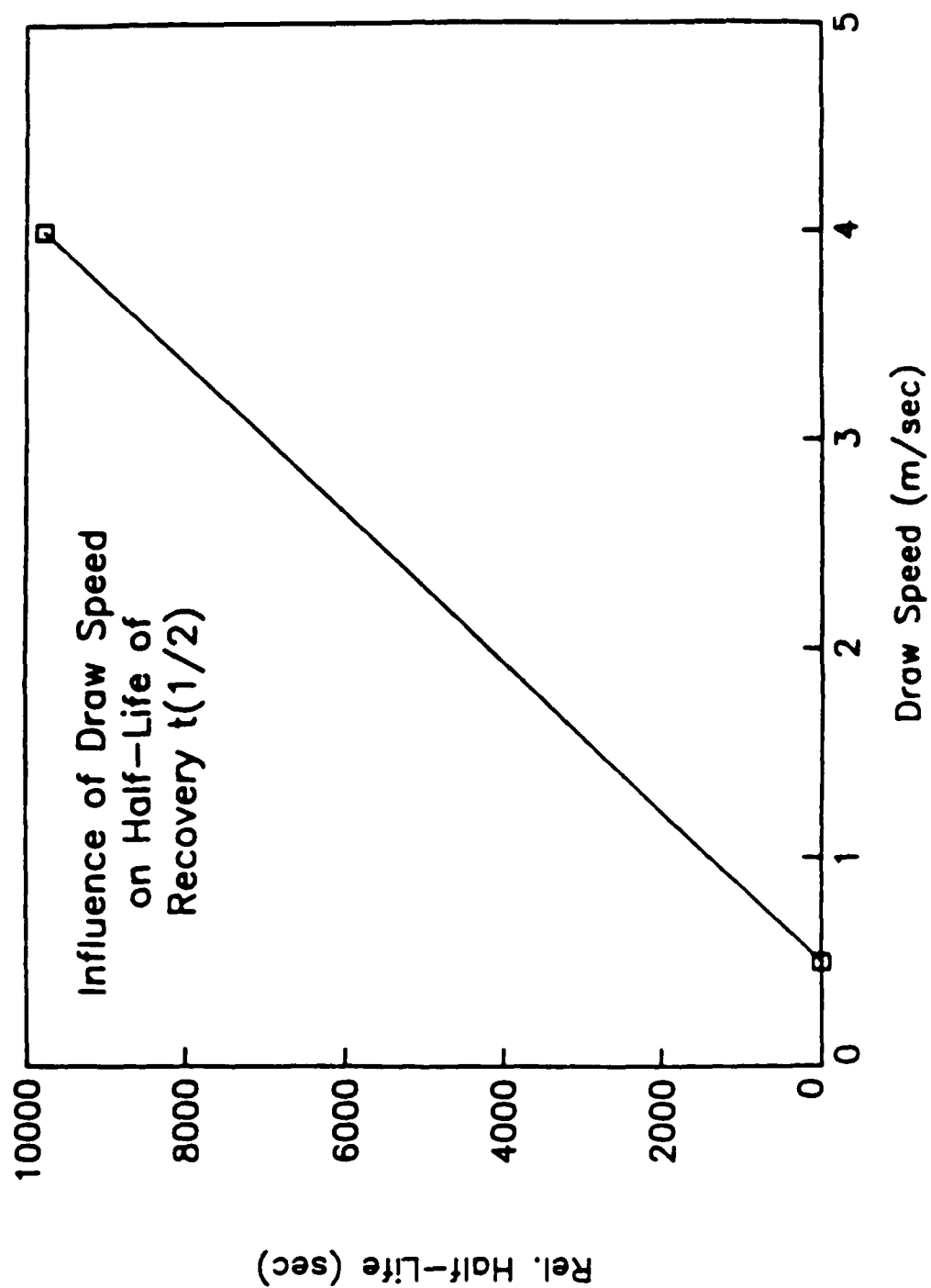


Figure 7.33 Effect of draw speed on the "half-life" τ of fibers of the first group.

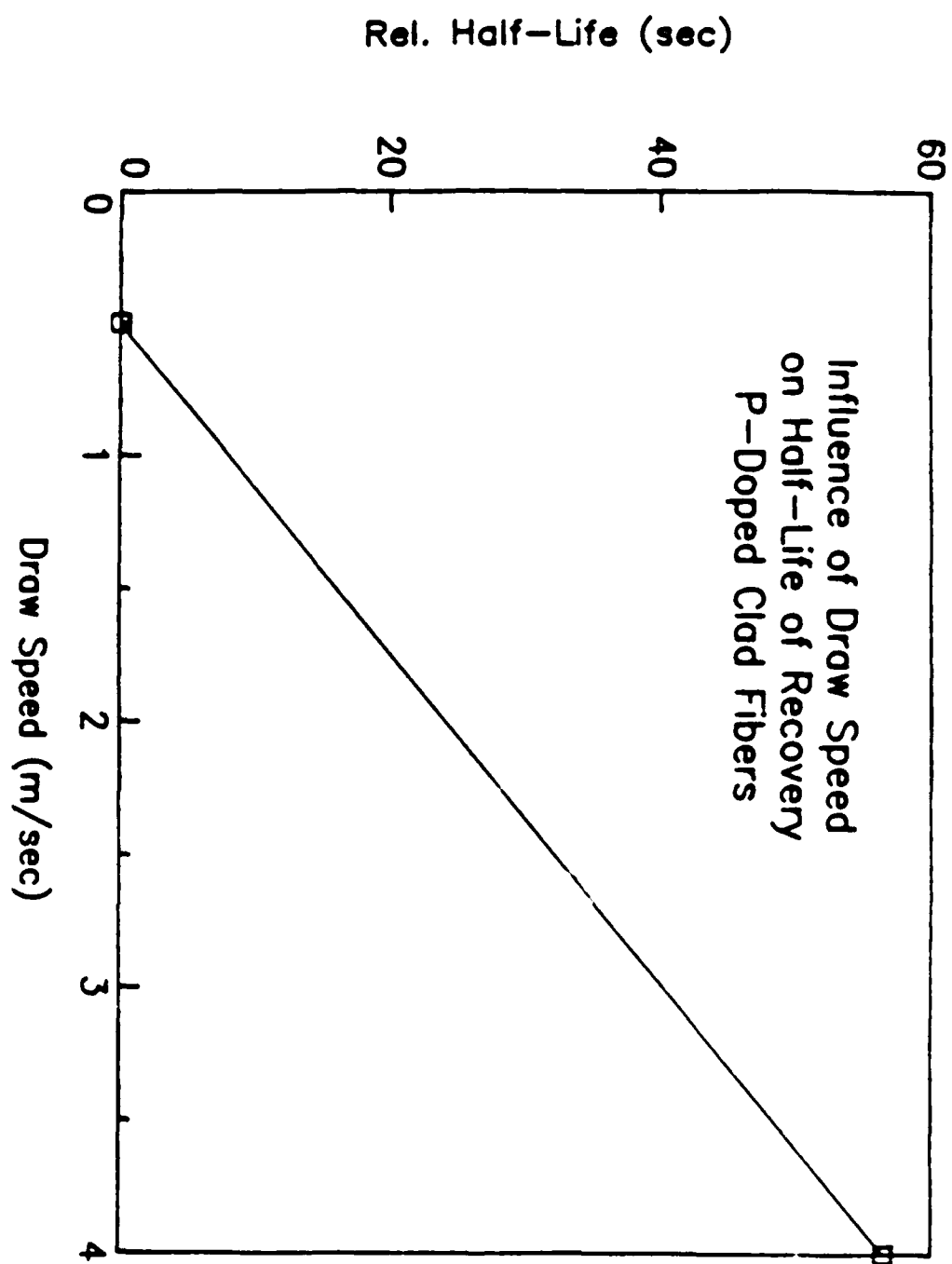


Figure 7.34 Effect of draw speed on the "half-life" τ of fibers of the second group.

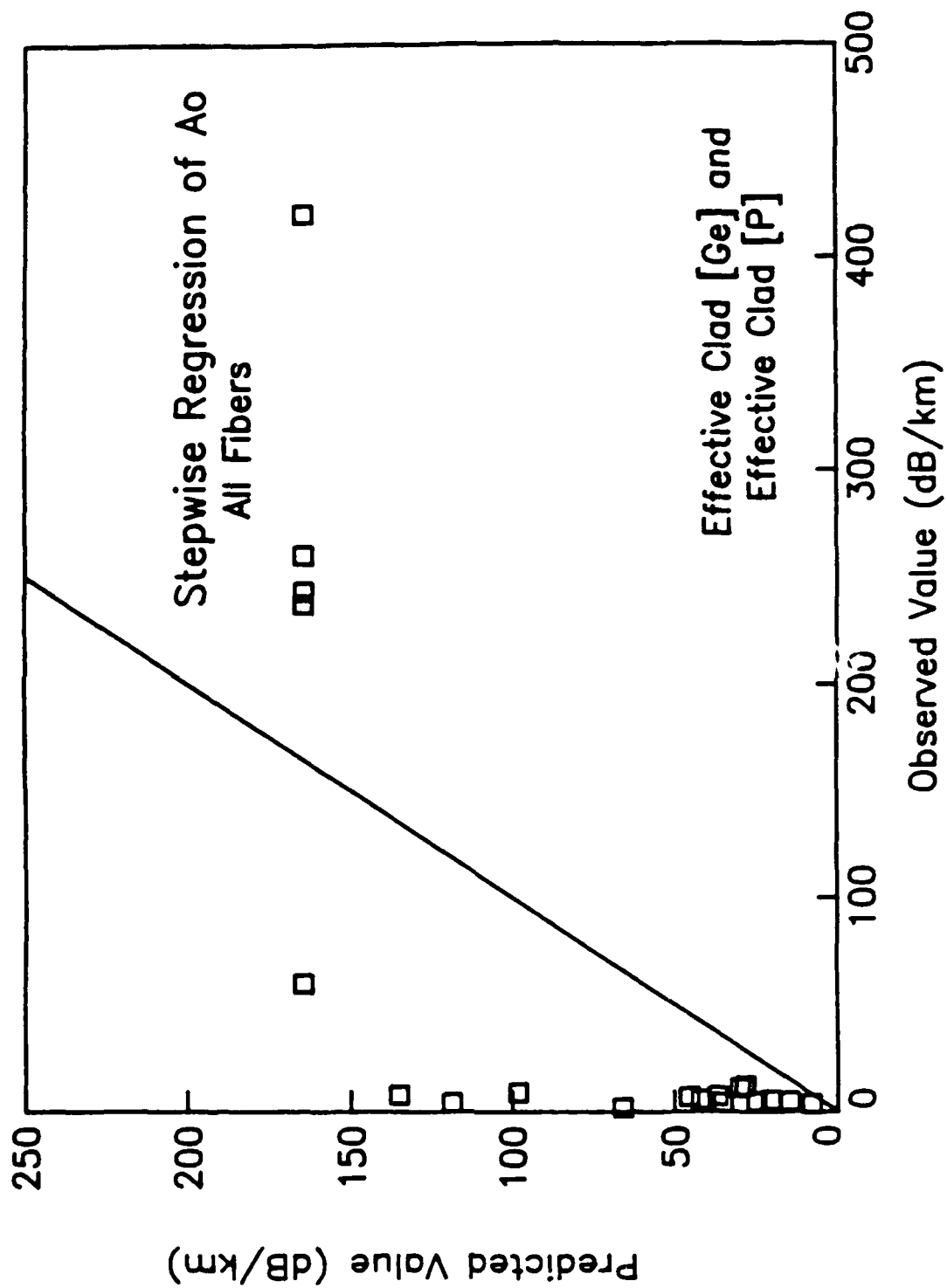


Figure 7.35 Stepwise multiple regression results of A_0 over all fibers using as the independent variables the clad [Ge] and clad [P], both normalized by the fractional optical power. The line represents a perfect fit of the model to the data and perfect predictive capability.

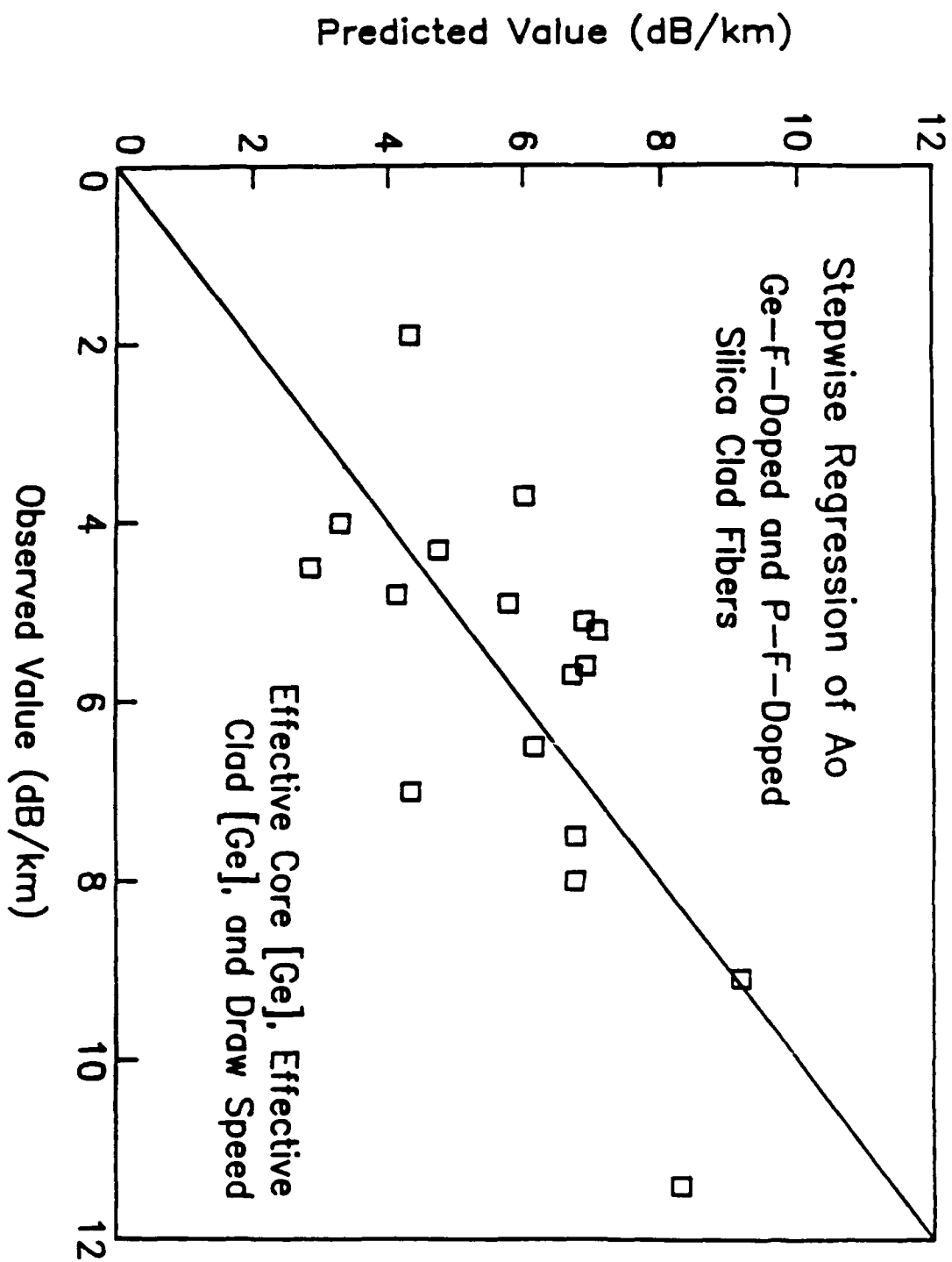


Figure 7.36 Stepwise multiple regression results of A_0 using a population of Ge-F-doped and P-F-doped silica clad fibers. The independent variables are the core and clad [Ge] normalized by the fractional optical power and the draw speed. The line represents a perfect fit of the model to the data and perfect predictive capability.

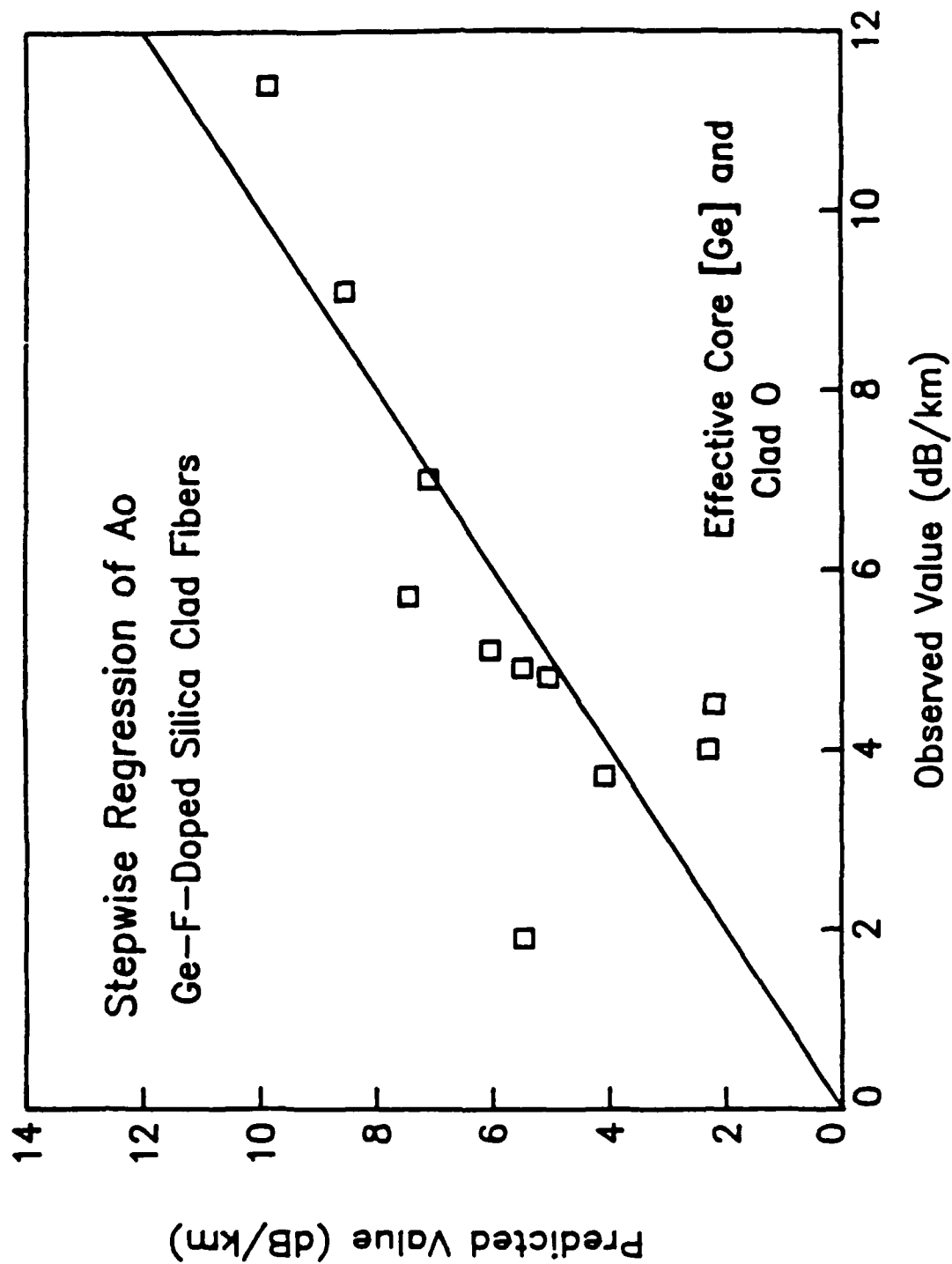


Figure 7.37 Stepwise multiple regression results of A_0 using a population of Ge-F-doped silica clad fibers. The independent variables are the core [Ge] normalized by the fractional optical power and oxygen-to-reagent ratio during clad deposition. The line represents a perfect fit of the model to the data and perfect predictive capability.

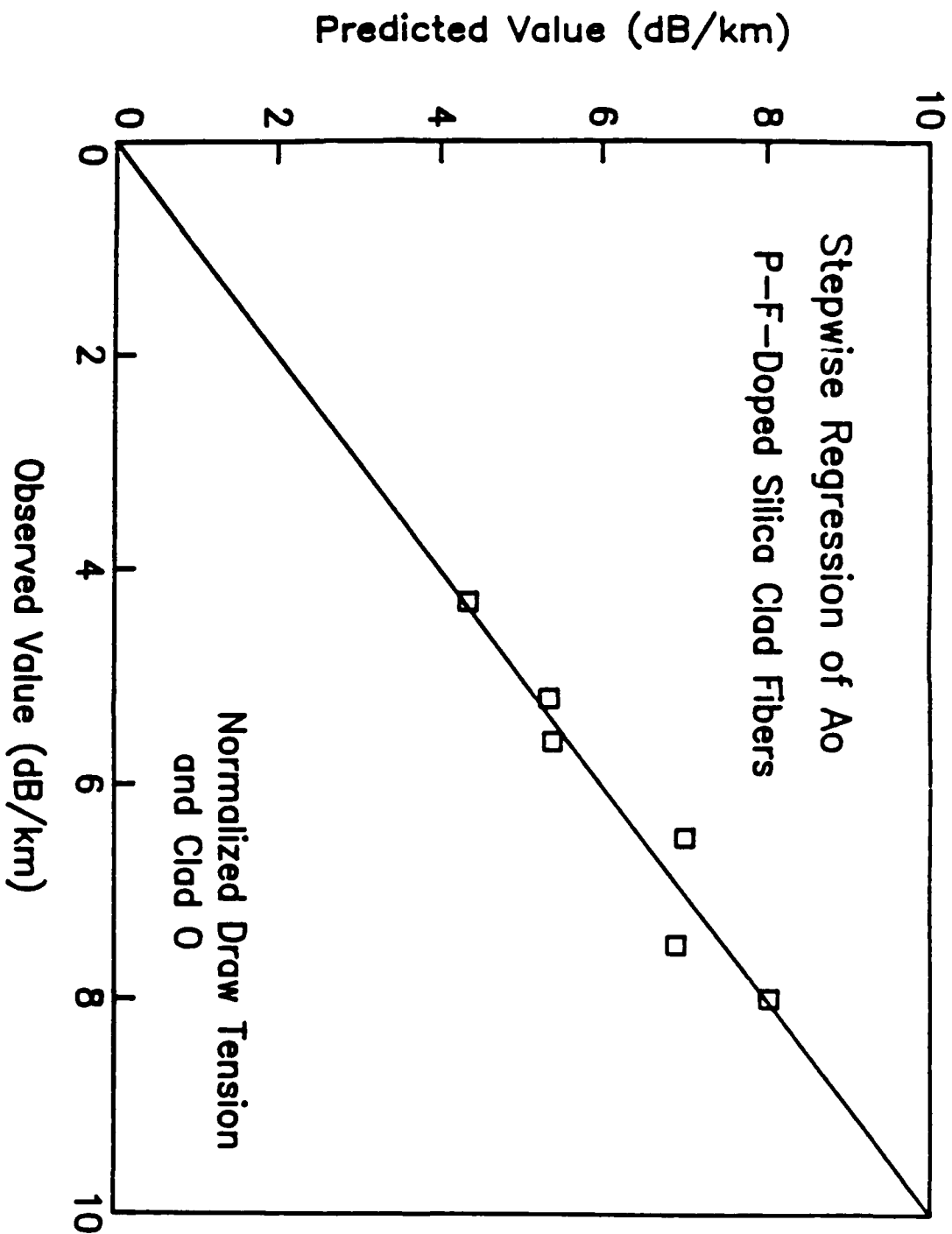


Figure 7.38 Stepwise multiple regression results of A_0 using a population of P-F-doped clad fibers. The draw tension divided by the fiber cross sectional area and oxygen-to-reagent ratio during clad deposition. The line represents a perfect fit of the model to the data and perfect predictive capability.

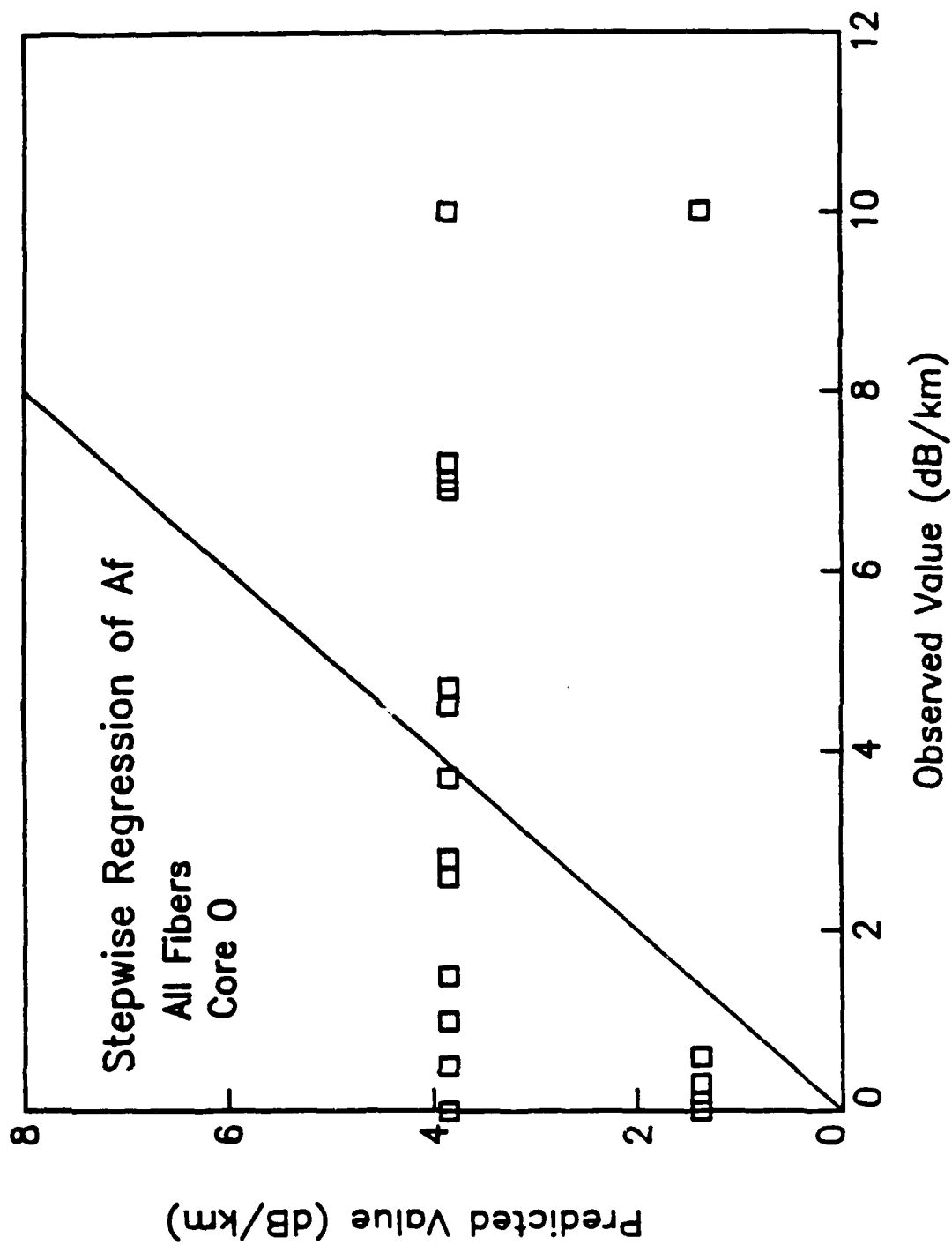


Figure 7.39 Stepwise multiple regression results of A_f using a population of all fibers. The independent variables is the oxygen-to-reagent ratio during core deposition. The line represents a perfect fit of the model to the data and perfect predictive capability.

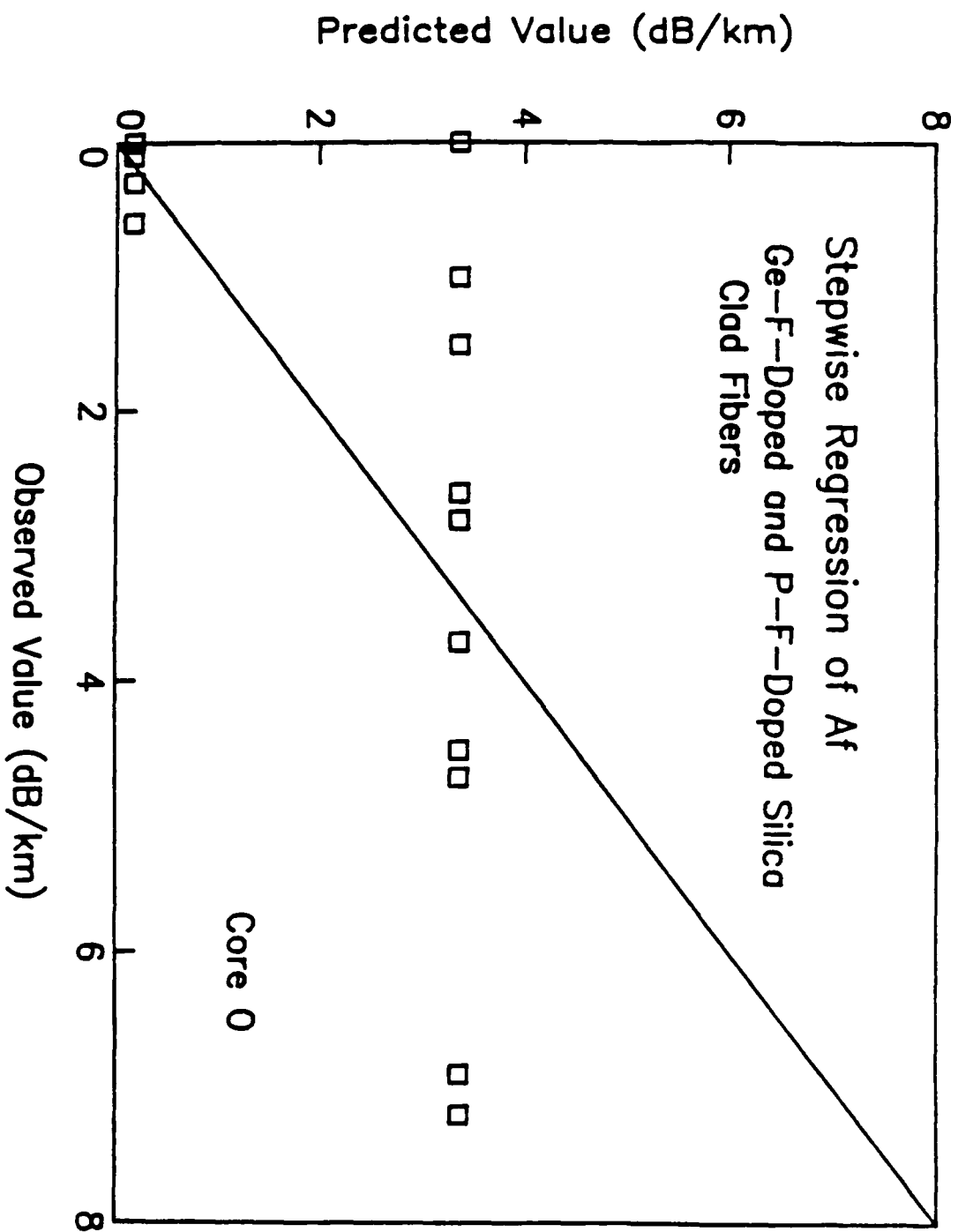


Figure 7.40 Stepwise multiple regression results of A_f using a population of Ge-F-doped and P-F-doped silica clad fibers. The independent variables is the oxygen-to-reagent ratio during core deposition. The line represents a perfect fit of the model to the data and perfect predictive capability.

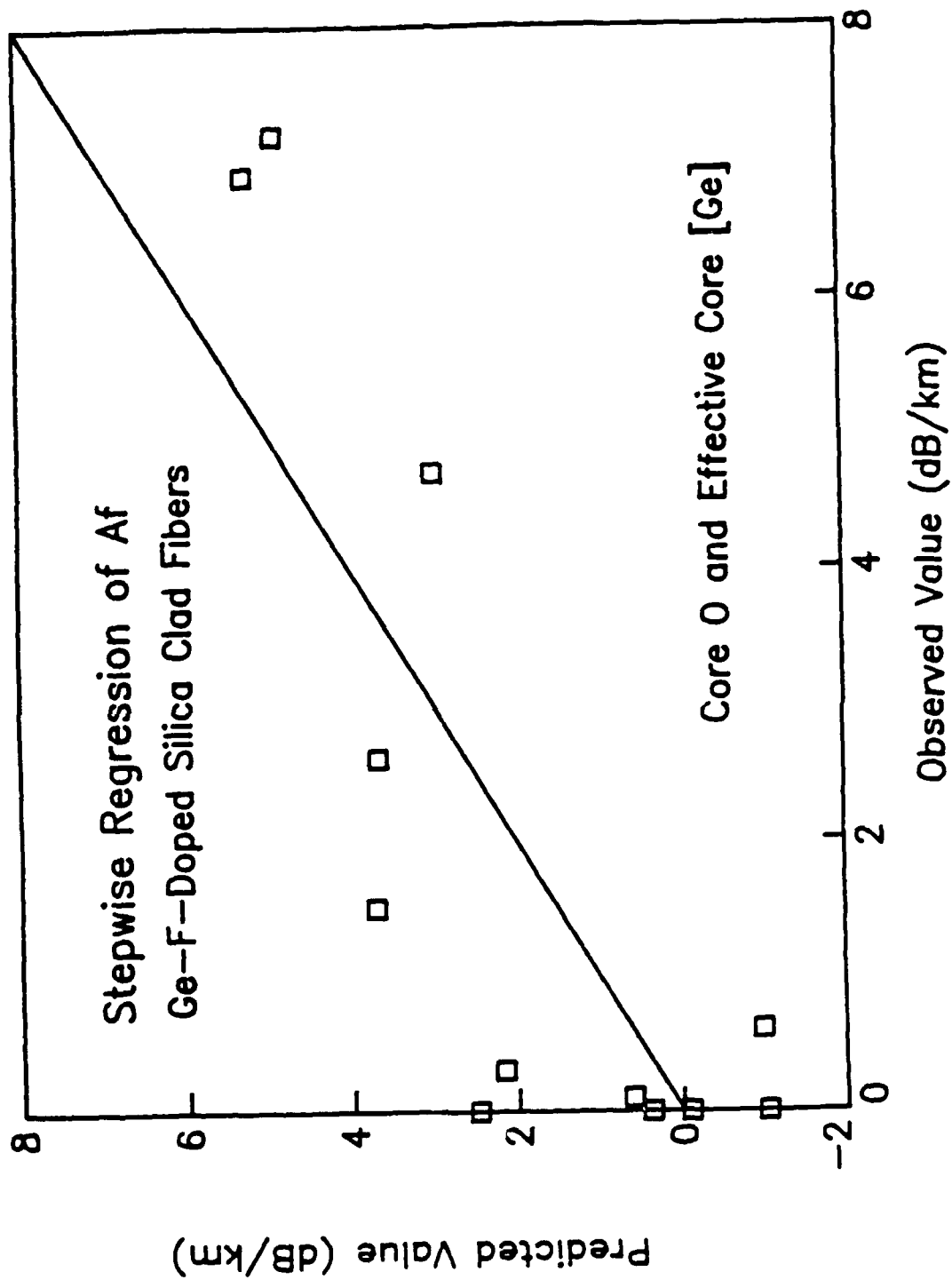


Figure 7.41 Stepwise multiple regression results of A_f using a population of Ge-F-doped silica clad fibers. The independent variables are the oxygen-to-reagent ratio during core deposition and the core [Ge] normalized by the optical power. The line represents a perfect fit of the model to the data and perfect predictive capability.

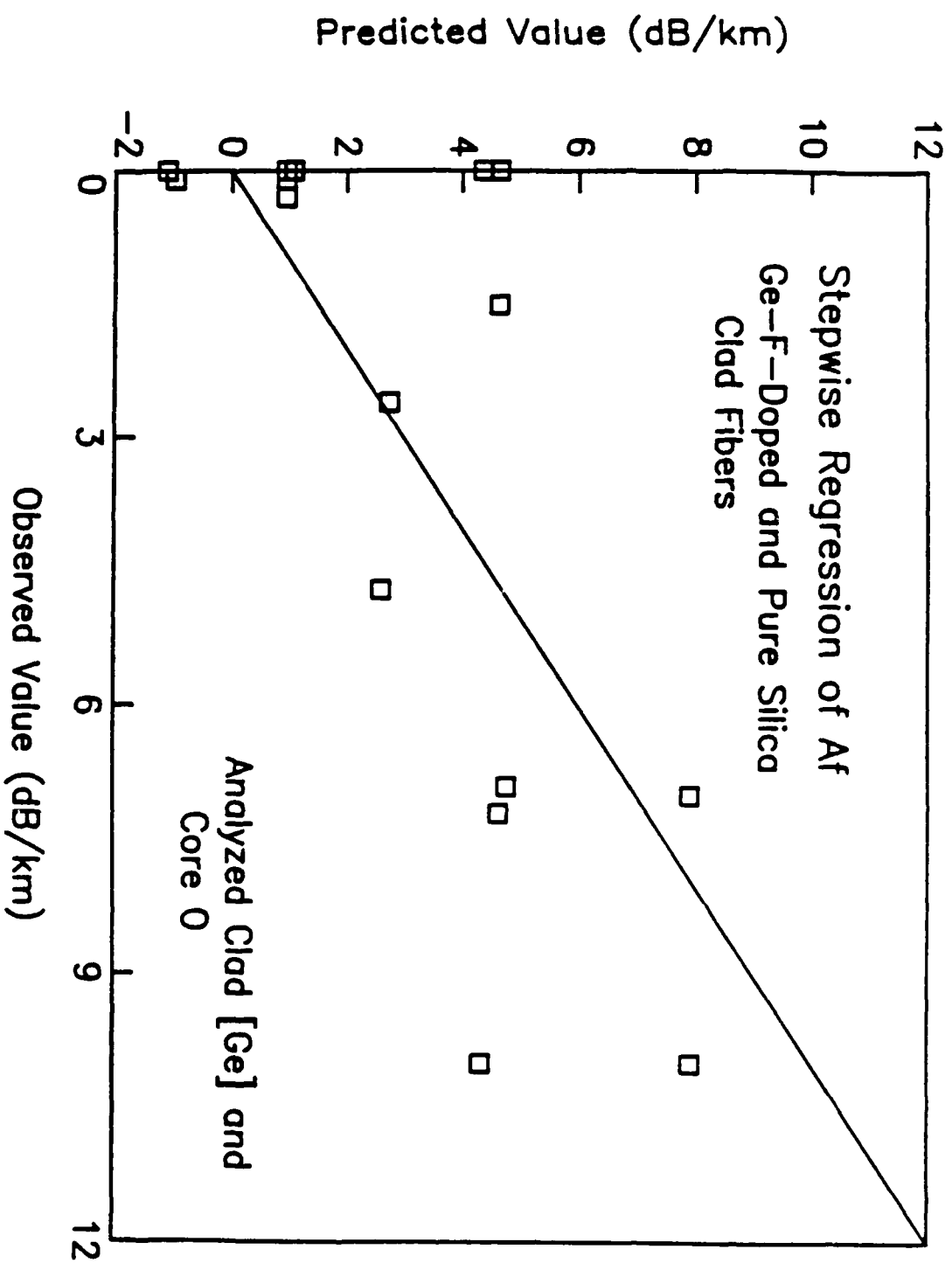


Figure 7.42 Stepwise multiple regression results of A_f using a population of Ge-F-doped and pure silica clad fibers. The independent variables are the oxygen-to-reagent ratio during core deposition and the clad [Ge] as determined by electron microprobe analysis and not normalized by the optical power. The line represents a perfect fit of the model to the data and perfect predictive capability.

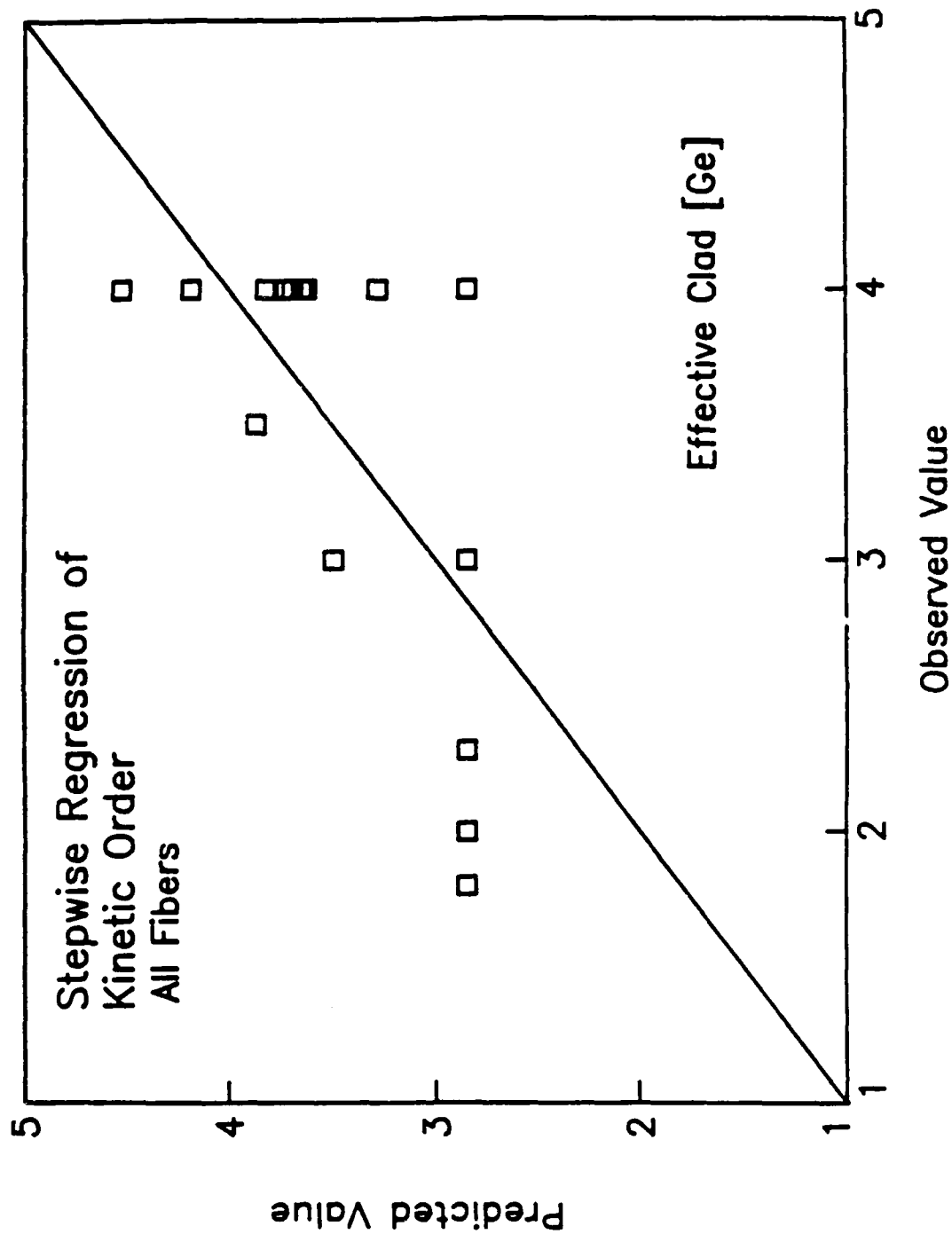


Figure 7.43 Stepwise multiple regression results of n using a population of all Ge-F-doped, P-F-doped, and pure silica clad fibers. The independent variable is the clad [Ge] normalized by the optical power. The line represents a perfect fit of the model to the data and perfect predictive capability.

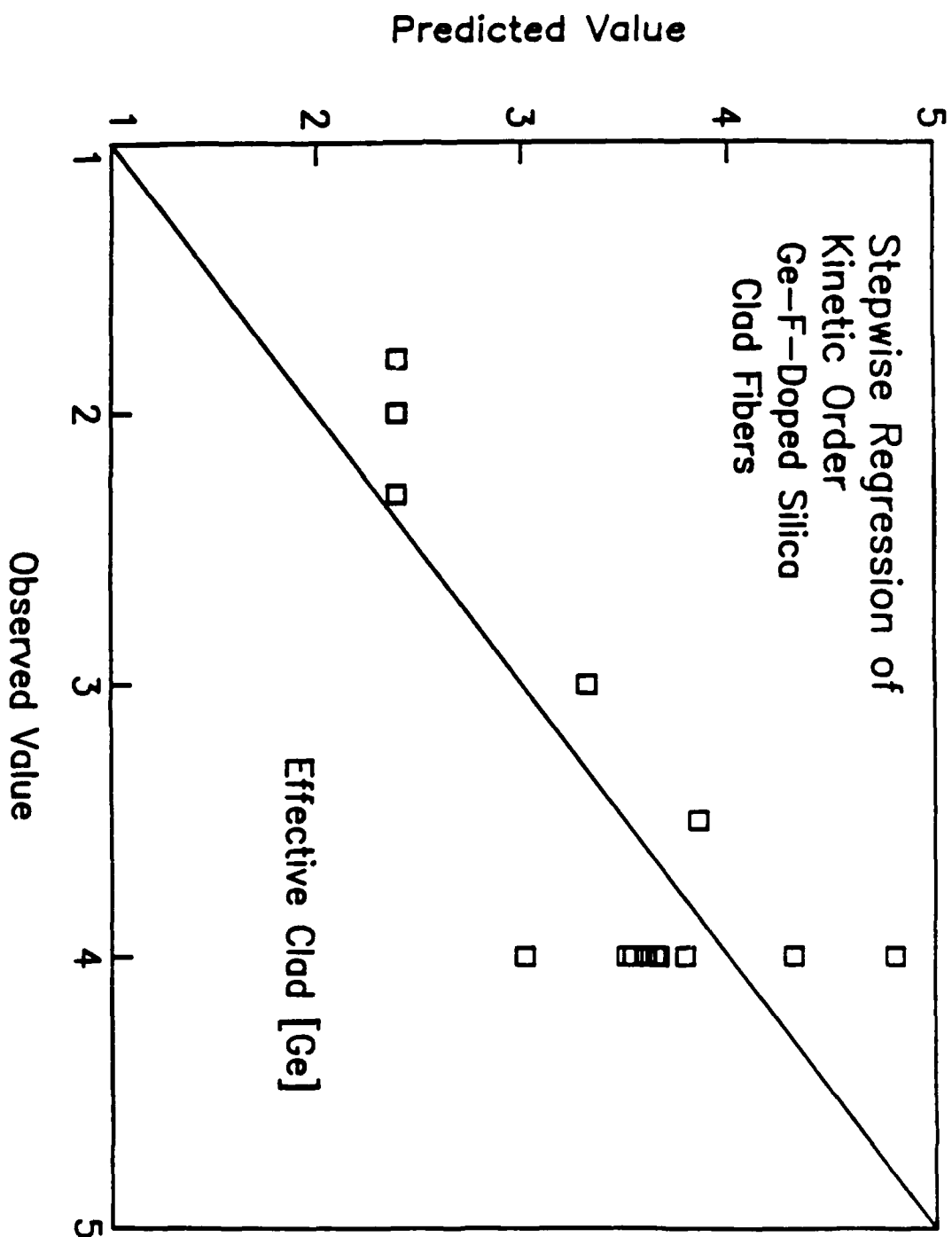


Figure 7.44 Stepwise multiple regression results of n using a population of all Ge-F-doped silica clad fibers. The independent variable is the clad [Ge] normalized by the optical power. The line represents a perfect fit of the model to the data and perfect predictive capability.

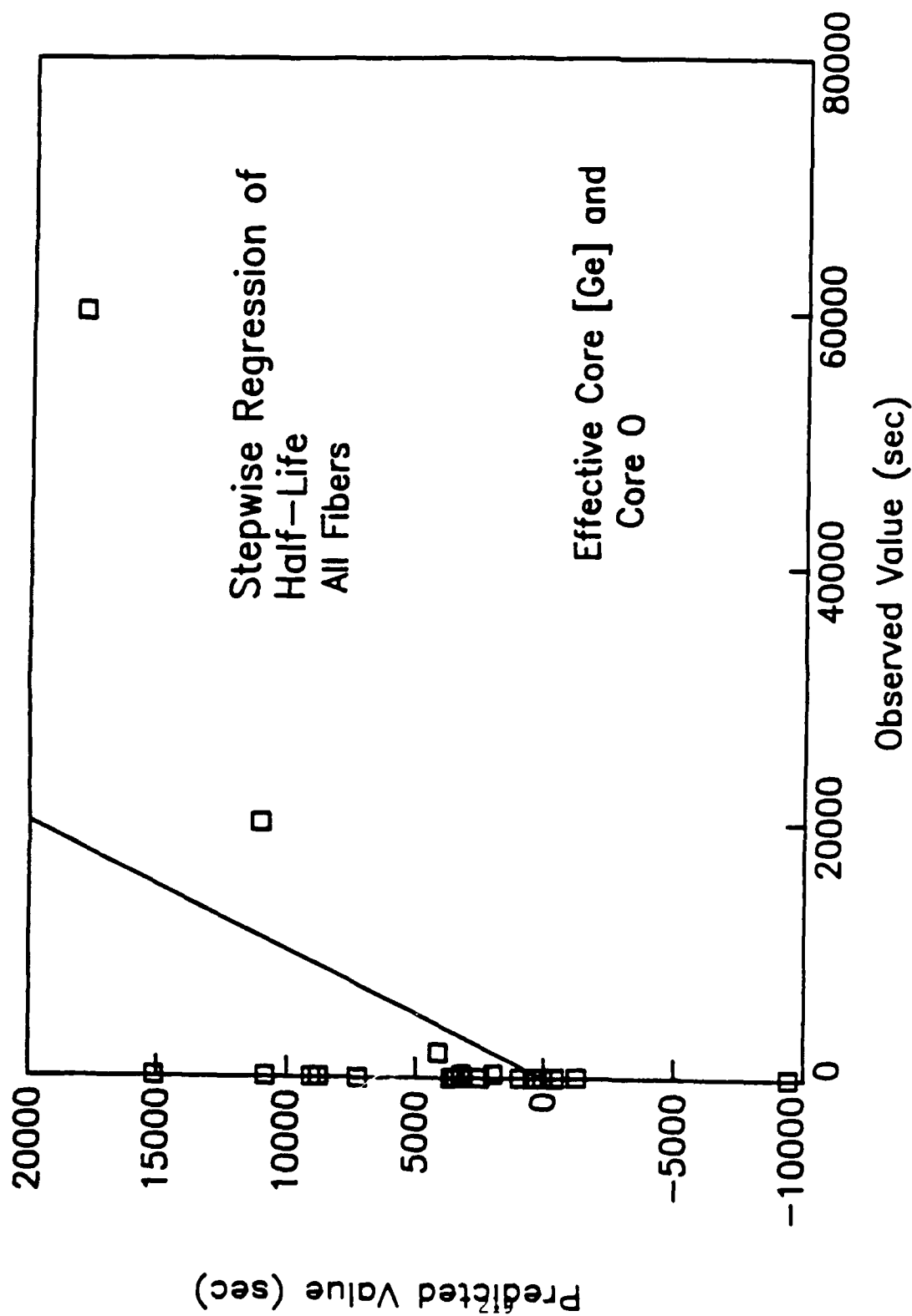


Figure 7.45 Stepwise multiple regression results of τ using a population of all Ge-F-doped, P-F-doped, and pure silica clad fibers. The independent variables are the core [Ge] normalized by the optical power and the oxygen-to-reagent ratio during core deposition. The line represents a perfect fit of the model to the data and perfect predictive capability.

CHAPTER 8

CONCLUSIONS AND FUTURE DIRECTIONS

CONCLUSIONS

The primary result of present study is the demonstration of the feasibility of a predictive capability whereby the optical attenuation induced by nuclear fallout in a matched clad single mode fiber can be determined via a linear regression model whose inputs are core and clad dopant concentrations and fabrication parameters such as draw speed and tension and oxygen-to-reagent ratio. The radiation response and recovery has been quantified by fitting the data to an n-th order kinetic equation. The "initial" loss is a measure of the response of the fiber to the delayed gamma component, while the "permanent" incremental loss is a measure of the fallout response.

The stepwise multiple regression procedure used here has shown that prediction of A_0 and A_f can be made with a fair degree of confidence in a few cases with one or two input variables:

1. For the Ge-F-doped silica clad fibers, A_0 is predicted from the effective core [Ge] and the oxygen flow used during clad deposition. A_f is predicted from the effective core [Ge] and the oxygen flow used during core deposition.
2. For the P-F-doped silica clad fibers, A_0 is predicted from the draw tension and the oxygen flow used during clad deposition.

The regression results are more tenuous in other cases, likely due to the small sample size. In particular, Mies and Soto [1] have shown a linear relationship between the effective phosphorus content in the clad and the loss induced by low dose rate exposure, which is roughly equivalent to A_f . The failure of the stepwise procedure to enter effective clad [P] into the equation for A_f in the present study can be attributed to the fact that only 6

fibers at 3 levels of P-doping were studied.

It was found in this study that no consistent, meaningful predictive capability could be derived for either the order of the kinetics n or the half-life of the radiation-induced loss τ . Once again, this result may be attributed to the small sample size, but additionally to the fact that there were significant outlying points in both populations. The value of kinetic order does not have a strong influence on either the delayed gamma or fallout radiation response, at least within the range of $2 \leq n \leq 4$. However, variations in the half-life τ do have a dramatic effect, and it is hoped that further studies will result in a predictive capability for this parameter.

Because of the large number of samples which would have been required to perform a series of one-dimensional experiments to establish relationships between the fabrication parameters and radiation response, an orthogonal matrix design was applied to the experiment. The resulting reduction to 24 fibers in which all parameters were varied over all levels yielded sufficient information to elucidate the various dependencies, which in general agreed with the regression results.

The preliminary regression model developed for predicting radiation response requires as input not only the analyzed core and clad compositions, but their effective value determined by normalizing by the relative optical power transmitted in the core and clad at the operating wavelength. The core and clad compositions are determined by electron microprobe analysis, while the core diameter (measured by scanning electron microscopy) and the near field radiation pattern are required for normalization. In addition, parameters such as oxygen flow during core and clad deposition, draw speed and draw tension are also required as input in some cases. The former parameters can be measured from the fiber, albeit tediously, while the latter must be provided by the manufacturer before the regression equation can be used.

Alternatively, fibers to be installed can be specified to have optimum parameters for radiation hardness. In any event, the present study has shown the capability of developing a regression model and has opened the possibility of further refinement to improve statistical confidence.

FUTURE DIRECTIONS

The limitations of sample size and parameter space used during the present work lead to the proposal of several tasks for future work:

1. Specific one-dimensional experiments should be conducted to further elucidate and quantitatively characterize the important interactions between fabrication parameters and radiation response shown in the present study. A sufficient number of preforms and fibers should be fabricated and tested to lend statistical confidence to the result. These experiments should also be designed to clarify conflicting results of the present study and to investigate and clarify suspected cross-correlations between parameters.

2. The experiments have been conducted at only one temperature in order to give a "worst-case" result. However, repetition of the measurements at several temperatures would allow an expansion of the kinetic modelling to include the activation energy and pre-exponential terms. This improved model would be more widely applicable than the present results at -35 C.

Further improvements are also necessary in the kinetic model so that it can be used to describe the recovery behavior of both well-behaved and "pathological" fibers.

3. A series of test experiments should be conducted to verify the model by procuring from industry well-characterized single mode fiber samples with well-documented core and clad compositions, deposition conditions, and draw parameters. These would serve as a blind test of the model, first by predicting their radiation responses from the model and then by experimental

measurement.

4. The indicated directions for radiation hardness derived from the present study should be pursued in order to develop more radiation resistant fibers. The trade-offs necessary between parameters should be investigated and optimized for the intended application. In particular, additional research into the effects of fluorine doping must be carried out as this has shown promise for greatly enhanced hardness, both in delayed gamma and fallout environments. Additional research areas include the effects of draw conditions, fluorine doping and oxygen stoichiometry on the nature and concentration of radiation-induced defect centers in the fiber which cause the incremental attenuation.

5. Finally, continued support for ongoing NCS programs should be provided; as new fibers become available from manufacturers, their radiation response to the NSEP environment should be evaluated to maintain a complete data base.

REFERENCES

1. E.W. Mies and L. Soto, Proc. ECOC '85 (Venice).